The Hengill Geothermal Area:

Seismological Studies 1978–1984

Gillian R. Foulger

The Hengill Geothermal Area:

Seismological Studies 1978-1984

Gillian R. Foulger

ABSTRACT

A seismological study of the Hengill geothermal area was conducted during the 7 year period 1978 - 1984. The aim of the study was to research the geothermal prospect and tectonic structure of the Hengill area and to evaluate the passive seismic method as a geothermal prospecting tool.

All seismological data from the area were reviewed, both natural earthquake and refraction. Both a pilot monitoring project and a further intensive project, involving the deployment of a dense radio telemetered seismometer network, were conducted. Recommendations for further work are made in this report (Section 7).

Large magnitude earthquake activity occurs in Ölfus in the S of the area outside the high temperature geothermal area. Seismic episodes occur in the fissure swarm. Superimposed on this activity, continuous small magnitude background activity occurs, predominantly associated with the geothermal area. Hypocentral depths lie mostly in the range 2 - 6 km.

The seismicity of the Hengill area is most notable for its ongoing nature. Mainshock and swarm sequences are observed. The area exhibits a b-value of 0.74 ± 0.06 in the magnitude range $-0.9 \leqslant M_L \leqslant 5.5$, and little spatial variation is observed within the area. The repeat time for $M_L \geqslant 6.0$ in the Hengill area and imediate vicinity is approximatly 100 yrs. Significant b- value variations were observed associated with a swarm sequence in Ölfus.

Focal mechanisms for 178 events indicated both shear type and tensile crack type movements. The directions of orientation of the principle axes of stress inferred from these events were consistent with local tectonics. The tensile crack type events occurred only in the high temperature geothermal area, and were confined to small magnitudes. Consideration of the tensile crack type events allowed the fault plane to be distinguished from the auxiliary plane for the shear events.

Examination of teleseismic and explosion data collected on the dense radio telemetered seismometer network indicated lateral inhomogeneities within the area. Volumes of rock with relatively high P-wave velocities were detected beneath Húsmúli and the area N of Hveragerði, contrasting with low velocity volumes beneath Grafningur, the fissure swarm and Ölfus. These velocity contrasts extend from the surface down to several km. They are interpreted as indicating dense, intrusive, relativly cool rock beneath Húsmúli and the area N of

Hveragerði and lower density, younger eruptives at shallow depth beneath the fissure swarm possibly underlain by partial melt at depth. The partially molten zone may widen with depth to underlie the area N of Hveragerði also.

The results of the study are consistent with the theory that two volcanic centers occupy the Hengill area : the presently active Hengill centre and the extinct Grensdalur centre, N of Hveragerði. The Grensdalur centre originally lay on the spreading boundary but was transported ESE at a rate of $1/2 - 1$ cm yr^{-1} by plate movements, became extinct and was replaced by the Hengill centre. A transverse tectonic structure marks the trajectory of migration of the Grensdalur centre.

The ongoing seismicity of the Hengill area is attributed to contraction cracking due to the action of cool groundwater fluids on hot rock. Their spatial distribution may thus provide a map of those volumes of rock at depth that are highly permeable and are delivering heat rapidly to the geothermal reservoir. Fracture in the predominantly tensile stress regime of the accretionary plate boundary results in the formation of tensile cracks. Volume calculations indicate that much aseismic widening of the fissures occurs subsequent to their formation.

It is concluded that the extensive high temperature geothermal system of the Hengill area is fed by two major heat sources associated with the two volcanic centres and possibly a third, minor source between them. Different parts of the geothermal area exhibit different reservoir characteristics as a consequence.

Local seismicity studies may be applied to other Icelandic high temperature geothermal areas as a tool to map those volumes of rock that are cooling down and feeding the geothermal reservoir.

The formation of cooling contraction cracks on accretionary plate boundaries offers an explanation for the mechanism of dyke injection.

Contents

List of Figures

List of Tables

INTRODUCTION

During the 7 year period 1978-1984, a seismological research programme was conducted in the Hengill area as a joint co-operative venture of Hitaveita Reykjavíkur, Orkustofnun and Raunvísindastofnun Háskólans. The main emphasis was on natural earthquake studies.

The aims of the programme were:
1. To research the geothermal prospect and tectonic structure of the Hengill area.
2. To evaluate the utility of natural earthquake (passive seismic) studies as a geothermal prospecting tool.

The study aspects were specifically:
1. A 3-dimensional map of the spatial distribution of local earthquake activity. Earthquakes accompany movements associated with faults and such a map thus gives a direct indication of the locations of active faults, and fault zones which might be aquifers in the geothermal reservoir.
2. A knowledge of the depth distribution of seismic activity. Earthquakes do not occur in rock above a certain temperature where it loses its elastic properties. The maximum depth of activity may thus be viewed as an isotherm. Variations in it within the area may be interpreted in terms of variations in the depth of the heat source.
3. An assessment of large magnitude earthquake activity - its periodicity and spatial distribution. This enables earthquake hazard assessment and may also contribute to volcanic hazard assessment.
4. An estimation of the seismic rate of the area prior to drilling and exploitation. This is a necessary prelude to the assessment of post-production induced seismicity.
5. An assessment of the b-value of the area as a whole and lateral variations in this parameter. The b-value of an area is a necessary parameter for a statistical estimate of the maximum magnitude event that could possibly occur within that area. Variations in b-value within the area may be interpreted in terms of stress variations in the crust (e.g. thermal stress, tectonic stress).
6. A focal mechanism study of the local earthquakes. Such a study indicates the mode of faulting, orientations of fissures, faults and fault zones and possible variations in these parameters within the area. It could, for example, indicate that subsidence was occurring and determine whether the area was undergoing compression or extension.
7. A study of earthquake S-wave attenuation. S-wave attenuation is to

be expected in the case of waves that pass through volumes containing partial melt. A study of this nature thus has the potential to delineate magma chambers in the crust if such exist.

8. An assessment of possible variations in Poissons ratio over the area. Low values of Poissons ratio have been associated with steam reservoirs. Such a study may thus give information about the phase of the geothermal fluid i.e. steam or water.

9. The study of refraction shots recorded over the dense seismometer network. These data give a 3 dimensional picture of seismic velocity variations within the area, (linear refraction or reflection profiles only yield a 2-dimensional picture) and may be interpreted in terms of structure. Such information may be of critical importance in interpreting other types of data e.g. gravity surveys.

10. A study of the relative attenuation of explosion generated P-waves. This may give information concerning lateral and vertical changes in reservoir properties such as degree of water saturation, pressure, temperature, the presence of gas, partial melting and degree of compositional heterogeneity.

11. A study of teleseismic earthquake arrival time delays. Teleseisms pass through the crust at very steep angles and hence sample the crust beneath the area at much greater depths than explosions or local earthquakes. Such a study can hence give information about the gross structure of the area at relatively large depths.

The programme was not planned in entirety at the beginning but proceeded in 4 phases. At the end of each phase the results to date were assessed and the decision to continue taken with a clear understanding of the expected returns. This is probably the single most important factor that guaranteed the success of the programme, on account of the uncontrolled and unpredictable nature of natural earthquake activity.

Information on most of the above listed study aspects is described in this report and omissions are a reflection of the limited amount of time that was available to interpret the vast amount of data collected.

The whole of the results, however, turned out to be greater than the sum of the constituant parts. The programme as a whole enabled significant advances to be made in our understanding of the structure of the Hengill area, especially the complex geothermal area. A new type of earthquake focal mechanism was observed which suggests an explanation for the seismicity of Icelandic geothermal areas in general. Evaluation of the utility of natural earthquake studies as a geothermal prospecting tool is left to the reader.

1. PROGRAMME STRUCTURE, DATA COLLECTION AND PROCESSING

1.1 Programme structure

1.1.1 The aims of the programme

The aims of the seismological research programme of the Hengill area were twofold:

1. To research the geothermal prospect and tectonic structure of the Hengill area using natural earthquake data augmented by explosions, and
2. To evaluate the utility of natural earthquake (passive seismic) studies as a geothermal prospecting tool.

1.1.2 Structuring passive seismological research programmes in geothermal areas

A literature survey of passive seismic studies in geothermal fields was conducted in order to assess the "state of the art" (Foulger, 1982). It emerged that many studies have been reported, using recordings of local, regional and teleseismic earthquakes made in areas of interest, sometimes augmented by explosions. Various different project designs and processing methodologies for dealing with different types of data were described. Much of the work, however, was of the "pilot project" type, involving small numbers of stations deployed for very short periods, sometimes with little or no foreknowledge of the seismicity of the area of interest. It was concluded that much of the work done thus far had suffered from poor programme design, but that in a number of instances natural earthquake studies had given useful information about geothermal prospects. No one "composite" study had been reported, designed to collect diverse data and apply the full spectrum of processing methodologies.

It is clear that a meaningful passive seismological research programme in a geothermal area should consist of four phases:

Phase 1   Survey of all pre-existing seismic data from the area.

Phase 2   Pilot field project, reduction of data.

Phase 3   Main field project, reduction of data.

Phase 4   Ongoing monitoring.

The design of each phase and indeed whether or not it is undertaken

should be decided on the basis of the results of the previous phase(s). Field projects should be structured to optimise the collection of data of various types to enable the application of as many different processing techniques as possible. Continual comparison should be made with the results of other geoscientific investigations.

Following this research plan should ensure that any investment made in this type of research is based on a clear understanding of the expected returns, an aspect important to consider in natural earthquake studies, and that those returns be maximised.

The seismological research programme of the Hengill area followed the plan outlined above closely. It was hoped that by running a programme such as this, based on sound theoretical and practical background research, and specifically aimed at geothermal research, the value of the method as a prospecting tool could finally be fairly evaluated.

1.1.3 The structure of the Hengill seismological research programme.

Phase 1   1978 - 1979
All data available were examined, including reports of historic destructive events and data recorded on the regional seismograph network. The locations of the instruments of this network are shown in Fig. 1.1. A broad picture of the spatial and temporal nature of the local seismicity emerged (Foulger and Einarsson, 1980).

Phase 2   1979 - 1981
On the basis of the results from Phase 1 a short (4 month) pilot field project was designed and conducted in 1979. Four additional temporary drum seismographs were deployed to augment the two permanent stations in the area. They were located in and around the most seismically active part of the area in order to enable accurate hypocentral determinations (Fig. 1.1). (These 4 temporary stations were later made permanent). With the addition of the results from this phase the pattern of activity in the Hengill area became fairly clear (Foulger, 1981).

Phase 3   1981 - 1984
On the basis of the results of Phases 1 and 2 the main field project was designed involving the deployment of a dense seismometer network for a 4 month period in 1981.

A radio telemetered network of 23 stations recording on magnetic tape was made available to the programme. It was decided that the deployment of a network of this size for one summer would provide data for a study of the spatial and temporal distribution of local
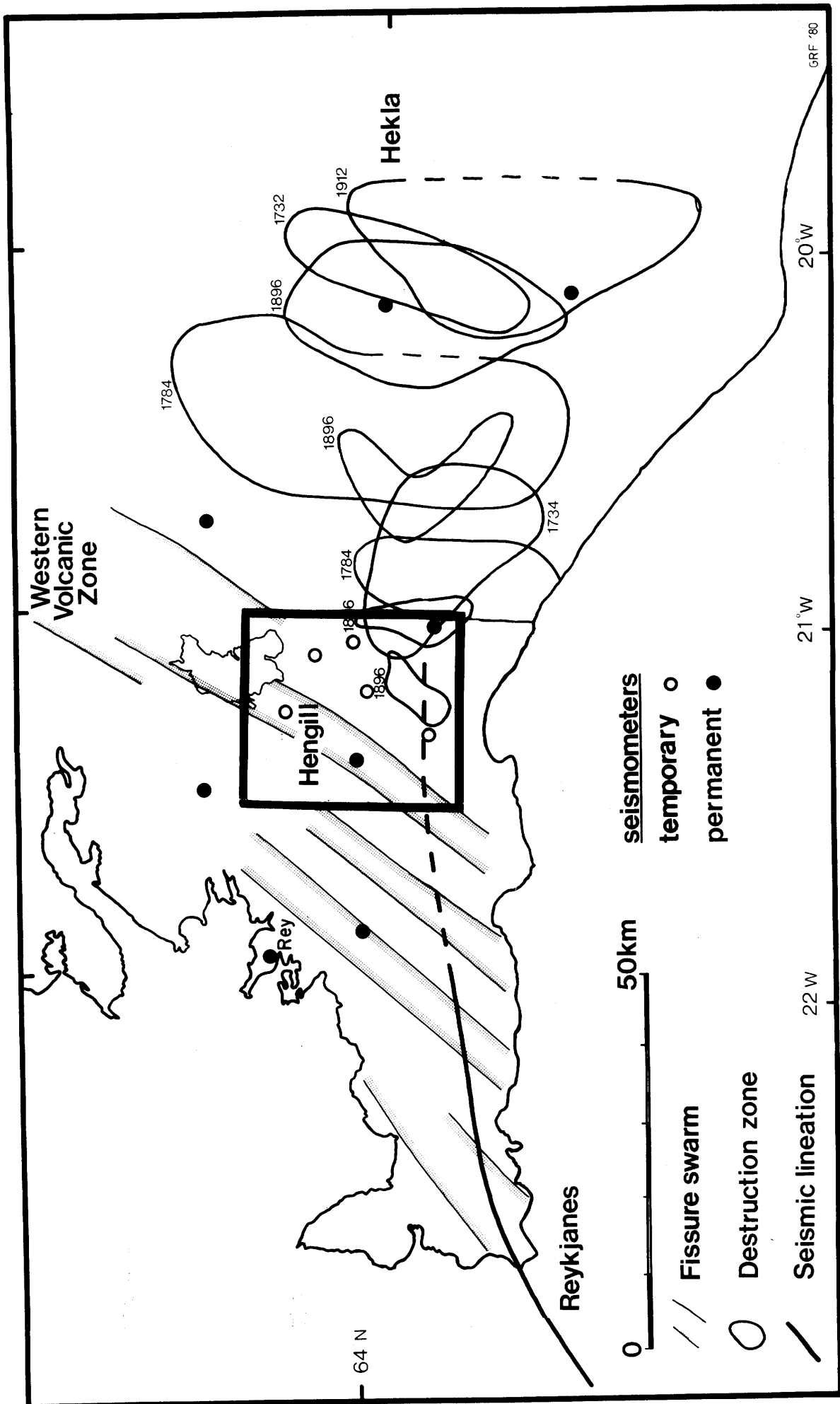
Fig. 1.1   Map of SW Iceland showing regional seismograph network and broad tectonic features.

earthquakes, frequency-magnitude relationships, focal mechanisms and teleseismic delay times. Local and regional explosions were also planned that would give data for a study of lateral and vertical velocity variations. This network augmented the network of 7 stations that was already installed in the area.

The network was centred on the most seismically active part of the area and its diameter made about three times the expected average hypocentral depth. Station coverage was fairly uniform but slightly denser in the middle. This network geometry enabled accurate locations to be calculated, especially hypocentral depths, and gave good constraint for focal mechanism solutions. Whilst maintaining this broad design, deviations were made for the following reasons:

1. 13 of the stations were deployed to form equidistant fan arrangements around the shot points. Such arrangements would yield arrival time delay and spectral data that would not have to be corrected for distance.
2. Line of sight had to be maintained between the transmitting and receiving aerials, therefore station coverage was poor in the neighbourhood and to the NE of Hengill and in the E, SE and SW of the area.

Station and explosion locations are shown in Fig. 1.2.

Phase 4   1984 –
The results of Phases 1 – 3 of this programme are presented in this report. On the basis of these results recommendations for Phase 4 (further monitoring) are made in section 7.1.
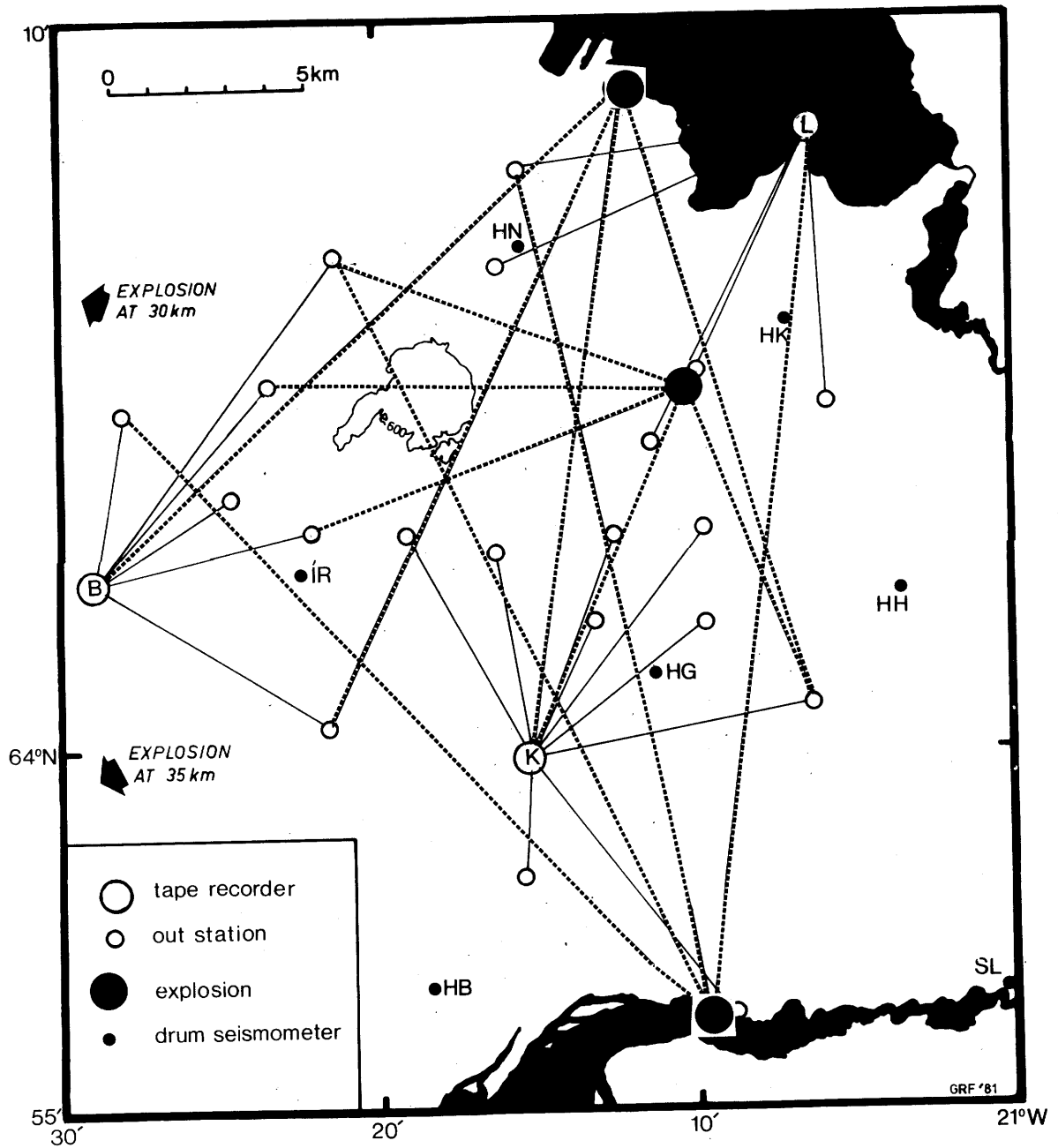
Fig. 1.2   Map of the Hengill area showing locations of the stations of the
           radio   telemetered   network   and   explosions. Ray paths from the
           explosions to the stations of the fan arrays are shown, and also
           radio transmission beams. Tape recorder stations   are   Blákollur
           (B), Kambar (K) and Lambhagi (L).

1.2 Data collection

1.2.1 The entire data set

The study of local earthquake activity presented in Sections 2-3 is based on data available concerning the seismicity of the Hengill area since the year 1700. The data are grouped as follows:

1. 1700-1983   historic macroseismic data
2. 1930-1983   data recorded at the regional station REY (Reykjavík)
3. Aug.1974-Jun.1981   data recorded on the regional seismograph network, which was occasionally augmented by additional temporary local instruments (the "drum data" set)
4. Jul.12-Oct.9 1981   data recorded on the radio telemetered network which augmented the regional seismograph network, (the "tape data" set).

Data groups 1-3 are "inhomogeneous" i.e. detection threshold and location accuracy did not remain constant (but usually improved) throughout the recording periods.

The teleseismic and explosion data discussed in Section 5 were collected on the radio telemetered network.

1.2.2 Historic macroseismic data

This was assessed by Sv. Bjornsson (pers. comm.). Documentation, and hence location and magnitude assessment, improved with time. The data group is considered to be complete for $M \geqslant 6.0$.

Locations of events in this group are based on reports of felt intensities and are accurate to within ten km. The data set contains 3-4 events.

1.2.3 Data recorded at the regional station REY (Reykjavík)

The station REY has response characteristics similar to the WWSSN stations. It is a 2 component set. The N instrument is a Sprengnether set at $T_s = T_g = 1.5$ sec and the Z instrument is a Willmore set at $T_s = 1$ sec, $T_g = 0.25$ sec. Recording is analogue on light sensitive paper at speeds of 30 and 60 mm min^{-1} respectively.

This station is operated by Veðurstofa Íslands which publishes data and event locations in its Seismological Bulletin. Event locations

were obtained directly from these bulletins, from Tryggvason (1978a, b; 1979) and from Ragnar Stefánsson and Þorunn Skaftadóttir (pers. comm.) of Veðurstofa Íslands. The instrumentation at REY was occasionally modernised during the period 1930-1983. Sensitivity and hence detection threshold thus progressively improved. The data set is probably complete for M $\geqslant$ 3.

Because instrumental data are only available from one station for most of the events (some of the larger events were also recorded at other stations operated by Veðurstofa Íslands) in general little more can be said about the event locations than that their epicentres lie somewhere in the Hengill area. The data set contains 116 events.

1.2.4   Data recorded on the regional seismograph network

The instruments comprising this network consist of vertical, short-period geophones (natural frequency 2-3 Hz) and paper drum recorders inscribing with pen and ink at a speed of 90 mm min^{-1}. Arrival times were read by hand from the seismograms to an accuracy of 0.1 sec.

The whole network consists of about 40 stations at the time of writing. Of these about 25 provided data for this programme, and 4 lie within the study area. The stations IR (IR skáli) and SL (Selfoss) were operational for the whole programme period. In addition four temporary stations were available, which were deployed intermittently (dependent on the whim of Krafla) at HG (Gufudalur), HH (Stóri-Háls), HN (Nesjavellir) and HB (Bjarnastaðir at Hjalli). These stations were first occupied for 4 months in the summer of 1979 during the pilot field project. In late 1980 semi-permanent stations were installed at these locations (Fig. 1.1). Because of this variability in station coverage, detection threshold and location accuracy is very variable within this data group. Fig. 1.3 illustrates the station coverage that was achieved within the Hengill area. The data set is complete for M $\geqslant$ 2.0 for the whole period, but a detection threshold as low as 0.3 was achieved when 6 stations were operated within the area.

In addition to these drum recorders, a station was operated at HK (Krókur) for part of the time. This station consisted of a 3 component set of Willmore Mk II seismometers with natural period adjusted to 1 sec. Recording was analogue on 1/4" magnetic tape. This station was loaned by Dept. of Geological Sciences, University of Durham, U.K. Tapes were played back on the processing system at Durham and paper records of events were written using a Siemens ink jet pen inscriber. Arrival times were read by hand and contributed to the computer

locations.

Both P- and S-waves were used in the computer locations of this data group (the S-wave arrival times were given half weight) which typically involve 5-10 readings. Locations are likely to be accurate to 1 km or so. The data set contains 1040 events.
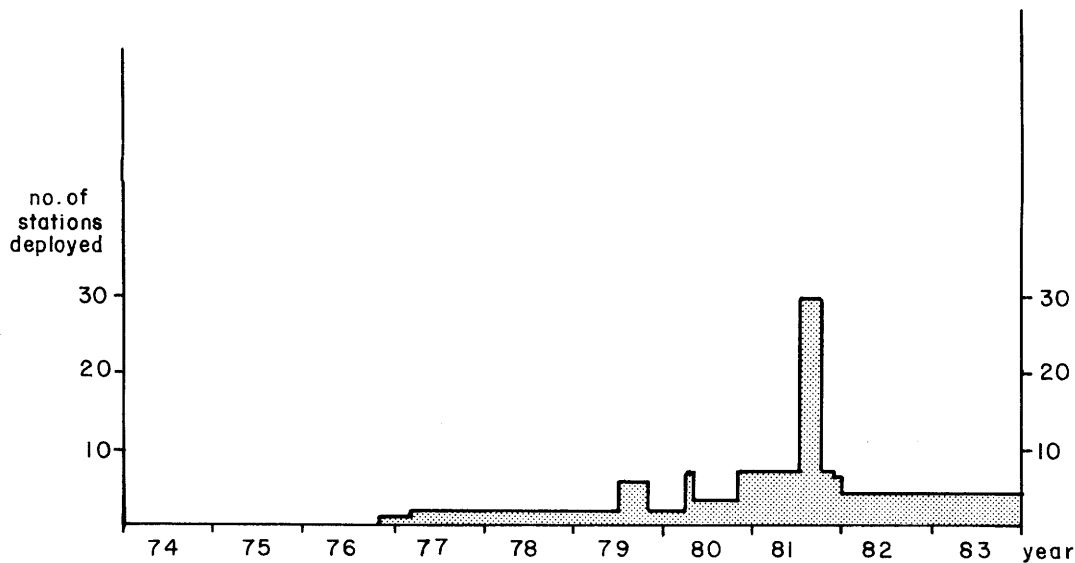
Fig.1.3 Station coverage achieved in the Hengill area 1974-1983.

1.2.5 Data recorded on the radio telemetered network

1.2.5.1 Instrumentation

Tape Recorders
Three tape recorders were used, recording analogue signals on 14 channel 1/2" magnetic tape at a speed of 15/320 in sec^{-1}. This gave an upper recording frequency limit of 32 Hz. One channel recorded time code generated by an internal crystal clock, flutter compensation signals were recorded on two channels, and a radio time signal was recorded on a fourth channel. The remaining 10 channels were available on each recorder for recording seismic signals. MSF Rugby radio time code receivers and aerials were provided with each tape recorder.

Seismometers

23 Willmore Mk III vertical seismometers were used, with natural period adjusted to 1 second. This is their minimum stable frequency. Each was paired with an amplifier-modulator. The seismometer/ amplifier-modulator pairs were each calibrated in the U.K. before shipment, so care had to be taken to match up the correct pairs. The instruments were not calibrated for frequency response in the field.

Radio links

20 radio links were deployed. They transmitted on 458-459 MHz at 0.025 MHz intervals. Each consisted of a transmitter, a receiver and a pair of UHF aerials.

Test Boxes

Two types were used. The Mk I type had both audio and visual (paper playout) displays, and was heavy. The Mk II type had audio display only but was light. The test boxes could be connected to the amplifier-modulator, the radio receiver or the tape recorder, to check the functioning of particular stations.

Replay equipment

A 7 channel Siemens ink jet pen inscriber, a 14 channel "store 14" playback tape recorder, an automatic time code decoder and a stereo audio playback set were used to monitor recording throughout the field season.

1.2.5.2   Field logistics

Out stations

In all cases the out station equipment was checked before setting off into the field.

A hole up to 1 m deep and 1/2 m diameter was dug at each site, with bedrock base. This was lined with a 20 1 paint drum with 1/2 of its base cut out. The drums used were made of steel, which was undesirable since metal objects can affect the functioning of the seismometer. Unfortunately this fact did not come to our notice until after all the out stations had been set up. The seismometer was placed on the bedrock, and adjusted to the vertical. Where necessary the bedrock was levelled with a hammer and chisel. The amplifier-modulator was stood in the paint drum on the half-base. The drum was sealed with its lid, and covered with a sheet of polythene.

A 2 m length of metal water pipe was used as a mast and was held upright by 3 steel wire guys. These were attached to the top of the mast by means of metal hooks, and to the ground to boulders or rock

outcrops. The guy wires were fixed with cable clamps, and tightened with cable tensioners. In order to prevent the mast from rotating in the wind, a 30 cm length of angle iron was screwed to its base by an exhaust pipe clip, and boulders piled onto this "foot".

The transmitting aerial was then clamped to the top of the mast. The transmitter, which was about the same size as a beer can (but sometimes less functional) was placed in a plastic bag and taped to the mast just below the aerial with the plugs pointing downwards. This was to prevent rain water leaking into the transmitter via the plug seals. The equipment was then connected up. The aerial was plugged into the transmitter, and the excess cable taped to the mast. The seismometer was plugged into the amplifier-modulator. The amplifier-modulator was then connected to the transmitter by running the cable along the ground to the base of the mast, up the inside of the mast, out of the top, and down to the transmitter. A branch cable connected a 12 volt lead acid battery to the transmitter. All cables on the ground were buried to camouflage them from sheep. Hence no visible cables were within chewing reach.

Batteries used were 60-70 amp hr lead acid batteries. A type with a carrying handle was used, which proved very useful when transporting them in the field. The batteries were placed in plastic bags and buried, to protect them from the weather and theft.

When all the equipment was installed, the test box was plugged into the amplifier-modulator and the gain adjusted. It was adjusted so that the low frequency background noise (1-2 sec. period) could be heard, but not high frequency wind and cultural noise. The gains were set variously at 4, 5, 6, 7 or 8. After recording commenced, however, it was found that the audio response of the test boxes was not the same as the response of the recording system as a whole. Several out stations had to be revisited and the gains increased by up to 3 settings (Table 1.1).

It was concluded from this experience that it would have been better to have set all the stations on gain 7 to start with, and to have adjusted them after the first paper playouts were examined.

Where time and circumstance allowed, the recording station was then visited, the receiving aerial and receiver set up, and the station tested for transmission integrity by plugging the test box into the receiver.

gain setting	no. of stations at beginning of recording	no. of stations at end of recording
4	2	-
5	2	-
6	5	3
7	13	20
8	1	-

Table 1.1 Gain settings of amplifier-modulators

Recording stations

2 m high masts accommodated the receiving aerials at the recording stations. Up to 6 aerials were placed on each mast, which was probably a little too crowded. However, no problems with cross talk were encountered as a result of this practice. The receivers were taped to the mast. Cables connecting the receivers to the tape recorders were shielded from sheep teeth by passing them through a length of plastic water pipe. The tape recorders were housed in waterproof aluminium boxes and stood on wooden frames to facilitate levelling. Cables passed into the boxes through a small hole cut in the underside. A seismometer was installed at each recording site, and connected directly to the tape recorder. Power was supplied by 12 volt lead acid batteries - a 60-70 amp hr battery for the seismometer, and a 110 amp hr battery for the tape recorder.

Installing the equipment

Accessibility was difficult in the area. Out of 23 sites, it was possible to drive up to 11 in the Land Rover, 9 sites were established and maintained by foot, and a pack horse was used for 3. For the recording sites it was imperative to select locations that could be driven right up to, because of the weight of the equipment and the great difficulty in making repairs and adjustments in the open.

When the radio transmitting stations were established by foot, the equipment necessary was transported in rucksacks, (a total weight of about 30 kg per station). The work of establishing the station fell naturally into two parts - placing and levelling the seismometer, and erecting the mast. Hence, it was found convenient to have two people. The addition of an extra person slowed the work and made it more difficult, and when there were four people it was impossible to get anything at all done.

þeim mun verr gefast heimskra manna ráð
er fleiri koma saman.

A pack saddle and saddle bags were hired for use with the horse. It was possible to pack equipment for two stations at a time.

During recording, when station maintenance was largely a matter of changing batteries, two wooden boxes with hooks were made, into which the batteries fitted. These could either be hung onto a rucksack frame or onto the pack saddle. This solved the problem of the batteries slipping about inside the packs and spilling acid.

Operating the equipment
Whilst recording was in progress the work naturally divided itself into two parts:
a) changing out-station batteries. This represented about 30 hours work per week.
b) changing tapes and playing them back on the replay equipment. This also represented about 30 hours work per week.

Time spent on maintenance and administration varied greatly, but averaged of the order of 100 hours per week.

Batteries at out stations were changed at intervals of 20 to 40 days, and recording station batteries more frequently. It should be noted for future projects using this equipment that there was a possibility of adjusting the power consumption of the transmitters, so it would have been possible to have lower power transmitters for the close stations. The reported range of the transmitters is 200 kms. For the short distances involved in this project, signals were relatively so powerful that orientation of the transmitting and receiving aerials was almost irrelevant to reception. In one case vandals turned the receiving mast (at Blákollur) through 90° but for none of the stations was reception affected. In one or two cases masts fell down, but the signal was never lost.

Explosions
Detonations were made, according to plan, in Ölfus, Djáknapollur, Þingvallavatn, Grænavatn in Krísuvík and outside Reykjavík harbour. 25 kg of dynamite were used for the local explosions and 50 kg in Grænavatn. It was found on playing back that 50 kg was too little at such a distance, so 100 kg was used in Reykjavík harbour.

Monitoring of the data collected on tape
During the recording period, all tapes were played back at speed of 7 1/2" per sec. (i.e. 80 x recording speed). Malfunctions could thus be

detected as quickly as possible. It was found necessary to play back the whole tape since some malfunctions, e.g. transmitters drifting off frequency, occurred only part of the time, and these stations often sounded good when they were checked out at tape changes. By playing the whole tape back as soon as it was changed, it was possible to keep as up to date an overview of the functioning of the equipment as possible. At this speed it took about 1 hour to obtain a paper record of seven of the channels.

Malfunctions

Data loss is calculated as follows as percentage lost recording time during the period 12th July to 9th October.

It should be noted that tape recorder breakdowns were much more damaging than radio link and other failures, since up to 10 stations were lost at a time in such cases.

	% data loss
tape recorder breakdowns	4.9
radio link breakdown and drifting	5.7
other	3.2
total	13.8

Total recording time = 90 x 3 = 270 tape days.
thus, the total data loss was equivalent to = 37.3 tape days

"Other" malfunctions included batteries running out, mechanical damage to tapes, amplifier - modulator failure, breakdown of insulation between receiving aerial and mast, vandalism, and cross talk.

No equipment was stolen or damaged. There were 3 instances of vandalism: a battery was disconnected, a receiving mast rotated through $90°$ and a mast was collapsed.

Data loss was very severe when recording first started, so some of the worst tapes were wiped and reused at the end of the project.

Cost

The whole field project cost about $50,000. This figure includes all expenses associated with the 4 month field project, and one year's salary for one scientist.

1.2.5.3 Data playback

Recording was conducted for about 90 days. The tapes were played back at the University of Durham using similar equipment to that used to monitor the tapes, but with a 16 channel jet pen. A playback speed of 3 3/4" sec^{-1} was used and paper records were produced on the scale 60 mm : 1 sec. About 15,000 individual paper records were made, and about 150,000 arrival times read, a process that took about 1 year.

Arrival times were read by hand to an accuracy of 0.01 sec. Station coverage during the recording period was constant, except for a few breakdowns of short duration, and hence detection threshold and location acuracy may be considered to be uniform for this data group. The data set is complete for M $\geqslant$ -0.9.

P-wave arrivals only were used for the computer locations, which typically involve 10-20 readings. The reading accuracy of this data is such that the error in the locations is probably chiefly dependent on the accuracy of the crustal model used. Relocation of local explosions indicates that epicentral locations are probably accurate to within 400 m (section 5.2.2). The data set contains 1918 events.

The teleseismic arrival times were also read from paper records, using the wave matching technique (see Section 5.1.2) The data set contains 21 events for which 328 arrival times were measured.

1.3 Data processing

1.3.1 The hypocenter locator and plot computer utilities

Earthquake locations were calculated using the programmes HYPO71 (Lee and Lahr, 1972), HYPOELLIPSE (Lahr and Ward, 1975), and HYPOINVERSE (Klein, 1978). When HYPOINVERSE, the most recent earthquake locator programme, was installed, a new velocity structure was calculated involving layers with linear velocity gradients. This structure replaced the previous one which used discrete velocity layers, and modelled the observational data more closely (Appendix 1). All events located using older programme versions and velocity structures were then relocated in order to standardise the data. For this reason the earthquake location maps presented in this report may differ in detail to those presented in reports dated prior to 1983. The overall picture, however, remains the same.

HYPOINVERSE is installed in the Reiknistofnun VAX/VMS machine, and is used in conjunction with the Earthquake Hypocenter Locator and Plot System (HLPS). HLPS is a system of user utilities that facilitates file editing, data handling, the running of Fortran programmes and data archiving.

A number of plotting utilities (EMAP, DMAP, TMAP) are also available in HLPS. These plot epicentral maps and depth and temporal profiles. Also installed is the utility BVALUE that plots frequency-magnitude diagrams and calculates b-values. Work commenced on HLPS and the plotting utilities late in 1979 and the present version is the result of continual maintainance, updating and enlarging work. HLPS is documented in a HELP facility in the same computer.

1.3.2 The teleseism computer utilities

The programme HYPERMAP, supplied by Dr. D.H. Tarling, University of Newcastle, was used to plot a map of world coastlines and teleseism locations in Mercator projection centred on Hengill (Fig. 5.1).

The programme MANETA (Savage, 1979) was used to calculate theoretical arrival times for the P- and PKP-waves of the teleseisms at the Hengill stations.

The programme SEPD (Savage, 1979) was used to calculate individual station delays from the raw delay times measured for a number of teleseisms.

These three programmes are currently installed in the NUMAC IBM system at Durham University.

2. LOCAL EARTHQUAKES: SPATIAL DISTRIBUTION

2.1 The historic macroseismic data

The events in this group may be listed:

M	Year	Day	Latitude	Longitude
6-6.5	1706	20.4	63 N 58.1`	21 W 13.6`
6-6.5	1789	10.6	64 N 00.0`	21 W 26.6`
6.0	1896	6.9	63 N 58.1`	21 W 13.6`
6.0	1935	9.10	64 N 00.0`	21 W 30.0`

The event of 1789 was a large earthquake swarm that activated at least 30 km of the fissure swarm passing through Hengill, and not a single large shock (Thoroddsen, 1899). The energy release of the whole sequence was equivalent to one magnitude 6-6.5 event (Tryggvason, 1973).

The events of 1706 and 1896 are located in the centre of the Ölfus lowlands, where population was dense enough to definitly constrain the epicentres to be south of 64° N. The event of 1935 is less well constrained because it occurred in an area of sparse population.

The main point that emerges, however, is that all 3(4) of these events are located on or south of the 64° line of latitude, and are hence probably not related to the geothermal area. As will be seen below, this picture is in stark contrast to that which emerges from a short-term study of small magnitude events.

2.2 Data recorded at the regional station REY

This station is about 35 km from the centre of the Hengill area. Events in this group were rarely recorded at any other station, and epicentres cannot be located more accurately than to permit association with the Hengill area. Study of this data group was hence limited to magnitudes and temporal distribution, which are discussed in Section 3.

2.3 The computer locations

2.3.1 Presentation of the data

Computer hypocentral locations were calculated for events recorded on the regional seismograph network and the radio telemetered network. These two data sets will be discussed together in this Section but will be presented separately in the Figures. They will be referred to as the "drum data" and the "tape data" respectively.

The natures of these two data sets are very different. The tape data set is far superior to the drum data set in terms of number and accuracy, and represents a different magnitude range and recording period. The drum data set, on the other hand, represents a much longer time period, and contains events of higher magnitude. These two data sets are thus inherently different and it should be appreciated that each gives information unobtainable from the other. However, despite these differences, the general pattern of seismicity is very similar for the two data sets, and for this reason they will be treated concurrently.

The drum data set shows the pattern of seismicity over the seven year period 1974-1981. The temptation to extrapolate to longer periods should be resisted, in the absence of supporting information. The tape data set shows the pattern of activity over the 3 month period July-Sept. 1981. Certain conclusions may be drawn about the persistance of the short term pattern of activity shown by this data set from comparison with the drum data set.

A similar argument may be applied to the magnitude aspect. The drum data set is comprised of events whose source volumes would typically have dimensions of tens of meters. This gives an indication of the scale of the structures in question. Extrapolation to hypothesise structures of larger size should only be considered in the presence of supporting information. Also, although events within the magnitude range in question ($M_L \leqslant 4.2$) form a certain pattern, it does not necessarily follow that events outside this magnitude range form a similar pattern. In fact historic evidence suggests the contrary (see Section 2.1). The tape data set typically contains events whose source volumes have dimensions of meters. Limited extrapolation may be made on the basis of comparison with the drum data set.

The entire data set contains almost 3000 events. The features displayed are hence often supported by a large bulk of data, which lends weight to the conclusions drawn.

The data set is 6-dimensional (space, time, magnitude and accuracy). It is only possible to represent two dimensions continuously on a sheet of paper. This necessitates the qualitative selection of data sets for each plot, and implies an inherent difficulty encountered in interpreting the data i.e. are the features delineated by the data being enhanced by the constraints used, or are they being produced by them? As a rule series of plots were made, progressively constraining the data. Spurious epicentral and hypocentral patterns were identified as those that were heavily dependant on the selection criteria.

Separate presentation of the drum and tape data sets may be regarded to some extent as the presentation of differing magnitude groups. In order to make some distinction between data of differing accuracy, each data set is divided into "epicentral data" and "hypocentral data", the latter being selected for accuracy in the depth determination, and the former for accuracy in the epicentral determination only. Definition of the selection parameters tabulated below are given in Klein, (1978).

epicentral data : The constraints imposed were:

	drum data	tape data
gap (azimuthal)	$\leqslant 180°$	$\leqslant 180°$
ERH (horiz. error)	$\leqslant 2.5$ km	$\leqslant 1.0$ km
RMS (of arr. times)	$\leqslant 0.15$ sec	$\leqslant 0.10$ sec
ERZ (vert. error)	$\leqslant 99.0$ km	$\leqslant 99.0$ km

hypocentral data : The constraints imposed were:

	drum data	tape data
gap	$\leqslant 180°$	$\leqslant 180°$
ERH	$\leqslant 1.3$ km	$\leqslant 1.0$ km
RMS	$\leqslant 0.15$ sec	$\leqslant 0.10$ sec
ERZ	$\leqslant 2.2$ km	$\leqslant 2.0$ km
no. arrival times	$\geqslant 8$	$\geqslant 12$
dist/depth	$\leqslant 2.0$ km	$\leqslant 2.0$ km

To obtain accuracy in the hypocentral depth of an event, comparable to that in the horizontal plane, stations very close to the epicentre are required. Hence additional parameters were constrained in selecting the hypocentral data. These were:

a) minimum number of arrival times used for the location, and
b) the ratio of the horizontal distance to the nearest station used in
   the location to the hypocentral depth (dist/depth). Constraining
   this parameter limits possible selected locations to cone shaped
   zones beneath each station. However examination of the data showed
   that very few hypocentres were located outside these cones.

These constraints were selected on a trial basis. The aim is to have
the effect of "focussing" a picture that would otherwise be blurred by
a scatter of poorly located events.

2.3.2 The seismicity in detail

2.3.2.1 General

Figs. 2.1 and 2.2 show the epicentral distribution of drum and tape
data sets respectively, and in Figs. 2.3 and 2.4, hypocentres are
plotted on NS cross sections.

The following are the main points to emerge from the spatial
distribution of events.
1. The general pattern of activity remained constant for both data
   sets, despite the contrasting recording periods and magnitude
   ranges.
2. The most active part of the area is a central cluster of activity
   roughly 20 km^2 in area NW of Hveragerði. This area is not circular
   in shape, but appears to display two trends, one striking NW-SE and
   the other NE-SW. This feature is most prominent in the drum data
   set. The tape data epicentral distribution is consistent with this
   pattern, but for this data set the activity falls into distinct
   subclusters.
3. A fault zone is delineated by epicentral locations in Nesjavellir.
4. A concentration of activity occurs NW of Hengill, on Mosfellsheiði.
5. Activity occurs S of 64° N in the Ölfus lowlands.
6. There is an EW belt of low activity about 64° N.
7. The most intensively faulted part of the area, the fissure swarm
   passing through Hengill, displays very low activity.
8. Hypocentral depths are generally in the range 1 - 8 km and mostly
   in the range 2 - 6 km.

2.3.2.2 The central cluster

The main epicentral area of activity lies approximately 5 km NW of
Hveragerði, and coincides with the area most abundant in hot springs
and fumaroles (Fig. 2.5). A topographic low formed by 3 NS trending
river valleys (Reykjadalur, Grensdalur and Sauðárdalur) occupies a
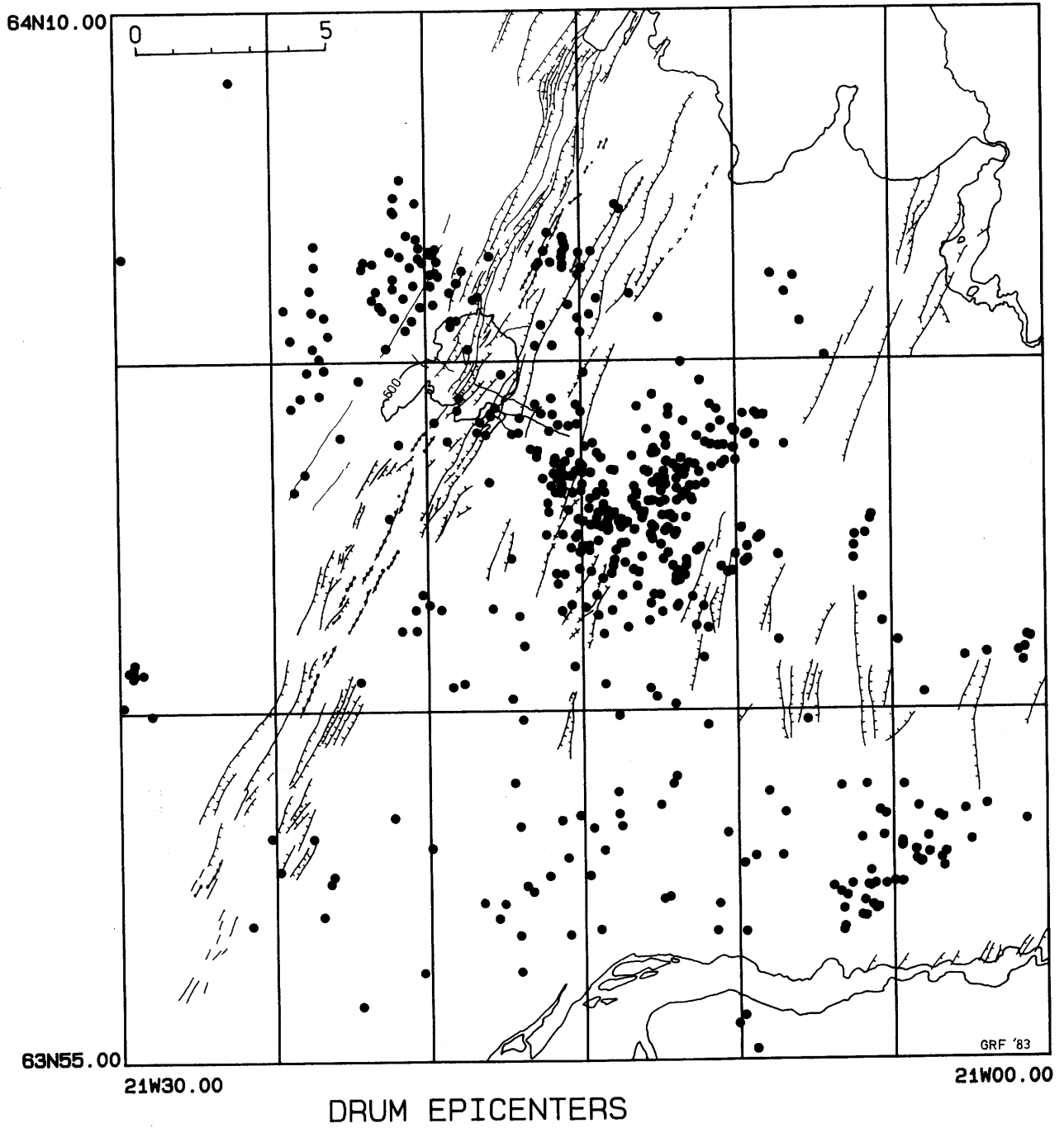
Fig. 2.1   Drum data epicentres.
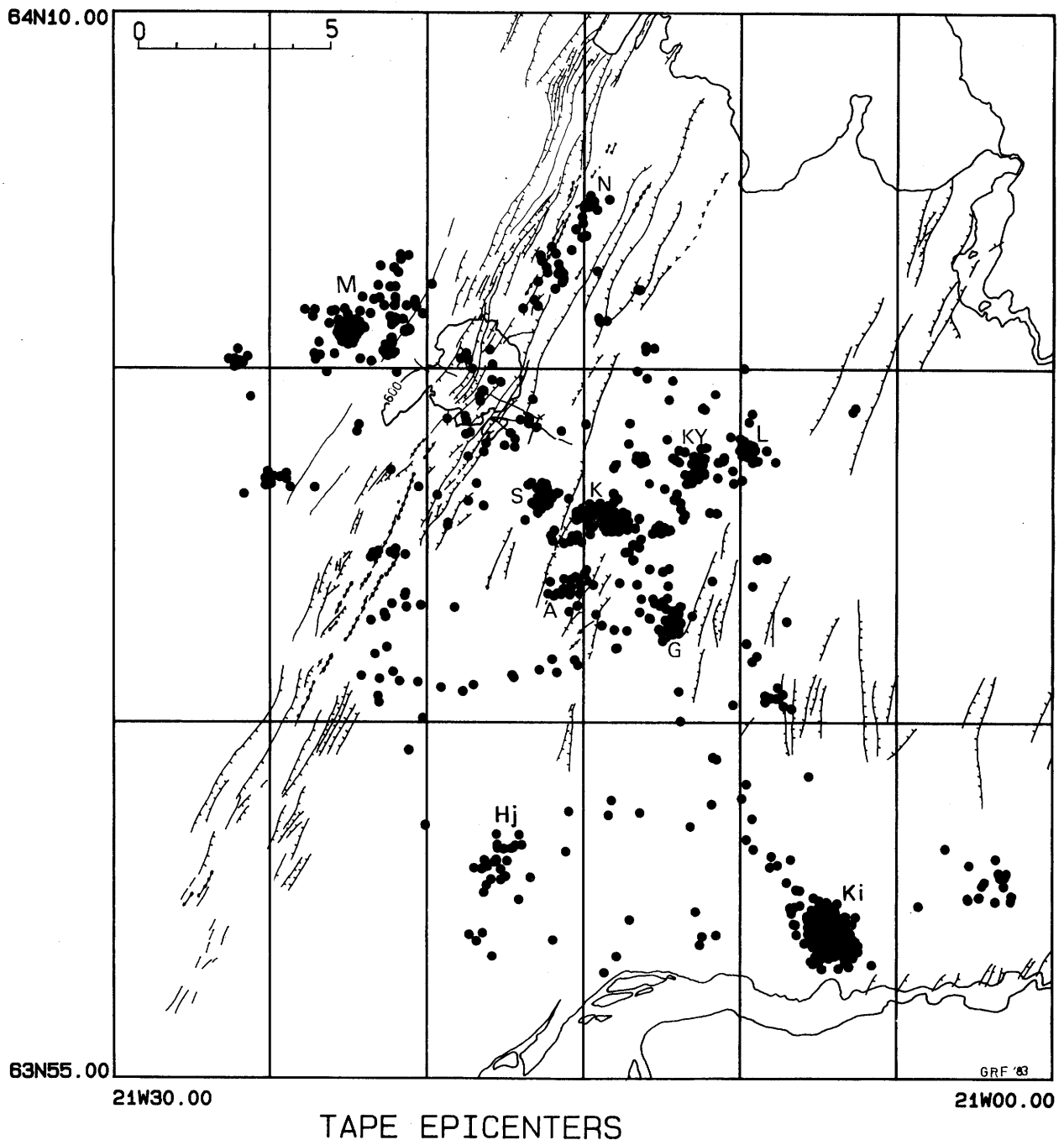
Fig. 2.2 Tape data epicentres. Subclusters discussed in the text are labelled.
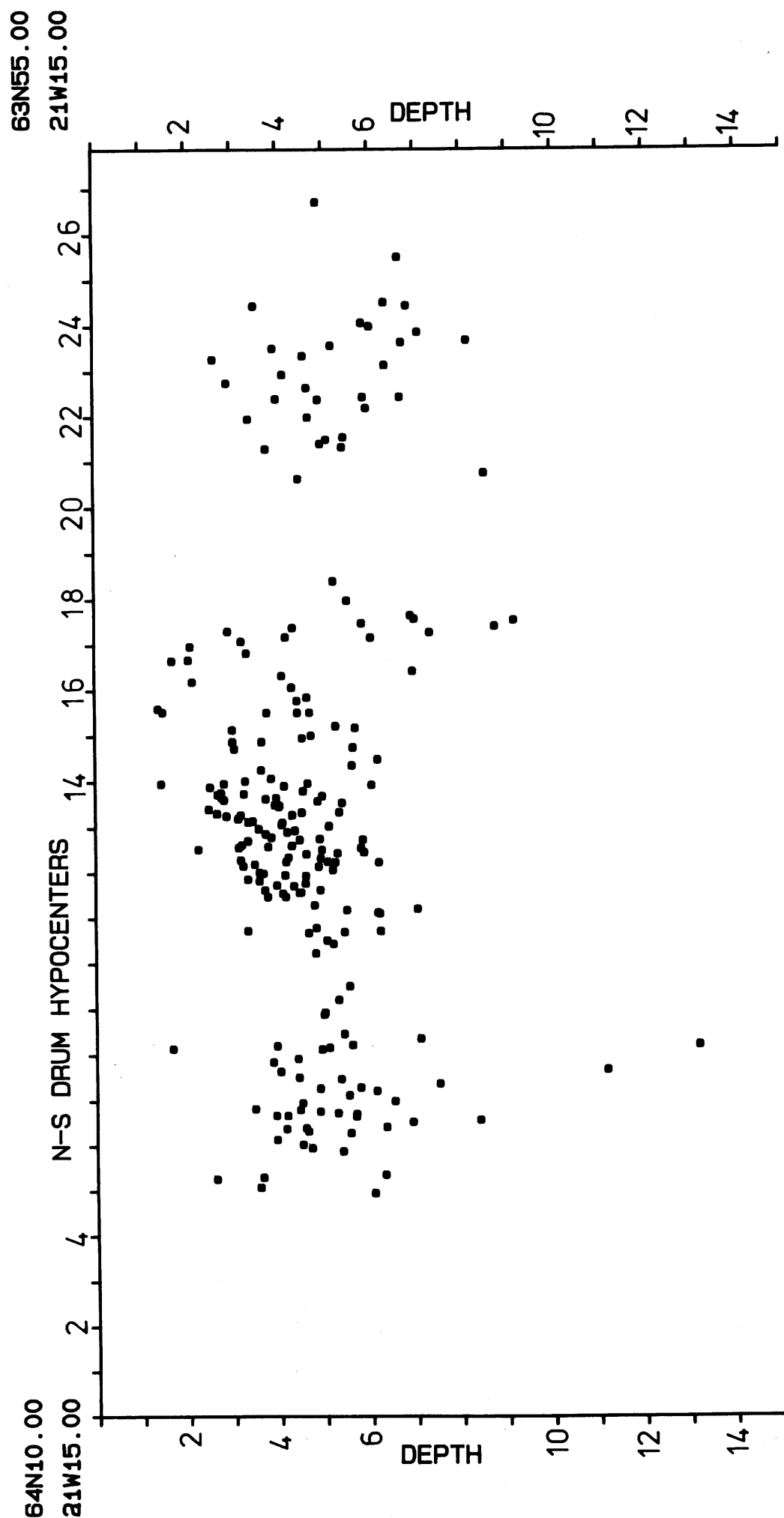
Fig. 2.3 NS cross section of drum data hypocentres.
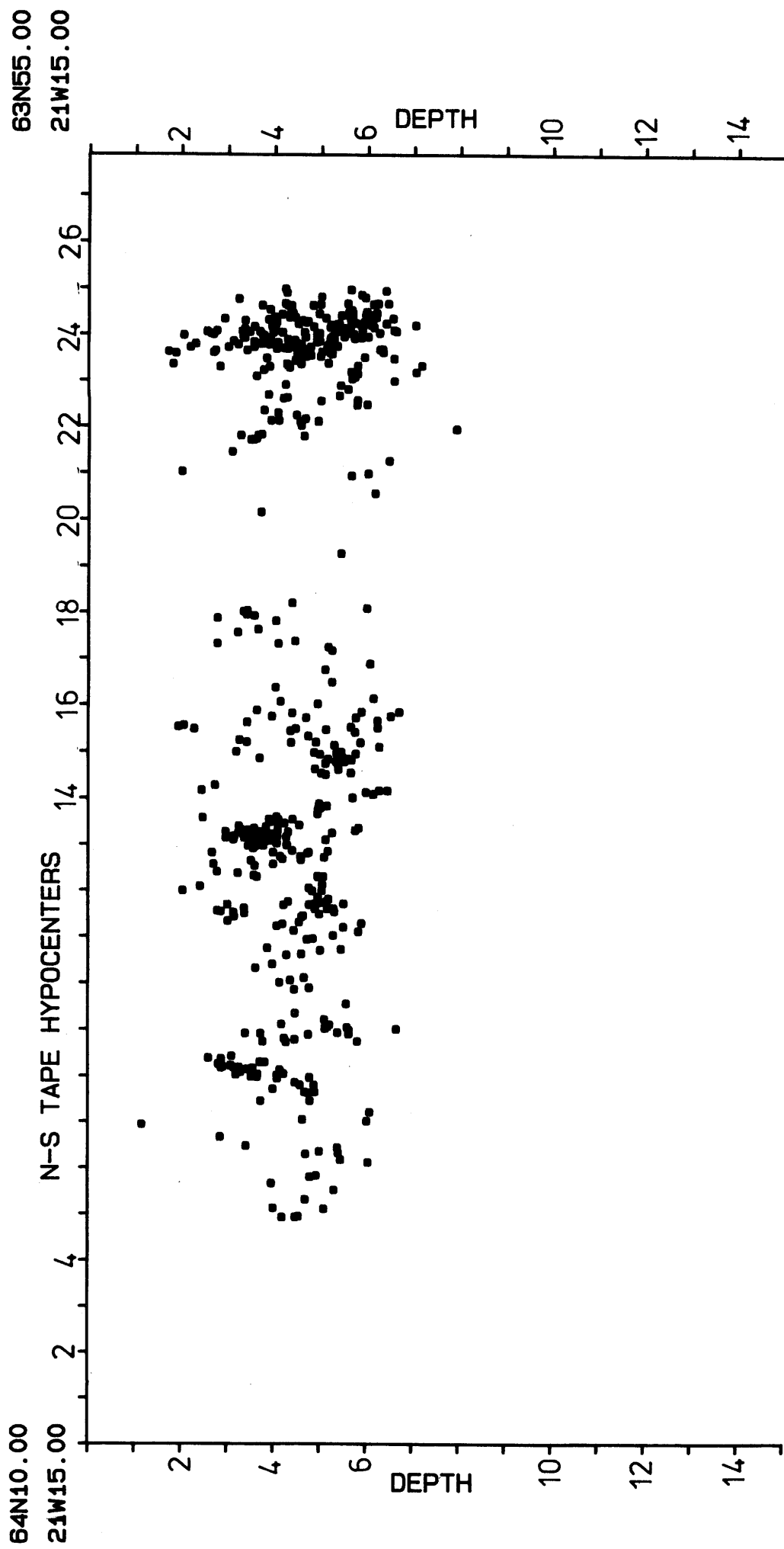
Fig. 2.4   NS cross section of tape data hypocentres.
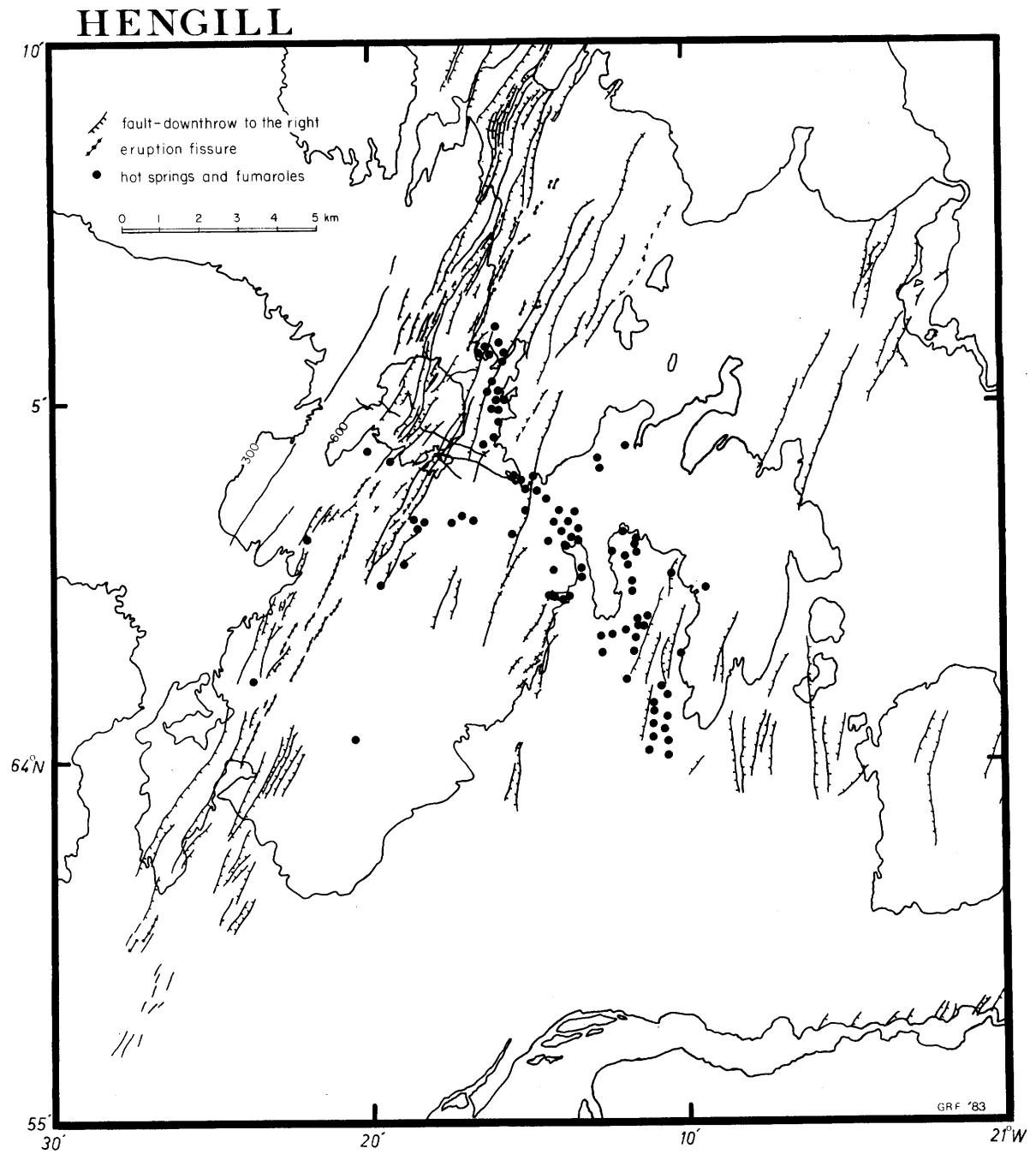
HENGILL

Fig. 2.5   Hot springs and fumaroles within the Hengill area.

large portion of the area of the cluster (Fig. 2.5). The activity does not extend as far south as Hveragerði.

Examination of the drum data epicentral distribution (Fig. 2.1) shows that activity in this area exhibits two trends:

1. NW striking trend.
2. NE striking trend. These trends intersect at an angle of about 90°. As is seen with other features, this tendency becomes clearer if the most accurately located events are selected. (Fig. 2.6).

In the tape data set (Fig. 2.2) the central cluster appears to divide up into about 6 subclusters, some of which were formed by single swarms, and others by continuous low level activity:

Single swarms	Continuous Activity
Svínahlíð (S)	Grensdalur (G)
Ástaðafjall (A)	Kyllisfell (KY)
Laxádalur head (L)	Klambragil (K)

The Klambragil cluster is by far the largest and 90 events were located within it. No sequences occurred during the recording period; activity stayed at a consistent level. The drum data epicentral map also shows some tendency for activity to be locally higher in this vicinity (Fig. 2.1).

In the following discussion, cross sections are as illustrated in Fig. 2.8.

Figs. 2.9 and 2.10 are cross sections colinear with the NW striking trend observed in the epicentral distribution presented in Figs. 2.1 and 2.6. These cross sections illustrate the progressive shallowing of the minimum hypocentral depth as one passes SE from Hengill to Reykjafell, and also the increase in activity. A shallowing of the maximum depth of activity is also apparent in the drum data of Fig. 2.9. On the tape section of Fig. 2.10 the dominant Klambragil cluster, about 10 km along the section, is very obvious, and enhanced activity is also visible in this region on the drum data cross section. The hypocentres shallow to a minimum at a distance of approximatly 13 km along the sections in both data sets, i.e. in the region of the Grensdalur (G) cluster. These cross sections hence display some doming of the seismically active zone in the central cluster.
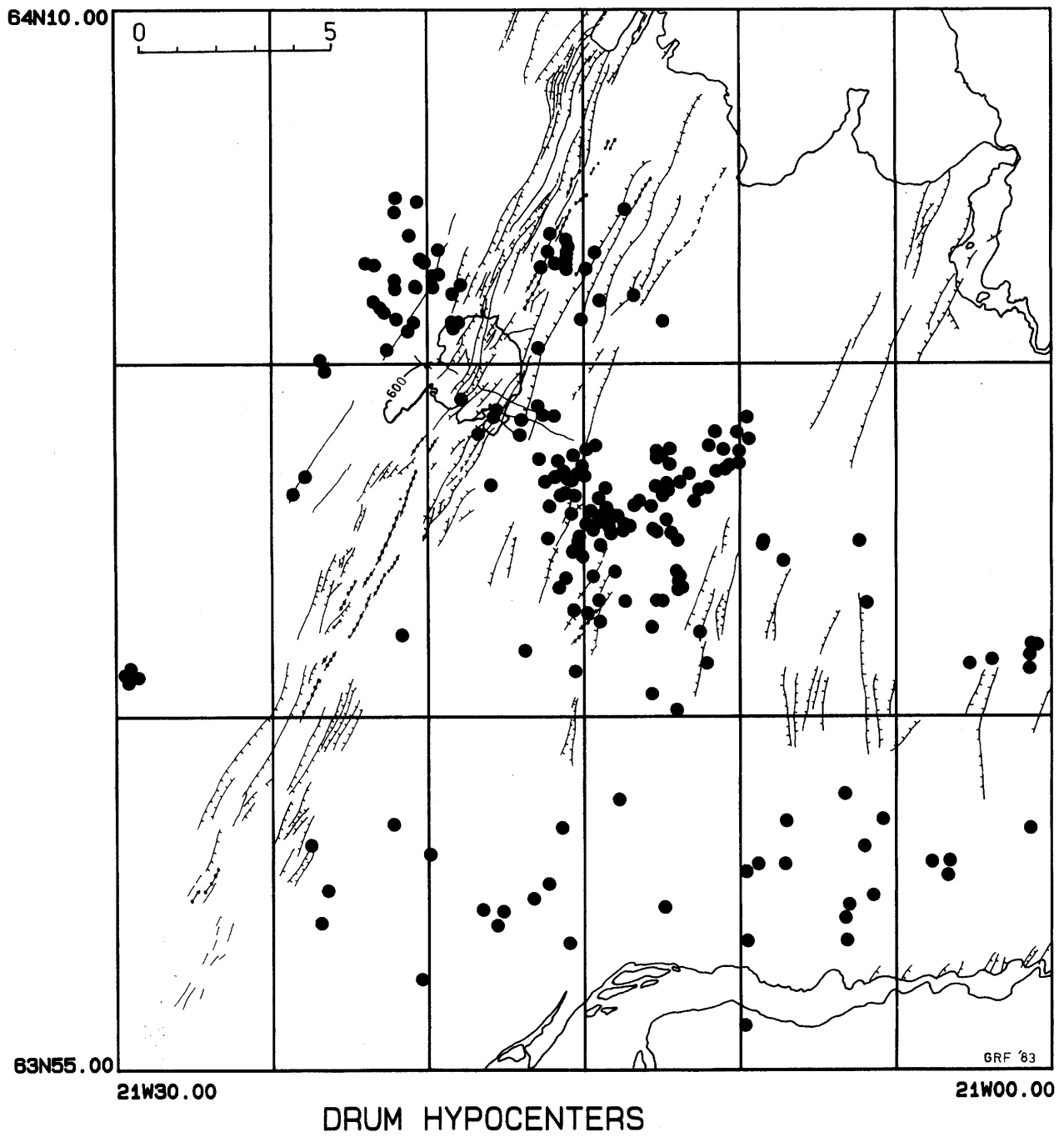
Fig. 2.6   Drum data hypocentres.
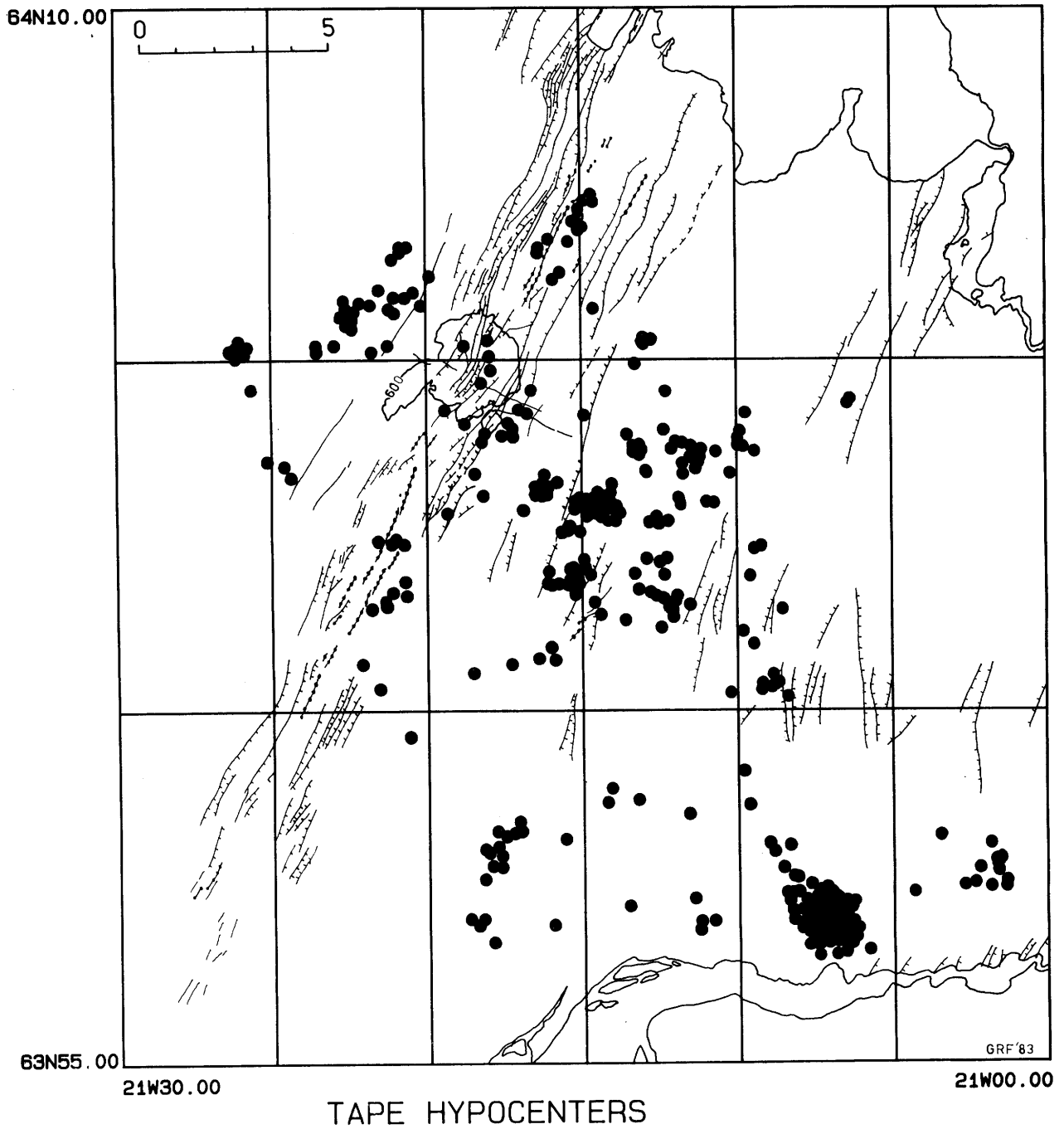
Fig. 2.7   Tape data hypocentres.
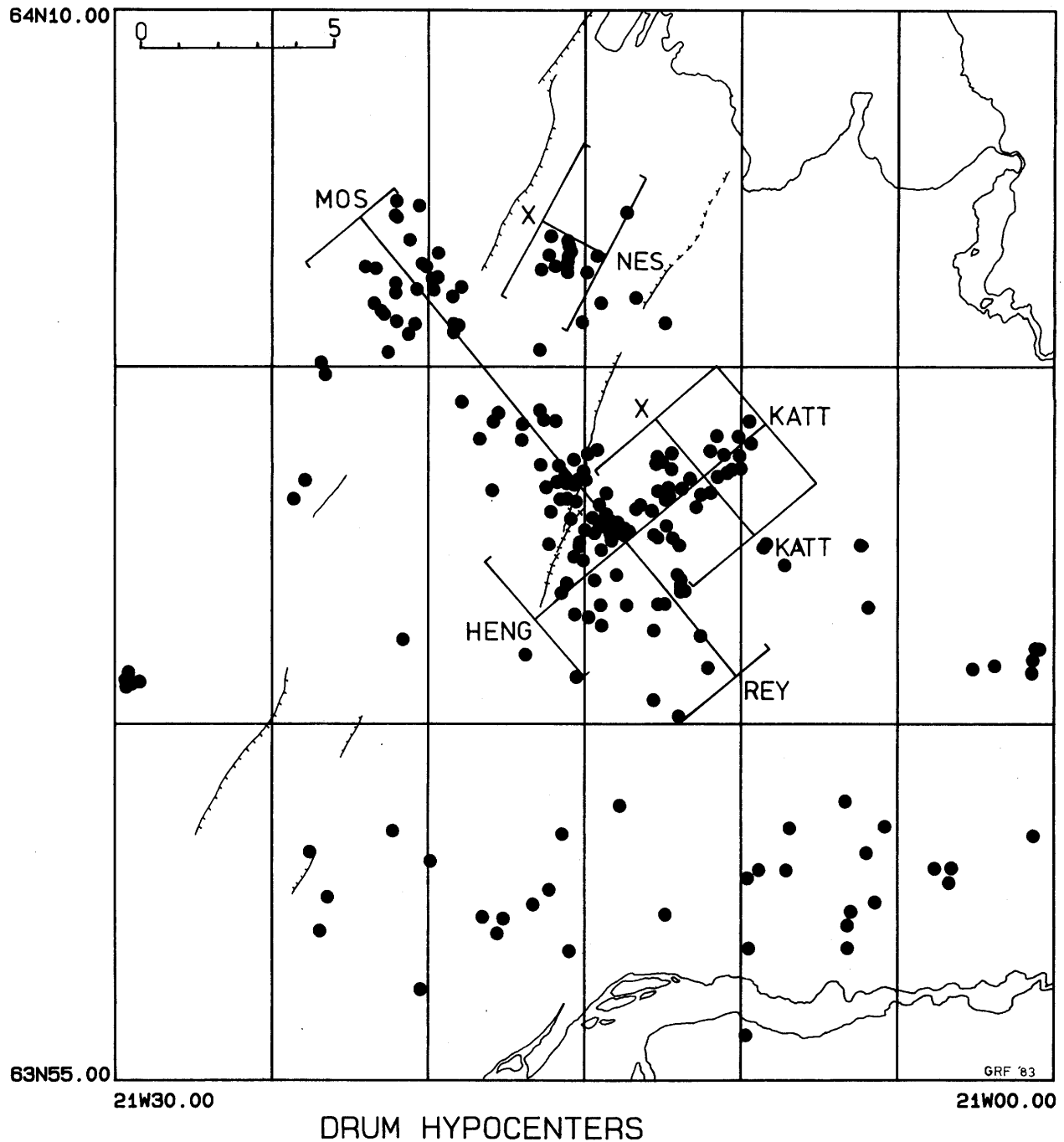
Fig. 2.8   Drum data hypocentral map showing the locations of cross sections presented in Figs. 2.9 - 2.14 and 2.16.

MOS   REY
64N07.02   64N00.58
21W22.57   1   2   3   DRUM HYP MOSFELSH.- REYKJAFELL   10 11 12 13 14 15   21W10.46
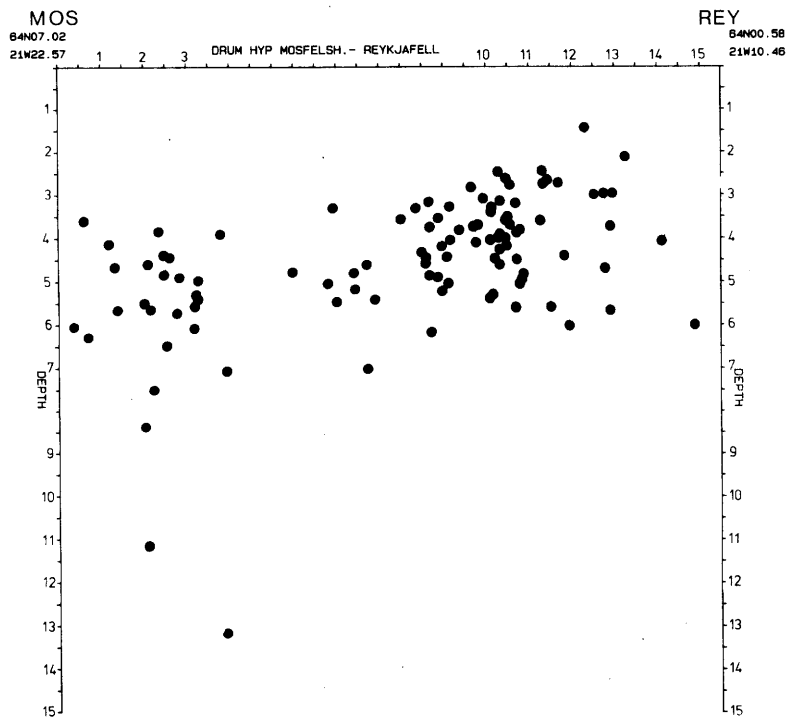
Fig. 2.9   NW-SE cross section Mosfellsheiði - Reykjafell. Drum data.

MOS   REY
64N07.02   64N00.58
21W22.57   2   4   6   8   10   12   14   21W10.46
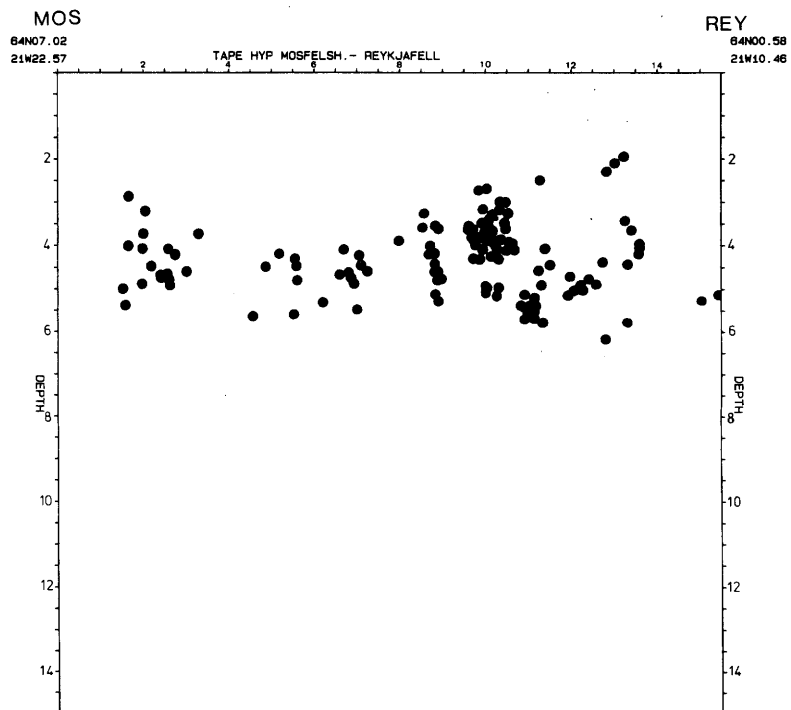
Fig. 2.10   NW-SE cross section Mosfellsheiði - Reykjafell. Tape data.

Figs. 2.11 and 2.12 are corresponding SW-NE cross sections across the central cluster. It may be noted that the left hand parts of these cross sections are transverse sections of the NW- SE trend, and the right hand parts are longitudinal sections of the SW-NE trend. Both sections show a higher level of activity in the region of the NW-SE trend than in the SW-NE trend. There is also some slight suggestion in the data that the NW-SE trend of hypocentres displays a zone with a SE dip. The doming of the seismic zone noted in Figs. 2.9 and 2.10 is also apparent in Figs. 2.11 and 2.12.

Figs. 2.13 and 2.14 are NW-SE cross sections across the SW- NE trend. These sections indicate that the events occupy the depth range 2 - 6 km and that the dip of the active zone is less than 10°.

2.3.2.3 Nesjavellir

The tape epicentral distribution clearly displays a linear array of events occupying Nesjavellir (Fig. 2.2). The fault dissected hills to the E and W were not active in the recording period. This linear feature is enhanced if the drum data and the tape data are presented together (Fig. 2.15). The lineation strikes at N 25° E, is parallel to the fissure swarm, and marks the continuation of a row of hot springs and a 2 km long fissure extending up onto Nesjaskyggnir.

A depth section of these events (Fig. 2.16) shows that they occupy the depth range 3.5 - 7 km depth, and that the feature is close to vertical.

The data set contains 31 events.

It should be pointed out that this feature came to light through the operation of the radio telemetered network, since prior to this, accurate locations were only available for events south of the drum seismograph on Nesjavellir which is situated approximately at the midpoint of the feature (Fig. 2.15).

2.3.2.4 Mosfellsheiði

These events form a diffuse cluster due W of Hengill (Figs. 2.1 and 2.2). The temporal distribution of these events shows that this area was continually active throughout the recording period July - Sept. 1981. Towards the end of the recording period a swarm occurred, and these events clustered between 2 and 4 km depth. The
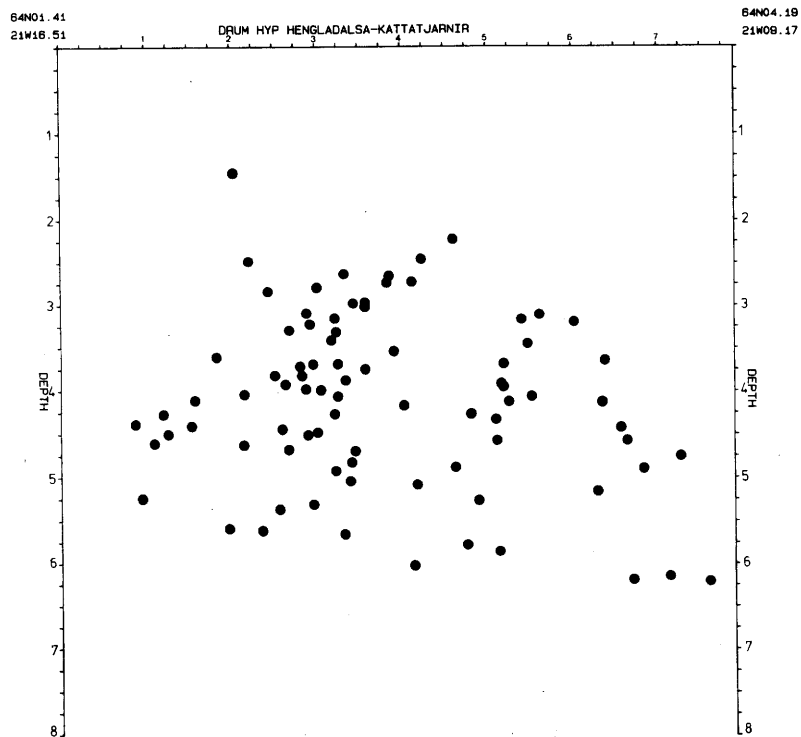
Fig. 2.11 SW-NE cross section Hengladalsá - Kattatjarnir. Drum data.
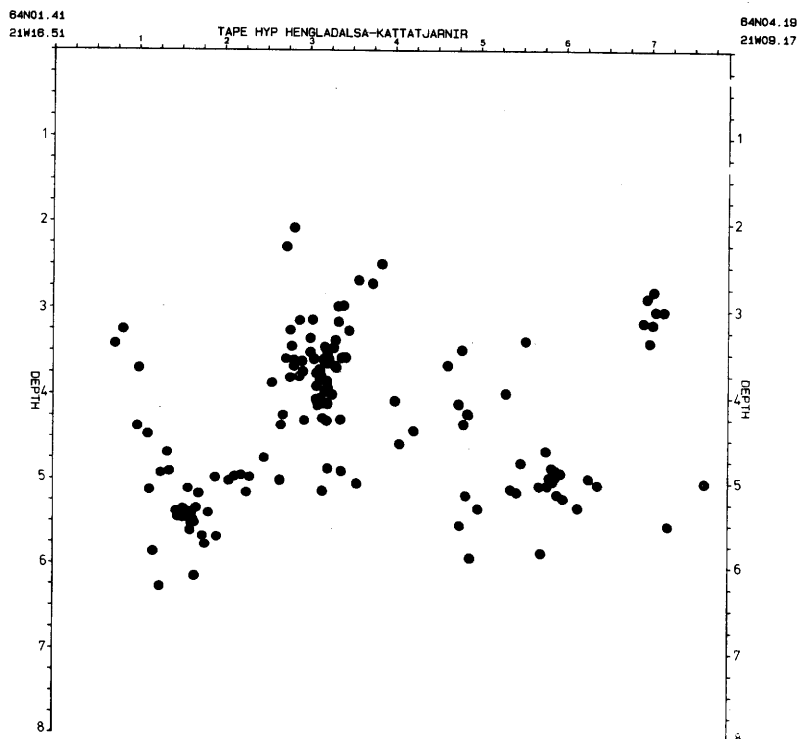
Fig. 2.12 SW-NE cross section Hengladalsá - Kattatjarnir. Tape data.

Fig. 2.14 NW-SE cross section across Kattatjarnir. Tape data.
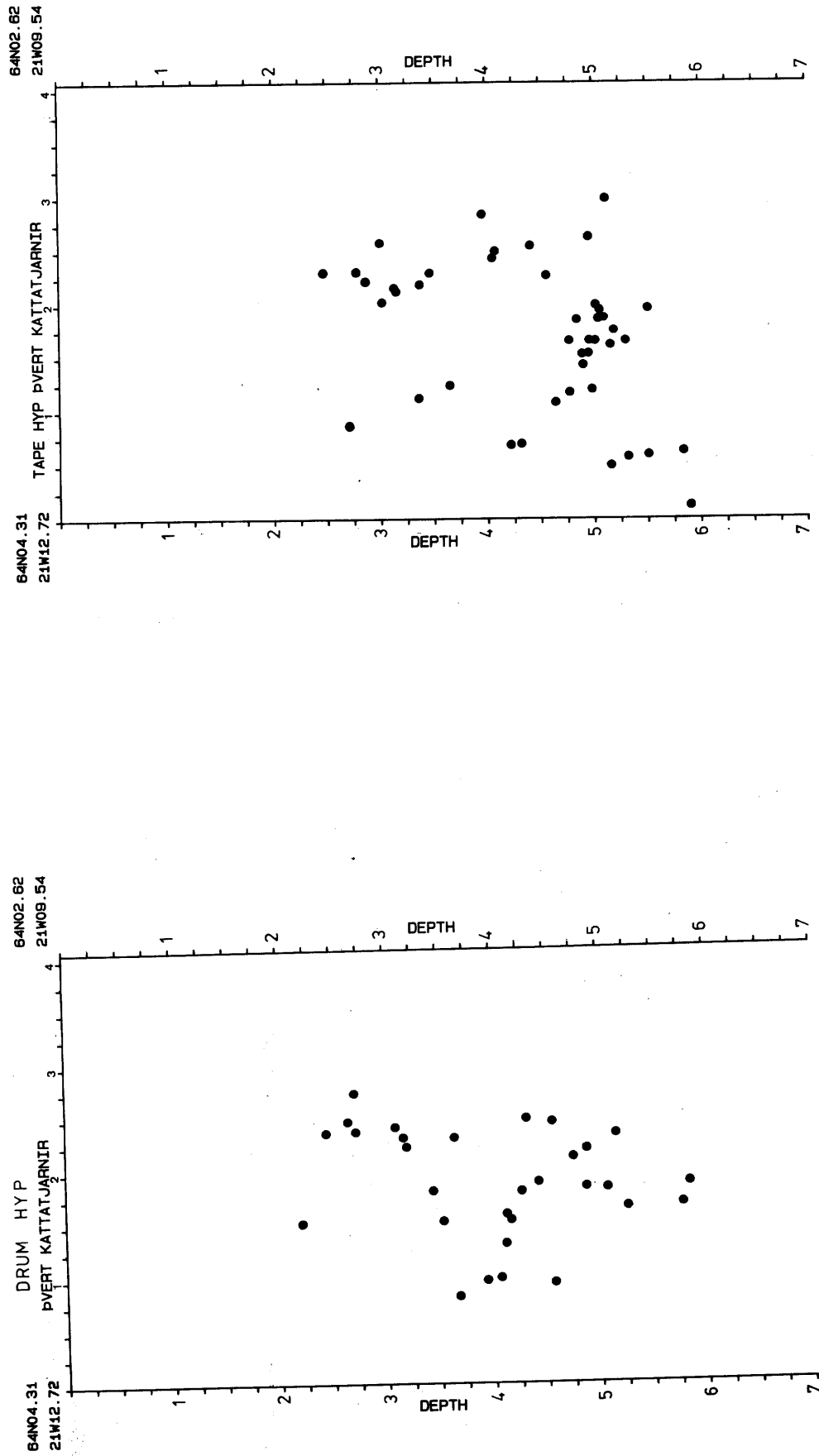
Fig. 2.13 NW-SE cross section across Kattatjarnir. Drum data.
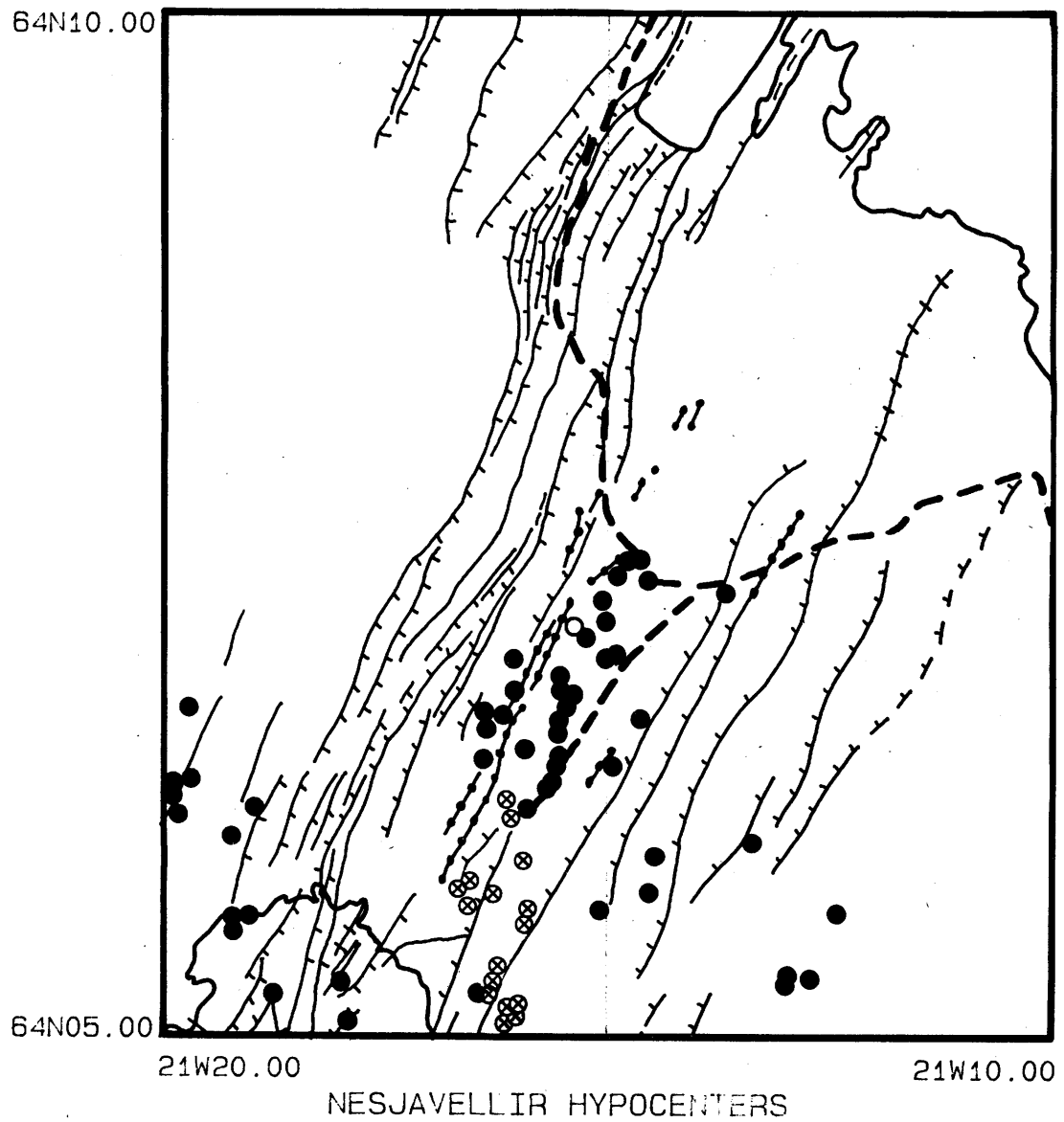
Fig. 2.15 Hypocentres located in the Nesjavellir area. Drum data and tape data. ● earthquake epicentres, ⊗ hot springs and fumaroles, O Nesjavellir drum seismograph.

X   NES

64N07.07   64N06.55

21W16.42   1   21W14.31
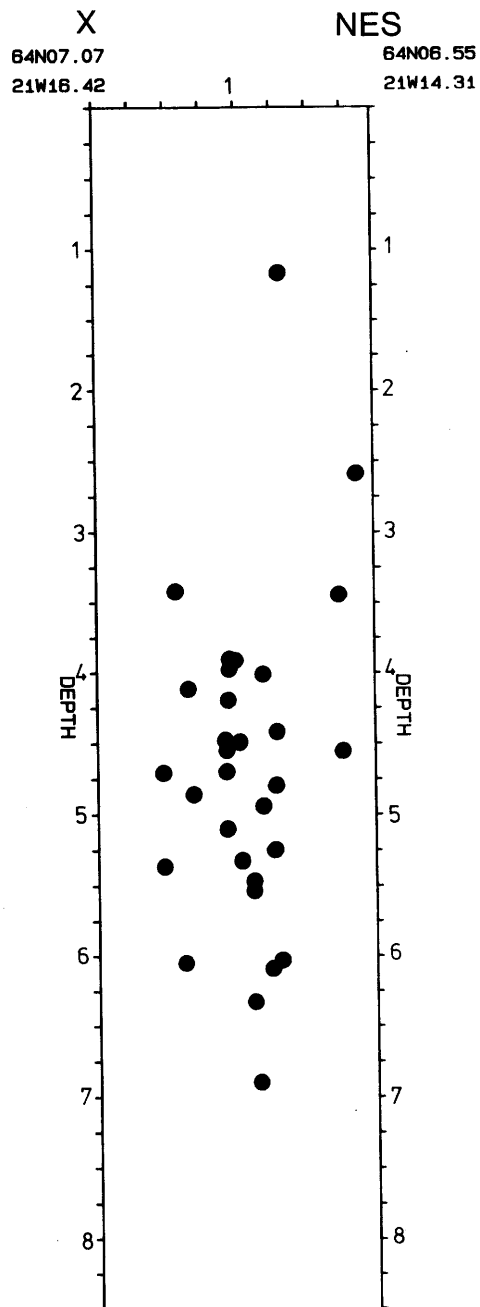
Fig. 2.16   NW-SE cross section across Nesjavellir. Drum and tape data.

easternmost boundary of the whole group of events is the westernmost fissure of the fissure swarm, i.e. as is typical in this area, the activity seems confined to areas where there is no surface faulting. Some events were located as far south as Húsmúli, but no activity appears to be associated with Kolviðarhóll, either in the tape or the drum data set.

Examination of Figs. 2.9 and 2.10 shows that hypocentral depths lie mostly in the range 3 - 6 km. The ocurrence of deep events is indicated in the drum data set (Fig. 2.9) but this is unsubstantiated by the tape data set (Fig. 2.10).

2.3.2.5 The Ölfus lowlands

S of 64° N a fairly continuous belt of diffuse activity stretches from Eldborgahraun in the W to the SW corner of Ingolfsfjall in the E at about 63°N 57`. The belt is diffuse, and does not coincide with any visible surface lineament. Concentrations of activity occur in the regions of Hjalli (Hj) and Kirkjuferjuhjáleiga (Ki). In the period September 19th-22nd 1981, whilst the radio telemetered network was in operation, a swarm occurred in the Kirkjuferjuhjáleiga area. 700 events were located in the depth range 1-8 km. This swarm was on the outer edge of the network, so accurate locations were not possible. The largest event (M_L = 2.2) in the tape data set occurred as part of this swarm.

Hypocentral depths mostly occur in the range 2 - 7 km (Figs. 2.3 and 2.4) and seismicity thus appears to extend to greater depths than events N of 64°N.

2.3.2.6 64°N

Separating the two areas discussed above is an EW trending belt of low seismicity, straddling the 64° line of latitude. It is best illustrated by the NS hypocentral cross sections of Figs. 2.3 and 2.4. Very few hypocentres are located in this zone, and earthquake sequences are confined either to the N of 64°N, or to the S - epicentral zones do not cross this "barrier".

2.3.2.7 The fissure swarm

Very few events were located within the most intensely faulted part of the area, the fissure swarm, during the period 1974-1981. It may hence be stated that for this period the fissure swarm was almost seismically quiescent down to microearthquake levels.

2.3.2.8 The hypocentral distribution

Figs. 2.3 and 2.4 are NS cross sections of the Hengill area. In the case of the tape data (Fig. 2.4) all the hypocentres lie in the range 1-8 km. In the case of the drum data the maximum hypocentral depth is 13 km. However, since only 7 events are located deeper than 8 km, this may be the result of poor locations in the drum data set. Most of the events of both data sets lie in the range 2-6 km. There is a tendency visible in both data sets for a shallowing of the average hypocentral depth in the central cluster (12-17 km along the profiles) relative to more northerly and southerly events (i.e. a doming of the seismic zone beneath the geothermal field), but this also may be a creation of the locator proceedure. Variations detected in the velocity structure within the Hengill area are precisely such as would produce this effect (see Appendix 1). Such distortion is estimated to be up to 5% of the hypocentral depth (see Section 5.2), and so may account for only part of the observed variation. However in the absence of a quantitative examination the variations in depth to the seismic zone described above remain unsubstantiated.

2.4 Summary

Examination of historic macroseismic data indicates that large magnitude earthquake activity is restricted to the area at or S of 64° N. The fissure swarm may periodically be activated by intense tectonic movements that cause seismicity and fault movements over tens of kilometers, e.g. the 1789 episode.

The monitoring of small magnitude earthquakes over an 8 year period yields a contrasting picture of spatial distribution. Most events cluster in a small area of approximately 20 km^2 NW of Hveragerði within which small subclusters of activity may be distinguished, and trends striking both NW-SE and SW-NE. Other localised areas of activity occur in Nesjavellir and on Mosfellsheiði. A low background of activity is observed in the fissure swarm and Ölfus. A belt of low activity occurs about 64^oN. In general the seismicity correlates negatively with those areas where surface faulting is observed.

Hypocentral depths mostly occur in the range 2 - 6 km and there is little evidence that seismicity extends to depths greater than 8 km.

3. LOCAL EARTHQUAKES: TEMPORAL DISTRIBUTION, FREQUENCY-MAGNITUDE RELATIONSHIPS AND B-VALUES

3.1 Temporal distribution

The temporal distribution of the seismicity of the Hengill area is characterised by its continuous nature and is dominated by the persistent, 20 km^2 cluster to the NW of Hveragerði, that comes to the forefront in every data set and time window.

A whole spectrum of sequence types is observed superimposed on a continuous background of single shocks. In addition a few small areas are characterised by continuous low level activity. These features are illustrated in Figs. 3.1 and 3.2 which show the temporal distribution of the drum and tape data sets respectively. In Fig. 3.1 the large increase in the rate of event location as a result of the setting up of additional stations in 1979 can be seen clearly. Both figures demonstrate continuous activity throughout the time period at all latitudes. Particularly prominent in Fig. 3.2 is the consistent belt of activity corresponding to the 15 km point on the horizontal axis. Comparison of Figs. 3.2 and 2.2. indicate that this activity corresponds to the Klambragil (K) subcluster. In addition, clusters of events may also be seen where many events occurred within a short space of time, and in a small area, e.g. the swarm that occurred in the Kirkjuferjuhjáleiga, Ölfus area in Sept. 1981 (about 3 km along the profile of Fig. 3.2). This sequence is discussed in more detail in Section 3.2.4.2.

Seismic sequences are roughly divided into three groups:

1. Mainshock - aftershock sequences
2. Foreshock - mainshock - aftershock sequences
3. Swarm sequences

A sequence is classed as a mainshock sequence if the magnitude of the largest event exceeds that of the second largest by at least 1 magnitude unit.

The Hengill area displays great variation in sequence type. All three types of sequence have been observed in the area in close proximity (Fig. 3.3). Sequences over a wide range of magnitudes are also recorded. No spatial pattern in the occurrence of different types of sequence has been observed.

DRUM DATA

	PERIOD		
FROM	1	1	74
TO	10	7	81
NO OF EARTHQUAKES			515

MAX GAP	180°
MAX RMS	0.15 SEC
MAX ERH	2.5 KM
MAX ERZ	99.0 KM

DEPTH (KM)
0.00 - 20.00
MAGNITUDE
-5.00 - 5.00
-5.00-5.00
5.00-5.00
5.00-5.00

WIDTH OF SECTION
24.50 (KM)

63 55.00
21 15.00

64 10.00
21 15.00
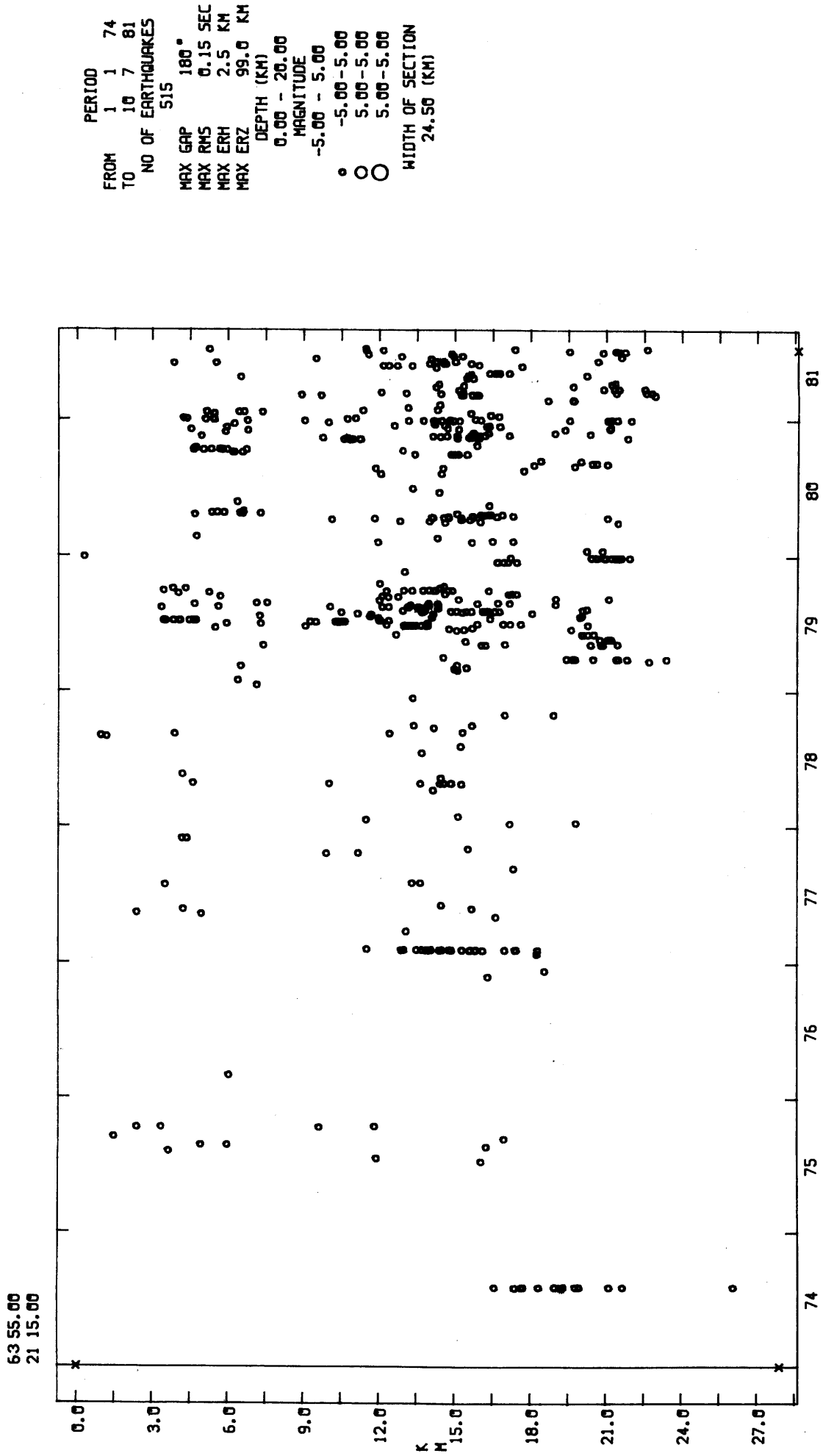
Fig. 3.1 Temporal distribution, drum data, in NS cross section. Horizontal scale in years.

TAPE DATA

PERIOD
FROM 1 7 81
TO   1 11 81
NO OF EARTHQUAKES
          858

MAX GAP   180°
MAX RMS   0.10 SEC
MAX ERH   1.0 KM
MAX ERZ   99.0 KM
  DEPTH (KM)
  0.00 - 20.00
   MAGNITUDE
 -5.00 - 5.00

 o -5.00-5.00
 O   5.00-5.00
OO   5.00-5.00

WIDTH OF SECTION
     24.50 (KM)

63 55.00
21 15.00

64 10.00
21 15.00

Fig. 3.2   Temporal disribution, tape data, in NS cross section. Horizontal scale in months.
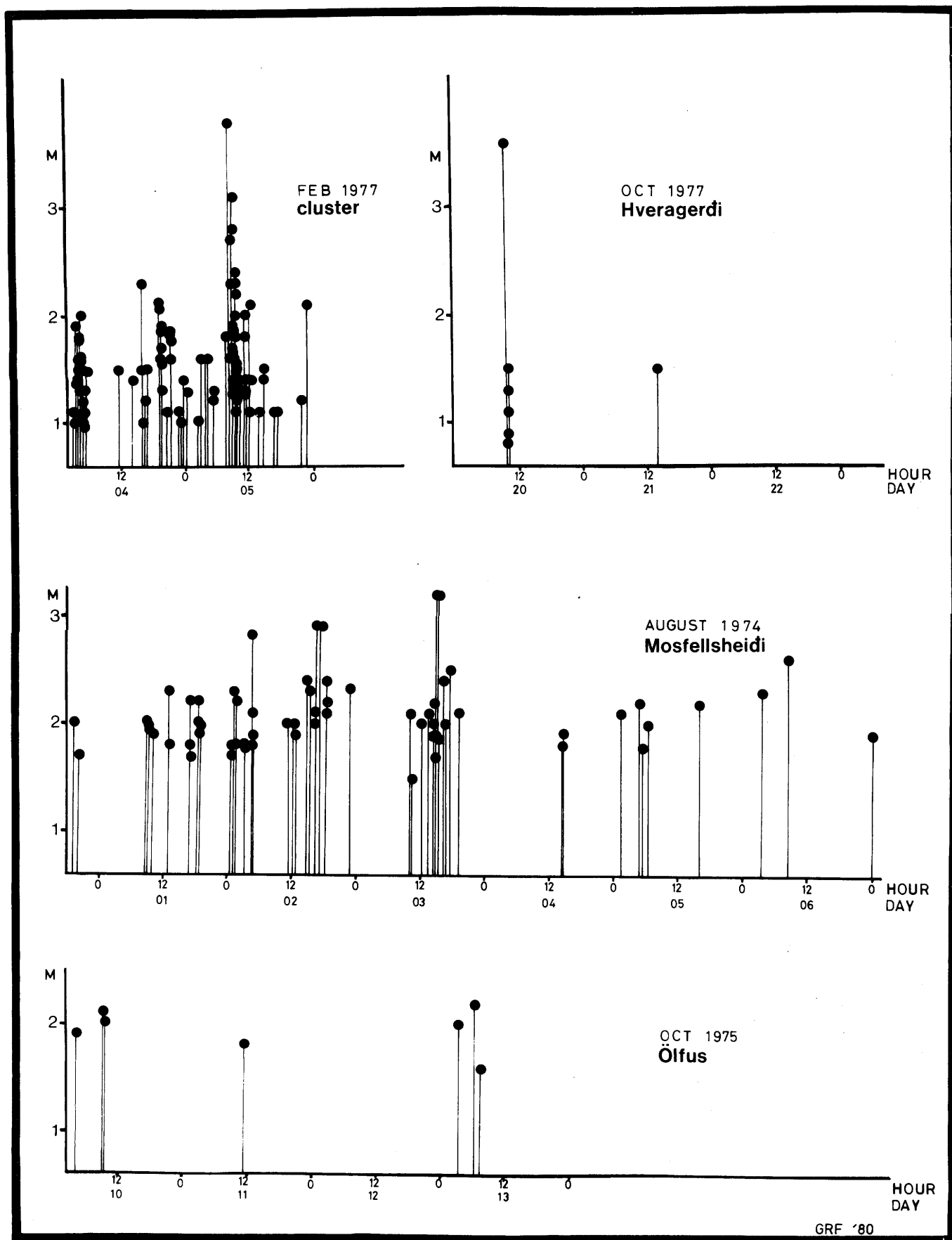
Fig. 3.3   Examples of sequences of various types that have occurred in the
           Hengill area.

3.2 Frequency magnitude relationships and b-values

3.2.1 Introduction

Richter (1958) found that a plot of $\log_{10}$ (cumulative number of earthquakes) against magnitude was roughly linear for the world at large and most of the limited areas studied. He expressed this in the equation

$$\log_{10} N = A-bM$$

where
N = number of shocks of magnitude M or greater per unit time
A,b = constants.

The A value is an indication of the seismic rate of the area and time period under investigation. The b-value is an indication of the rate of decrease in frequency with increase in magnitude. A b-value of about 1 is typical for most seismic zones.

Variations in the value of b between different areas, and with time have been investigated and the possibility considered that they could be used as a tool for evaluating and detecting variations in properties of the brittle earth's crust, e.g. homogeneity or stress. It is the aim of this section to attempt to clarify the present status of thinking about b-values and the possible causes of variations in them so the results from the Hengill area can be discussed in context. The ideas presented here draw on the work of Francis (1968 a, b), Sykes (1970) and Einarsson (1984).

Fig. 3.4 is an idealised magnitude-frequency plot. Examination of this plot shows that the b-value (negative slope) varies with magnitude. At low magnitudes the slope decreases to zero. This is a general feature of magnitude frequency plots and is caused by incomplete detection of the smallest events over the whole area. The detection threshold is the magnitude at (and above) which detection is complete over the area under investigation.

At high magnitudes the slope increases to infinity as the maximum magnitude supportable by the rock volume under investigation is reached. This progressive increase in slope above a "knee" magnitude is not well supported by observational data, but arguments, discussed below, have been made for its existence.
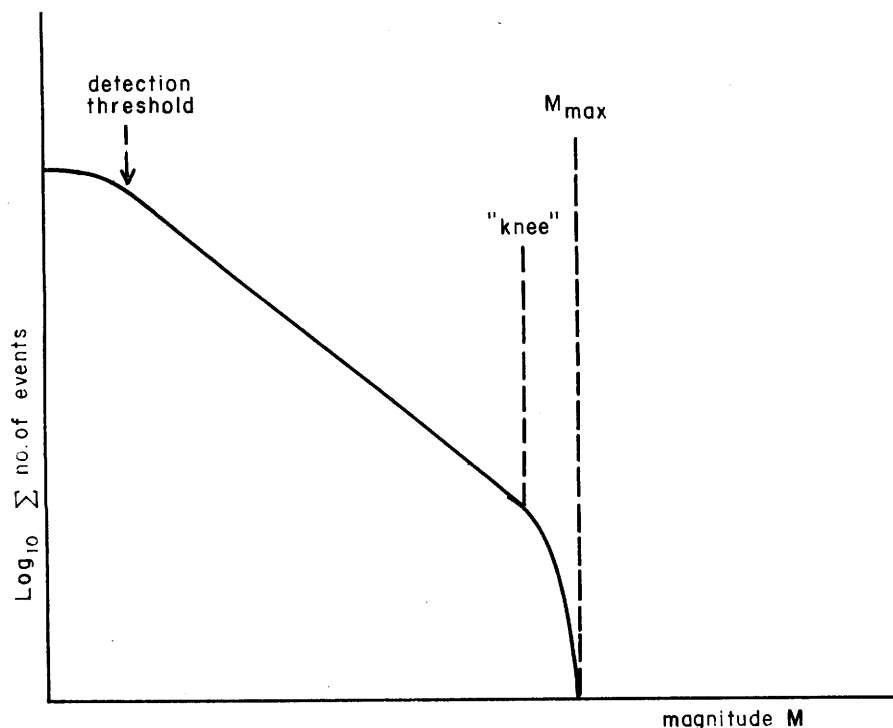
Fig. 3.4 Idealised frequency-magnitude plot.

The magnitude of an earthquake is related, through its seismic moment, to its source dimensions. For a volume of rock to fracture in a single event, it must behave as a single unit. To do this the volume of rock must be homogeneous on the scale of the fracture activated, uniformly stressed and the fracture must be uniform along its length. Hence the maximum magnitude earthquake that can occur in an area is governed by the dimensions of the maximum volume of rock that behaves as a single unit. It follows that the upper limit of earthquake magnitude is governed by the size of first order inhomogeneities in the earth's crust.

The frequencies of small magnitude events relative to each other will not be affected by this upper limit of the homogeneity scale (i.e. the fact that the volume of rock active is of finite size). At larger magnitudes however, it might be expected that this fact would have the effect of decreasing the likelihood of an event occurring. A "tailing off" of the magnitude-frequency plot (i.e. a progressive increase in slope) would then occur in the magnitude range where earthquake source volume is of the same order of magnitude as the volume of rock.

This principle appears to be displayed by laboratory specimens, where high b-values are found to be associated with heterogeneous material,

i.e. in the case of such samples we may be observing above the "knee". For data sets taken for the ridge and fracture zone portions of the mid Atlantic plate boundary, the b-value exhibited by ridge events is found to be much higher than that exhibited by fracture zone events in the range $4.5 \leqslant m_b \leqslant 6.0$. Here again, we may be observing above the "knee" for ridge seismicity. This would imply inhomogeneities of the order of 1-10 km in extent for the ridges, but much larger for the fracture zones, a perfectly plausible circumstance. For the Geysers geothermal field, which has an areal extent of about 40 km , the "knee" is around $M_L = 3.5$.

It might thus be expected that observation in the magnitude range above the "knee" would give an indication of the largest event expected in an area. In most cases, however, including that of the Hengill area, the repeat times of relatively large earthquakes are several decades and an instrumental observation time of centuries would be required.

Some examples of b-value variations with time have been documented. The best known of these are cases where a low b- value has been associated with the foreshocks of a large earthquake, and a higher b-value associated with the aftershocks (e.g. Suyehiro et al., 1964; Bufe, 1970; Wyss and Lee, 1973). The reason why a high b-value is associated with aftershocks may be that the source area was made highly inhomogenous by the main rupture, but this does not explain the anomalously low b- value associated with the foreshocks. It has been hypothesised that b is inversely related to stress in the rock volume (Scholz, 1968; Wyss, 1973). This would explain the observations since stress would be expected to be higher at the beginning of a sequence than later on, after it had been partially released. If this is the case, variations in b from area to area might be exhibited, that would provide a tool for mapping the stress state of the crust.

The possibilities of doing this are somewhat limited, however, because b varies only over a small range, and such variations are usually of the same order of magnitude as the associated uncertainties. The two most serious sources of error are the use of different magnitude scales and small data samples. In order to detect significant variations in b large numbers of earthquakes must be used and their magnitudes determined by a consistent method. This was achieved by Klein et al. (1977) on the Reykjanes Peninsula. They determined b-values of 0.85 ± 0.07, 1.02 ± 0.07 and 0.75 ± 0.11 for 3 portions of their study area. The value 1.02 was shown to be significantly different from the other two. Values comparable to these of 1.09 ± 0.06 and 1.06 ± 0.06 were obtained by Einarsson et. al. (1977) for the Borgafjörður area. These values are broadly comparable to each other

and to the values obtained for the Hengill area, discussed below, since in all cases the magnitudes used were based on those measured at REY.

In conclusion, the following points may be made:

(a) A "typical" value of b is 1.0.
(b) It is argued that b may be influenced by inhomogeneities in the earths crust. In a single area the value of b would increase above a certain "knee" magnitude (whose value is governed by the scale of first order inhomogeneities). Different "knees" may be exhibited by different areas if the scale of first order inhomogeneities varies.
(c) It has been hypothesised that b is inversely related to stress. This may explain variations in b observed e.g. anomalously low b-values associated with foreshocks and variations in b at low magnitudes between different areas, that cannot easily be explained by variations in homogeneity.
(d) Variations in b are difficult to assess since they are commonly small compared with the associated errors. Large uncertainties are especially introduced by the use of different magnitude scales and small data samples.

3.2.2 Composite frequency-magnitude plot

3.2.2.1 The data

In order to investigate this aspect of the seismicity of the Hengill area over as large a magnitude range as possible, 4 data sets are combined in the composite frequency-magnitude plot shown in Fig. 3.5. The b-values were calculated using the method of maximum likelihood (Page, 1968).

1. Historic macroseismic data
Three or four events of magnitude 6-6.5 are known to have occurred in the Hengill area since 1700 (see Section 2.1). The magnitudes of the events were estimated from macroseismic data.

The annual rate of events in the range $M_L \geqslant 6$ is variable according to the time window taken in the period 1700-1983, and uncertainties are introduced by the arbitrary nature of the end points. Fig. 3.6 is a plot of rate of occurrence of $M_L \geqslant 6.0$ events against time. It can be seen that as the data sample becomes progressively larger with time the occurrence rate tends to about 1 event per 100 years, or about 1 event per 75 years if 4 events are counted.
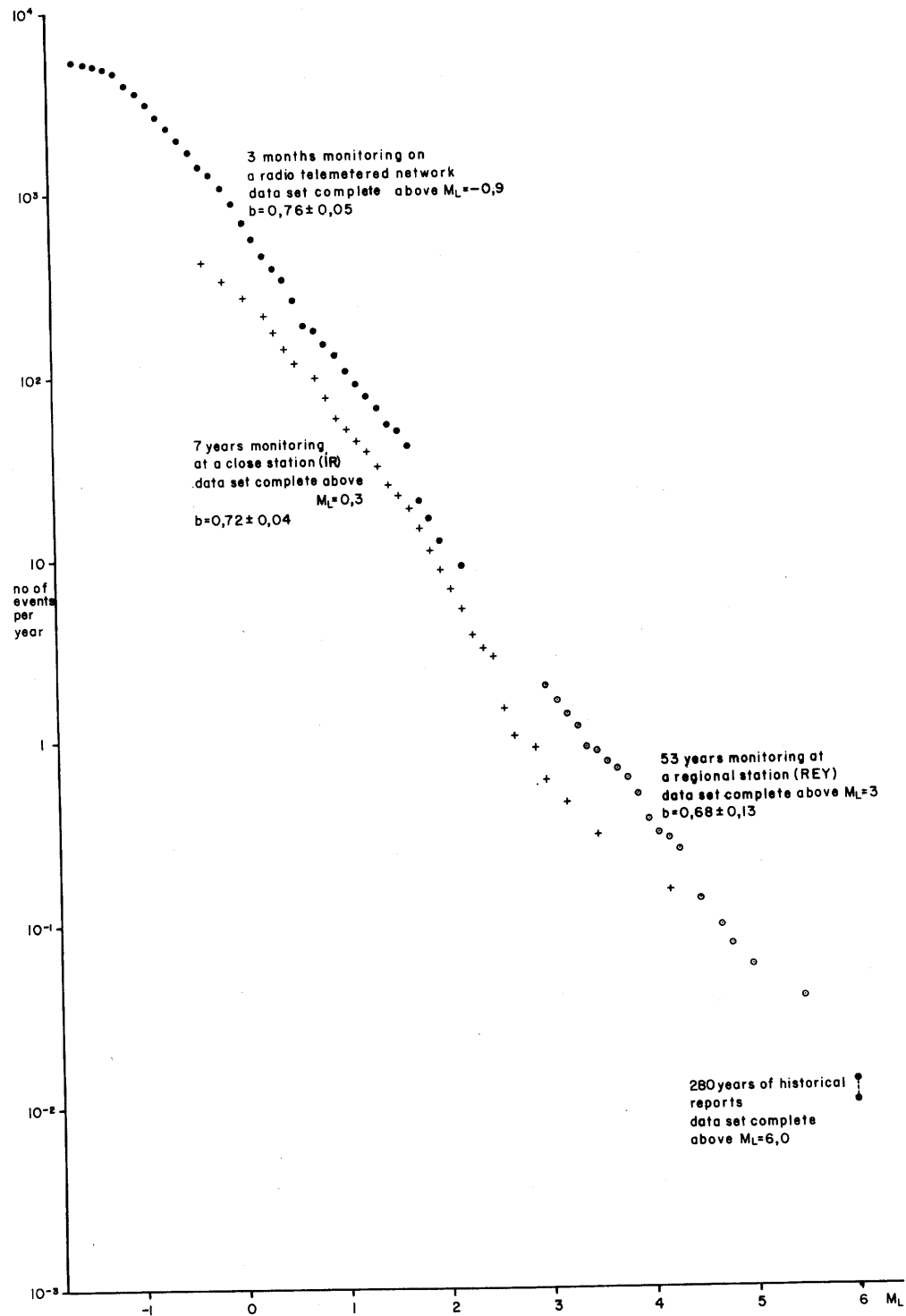
Fig. 3.5   Composite frequency – magnitude plot of events occurring in the
Hengill area.

These data are plotted at $M_L = 6$ in Fig. 3.5.

2. Data recorded at the regional station REY

Data from this station were taken from the published literature (see Section 1.2.3). The magnitudes are instrumentally determined, but macroseismic data were also used in determining the locations. The instruments deployed were replaced by more modern and sensitive equipment several times during the 54 year period studied, but the linearity of the frequency- magnitude plot described below (Section 3.2.1) indicates that the data set is complete for $M_L \geqslant 3$. The data set is 116 events $M_L \geqslant 3$. Plots of seismicity with time for this data set are presented in Figs A3.1-A3.9

For this data set the frequency-magnitude plot is linear and continuous for $3.0 \leqslant M_L \leqslant 4.3$. For $M_L \geqslant 4.3$ the plot becomes discontinuous. The b-value was calculated to be 0.68 ± 0.13 for $M_L \geqslant 3$

3. Data recorded on the local seismograph IR

This station is located within the Hengill area and is part of the regional seismograph network. It has been in operation since March 1977. A coda length magnitude scale was calculated for this station for the Hengill area based on the maximum amplitude scale of the station REY. The relation obtained was:

$$M_L = 2.85 \log_{10} \text{Tsec} - 2.32$$

T sec = time in seconds that the recorded P-P amplitude of the event was greater than 2 mm at 36dB magnification.

For the 7 year period 1977-1983 an average of 1.9 events per day were recorded at IR from the Hengill area. Plots of seismicity with time for this data set are presented in Figs. A3.10-A3.16. The data set is complete above $M_L = 3.0$ and contains 1500 events $M_L \geqslant 0.3$.

The frequency-magnitude plot for IR is linear and continuous for $0.3 \leqslant M_L \leqslant 2.3$. The b-value calculated for $M_L \geqslant 0.3$ is 0.72 ± 0.04.

4. Data recorded on the radio telemetered network

Coda length magnitude scales were calculated for 3 stations in this network (1 station for each tape recorder operated) by comparison with the stations IR and REY. The relationships obtained were:

station   BMO $M_L = 2.51 \log_{10} \text{T mm} - 3.37$
      "   KHA $M_L = 2.26 \log_{10} \text{T mm} - 2.69$
      "   LDJ $M_L = 2.46 \log_{10} \text{T mm} - 3.30$

61
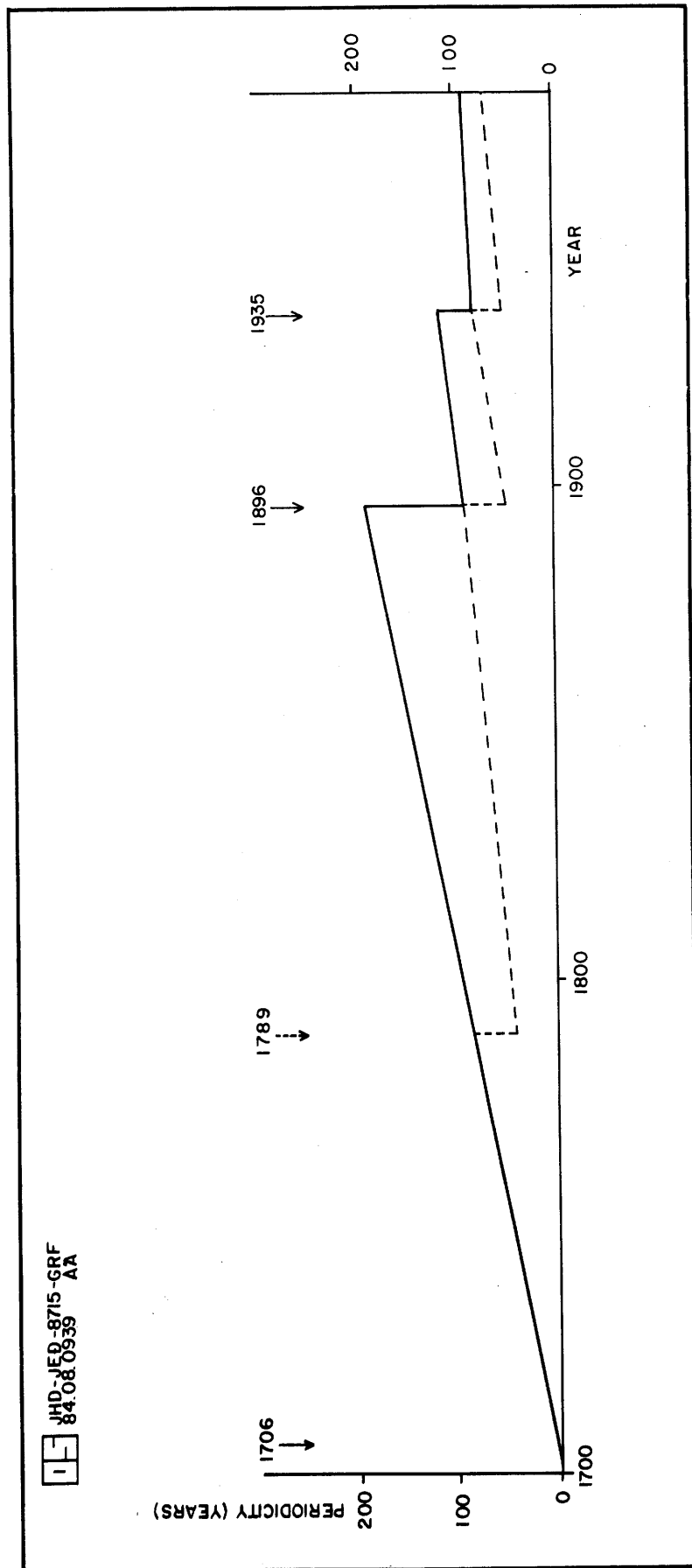
Fig. 3.6   Rate of occurrence of $M_L \geqslant 6.0$ events vs. time.

T mm   = coda length in mm of seismogram for which the P-P amplitude
        was $\geqslant$ 2mm (measured on the 147 mm/minute fast playouts. T mm =
        2.45Tsec)

Magnitudes were calculated by averaging all the magnitudes available
for a given event.

These magnitude scales, and that of IR are illustrated in Fig. 3.7.
It may be seen from this figure that the radio telemetered stations
(natural frequency 1 Hz) were more sensitive at higher magnitudes, at
the gain used, but had similar detection capabilities as the drum
seismograph IR (natural frequency 2-3 Hz) at lower magnitudes.

For the 90 day period July 12th - Oct 9th 1981 an average of 21 events
per day were located on this network. The data set is complete for
$M_L \geqslant$ -0.9, and contains 888 events in this range.

For the data recorded on this network, the frequency-magnitude plot
is linear and continuous for -0.9 $\leqslant M_L \leqslant$ 1.7.   The b-value calculated
for $M_L \geqslant$ -0.9, was 0.76 $\pm$ 0.05.

3.2.2.2   Discussion

b-values of 0.68 $\pm$ 0.13, 0.72 $\pm$ 0.04 and 0.76 $\pm$ 0.05 were obtained for
the 3 instrumental data sets. A value of b around 0.74 for the
Hengill area in the range -0.9 $\leqslant M_L \leqslant$ 5.5 is hence constrained by a
large body of data.

The small (statistically insignificant) variations in these 3 values
may be in part due to the fact that different instruments with
different calibration scales were used for magnitude determination.

The data set from the radio telemetered network is offset from that of
the close station because the seismicity rate during the recording
period in 1981 was about twice the average due to the
Kirkjuferjuhjáleiga, Ölfus swarm of September 19th - 22nd. The IR and
REY data sets are not offset, however, indicating that the seismic
rates for these data sets were similar. In the range M $\geqslant$ 2 the data
points of the IR data set plot below those of the REY data set
indicating that activity in this magnitude range was lower in the
period 1977-1983 than the average over the last 54 years. Examination
of Figs. A3.1 to A3.16, however shows that the occurrence of large
events is very irregular. The longest quiescent period at $M_L \geqslant$ 3.0 to
have occurred since 1930 is the 6   year period 1962-1968. This
quiescent period was terminated by an event of M_L = 4.7.   At the time
of writing no event of $M_L \geqslant$ 3.0 has occurred since 1978, a quiescent
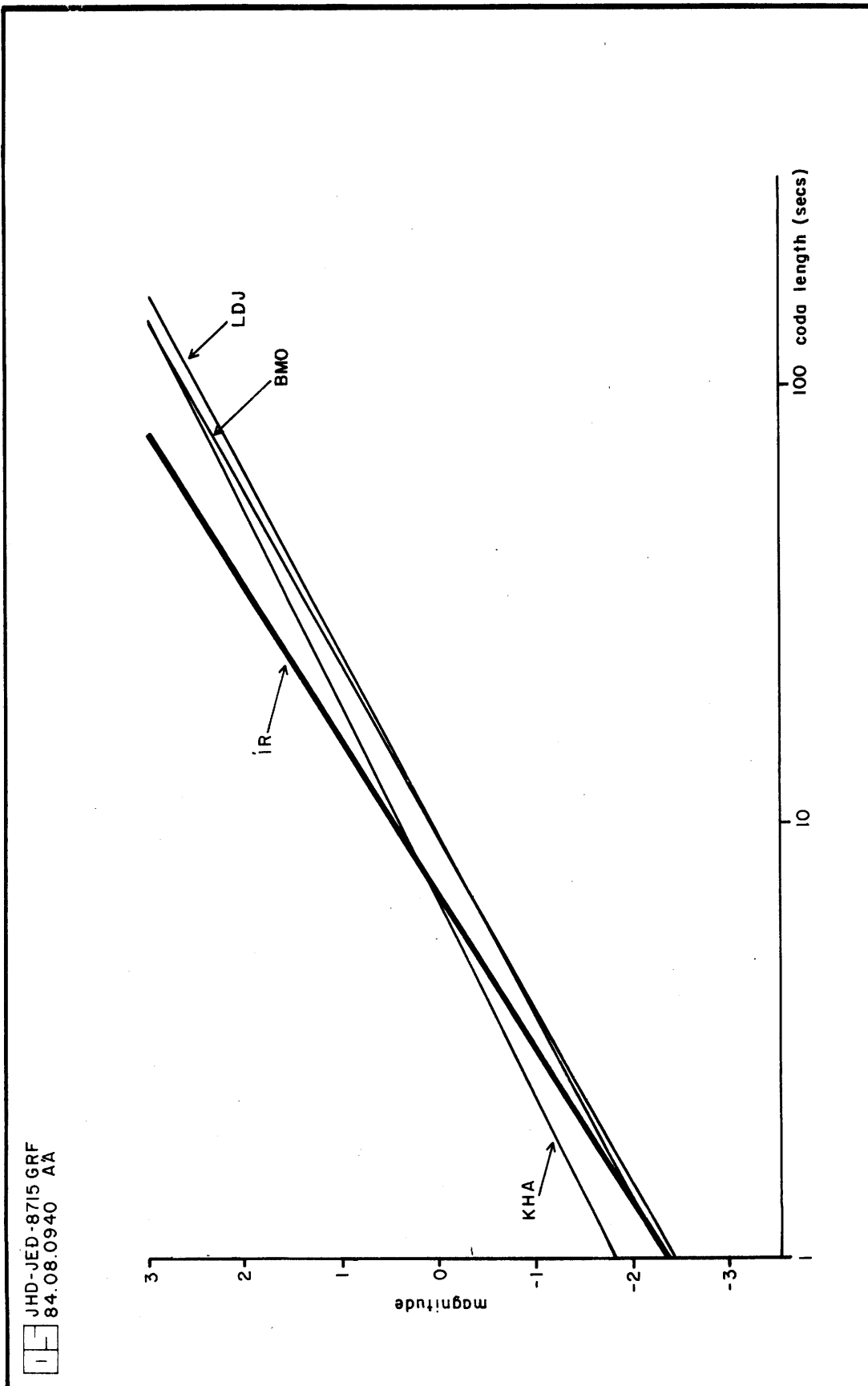
Fig. 3.7   Magnitude scales for stations within the Hengill area.

64

period of 6 years.*

The average seismic rate of the area is one event M_L = 3.5 per year or one event M_L = 0 per day.

The frequency predicted for $M_L \geqslant 6$ earthquakes by extrapolation of data from the regional station, is one event per 60 years. The observed frequency is considerably less than this (probably 1 event per 100 years) and hence the M_L = 6 datum point plots below the continuation of the trend of the other data groups. This is consistent with an increase in b at high magnitude but not statistically significant by itself. It can be seen from the other 3 data sets plotted in Fig. 3.5 that a large scatter is common for data points based on less than 10 events. However, an upper limit of M = 6-6.5 for events in the Hengill area would also be in agreement with historical evidence.

Historical evidence suggests that all these destructive earthquakes are associated with Ölfus and that no such large event has occurred in the high temperature geothermal area. This implies that the Hengill area may be subdivided into two units on the basis of seismicity:

(1) Ölfus, and
(2) the high temperature geothermal area.

For each of the 3 instrumental data sets the b-value plot is linear and the value of b the same within the 95% certainty limits. This indicates that no large difference in b-value exists between Ölfus and the high temperature geothermal area since the combination of two data sets with different b-values would yield a non-linear curve (Appendix 3). Indications are, however, that the maximum size of event sustainable by the Ölfus area is larger than that of the high temperature geothermal area. The two areas are roughly of similar areal extent so this would imply that inhomogeneities occur on a smaller scale in the high temperature geothermal area than in Ölfus (Section 3.2.1). Possible forms of the b-value plots for the two areas are shown in Fig. 3.8.

The two areas exhibit frequency-magnitude plots with similar b-values but with "knees" at different magnitudes. Also shown is the form that would result for a composite plot. Two "knees" would be expected, corresponding to the "knees" of Ölfus (at higher magnitude) and the high temperature geothermal area (at lower magnitude). The lower magnitude "knee" would give an indication of the maximum magnitude event to be expected in the geothermal area.

*Note added in proof: On 840905 0843 an M_L =3.9 event occurred close to Hjalli in the S of the area, thus terminating a quiescent period of 5yrs 10 months.
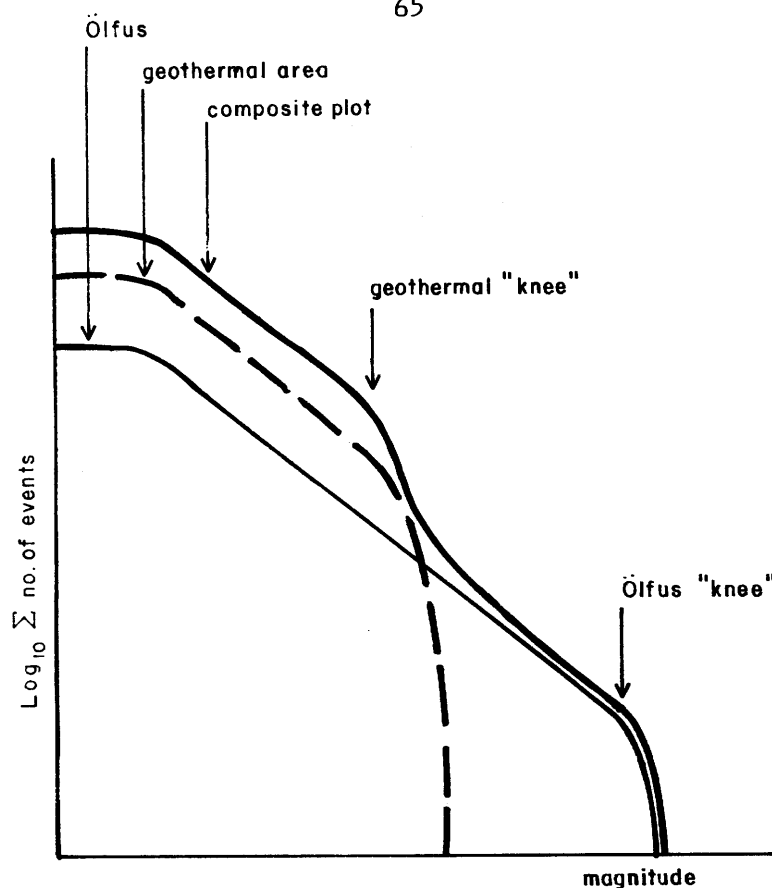
Fig. 3.8 Diagram illustrating the hypothesised forms of the
frequency-magnitude plots for the high temperature geothermal
area and Ölfus and the form of the plot that might be
expected from a combination of the two.

Although there is a slight indication of a high magnitude Ölfus "knee"
in the region of $M_L = 6$, there is almost no evidence of a second
"geothermal knee" at a lower magnitude. If it exists it must occur at
$M_L > 4.2$ since the plot is linear up to this magnitude and also an
event of this magnitude has been located in the geothermal area (Oct.
1977).

3.2.3 Variations in b within the Hengill area

The data collected on the radio telemetered network is a homogeneous
data set from which were calculated 1918 earthquake locations and
corresponding magnitudes in the range $M_L \leqslant 2.2$. For this low magnitude
range it would be expected that b would be uninfluenced by the effects
of inhomogeneity that act to increase b at high magnitude. However,
there remains the possibility that variations in stress e.g. due to
tectonic or thermal influences, may be reflected in variations in
b-value within the area. b-value plots were made for 9 geographical
subdivisions of this data set (see Section 2.3.2). The results are
summarised in Table 3.1 and Fig. 3.9. Individual plots are
illustrated in Figs. 3.10 to 3.19.

From Fig. 3.9 it may be deduced that the b-values obtained for many of the geographical subdivisions are not statistically different from one another. The b-values for the areas N of $64°N$, S of $64°N$, Klambragil, the central cluster, the fissure swarm, the Kirkjuferjuhjáleiga, Ölfus swarm and 2.00-3.99 km depth are all within or very close to the 95% confidence range for the b-value for the entire area. Examination of Figs. 3.10- 3.19 indicate reasonable linearity for these data sets in the magnitude range about $-1.0 \leqslant M_L \leqslant 2.0$. If one accepts that the b-value is influenced by the stress state of the source volume then one must conclude that stress in the parts of the Hengill area listed above is similar.

Area	b-value calc. betw. M_L	size of data set for b-val calculation	error ±	b
N of $64°N$	-0.9/2.2	318	0.09	0.80
S of $64°N$	-0.9/2.2	570	0.06	0.74
Klambragil	-1.2/1.3	51	0.22	0.80
Mosfellsheiði	-1.2/0.5	116	0.18	1.00
cluster	-1.1/2.2	181	0.11	0.76
fissure swarm	-1.2/0.8	87	0.14	0.68
Ölfus swarm	-0.3/2.2	184	0.11	0.76
2.00-3.99 km depth	-1.1/1.7	243	0.09	0.73
4.00-5.99 km depth	-0.1/2.2	149	0.14	0.86
entire area	0.3/4.2	1424	0.04	0.72

Table 3.1 b-values calculated for subdivisions of the Hengill area

A b-value of 0.86 ± 0.14 was obtained for the 4.00-5.99 km depth range. This is slightly high, and may be an indication of reduction in stress with depth. This might be expected if increase of temperature with depth causes reduction of strength of the rock, as
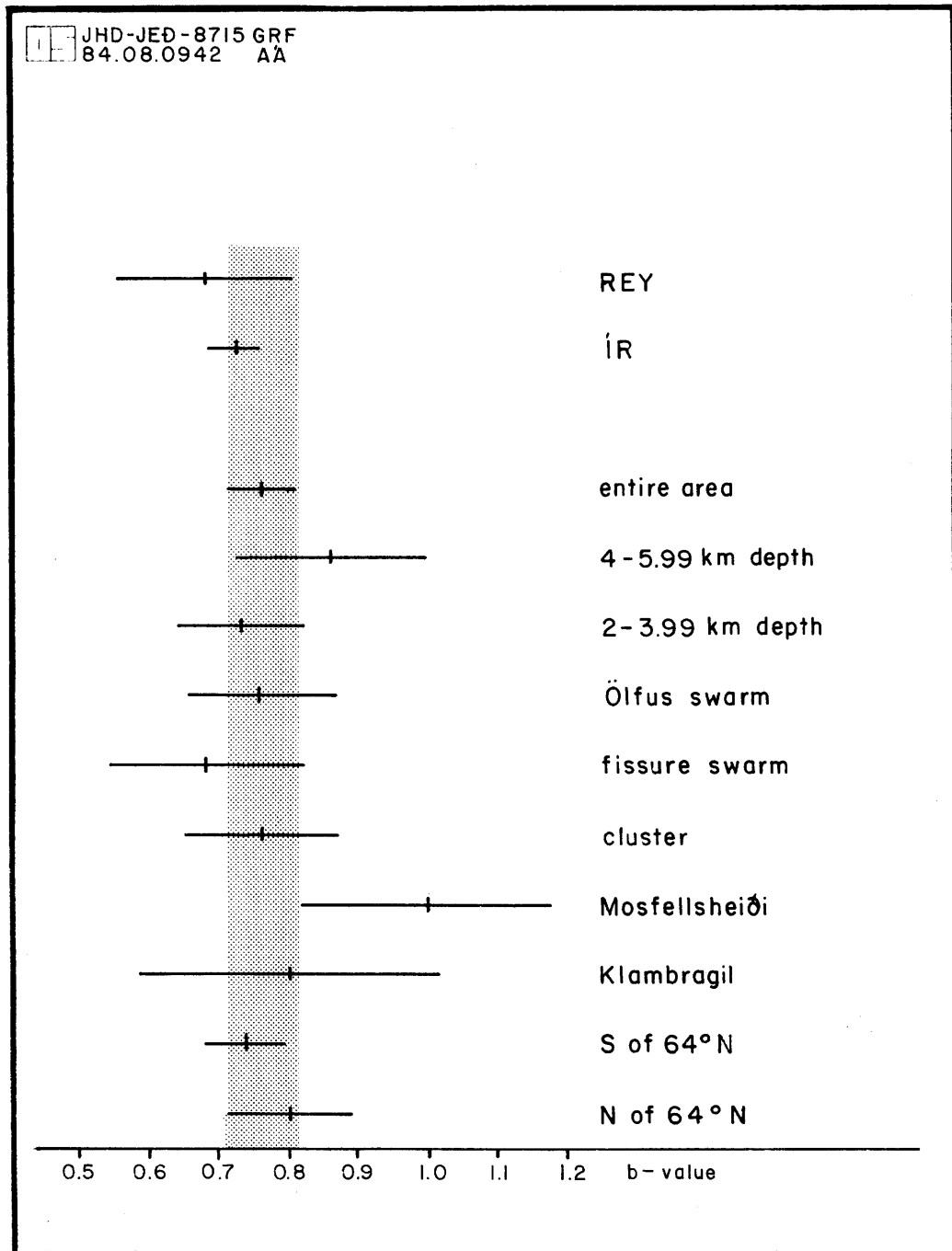
Fig. 3.9   b-values calculated for subdivisions of the Hengill area.
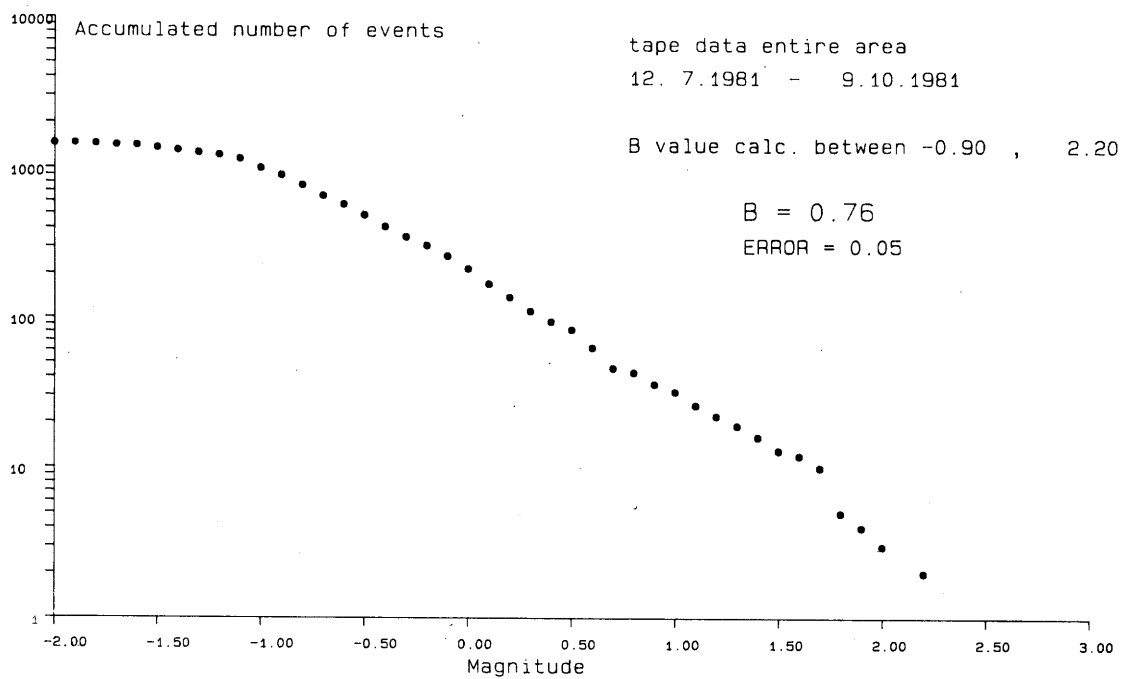
Fig. 3.10 Frequency - magnitude plot - tape data entire area.
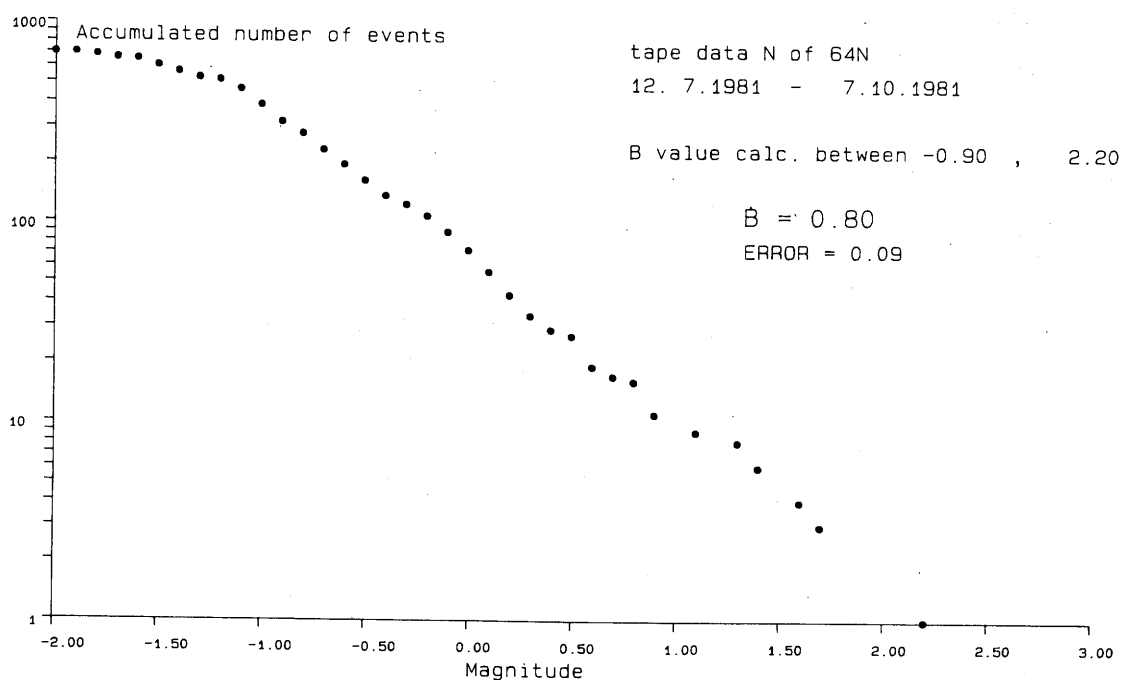
Fig. 3.11 Frequency - magnitude plot - area N of 64°N
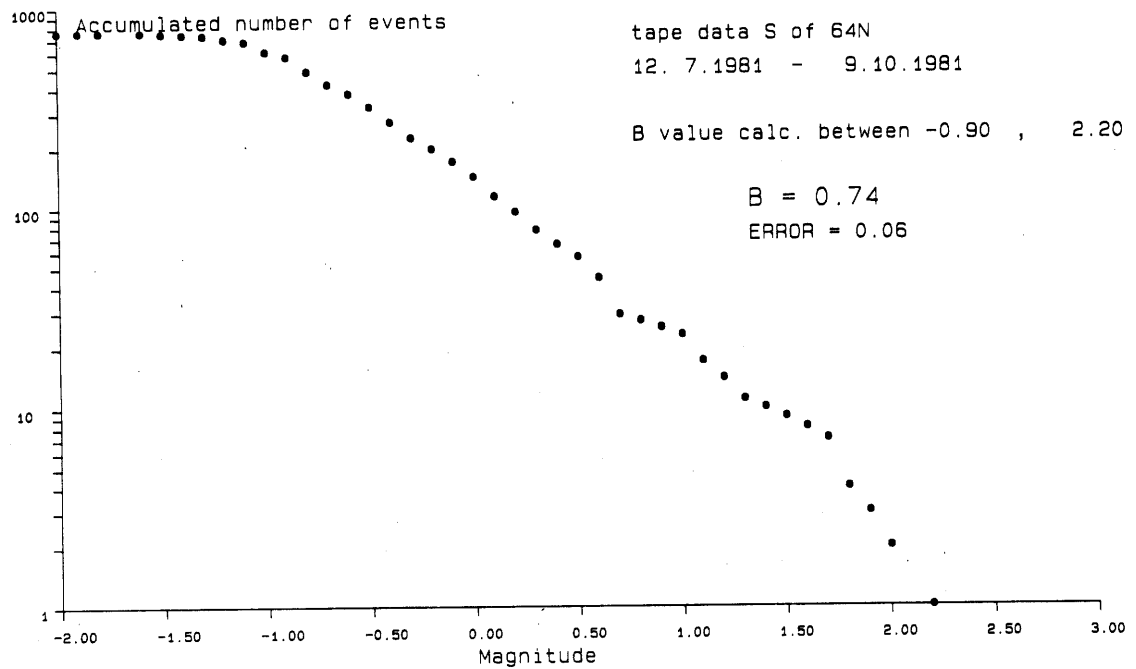
Fig. 3.12 Frequency - magnitude plot - area S of 64°N.
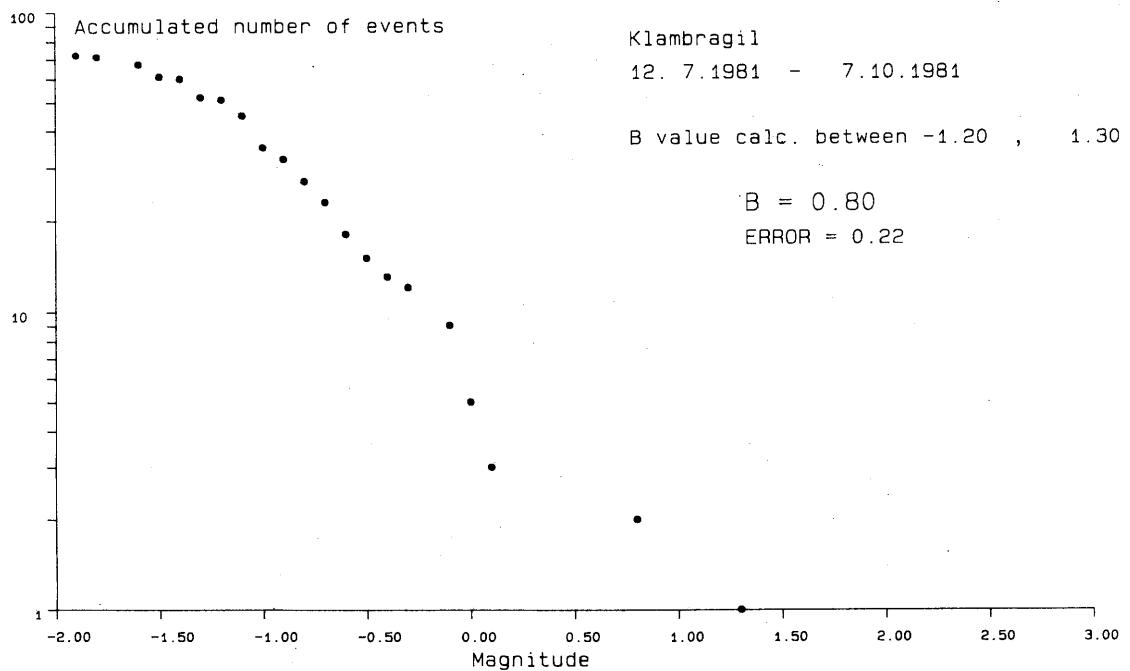
Fig. 3.13 Frequency - magnitude plot - Klambragil area.
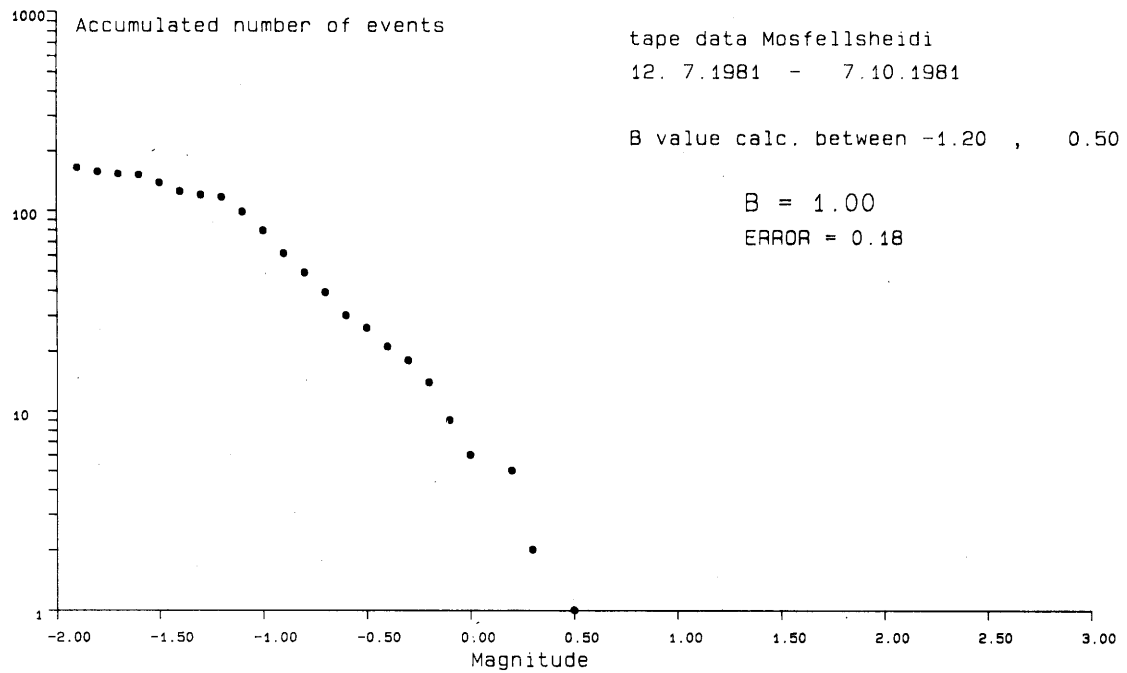
Fig. 3.14 Frequency - magnitude plot - Mosfellsheiði area.
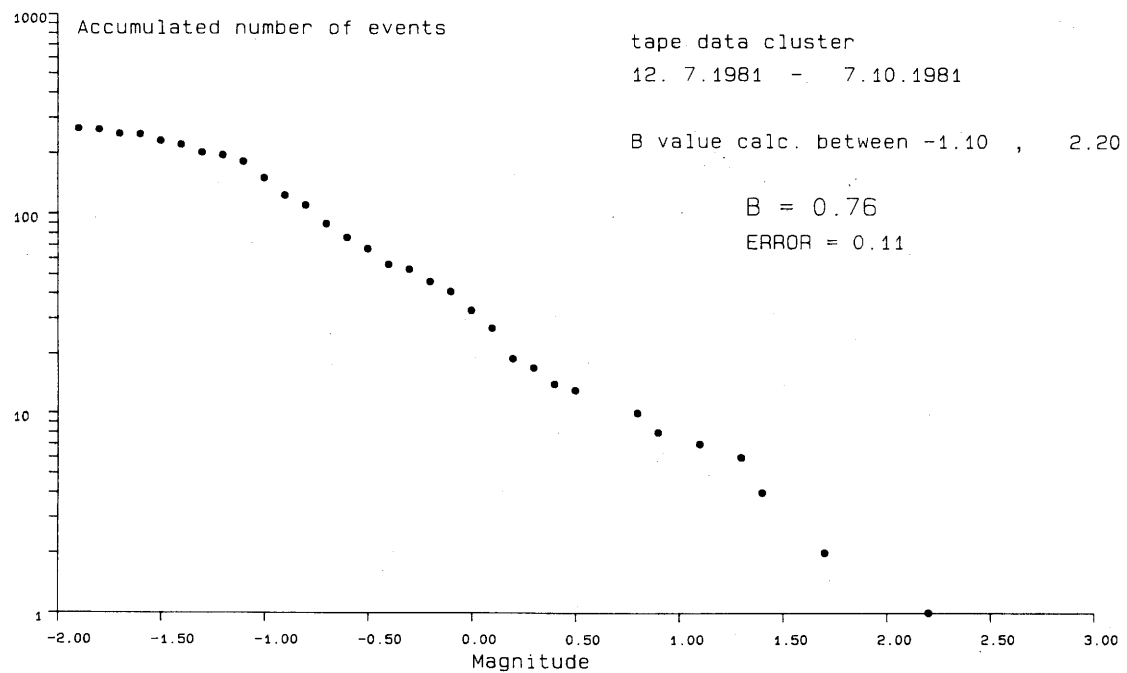
Fig. 3.15 Frequency - magnitude plot - central cluster.
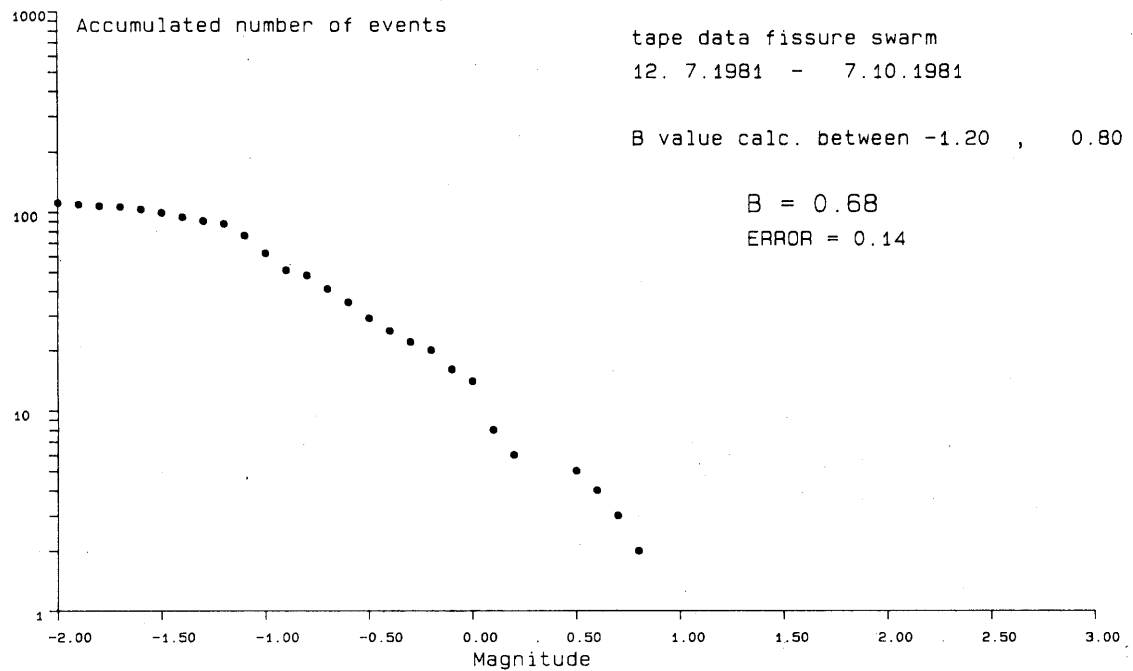
Fig. 3.16 Frequency – magnitude plot – fissure swarm.
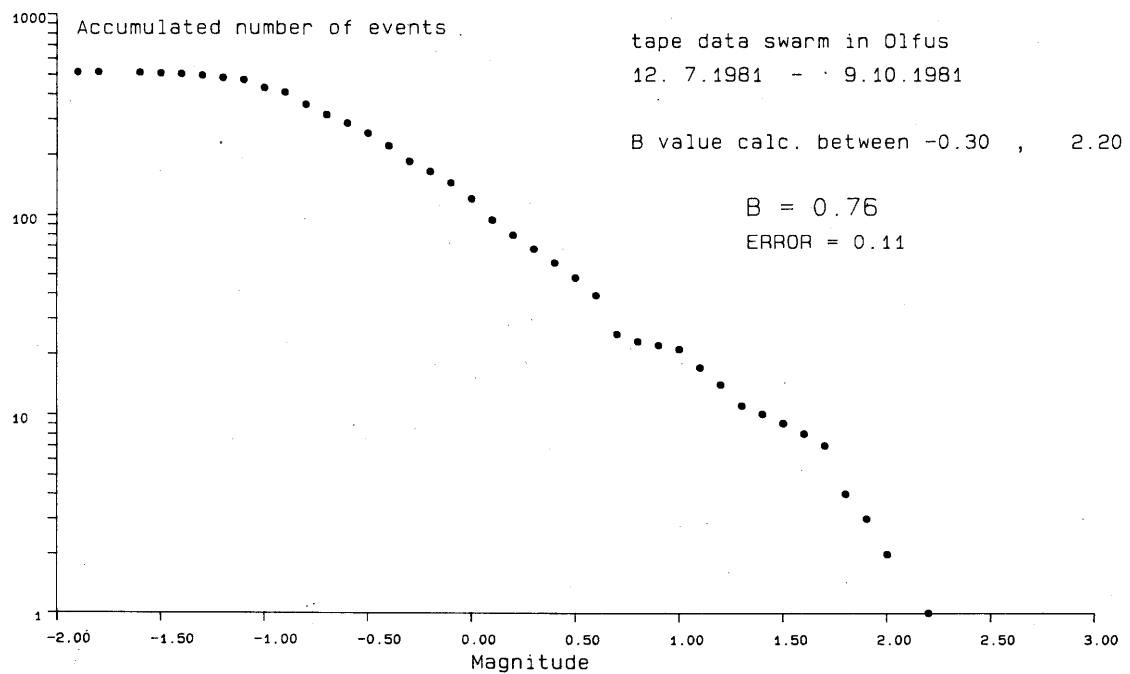
Fig. 3.17 Frequency – magnitude plot – Kirkjuferjuhjáleiga, Ölfus swarm.
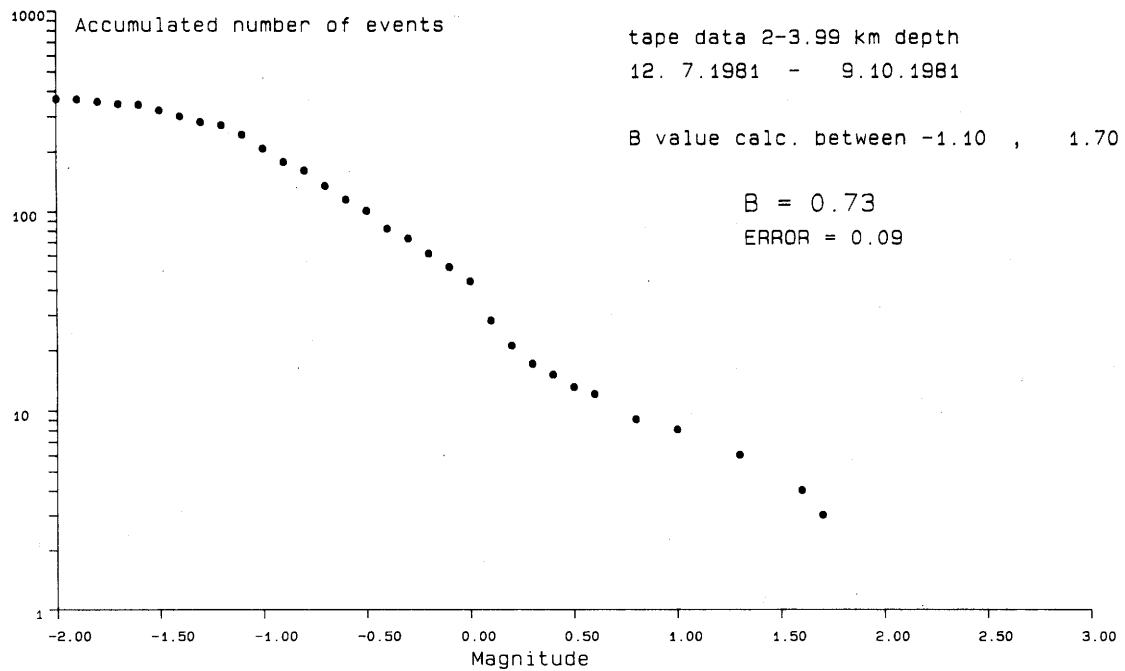
Fig. 3.18 Frequency - magnitude plot - 2.00 - 3.99 km depth.
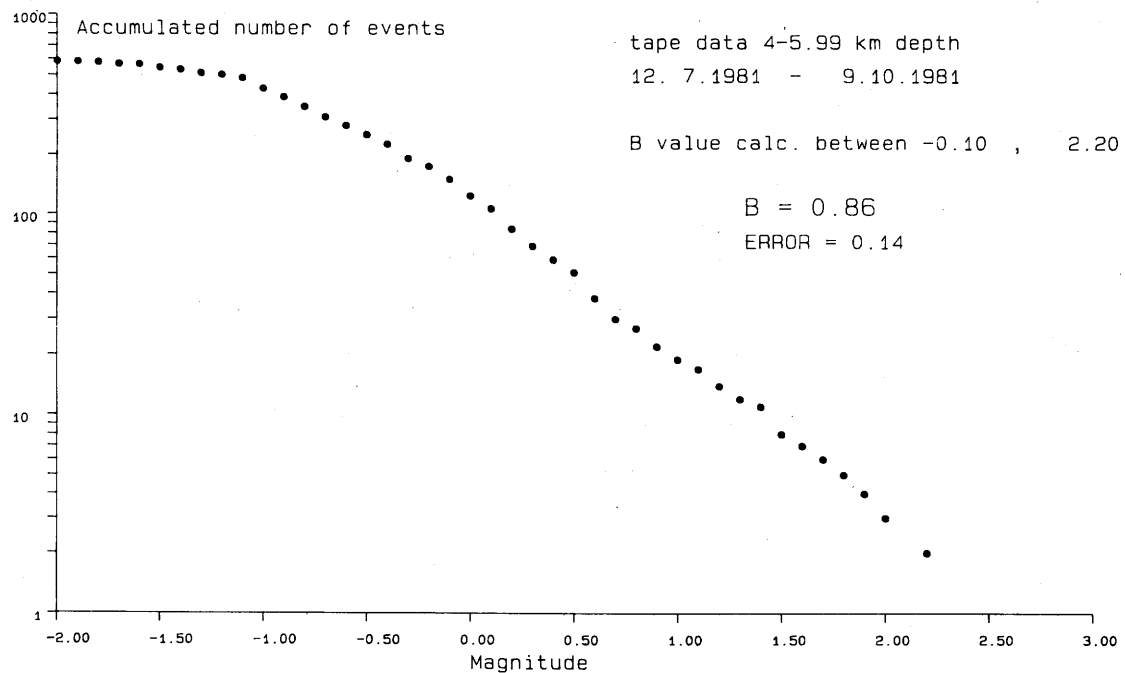
Fig. 3.19 Frequency - magnitude plot - 4.00 - 5.99 km depth.

has been hypothesised for SW Iceland in general.

A b-value of 1.0 $\pm$ 0.18 was obtained for the Mosfellsheiði subdivision. This is significantly different from that obtained for the entire area, and higher, which may indicate lower stress than over the rest of the Hengill area. This b-value contrasts with that obtained for the fissure swarm immediately adjacent, indicating that an abrupt change occurrs on the W boundary of the fissure swarm. It may indicate a change from the anomalously low b-values associated with the Hengill area in general to more "normal" intraplate values such as those observed for the Borgafjörður area.

3.2.4 Running b-values

3.2.4.1 Data recorded on the local seismograph IR

Fig. 3.20 is a running b-value plot over the period April 1977-December 1983. The vertical axis is b-value and covers the range 0.5-1.0. A sample size of 200 was taken, which results in an uncertainty of 0.08-0.11 in the data points. The incremental number of earthquakes was 20.

The b-value varies from 0.64 to 0.79, i.e. over a range of 0.15 units. Also shown in Fig. 3.20 are events of $M_L \geqslant 3.0$ that occurred in the Hengill area during the 7 year period. All of these 4 events occurred in 1977-78 and were accompanied by a decrease in b-value from 0.79-0.65. However, a similar decrease occurred May 1981-June 1982 with no accompanying $M_L \geqslant 3.0$ seismicity.

The variations in b found in the IR data set are not statistically significant and at the time of writing have not been correlated with any ongoing process in the Hengill area.

3.2.4.2 Data recorded on the radio telemetered network

Fig. 3.21 is a running b-value plot over the period July - Oct. 1981. The vertical axis is b-value and covers the range 0.0 - 1.5. A sample size of 200 was taken which results in an uncertainty of 0.8 - 0.12. The incremental number of earthquakes was 20.

The Figure is dominated by a feature around mid September which corresponds to the swarm near Kirkjuferjuhjáleiga, Ölfus. In Fig. 3.22 events confined to the source region of this swarm are plotted separately. A sample size of 100 and an increment of 10 was taken since the data set was small (320 events). In Table 3.2 the data points plotted in Fig. 3.22 are listed with their uncertainties. In
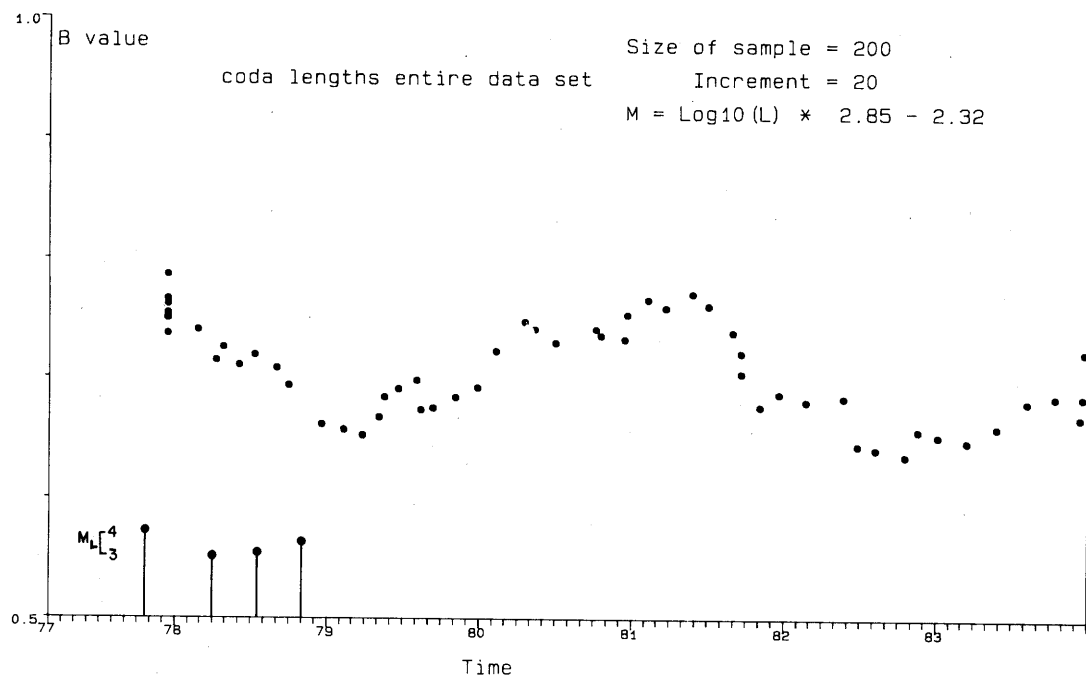
Fig. 3.20 Running b-value plot, data from IR.
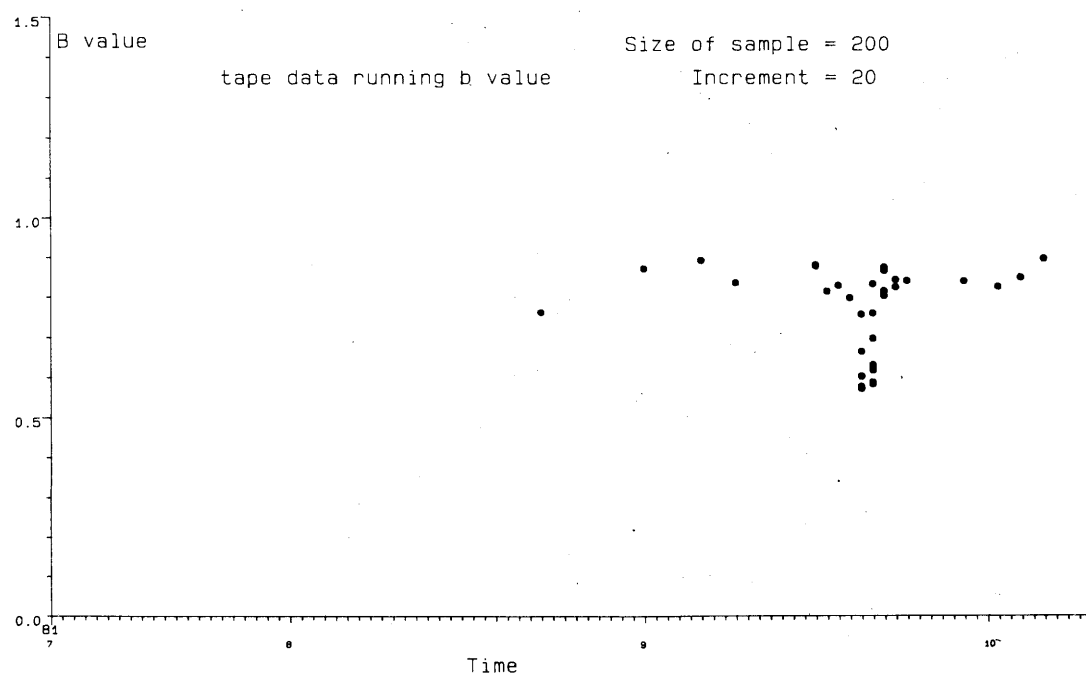
Fig. 3.21 Running b-value plot, tape data.

Fig. 3.23 all the events of $M_L \geqslant 0$ are plotted against time for the period of the swarm alongside the b-value.

The b-value varies from 0.56 to 1.01, i.e. over a range of 0.45 units and the uncertainties vary from 0.11 to 0.2. This is a statistically significant variation. It can be seen from Fig. 3.23 that during the period prior to the swarm the b-value exhibited was high - about 0.9 ± 0.18 but with the onset of the swarm it rapidly decreased to reach its lowest value of 0.56 ± 0.11 by the end of the 19th September. During the following day it remained low, but on the 21st September it rose to approach its original value.

Interpreted in terms of variation in stress within the source region, these results indicate that prior to the swarm stress was relatively low. The onset of the swarm accompanied an increase in stress in the source region. Most of the largest events occurred at the beginning of the swarm also (1.5 $\leqslant M_L \leqslant$ 2.2) but it should be appreciated that this fact alone will not alter the b-value, which is a measure of the relative proportions of events of various magnitudes. The continuation of the swarm resulted in a gradual reduction of stress, and activity stopped when stress had returned to its former level.

These changes in b-value are in a similar style to others reported for earthquake sequences and are consistent with those predicted by theory (Section 3.2.1). However, several other factors may account for part, but probably not all of the observed variations, e.g. the selective picking of large magnitude events early on in the swarm and the possible migration of activity in depth. Quantitative assessment of these errors should preceed any further analysis of these results.

Time from - to		B - value	Error
12.07.81 - 05.09.81 -		0.88	0.17
05.09.81 - 13.09.81 -		0.99	0.19
13.09.81 - 16.09.81 -		0.94	0.18
16.09.81 - 16.09.81 -		0.91	0.18
16.09.81 - 18.09.81 -		0.91	0.18
18.09.81 - 19.09.81 -		0.80	0.16
19.09.81 - 19.09.81 -		0.70	0.14
19.09.81 - 19.09.81 -		0.69	0.14
19.09.81 - 19.09.81 -		0.58	0.11
19.09.81 - 19.09.81 -		0.56	0.11
19.09.81 - 20.09.81 -		0.62	0.12
20.09.81 - 20.09.81 -		0.64	0.13
20.09.81 - 20.09.81 -		0.64	0.12
20.09.81 - 20.09.81 -		0.64	0.12
20.09.81 - 20.09.81 -		0.63	0.12
20.09.81 - 21.09.81 -		0.64	0.13
21.09.81 - 21.09.81 -		0.72	0.14
21.09.81 - 21.09.81 -		0.80	0.16
21.09.81 - 22.09.81 -		0.99	0.19
22.09.81 - 23.09.81 -		1.01	0.20
23.09.81 - 29.09.81 -		0.94	0.18
29.09.81 - 02.10.81 -		0.91	0.18
02.10.81 - 05.10.81 -		0.97	0.19

Table 3.2 Data points plotted in Fig. 3.22.
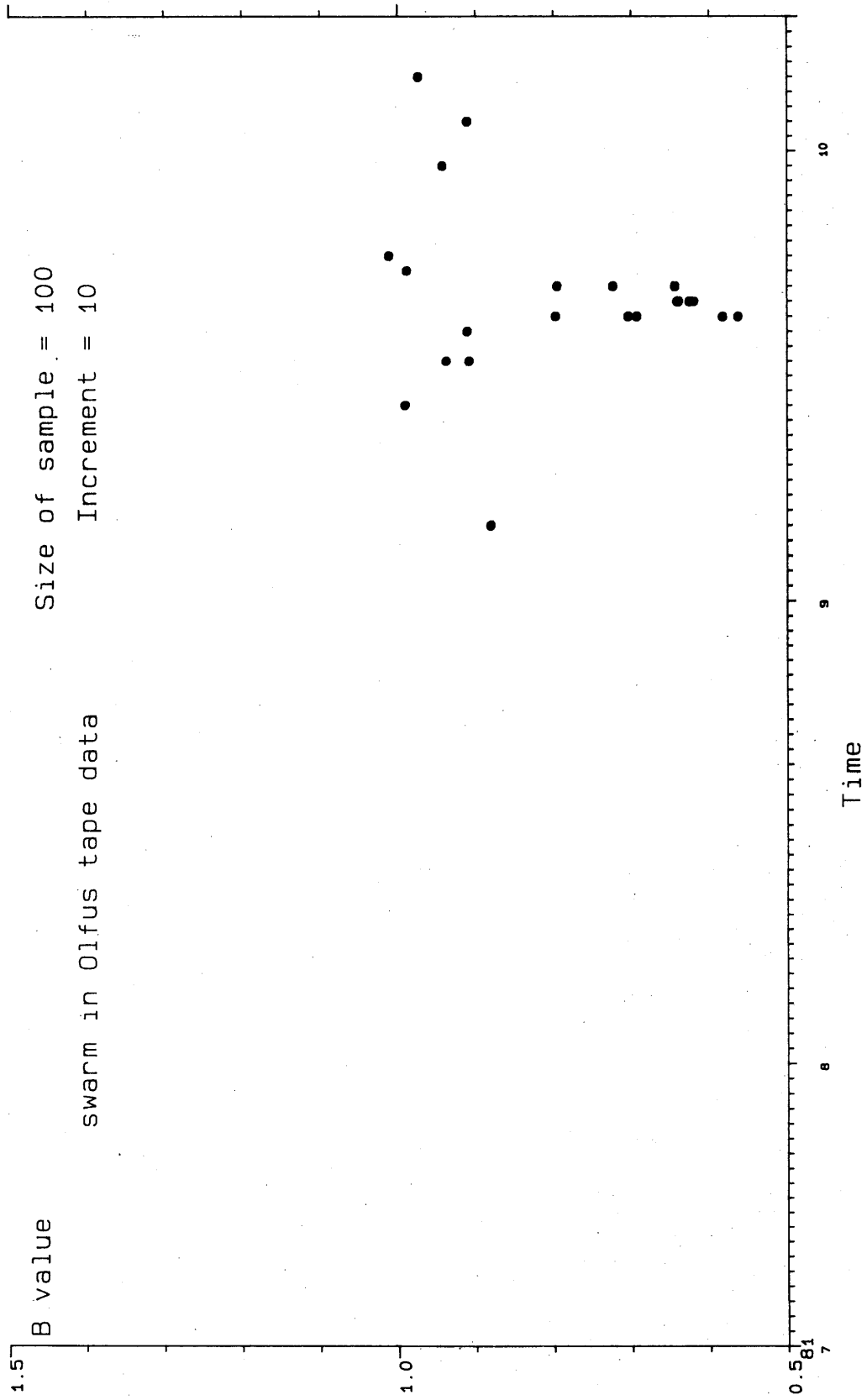
Fig. 3.22 Running b-value plot, Kirkjuferjuhjáleiga, Ölfus swarm.
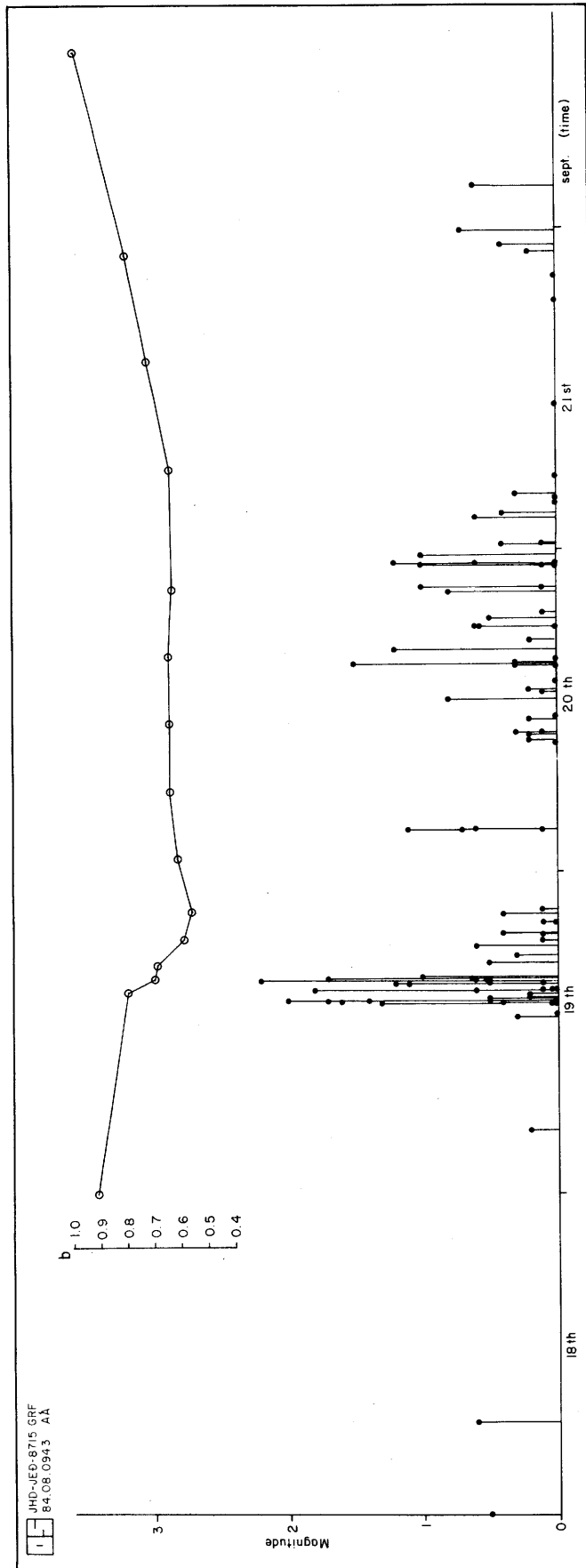
Fig. 3.23 Magnitudes of events of Kirkjuferjuhjáleiga, Ölfus swarm and associated b-values. b-values plotted were calculated for the preceeding 100 events in the hypocentral volume.

3.3 Summary

The temporal nature of the seismicity of the Hengill area is remarkable because of its continuous day to day nature. In this respect it contrasts with all the neighbouring seismic areas. The continuity of the activity is most striking in a 20 km^2 area to the N of Hveragerði, but is also observed for other parts of the area. This fact is the single most important one that facilitated the design of the 1981 radio telemetry monitoring project and guaranteed its success. Sequences of various types are superimposed on continuous background activity.

A b-value of 0.74 $\pm$ 0.06 for the Hengill area is constrained by a large body of data. This is low compared to the value 1.0 usually quoted for the global average. Comparable b-value studies on the Reykjanes Peninsula yielded estimates of b of 0.85 $\pm$ 0.07, 1.02 $\pm$ 0.07 and 0.75 $\pm$ 0.11 and in the intraplate Borgafjörður area of 1.09 $\pm$ 0.06 and 1.06 $\pm$ 0.06. The b-value for the Hengill area is therefore significantly lower than these.

Evidence has been discussed above that variations in b-value may be due to variations in rock homogeneity or stress. Since homogeneity is only thought to affect b in the higher magnitude range, it is difficult to see how this could cause the variations cited above, which appear in b-value determinations at low magnitudes. If stress variations contribute to these b-value variations, then there may be an indication here that the crust in the Hengill area in general is more highly stressed than that of the Reykjanes Peninsula and the Borgafjörður areas. This enhanced stress level may be due to thermal or tectonic effects.

An upper magnitude limit of M_L = 6-6.5 is likely for events in Ölfus but indications are that it is lower for the high temperature geothermal area. It appears that the South Iceland Seismic Zone of destructive earthquakes extends into the Hengill area in Ölfus, but does not encompass the high temperature geothermal area i.e. the area N of 64°N. At the time of writing the Hengill area has been quiescent at $M_L \geqslant 3.0$ for an unusually long time.[*]

Investigation of local variations of b within the area indicated elevated b-values for the Mosfellsheiði area and the deeper events in general. This may indicate lower stresses in these areas. For all other subdivisions of the area b was statistically constant. If these variations are stress induced then it may be that stress decreases with depth beneath the Hengill area, because of temperature elevation. The high b-value of Mosfellsheiði, relative to the rest of

[*]see note added in proof p. 64

the area, may indicate that the high stress regime associated with the Hengill area, possibly due to thermal or tectonic effects, terminates abruptly on the W boundary of the fissure swarm. On Mosfellsheiði the stress regime is more characteristic of that observed on the Reykjanes Peninsula and in the intraplate Borgafjörður area.

Calculations of running b-values show that no statistically significant variation was detected over a 7 year period at a local instrument (ÍR) with detection threshold M_L = 0.3. However, significant variations occurred during a single swarm in the Kirkjuferjuhjáleiga, Ölfus area in Sept. 1981. One possible explanation for these variations is that the source volume experienced a stress pulse accompanied by seismic activity.

4. FOCAL MECHANISMS

4.1 The Data

4.1.1 Theory

A foreknowledge of the spatial distribution of the seismicity of the Hengill area meant that the radio telemetered network could be deployed to provide the optimum net geometry for focal mechanism determinations. Well constrained radiation patterns were determined for 178 events, 50% of which were not consistent with a shear (double couple) source mechanism. The theoretical treatment of the anomalous events is dealt with in brief in Appendix 2, and they have been described and discussed by Foulger and Long (1984).

It has been generally assumed that all earthquakes occur as a result of shear slip on buried faults. Theory predicts that the P-wave radiation pattern generated by such movement would exhibit equal areas of compression and dilation when projected onto the focal sphere, an imaginary sphere with the earthquake focus at its centre. It should be possible to separate these areas of compression and dilation by drawing two orthogonal great circles on the focal sphere, thus dividing it into 4 "quadrants" - two compressional and two dilational. One of the great circles represents the fault plane and the other is named the "auxiliary plane". For the Hengill events, in only 50% of cases could the dilational and compressional portions of the focal sphere be separated by a pair of orthogonal great circles. It was concluded that the "anomalous" events were not generated by shear slip on fault planes.

The anomalous events are characterised by compressional radiation fields that occupy far more than 50% of the focal sphere, and correspondingly severely reduced dilational fields. The dilational arrivals are of normal amplitude. These facts imply that the sources that generate these events exhibit a net explosive component (i.e. a "volume increase"). The interpretation of them favoured here is that their source mechanisms involve fault planes, but that movement is in the direction normal to the fault plane instead of parallel to it as is the case for a shear dislocation, i.e. that they may be approximated to tensile cracks. The reasons why this model is taken are that the observed anomalous radiation patterns are very similar to that predicted by theory for a tensile crack and also that this model is a reasonable one in an area such as Hengill that displays features clearly indicative of a tensile stress regime (e.g. open surface fissures, geological offsets). It should be pointed out, however, that this interpretation is a hypothesis and that although other

reports of anomalous earthquake radiation patterns have been made, (see Foulger and Long, 1984, for summary) this is the first time that they have been interpreted as being due to tensile crack formation at depth in the earth's crust.

4.1.2. Presentation

For completeness of documentation, all events for which reasonably good polarity plots were obtained are illustrated in Figs. A2.1 to A2.14 in Appendix 2. The minimum number of data points used to constrain any one solution is 10. Where possible, a shear solution is preferred. The data have been divided into 12 groups that are suggested by the epicentral distribution (see Section 2.3.2.1). Each event is labelled by its origin time, so an exact hypocentral location for any one event may be obtained from the location listings. The groups are Nesjavellir (N), Mosfellsheiði (M), the fissure swarm (F= all events within the fissure swarm but not included in any other group), Svínahlið (S), Örustuhólshraun (Ö), Ástaðafjall (Á), Klambragil (K), Kyllisfell (KY), Laxárdalur (L), the central cluster (C= all events within the cluster NW of Hveragerði but not included in any other group), Hveragerði (H) and Ölfus (Ö).

For each group, a summary diagram is also presented in the form of a stereographic projection. All the events associated with the particular group for which an unambiguous interpretation could be made are represented on these. For the shear solutions the pressure (P) axes and tension (T) axes are represented by open circles and dots respectively. (The P and T axes of a shear focal mechanism solution are axes that lie normal to the null axis and at 45° to the fault and auxiliary planes, in the dilational and compressional quadrants respectively). For the tensile crack solutions the planes of the cracks (which, in stereographic projection, disect the dilational belts) are represented by great circles. The events for which no solution could be obtained or for which either type of solution would fit equally well are not represented on the summary diagrams. The summary diagrams are displayed together in Fig. 4.1.
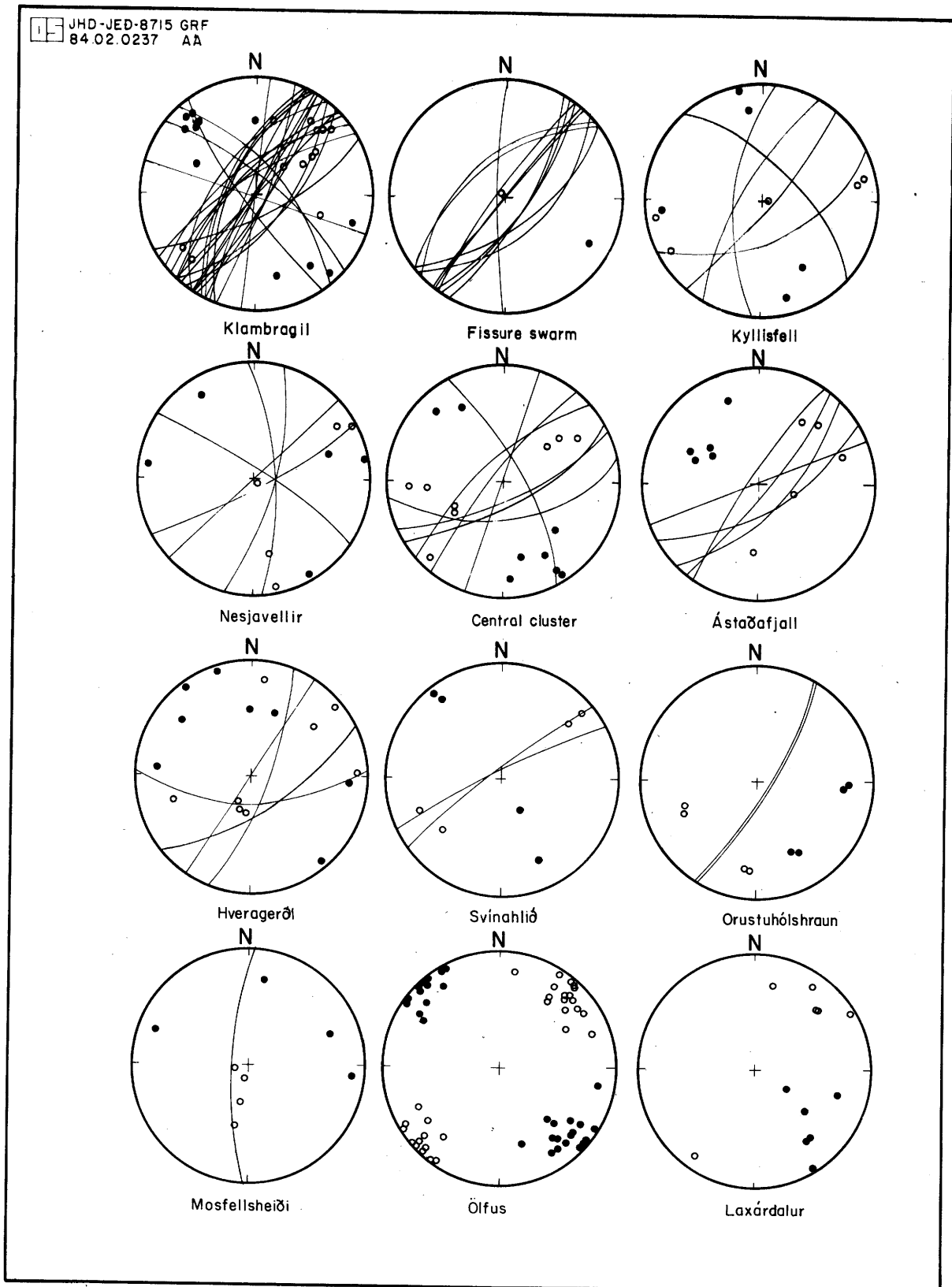
Fig. 4.1   Summary diagrams for focal mechanism data groups.   O = P axes,   ● = T axes of shear solutions, great circles represent planes of tensile crack solutions.

4.2 The mode of strain release in the Hengill area

4.2.1 The tensile crack events

Examination of Fig. 4.1 indicates that most of the tensile crack events occurred on near vertical planes. The greatest hade measured was 40°. The dominant direction of strike was about N 35°E (see Fig. 4.2) but a few events exhibited N, NW and EW orientated crack strikes. The width of the dilational belt varied but was never larger than $2\theta = 60^{\circ}$. If the tensile crack interpretation is correct, that the dilational belt is generated by a pressure drop in the pore fluid at the instant of fracturing (see Appendix 2), it would be expected that the width of the belt would be dependent on the magnitude of the pressure drop. The width of the dilational belt might then be governed by such factors as the type and phase of the pore fluid and the porosity of the rock, that would influence the speed of pore fluid flow. It would be expected that tensile cracks would form normal to the direction of least compressive stress (i.e. greatest tension). Hence the direction of greatest compressive stress would lie in the crack plane. This implies a direction approximatly horizontal N 125° E for the least compressive stress (σ_3) in the depth range 2 – 6 km. The strike and hade of surface extensional features indicates an orientation of horizontal N 115°E for the least compressive stress (horizontal and normal to the orientation of the fissure swarm). It is therefore possible that σ_3 rotates dextrally with depth, but it is also possible that there is a component of double couple mechanism in some of the tensile crack events. This would have the effect of biasing the apparent orientation of σ_3 dextrally.

The implications of the findings described above are far reaching. It is recognised that fissure opening can occur at the surface and near it since the overburden pressure is zero or small but such fissuring was not considered likely to extend very deep since at great depth the confining pressure is very large. That such a process is ongoing in the Hengill area, down to depths of 6 km where confining pressures of about 1.5 kbar would be expected, implies that a very strong tensional stress regime is superimposed onto, and outweighs, the compressional field generated by the overburden. Plate movements are an obvious process that could generate such a tensional stress field.

4.2.2 The shear events

The solutions obtained exhibited faulting which, in general, ranged from strike slip on near vertical NS or EW orientated planes to normal dip slip movement on NE orientated planes. The normal movements indicate subsidence and subsurface faulting on planes with a similar

4-DEGREE RUNNING AVERAGES

Number
of events

Orient[n] of P-axes
Ölfus events

Orient[n] of P-axes
shear events N of 64°N

Orient[n] of crack
tensile crack events

Degrees E of N
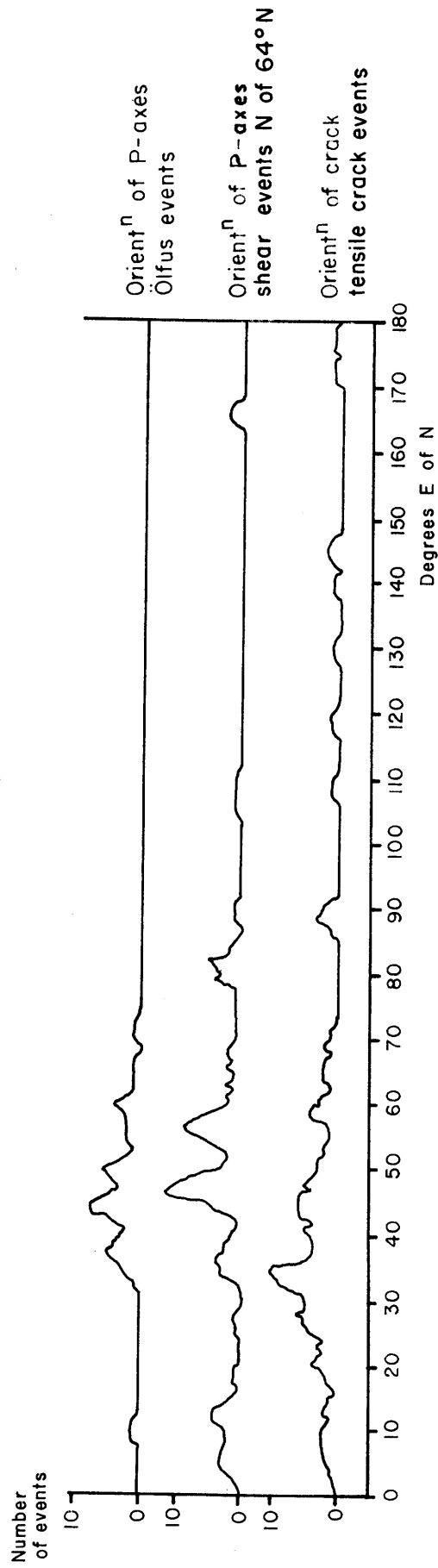
Fig. 4.2 Smoothed plot of orientation of P axes for Ölfus shear events, and shear events located N of 64°N, and orientation of the crack planes of the tensile crack events.

orientation to fault planes observed at the surface. The P axes are orientated preferentially about N 45°E (see Figs. 4.2 and 4.3). They are often close to horizontal but range through to vertical (Fig. 4.3). The T axes are normal to the P axes, and usually close to horizontal. Although the P and T axes of the double couple events are not exactly equivalent to the directions of greatest and least compressive stress (see Section 4.2.5), they nevertheless imply an approximately horizontal NW orientation of the direction of least compressive stress, σ_3 , and variation from horizontal, approximately NE, to vertical for the direction of greatest compressive stress σ_1 .

4.2.3 Spatial variations in mechanism

Table 4.1 is a breakdown of events of different type in the data groups depicted in Fig. 4.1. From this table it can be seen that the sizes of the data groups vary from 45 events for Klambragil to only 5 for Mosfellsheiði. Also the proportion of double couple to tensile crack solutions is variable. These variations are displayed in Fig. 4.4. A circle is drawn in the location of each data group and the proportion of events that are unambiguously tensile crack is equal to the proportion of the circle filled.

	number of shear events	number of t.c. event	number with no solution	Total
Klambragil	13	26	6	45
Fissure swarm	1	11	4	16
Kyllisfell	5	5	2	12
Nesjavellir	5	5	–	10
Central cluster	8	8	3	19
Ástaðafjall	6	5	1	12
Hveragerði	7	3	–	10
Svínahlið	4	2	–	6
Orustuhólshraun	4	2	–	6
Mosfellsheiði	4	1	–	5
Ölfus	31	–	–	31
Laxárdalur	6	–	–	6
totals	94	68	16	178

Table 4.1 Breakdown of events of different type in the data groups.
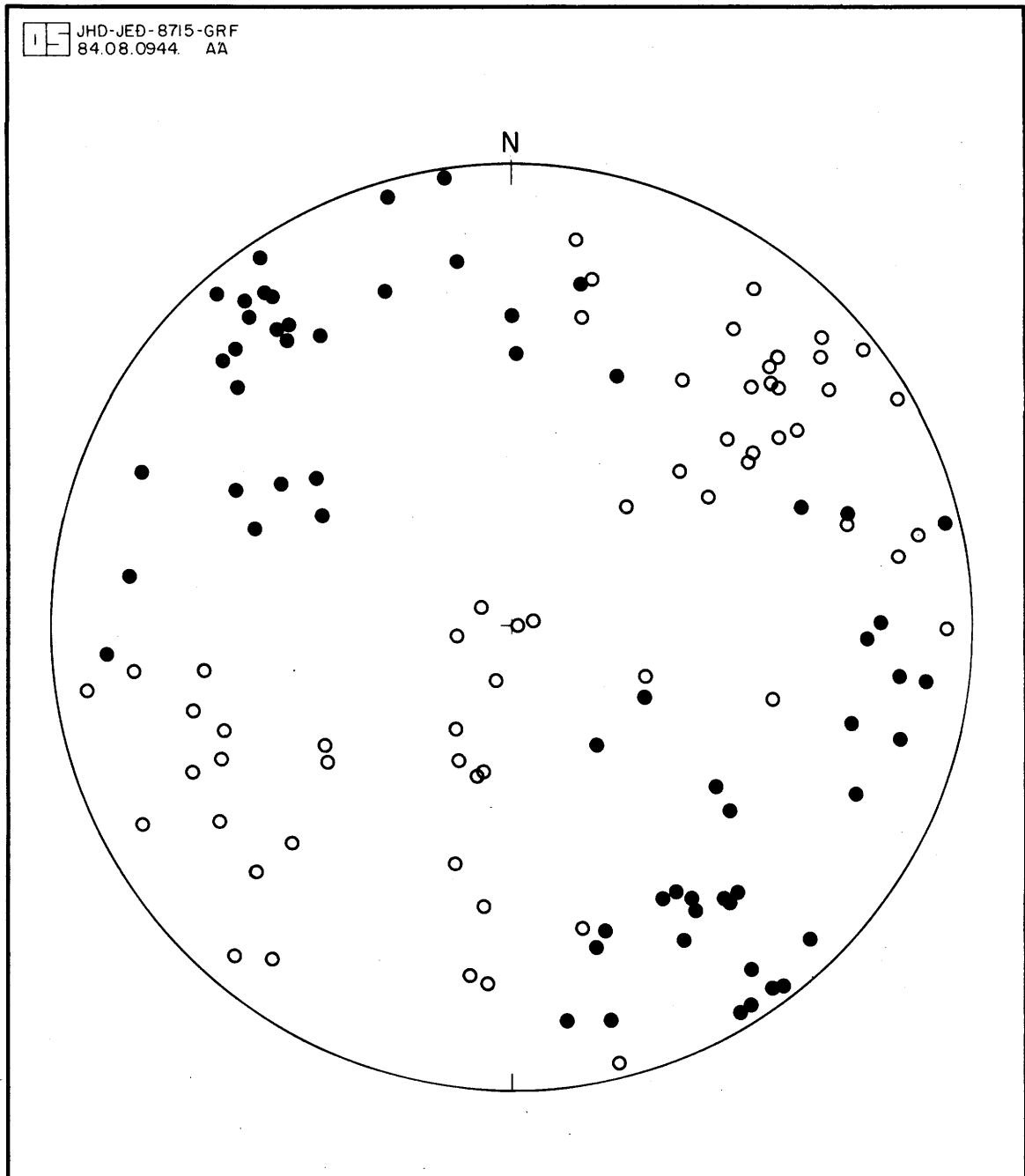
Fig. 4.3. Plot of P - and T - axes of all shear events in stereographic
projection. O = P axes, ● = T axes.
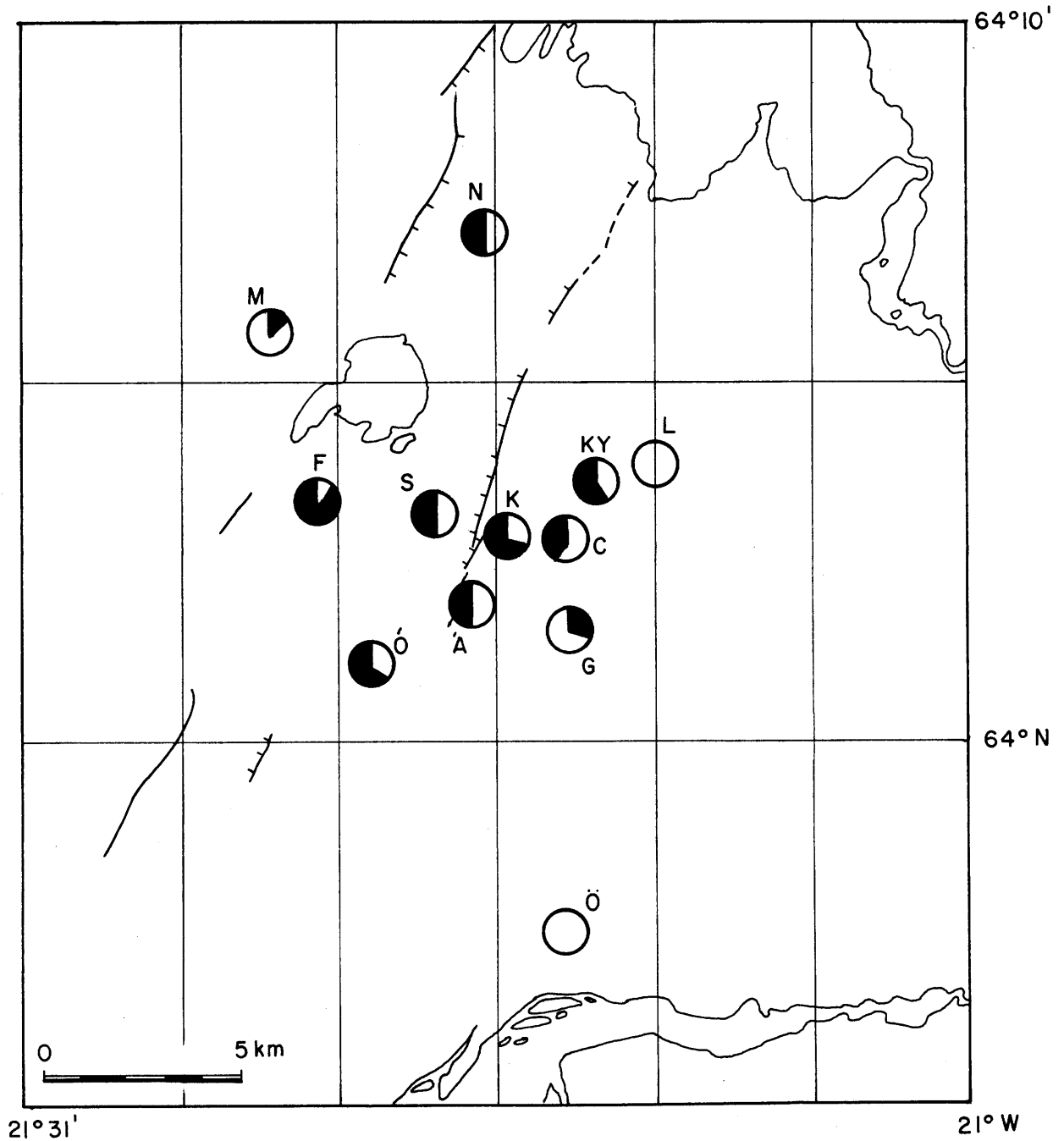
Fig. 4.4   Proportion of tensile crack events represented as proportion of
circles filled for the data groups depicted in Fig. 4.1.

It can be seen that tensile crack solutions occur preferentially in the cluster NW of Hveragerði and the fissure swarm, i.e. the high temperature geothermal area. In the Hveragerði, Mosfellsheiði, Laxárdalur and Ölfus areas, which are peripheral to or outside the high temperature area tensile crack type events are subsidiary or absent. The transition from tensile crack type to shear type strain release is abrupt on the W boundary of the fissure swarm. There is hence a clear indication that the tensile crack type events are associated with some deep process in the high temperature geothermal area.

In the case of the shear events, the data group for Ölfus exhibits primarily strike slip movement whereas events that exhibit a large normal component of faulting are confined to the area N of 64°N (Fig. 4.1).

Fig. 4.5a illustrates depth distribution for the tensile crack and the double couple data groups. For the depth distribution the data are divided into 3 sets representing different parts of the area. The depth distribution for Klambragil shows similar ranges for both types of event except that the tensile crack events extend to greater depths. The seismicity in this small area is also at a shallower level than for the rest of the high temperature area. The depth distribution for all areas except Klambragil and Ölfus shows a definite tendency for the tensile crack events to occur at greater depths than the double couple events. It is possible that the tensional stress field that enables tensile crack formation is strongest in the deeper part of the seismic zone and that strain is preferentially released by shear movements at shallower depth. The distribution of double couple events in Ölfus shows the greater depth range of events in this part of the area, in agreement with the observations described in Section 2.3.2.8.

4.2.4 Magnitude variations in mechanism

The plot of magnitude distribution (Fig. 4.5b) shows that the shear events occupy the range $-2.0 \leqslant M_L \leqslant 2.2$ and the tensile crack events $-2.0 \leqslant M_L \leqslant 1.4$. Hence for the set of events for which solutions were obtained (representing 3 months recording) the largest shear event was 0.8 magnitude units larger than the largest tensile crack event. In terms of energy, for this data set 95% of the seismic strain energy release was by shear failure and 5% by tensile crack failure.

The swarm that occurred in the Kirkjuferjuhjáleiga, Ölfus area 19th-22nd Sept. 1981 is not included in the data set since it was located too far outside the tape network for the radiation patterns to

MAGNITUDE AND DEPTH DISTRIBUTIONS

JHD-JED-8715 GRF
84.02.0230   AÅ
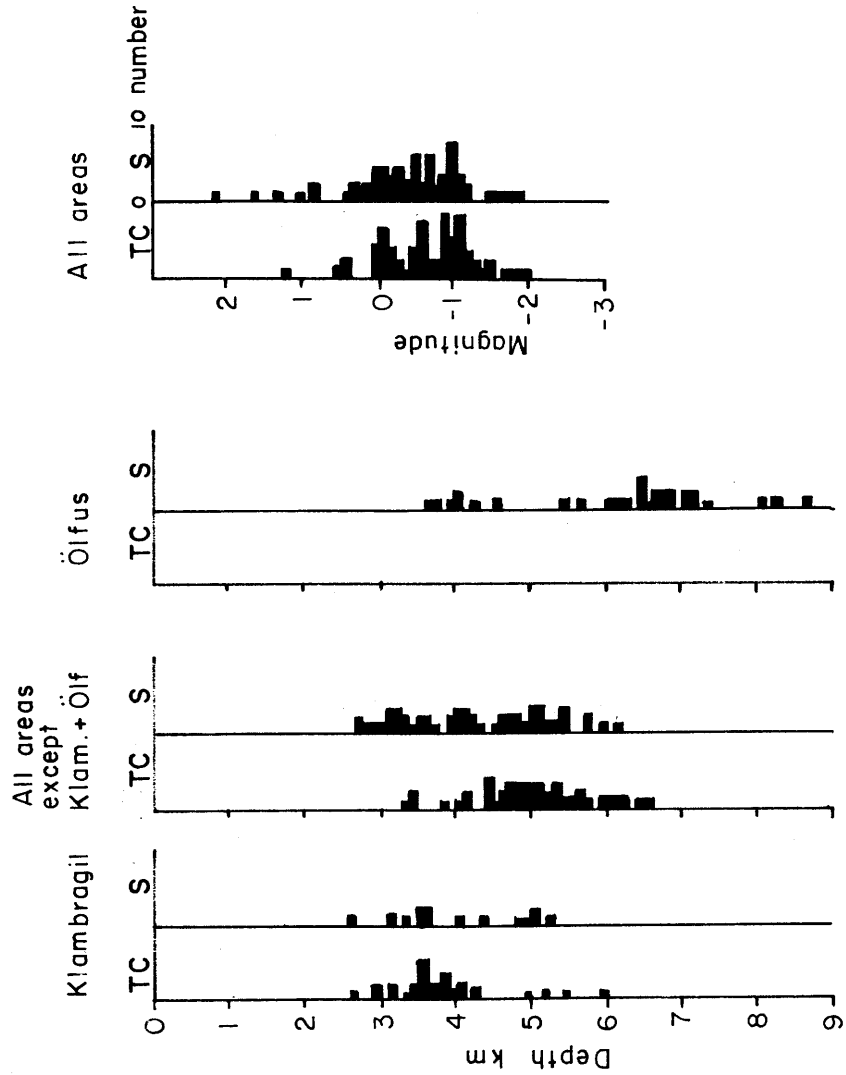
(a)

(b)

Fig. 4.5   (a) Depth distributions of tensile crack and shear events for
the Klambragil and Ölfus data groups and all other areas.
(b) Magnitude (M_L) distributions of tensile crack and shear
events, entire data set.

be well constrained. Because of this, the data presented in Fig. 4.5 are a typical 3-month sample as regards number of events (Section 3.2.2.2).

These observations are in agreement with the hypothesis that tensile crack type events are limited to small magnitudes and thus account for only a very small percentage of the total seismic strain energy release of the Hengill area. However the recording period of 3 months was too short to provide definite proof of this.

4.2.5 Implications for fault plane determination for the shear events.

That the shear and tensile crack events are interspersed in the same volume of rock, is demonstrated by the depth distribution. Also both types of event may occur in a single sequence (e.g. the 810905 sequence in the Ástadafjall area, Fig. A2.14). This may be explained by the process illustrated in Fig. 4.6.

The opening of tensile cracks close together results in the build up of stress in the intermediate rock volume which is then released by shear failure on a plane connecting the cracks (Hill, 1977). For tensile cracks forming at the same depth (i.e. with horizontal separations only) strike slip earthquakes would be generated. For tensile cracks forming at different depths (i.e. with vertical separations) earthquakes with a normal component of shear movement would be generated. Strike slip shear faulting preferentially occurs on either NS or EW orientated planes (Section 4.2.2). These two alternatives are illustrated in Fig. 4.6. It can be seen that release of shear stress on EW orientated vertical planes implies a left lateral tensile crack configuration, and movement on NS orientated vertical planes implies a right lateral tensile crack configuration.

According to McKenzie (1969), for a fresh break in homogeneous rock the direction of greatest compressive stress (σ_1) lies between the P-axis of the shear focal mechanism solution and the fault plane (see Fig. 4.7). In the case of the Hengill events the P axes of the shear events are preferentially orientated about N 45° E whereas the orientation of the tensile crack events indicates an average horizontal direction of about N 35° E for the greatest compressive stress in the depth range of the events (Sections 4.2.1 and 4.2.2). With this information, and from inspection of Fig. 4.7 it may be deduced that in the case of the strike slip shear events, the plane of fracture will be the more northerly striking plane, and a right lateral tensile crack configuration is implied. The strike slip shear seismicity associated with the high temperature geothermal area therefore indicates that right lateral movement on northerly striking

91
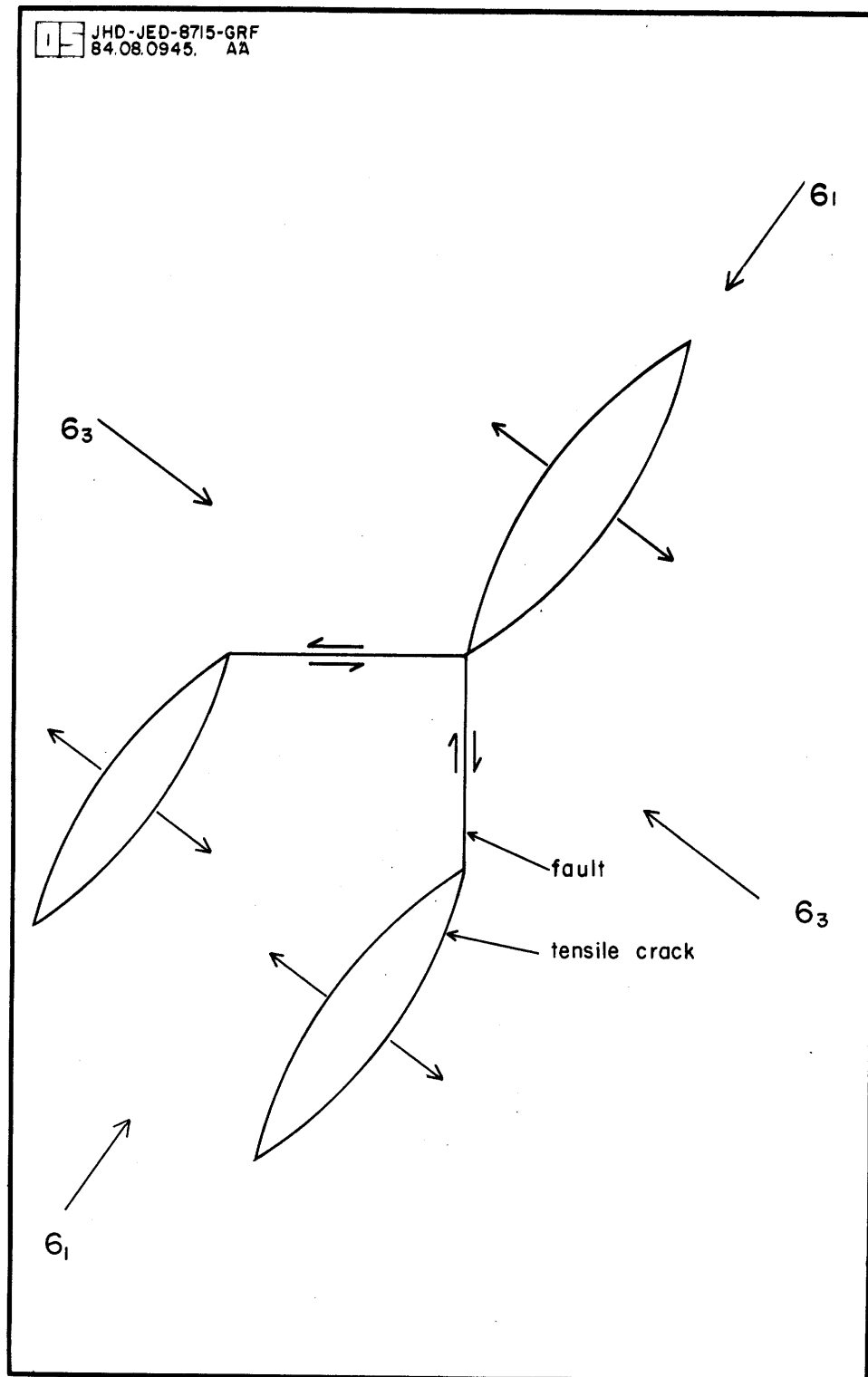
Fig. 4.6   Schematic   diagram   of   tensile   crack   opening and accompanying
shear seismicity on planes connecting the cracks.

fault plane

6_1 in this range

P

T

auxiliary plane

T

P

6_1 = greatest principal stress

6_2 = intermediate

6_3 = least principal stress
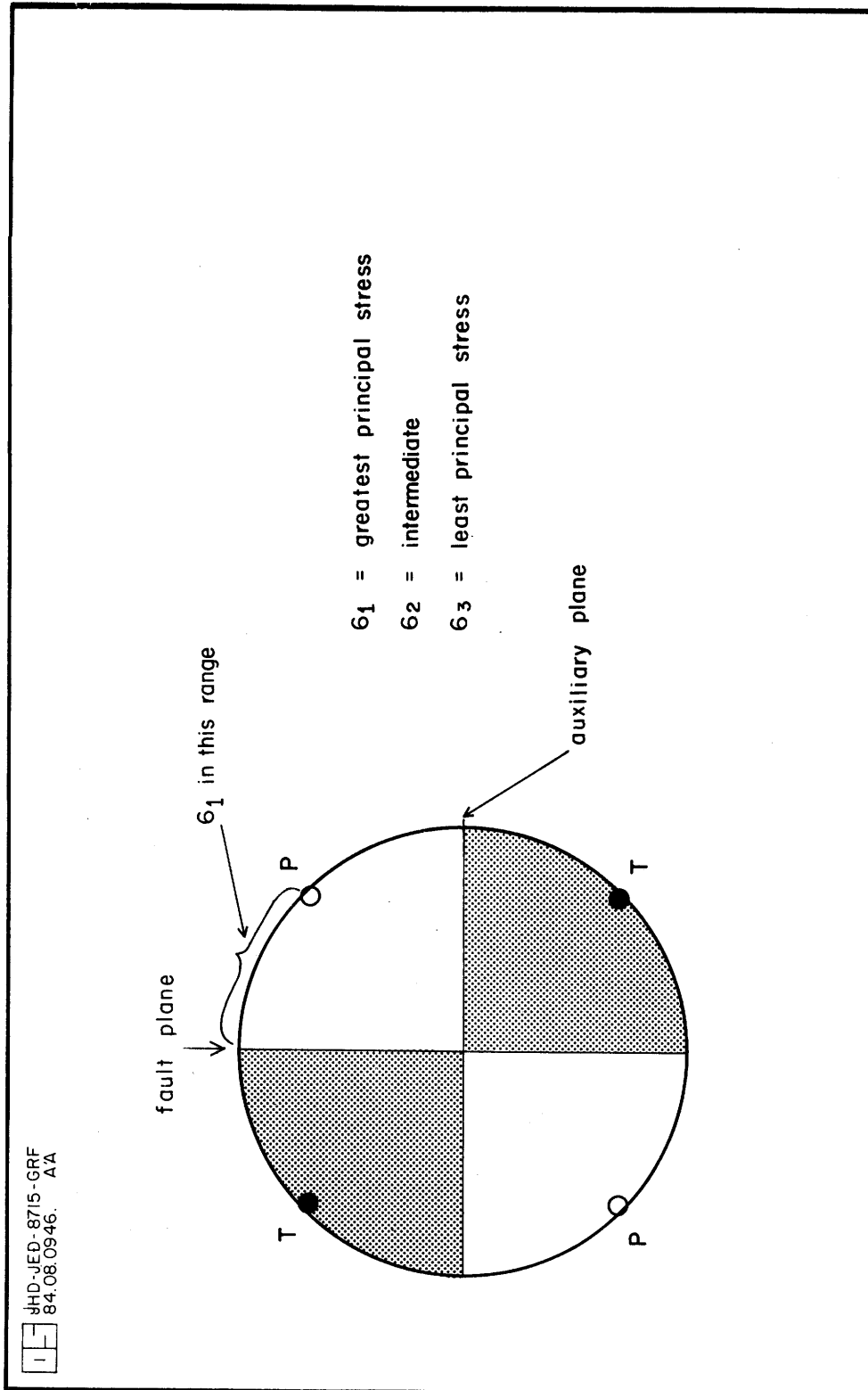
Fig. 4.7   Diagram showing relationship between P - and T - axes,   and the fault and auxilliary planes of a shear earthquake focal mechanism.

planes is the most common mode of faulting. It can be seen from Fig. 4.6 that if fracturing of this nature occurred in a zone, then the orientation of the entire activated zone would be intermediate between that of the tensile cracks and the shear fault planes. As has been described above this situation is observed at the surface in the Hengill area. The trend of surface faulting is N 25° E, intermediate between the NS striking fault plane typical of the double couple focal mechanism solutions and the N 35° E strike typically exhibited by the tensile crack events. This is a strong indication that the deduction of fault plane made above is correct. If it is assumed that the mode of faulting observed for the high temperature geothermal field extends S into the Ölfus area then this implies that faulting there is right lateral strike slip on NS orientated planes. This is consistent with the mode of faulting observed for large destructive earthquakes in the South Iceland Seismic Zone, of which Ölfus forms the westernmost part (Einarsson et al., 1981; Einarsson and Eiriksson, 1982).

4.3 Summary

Good constraint was obtained for the radiation patterns of 178 small earthquakes located within the Hengill area. Of these, 50% were interpretable as demonstrating shear movement on fault planes, 40% as movements normal to the fault plane (tensile cracks) and 10% did not fit either interpretation, and may have been intermediate events.

Preferential orientation of the dilational fields of the tensile crack events indicates a direction of horizontal N 125° E for the least compressive stress (σ_3) in the seismic volume. That these events occur at depth in the earths crust indicates that σ_3 must be negative and large enough to outweigh the overburden pressure of several kilometers of rock. The shear events observed indicated strike slip and normal movements and an orientation of the axes of principal stress consistent with that demonstrated by the tensile crack events.

The tensile crack events were confined to the high temperature geothermal area. The ratio of tensile crack type events to shear events was greatest in the interior of the high temperature area where the heat loss is highest, and was lower in peripheral areas. Outside the high temperature area faulting was almost entirely shear. The tensile crack events indicate a strong tensional stress regime, but their occurrence also appears to be dependent on some high temperature geothermal process. Normal shear faulting was almost absent in Ölfus. The events for which focal mechanism solutions were obtained occupied the depth range 2 – 6 km. There was a tendency for the tensile crack type events to occur at greater depth than the shear events beneath the high temperature geothermal area. This may indicate that the conditions under which tensile crack type events form occur preferentially at greater depth within the seismic volume. The Klambragil data group exhibits activity at anomalously shallow depth and a very high proportion of tensile crack type events. The strike slip shear events of Ölfus occur to greater depths than earthquakes occurring N of 64°N.

During the 3 month recording period tensile crack type events were confined to small magnitudes and accounted for only 5% of the seismic strain release. This is consistent with the hypothesis, but not proof that such events are confined to small magnitudes.

The tensile crack events were interspersed with shear events in space, and also the two types were seen together in sequences. It was concluded that the shear events represented movements on fault planes connecting the tensile cracks, a process originally hypothesised by Hill (1977). The deduction of the direction of least compressive

stress from the orientation of the tensile cracks, allowed the fault plane of the strike slip shear events to be identified as primarily the NS striking one. In the case of the mixed earthquake sequences this implies that activity occurs on right laterally arranged en echelon tensile cracks connected by NS orientated shear fault planes. The combined trend of the whole activated zone would then be expected to be more northerly than that of the tensile cracks. This is consistent with observations of the trend of surface tectonic features. Extrapolation of these deductions to the Ölfus area indicates that the type of faulting there may be right lateral strike slip on NS orientated planes. This is consistent with the mode of faulting of the South Iceland Seismic Zone.

5. TELESEISMS AND EXPLOSIONS

5.1 Teleseisms

5.1.1 Introduction

During the 90 day period of recording on the radio telemetered seismometer network in 1981, 21 well recorded teleseisms were monitored. Teleseismic arrivals approach recorders at steep angles, and hence sample the crust beneath the stations at much greater depths than local or regional seismic sources. The absolute travel times of such events to stations are of little use in examining local anomalies, since they contain perturbations (due to mislocation of the hypocenter, lateral variations in the earth`s velocity structure etc.) that may be much larger than the expected variations due to local anomalies.

However, the differences in arrival time of an event at the various stations of an array are mostly influenced by conditions immediately beneath the array and may be interpreted in terms of local structure. This treatment of teleseismic arrival time data is known as the method of relative delays.

5.1.2 Delay measurement

Paper playouts of the teleseismic records were made on a scale of 5 cm:1 sec. In order to measure the relative onsets of the first P arrival as accurately as possible, a "typical" P waveform was selected for each event. This was traced onto transparent paper and the first arrival marked. The tracing was then superimposed onto the waveforms recorded at all the other stations for that event and the picking of the rest of the first arrivals aided by comparison of the total waveform. The absolute arrival times of the first P-wave onsets at the stations were thus measured. This picking method is reported by Corbishley (1969) and Savage (1979) to give the best accuracy.

The theoretical arrival times of the events at the stations were calculated using programme MANETA (Savage, 1979). This programme reads in the station and source locations (the source locations were taken from the Preliminary Determination of Epicenter (PDE) listings of the U.S. Coast and Geodetic Survey (USCGS)). It calculates epicentral distances, and estimates P- and PKP- travel times by referencing the Herrin travel time tables (Herrin et al., 1968). Corrections are calculated and applied for the earth`s ellipticity and the station height above datum (sea level). In order to make the latter correction the average velocity of that part of the crust above

sea level was required. A velocity of 3.0 km per sec. was used since this was the value obtained by Palmason (1971) for the surface layer in Grafningur (Profile 42) and was shown to be a reasonable average by refraction shots fired in 1981 (see Section 5.2 and Appendix 1. Program MANETA is described in detail by Savage (1979).

The "raw delay times" were then obtained by subtracting the calculated theoretical arrival times from the observed. According to Long and Mitchell (1970), each raw delay time may be expressed as the sum of six terms:

$$T = S + To + Te + Tt + Ti + e$$

where
T   is the raw delay time
S   is the delay due to material with anomalous velocity beneath the station.
To   arises from errors in the earthquake focal data,
Te   is the delay due to material with anomalous velocity beneath the source,
Tt   is the error due to inaccuracies in the travel time tables and calculations,
Ti   is the instrumental delay for which correction may be made, and
e   is the error due to misreading and poor timing of the seismogram.

This may be expressed as:

$$T = S + E$$

where
E is a composite error term (= To + Te + Tt + Ti + e)

For a single event, the value E will be approximately the same at all stations, because for a very distant event the source to station path is virtually the same except for directly beneath the station network. S will vary from station to station due to velocity anomalies directly beneath the station array. Each event will be associated with a different E value. The S-value profile across the station network will also vary for the different events because the events approach the stations from different azimuths and angles and hence sample different portions of the volume beneath the station array.

In order to calculate S-values, i.e. the delays associated with anomalous material directly beneath the stations, the programme SEPD (which is described in detail by Savage, 1979) was used. This

programme reads in all the raw times and calculates least-squares values for the error terms E and the station delays S. An arbitrary zero was declared for the station delay at KDN. In order to examine azimuthal variation in the station delays, the events were grouped according to geographical location of the sources and separate runs of SEPD were made.

5.1.3 Discussion of the results

Fig. 5.1 is a stereographic plot of the world coastlines centred on Hengill, and drawn out to 90°. The locations of all the teleseisms used in this study are plotted. Lower hemisphere epicenters are indicated by crosses. These events are all in the Tonga-Fiji area. The epicenters fall roughly into four groups :-

- Europe and W Asia
- Japan - Kuriles
- West Indies - Atlantic
- Tonga - Fiji

In the case of the latter two groups, P-wave onsets were poor.

The angles of incidence of the incoming rays varied from 32° to 10° with increase in epicentral distance, but was, for the majority of rays, in the region 27° to 15°. This is illustrated in Fig. 5.2.

In Table 5.1 the relative station delays are listed, calculated using all events equally weighted. As was mentioned above, an arbitrary zero was assigned to KDN, this station being peripheral to the main area of interest. Because of this arbitrary zero, the error associated with each station delay does not indicate significance (or insignificance) in that delay in an absolute sense, but only relative to the other stations.

e.g. Stations KKA and KHE:

delay KKA - delay KHE = +0.02 sec
error KKA + error KHE = ±0.05 sec

hence the station delays calculated for KKA and KHE are not significantly different.

However, in the case of stations KHE and KST:

delay KHE - delay KST = -0.11 sec
error KHE + error KST = ±0.05 sec
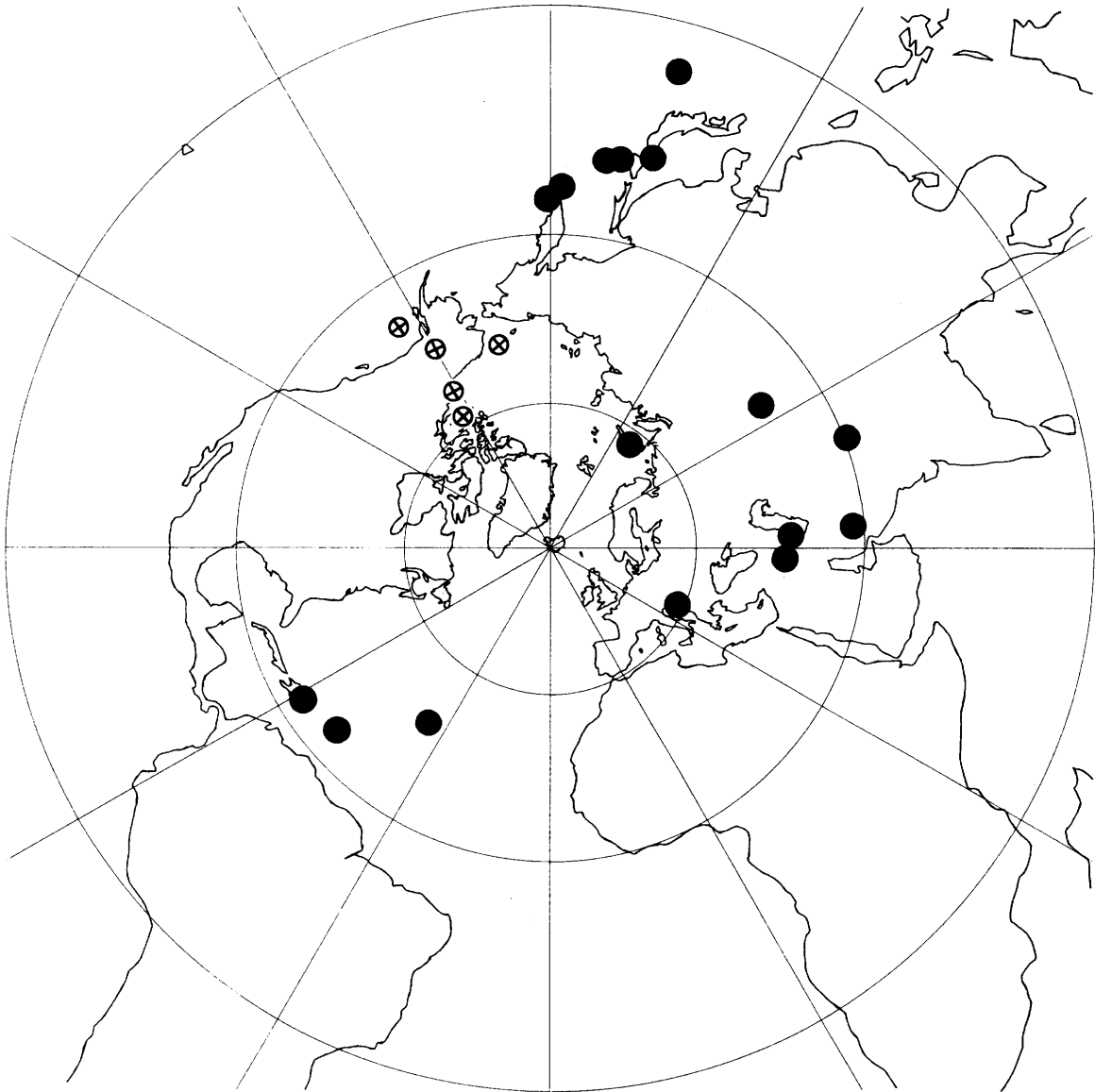
Fig. 5.1   Plot   of   world   coastlines   and   teleseism   locations   in
stereographic projection centred on the Hengill area.
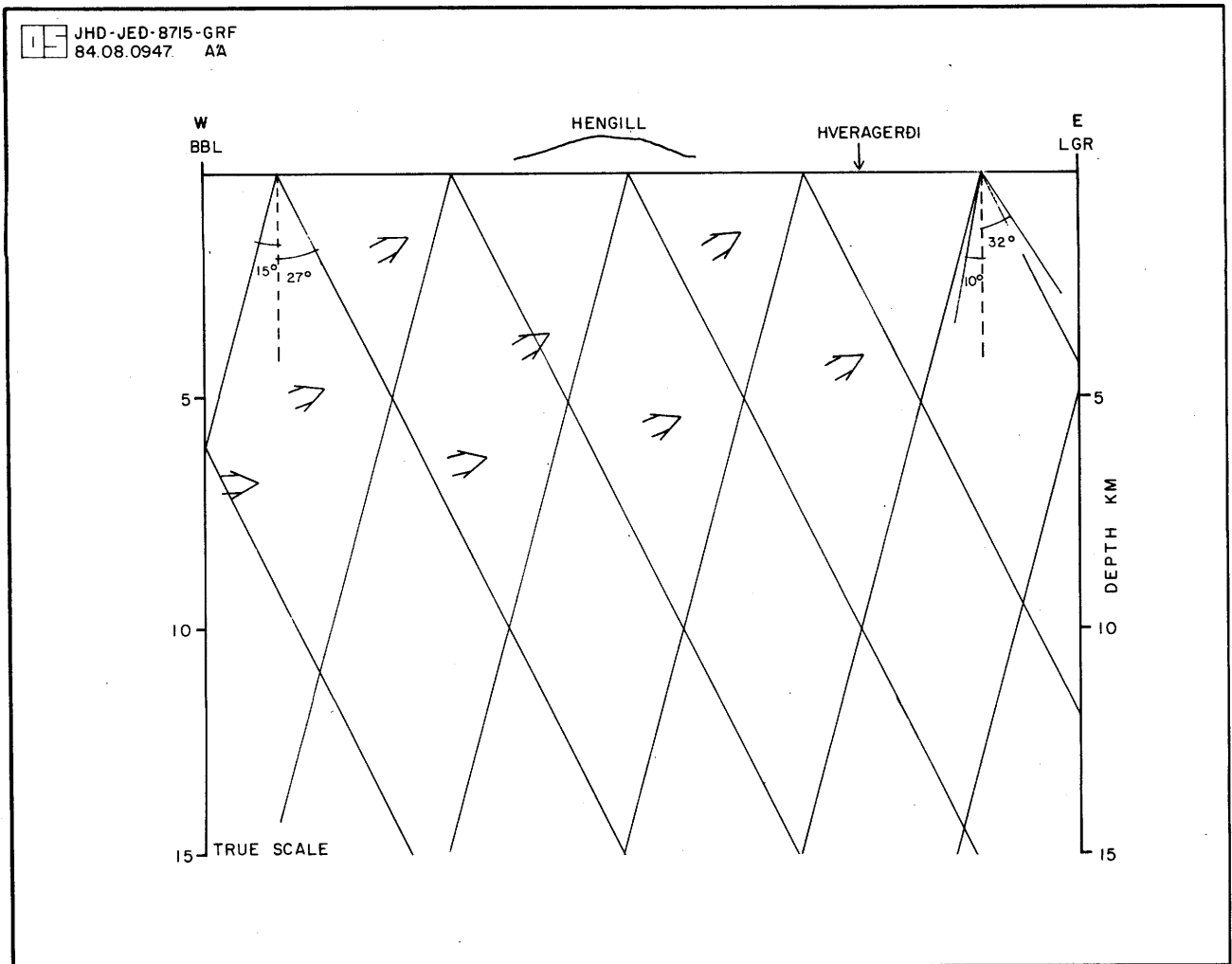
Fig. 5.2 WE cross section of the Hengill area showing angles of incidence
of the teleseismic and regional explosion arrivals.

hence the station delays calculated for KHE and KST are significantly
different.

Fig. 5.3 is a contoured plot of the delays listed in Table 5.1.   The
features displayed by this Figure reflect some kind of average
structure for the volume beneath the station array down to
indeterminate depth, since the different rays used to calculate each
relative station delay sampled slightly different portions of the
volume (Fig. 5.2).   It should also be borne in mind that the scale of
resolvable structures is limited by the wavelength of the incoming
rays, which is about 6 km in this case.

Station Name	Delay time (sec)	no. of events	error (sec)
BBL	0.01	9	0.03
BHU	-0.12	15	0.02
BSL	-0.04	12	0.02
BVA	-0.06	13	0.02
BLA	-0.05	10	0.02
BEN	-0.03	14	0.02
BMO	-0.04	17	0.05
KST	0.07	13	0.03
KDN	0.00	21	0.02
KKL	-0.04	18	0.02
KDL	-0.04	14	0.02
KDA	-0.05	19	0.02
KMI	0.09	15	0.01
KHE	-0.04	14	0.02
KHA	0.03	16	0.02
KKA	-0.02	14	0.03
KSA	-0.08	10	0.02
LBO	0.07	9	0.02
LDY	-0.02	17	0.02
LLA	0.02	15	0.01
LGR	-0.04	11	0.02
LDJ	-0.04	17	0.02
LKA	-0.09	15	0.02

Table 5.1 Station delays calculated using all 21 events

The broad picture that emerges from Fig. 5.3 is that positive delays
(= low velocity (Vp)) are associated with Nesjavellir, Hengill and
Ölfus relative to Húsmúli and the area N of Hveragerði (respectively W
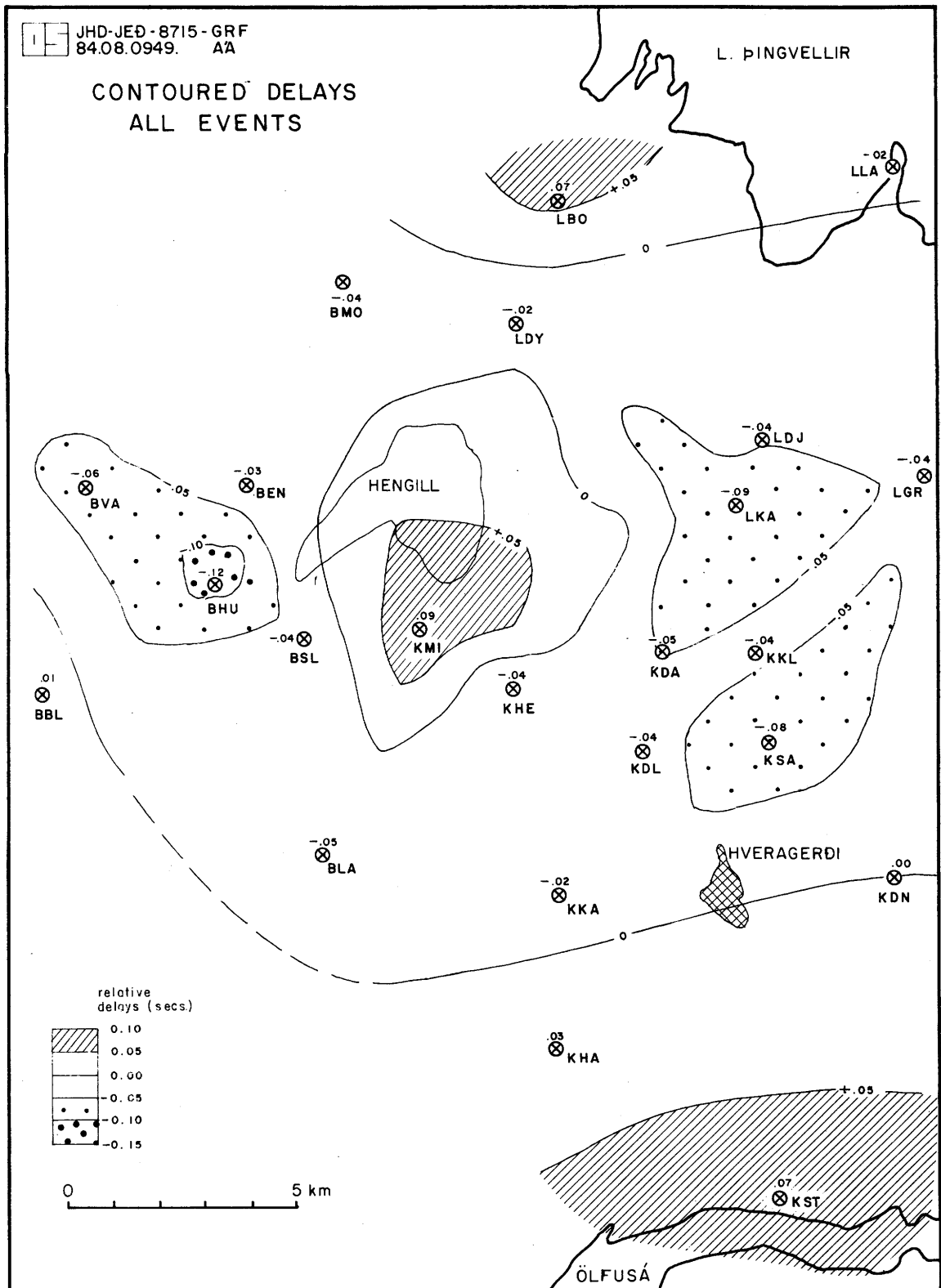
Fig. 5.3   Contoured plot of teleseismic delays.

and E of Hengill). The maximum relative delay is associated with KMI, directly S of Hengill, which is about 0.2 ± 0.03 sec slow compared with BHU to the W and LKA to the E. The gradient of the delay contours is steeper to the W than to the E. The shape of the positive delay anomaly associated with KMI is not well constrained to the N because no stations could be deployed on or to the N and E of Hengill, but it does not extend as far as the station LDY. Passing further N to station LBO, N of Nesjavellir, the delay is seen to increase again. It is possible that a low velocity anomaly is associated with Hengill that is cut off from a more northerly anomaly of unknown extent in the fissure swarm that extends little farther S than Þingvallavatn. That the positive anomaly associated with KMI does not extend very far S is fairly well constrained by the stations BLA and KHE. The areas of relatively early arrivals to the W and E of Hengill are fairly well constrained by several stations in each case.

This picture remains constant if the data set is narrowed down to the best arrivals only, or subdivided into azimuthal groups. Thus it very likely shows real relative arrival time variations over the Hengill area that are of the scale of the resolving limit of the seismic waves (∼6 km diameter).

In Fig. 5.4 the relative delays associated with different azimuths have been plotted for each station. Positive delays (low Vp) relative to the arbitrary zero are plotted as solid lines and negative delays (high Vp) as dashed lines. The length of the ray path drawn is the projection onto the surface of the ray paths down to approximately 10 km, and the lengths of the "delay lines" are proportional to the size of the relative delays.

In order to obtain depth constraint on the structures causing the relative delays, azimuthally separated delays must be examined where ray paths cross, and attempts made to maximise consistency in the data by varying the depth of the delay lines. In Fig. 5.4 the mid points of the delay lines are projected at 5 km depth. Projection at greater depths would result in the mid points of the delay lines migrating outwards from the station along the ray paths.

It can be seen by inspection of Fig. 5.4 that fairly good consistency of the data is displayed. In the region of the KMI positive anomaly, rays approaching BSL and BEN from the E exhibit positive delays relative to those from the N and SW. Rays approaching stations LDJ and LKA from the SW, and KDA and KKL from the N exhibit positive delays whereas those from other azimuths exhibit negative delays. This may be an indication that the negative anomaly in the area N of Hverageröi does not extend much farther W than the stations LDJ and
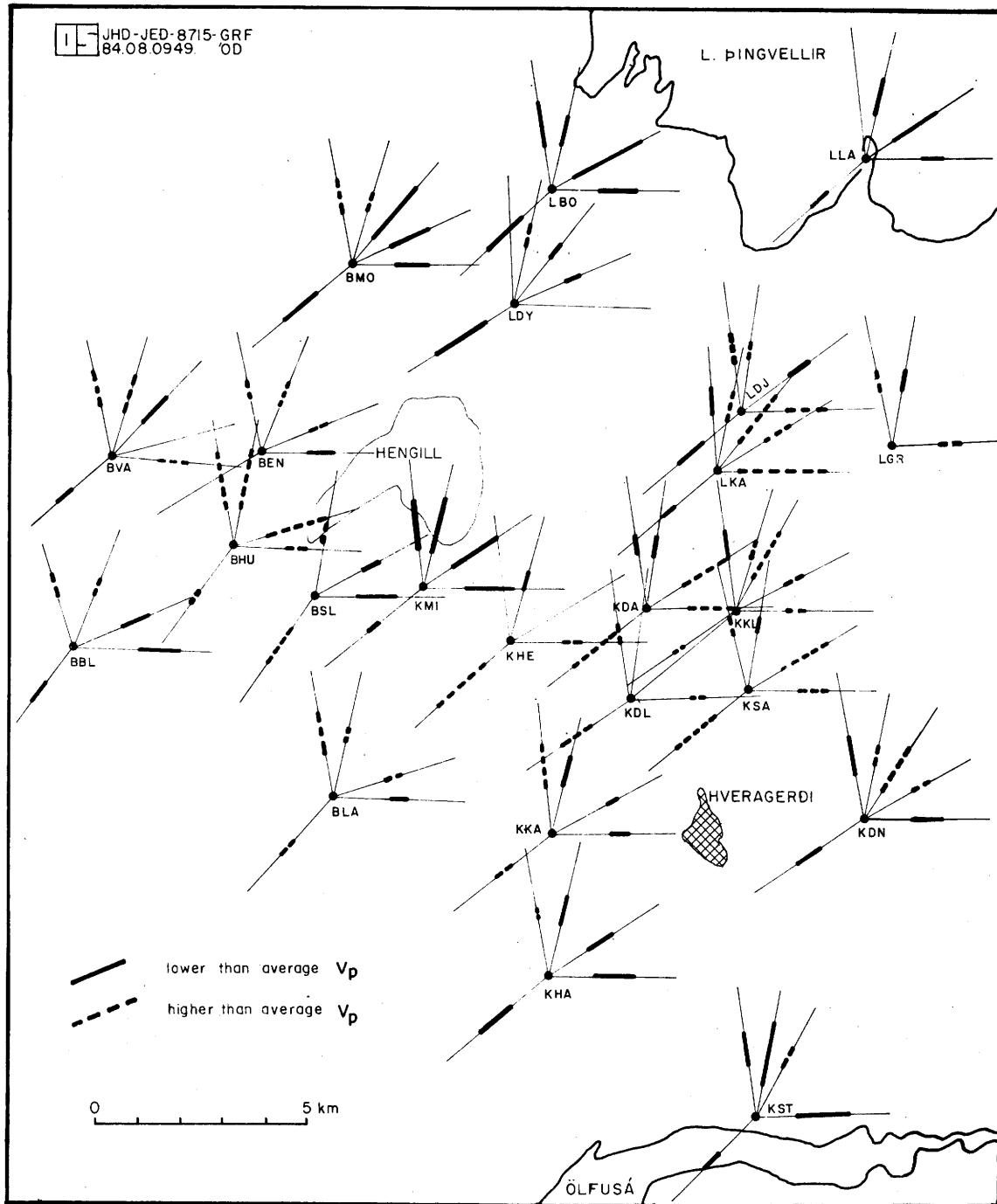
Fig. 5.4   Azimuthal plot of teleseimic delays.

LKA.

It can also be seen from Fig. 5.4 that a progressive increase of the projection depth of the delay lines would not significantly change the consistency of the data until about 15 km depth, when deterioration would begin. This is most easily seen in the area of the KMI positive anomaly because of its limited areal extent. There is also the possibility that the anomalies apparent in the data result from structures at different depths. If variation in the relative depths of the anomalous structures is also allowed then it becomes practically impossible to place any depth constraint on them. However, if it is assumed that the anomalous structures are all at approximately the same depth, then it may be concluded that they are likely to be shallower than 15 km.

5.2 Explosions

5.2.1 Introduction

During the period of deployment of the radio telemetered network, five explosions were made. Three of these were located within the Hengill area, and two at more distant sites. They were, respectively, the Ölfus, Djáknapollur, Þingvallavatn, Grænavatn and Reykjavík explosions. Their coordinates are given in Table 5.2.

5.2.2 Delay measurement

The crustal model used to locate the local earthquakes, referred to here as the Hengill-South Iceland crustal model, is an average model that fits the observational data of a number of refraction profiles made in the Hengill area and South Iceland by Palmason (1971) (see Appendix 1). In order to test the locator procedure for accuracy the 3 local explosions were located using the Hengill-South Iceland model and HYPOINVERSE. The results of this are shown in Table 5.2, and give some idea of the accuracy of the earthquake locations discussed in Section 2.3.2. It should be pointed out, however, that if one assumes that the majority of the error in the earthquake locations is due to the departure of the real crustal structure from the model, then the relative locations of events in a small area will not be significantly affected, only the absolute location of the group.

All five explosions were located a second time, using the true location as a trial hypocenter. The first iteration of the programme was printed out (see Appendix 1) which listed calculated travel times to all the stations from the true locations, and the differences between these and the observed travel times. These delays give information about the departure of the Hengill-South Iceland crustal model from the true.

For the three local explosions, 59 travel times were observed. The average delay for all 59 observations was +0.01 sec. This indicates that in general the Hengill-South Iceland crustal model contained slightly too high velocities. Expressed another way, the upper 3 km or so (Fig. 5.7) of the crust in the Hengill area exhibits slightly lower seismic velocities than is average for the Hengill-South Iceland region.

explosion	co-ordinates	HYPOINVERSE location	error in location	epicentral distance from stations km
Ölfus	63N56.27 21W09.50	63N56.39 21W09.18	400m to NE	0.3-22.8
Djáknapollur	64N05.17 21W10.10	64N05.02 21W09.92	320m to SE	0.2-16.1
Þingvallavatn	64N09.07 21W11.40	64N09.07 21W11.40	none	3.7-20.5
Grænavatn	63N53.05 22W03.40		-	32.9-54.5
Reykjavík	64N11.07 21W51.12		-	22.1-43.6

Table 5.2 1981 explosion data

In order to examine lateral variations in crustal structure within the area, a ray diagram is presented in Fig. 5.5. Here the ray paths are projected onto the surface as lines. Positive delays, (i.e. late arrivals, indicating Vp lower than defined in the Hengill-South Iceland crustal model) are indicated by solid lines placed at the mid point of the ray path, with length proportional to the size of the delay. Negative delays (i.e. early arrivals, indicating Vp higher than defined in the Hengill- South Iceland crustal model) are indicated by dashed lines. Fig. 5.5a shows the delays measured for the 3 local explosions.

In the case of the two regional explosions, the velocity structure of the crust between the shots and the Hengill area is known to be different from that defined in the Hengill-South Iceland model. In the case of the Grænavatn explosion, this resulted in systematic early arrival of the waves by about 0.28 sec at the stations of the network. In order to correct for this a 0.28 sec delay was added to all delays calculated. This gave an average delay of zero for the stations that recorded the shot. In the case of the Reykjavík explosion, waves recorded arrived at the stations progressively earlier with increasing distance from the shot point. Hence a correction was made to the arrivals that was proportional to distance. The relationship used was:

108

HENGILSSVÆÐI EXPLOSION DELAYS

GRÆNAVATN AND REYKJAVÍK EXPLOSION DELAYS

JHD-JED-8715-GRF
84 02 0232

HVERAGERÐI

Vp lower than average
Vp higher than average

0   5 km
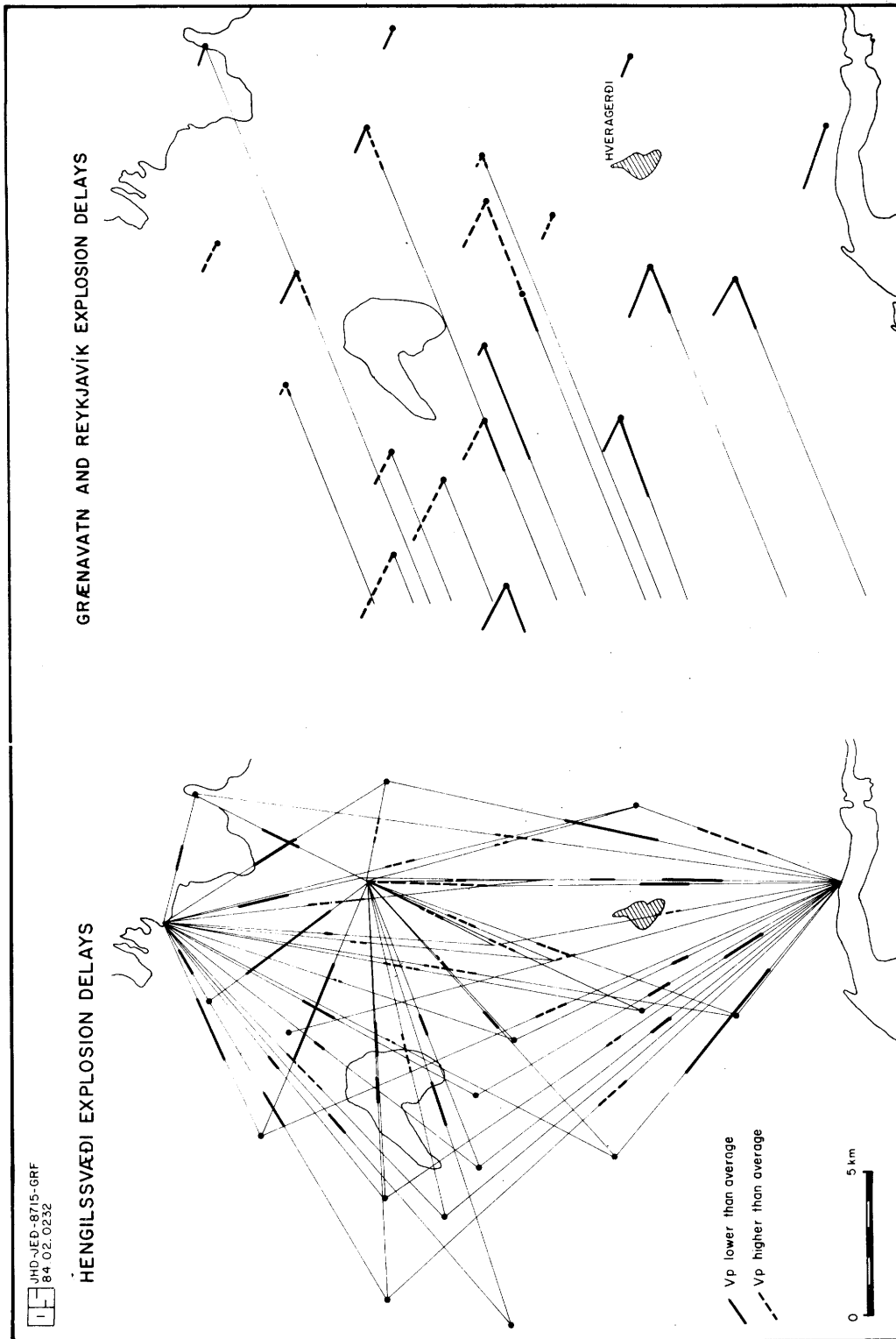
Fig. 5.5   Ray diagram of explosion data (a) the local explosions, (b) the regional explosions.

correction factor(sec) = 1.52 - 0.0243 x epicentral distance (km)

This relationship is a least squares linear fit to the observational data, and yielded a correlation coefficient of 0.84 (see Fig. 5.6). The 1.52 sec threshold is arbitrary since the shot instant was not recorded for this explosion. Application of correction factors calculated by this formula gave an average delay of zero for the stations that recorded the shot.

The corrected delays are plotted in Fig. 5.5b. In examining Fig. 5.5, it should be borne in mind that the delays from the 3 local, the Grænavatn and the Reykjavík shots are all relative to different crustal models and their magnitudes are hence not directly comparable. However, the variation in the delays over the area within each of the 3 data groups are comparable.

5.2.3 Discussion of the results

The depth of penetration of the rays increases with increasing ray path length in the manner shown in Fig. 5.7. This Figure shows the maximum depth of penetration against shot- reciever distance for the Hengill-South Iceland crustal model. This penetration depth would be achieved beneath the shot- station mid point. The majority of the ray path will, of course, pass through the crust at shallower depths than the maximum. At shot-receiver distances greater than 4.5 km the rays will penetrate deeper than 1 km and in the range 9-25 km the depth of penetration will be 2.5 - 3.5 km with a considerable portion of the ray path falling in this depth range. The regional shots, that were 22-55 km distant from the receivers penetrated up to 9 km depth, though not beneath the Hengill area. Approximate path trajectories for the regional events are shown in vertical cross section in Fig. 5.2.

It can be seen in Fig. 5.5a that for the local shots the negative delays (Vp higher than average) mostly cluster in the area to the N of Hveragerði, whereas positive delays, sometimes relatively large, are restricted to the Grafningur - fissure swarm - Ölfus zone. This strongly indicates the presence of a body N of Hveragerði that exhibits higher seismic velocities than those of the surrounding areas. Because of the great variation in the shot-receiver path lengths, firm depth constraint cannot be placed on this body by the simplistic treatment of the data presented here. However, it can be said that the majority of the rays penetrated the crust in the range 1-3.5 km, and the fact that great consistency is displayed despite the variation in penetration depth strongly indicates that a real anomaly is present.
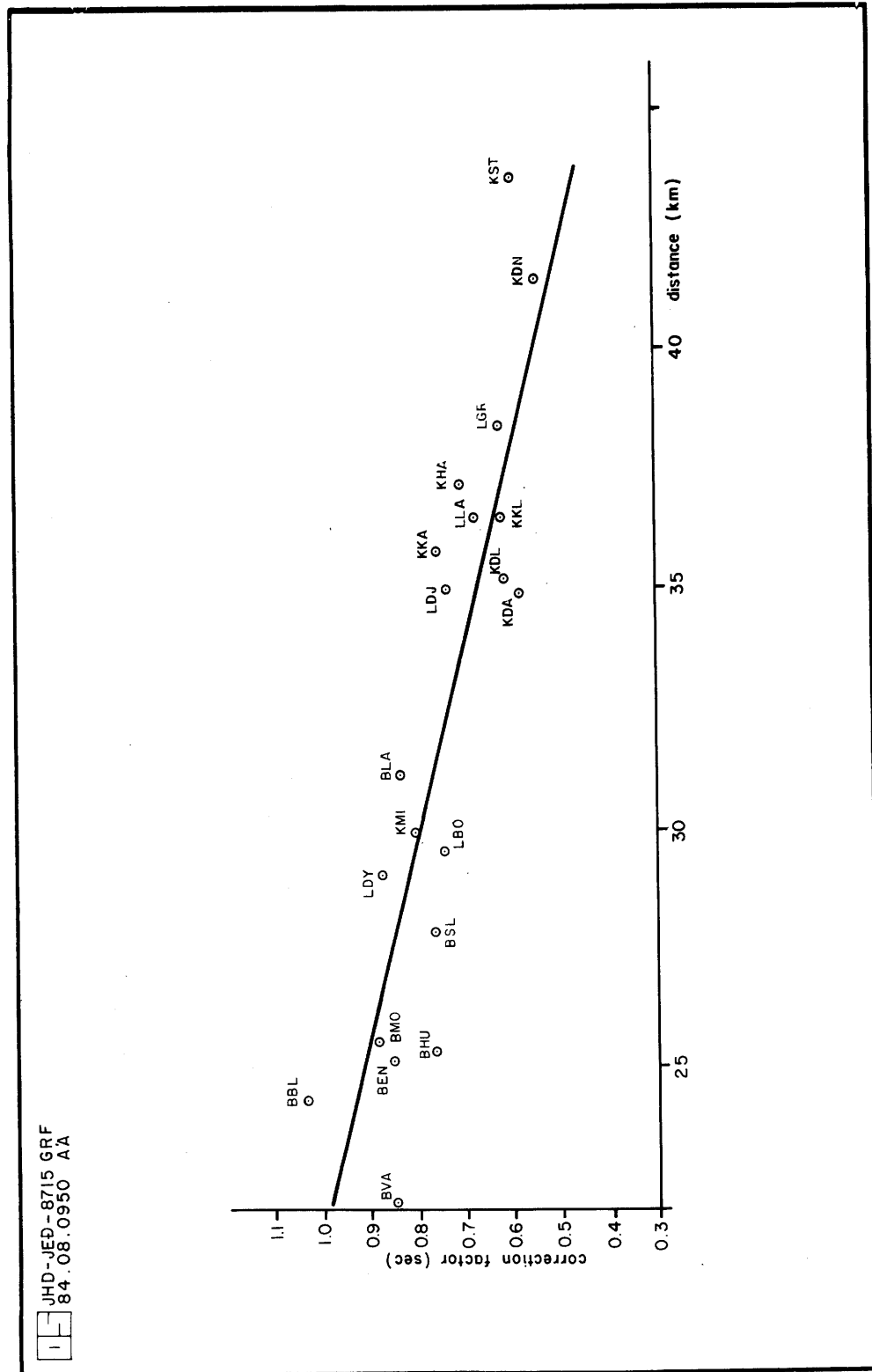
Fig. 5.6   Correction relationship applied to the arrival times of the
Reykjavík explosion data.
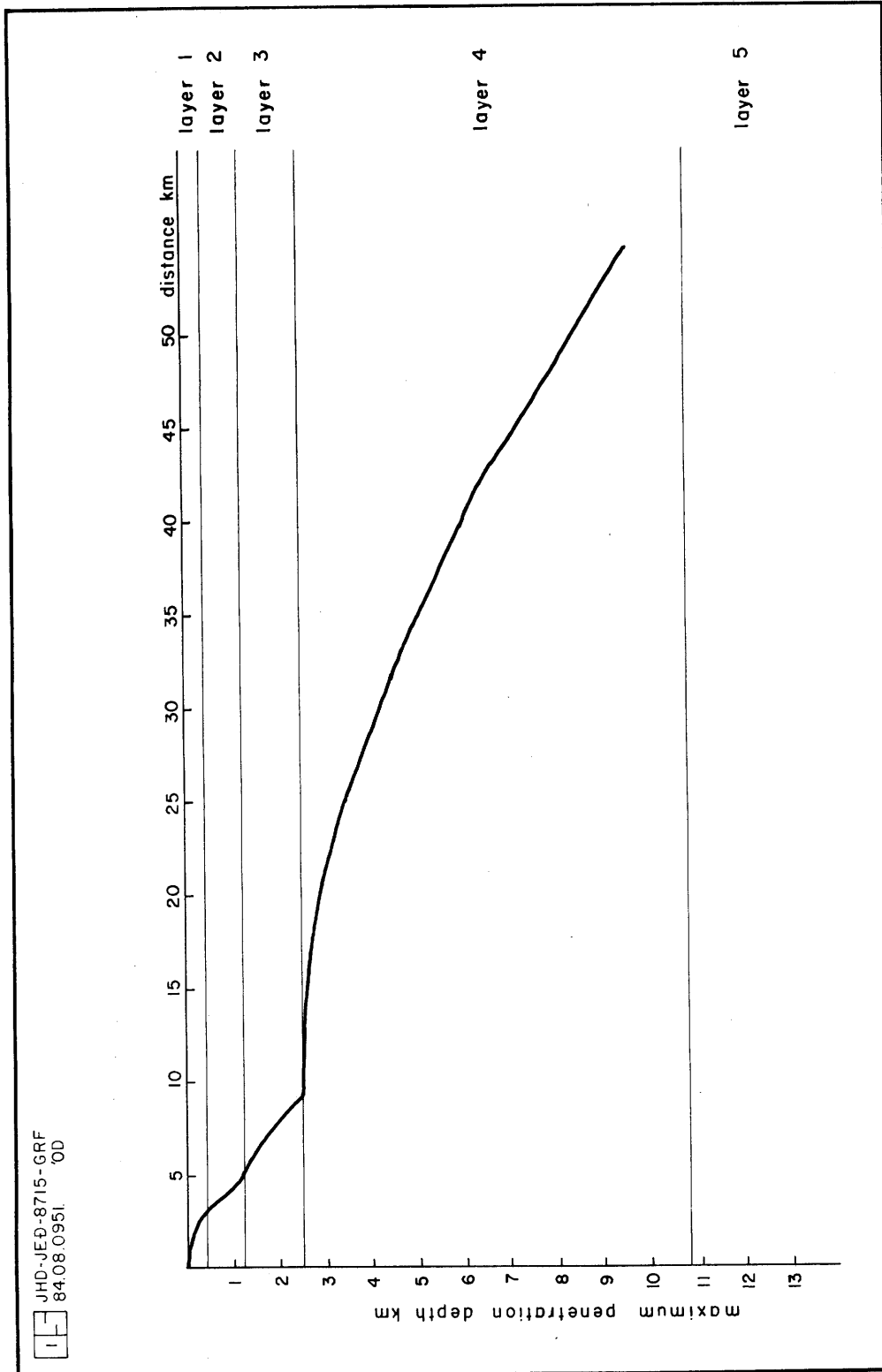
Fig. 5.7 Plot of source – reciever distance : maximum penetration depth for a surface source and the Hengill – South Iceland crustal model.

In the case of the regional event delays presented in Fig. 5.5b a similar pattern is observed. Rays recorded at the stations immediately N of Hveragerði appear to have an enhanced apparent velocity relative to those recorded at stations in the Grafningur - fissure swarm - Ölfus zone. An exceptionally low apparent velocity is associated with the station KMI for the ray approaching from the SW. In addition, a high apparent velocity is displayed by rays recorded by the stations W of the fissure swarm, especially those in the Húsmúli area. The data are again highly consistent.

In conclusion the local and regional explosion data indicate a body in the area N of Hveragerði that exhibits high Vp relative to that of the Grafningur-fissure swarm-Ölfus zone. In addition, the presence of a relatively high velocity body is indicated beneath Húsmúli. Accurate depth constraint cannot be placed on these bodies, but the majority of the ray paths beneath the Hengill area lay in the range 2-5 km.

5.3 Synthesis

A superficial perusal of data from teleseismic sources and local and regional explosions indicates a consistent pattern of relative seismic delays over the Hengill area. On average the seismic velocities of the near surface rocks of the Hengill area are slightly lower than is average for the Hengill - South Iceland region. Seismic velocities in the area to the N of Hveragerði and the Húsmúli area are high relative to the Grafningur - fissure swarm - Ölfus zone, and exceptionally low velocities are associated with bodies of rock beneath N Nesjavellir, Hengill and Ölfus. That this general pattern is exhibited by all the data sets suggests that the bodies associated with these velocity contrasts may extend from near surface to several kilometers depth.

The local and regional explosion data indicate that velocities vary from the average by ± 5% in the upper few kilometers. In the case of the teleseismic data slightly higher velocity contrasts are required at depth if the whole anomaly is to be accommodated in the upper 10 km or so of crust. Velocity variations of ± 10% from the average at depth were taken in the model presented here.

A suggested interpretation of these data is shown in Figs. 5.8 and 5.9 which are, respectively, a WNW cross section S of Hengill and a SSW cross section longitudinal along the fissure swarm (see Fig. 5.3). The velocity in the depth range 0-2 km is allowed to vary by ± 5% and that in the range 2-10 km by ± 10%. Velocity gradations doubtless occur, but are not shown in these simplistic cross sections. The main features exhibited are:

(a) A `chimney` of low velocity material rising beneath Hengill, flanked to the W and E by high velocity bodies. The low velocity body may widen with increasing depth, and underlie the area to the E (i.e the area N of Hveragerði).

(b) The low velocity body associated with Hengill is not continuous along the fissure swarm but disappears in the area of the fissure swarm between Hengill and Þingvallavatn

Because the sizes of the bodies exhibiting anomalous velocities could not be resolved, neither could the absolute velocity contrasts. The model presented above is one possible model that could account for the observations. Smaller bodies (not less than 6 km in diameter) and larger velocity contrasts would also produce the same delay data.

The relatively high velocities may indicate dense, intrusive, relatively cool material, and the low velocities low density, younger eruptives at shallow depth possibly underlain by partial melt.
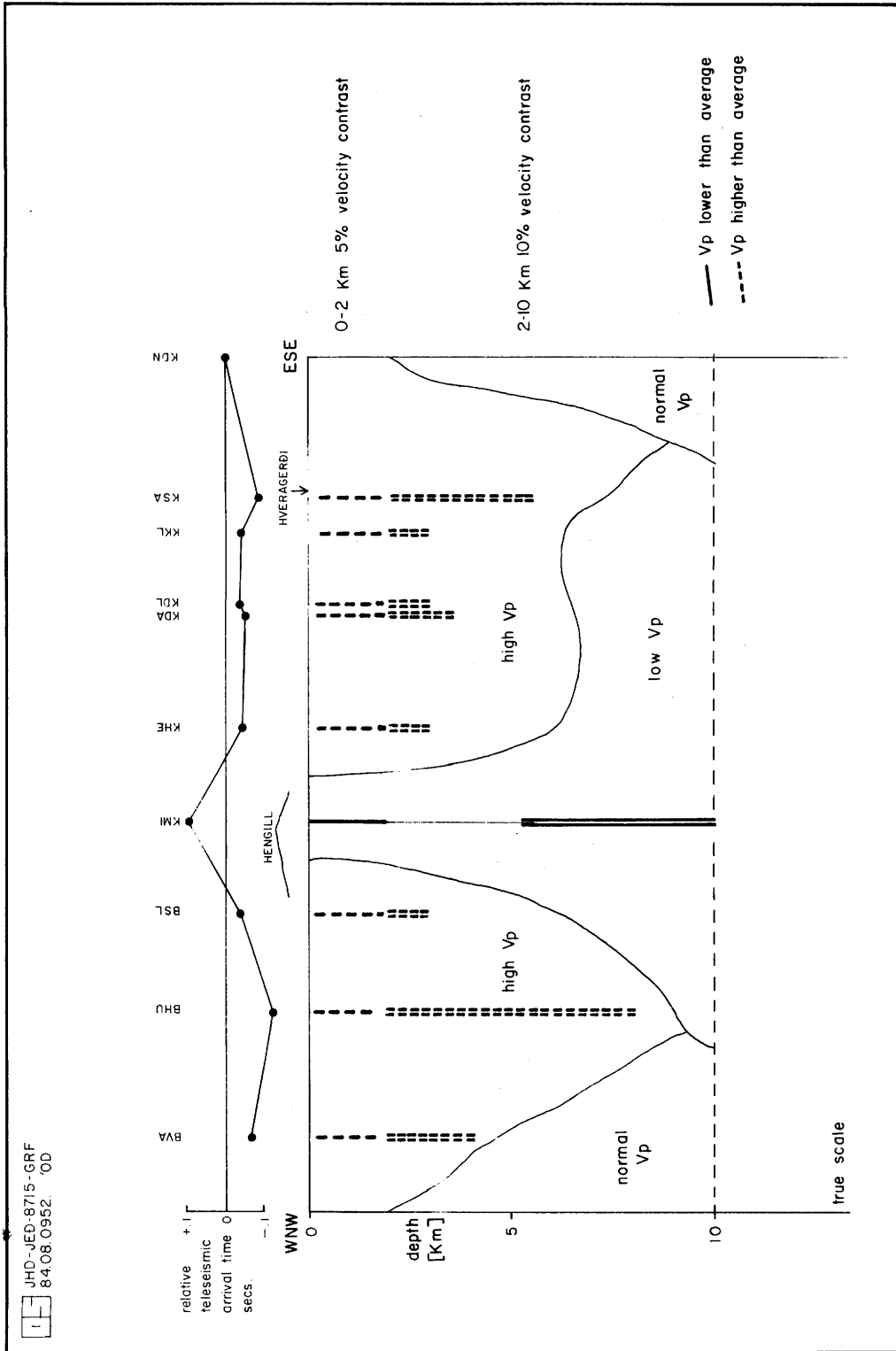
Fig. 5.8   WNW – ESE cross section of the Hengill area S of Hengill illustrating the proposed model of the teleseismic and explosion delay data.

115
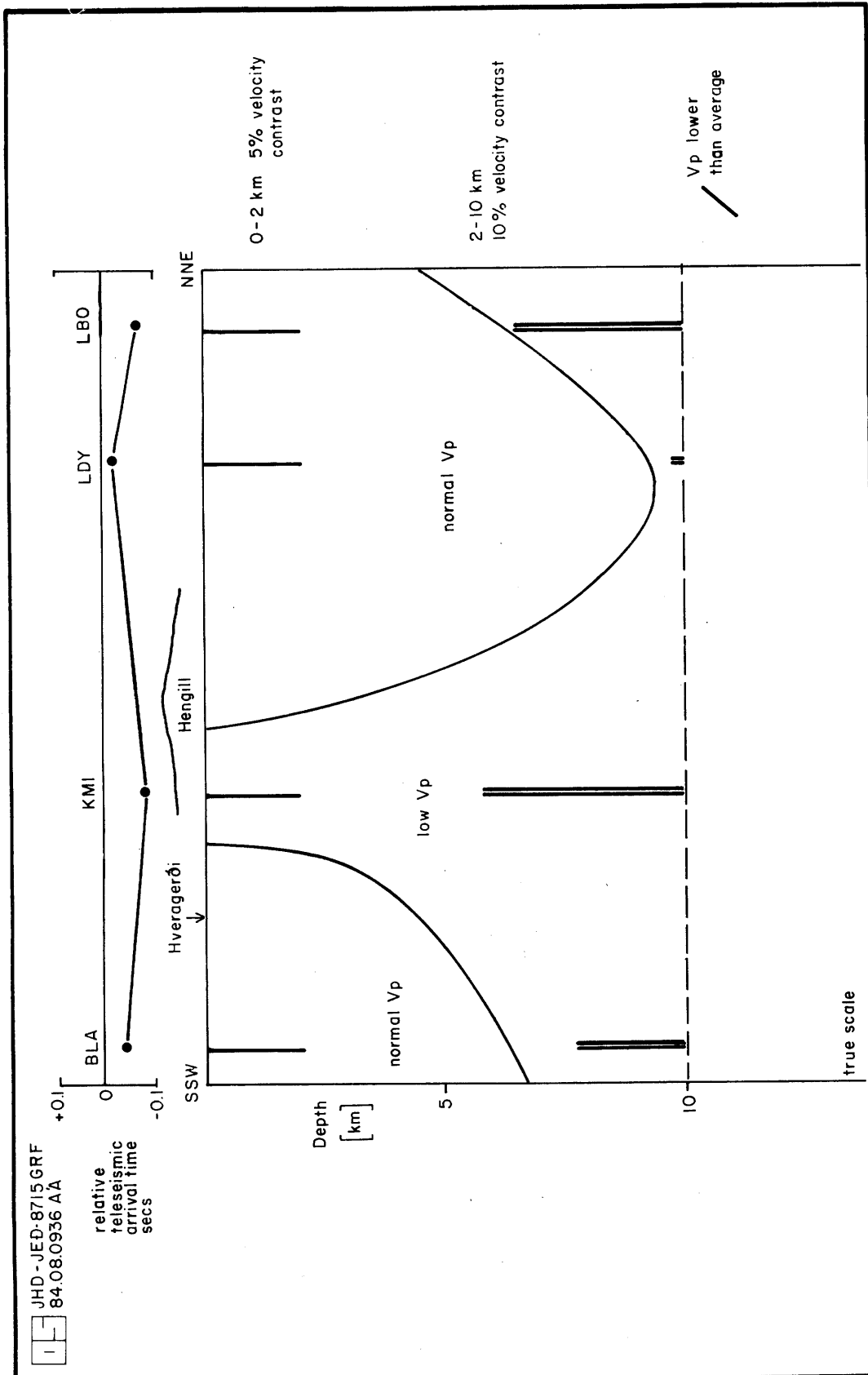
Fig. 5.9   SSW - NNE cross section of the Hengill area along the fissure swarm illustrating the proposed model of the teleseismic and explosion delay data.

6. SYNTHESIS

6.1 Summary of the results

The seismicity of the Hengill area has been investigated in the magnitude range -3 to 6+. Large magnitude activity is confined to Ölfus, whereas persistant, ongoing, small magnitude seismicity characterises the high temperature geothermal area. The majority of this activity occurs in a 20 km^2 area NW of Hveragerði. Clustering was also observed on a smaller scale during the 1981 monitoring project. Continuous low magnitude earthquake activity delineated small volumes within the geothermal area, of which the Klambragil subcluster was most notable. Earthquake activity in the fissure swarm, the most intensely faulted part of the area, was rare except in Nesjavellir, where the earthquake epicentral trend defines a linear zone at depth 3.5-7 km. Ongoing seismicity was also associated with the Mosfellsheiði area, W of Hengill, and the Ölfus area, where a swarm of over 100 events was recorded near Kirkjuferjuhjáleiga. Epicentral depths of the located events mostly occupy the range 2-6 km.

The Hengill area exhibits a b-value of 0.74 ± 0.06 in the magnitude range -0.9 ≤ M_L ≤ 5.5. This is significantly lower than comparable values obtained for the Reykjanes Peninsula and the Borgafjörður areas. Separate calculation of the b-value for small subdivisions of the area showed that its value does not vary significantly within the Hengill area except on Mosfellsheiði, where a value of 1.0 ± 0.18 was obtained, and for the deeper events in general where a value of 0.86 ± 0.14 was calculated. With the data available no significant variation of b-value with time could be found except that associated with the Kirkjuferjuhjáleiga, Ölfus swarm of Sept. 1981. A decrease of b was observed during the early part of the swarm, with a subsequent return to a normal level. Historical evidence indicates that activity of magnitude 6 and higher is confined to Ölfus. It is argued that earthquakes occuring within the high temperature geothermal area may be restricted to magnitudes considerably lower than this.

For the data collected on the radio telemetered network, a focal mechanism study was possible. 178 well-constrained solutions were obtained, of which only 50% were consistent with a source involving shear slip on faults. The anomalous events are characterised by expanded compressional quadrants, which implies a net explosive source. These events are interpreted as being generated by tensile crack formation at depth. They were interspersed with shear events. Both the tensile crack and shear type events indicate an orientation of about NW for the direction of least compressive stress σ_3 and

variation from horizontal NE to vertical for the direction of greatest compressive stress $\mathcal{G}_1$. This is consistent with the regional and local tectonics. Comparison of the two types of event enabled the NS striking plane to be identified as the fault plane in the case of the strike slip shear events. This is consistent with the mode of faulting observed in the South Iceland Seismic Zone.

The tensile crack type events were confined to the high temperature geothermal area. Their relative proportion to shear events was greatest in the interior of the area, and lower in peripheral areas. Outside the geothermal area in Ölfus events were shear type without exception. There is a tendency for the tensile crack type events to occupy a deeper zone than the shear type events. The observations were consistent with tensile crack type events being restricted to small magnitudes.

A relative delay time analysis performed on teleseismic data collected on the radio telemetered network revealed features with dimensions approximately equal to the wavelength of the signals used. The Húsmúli area and an area N of Hveragerði were associated with relatively early teleseismic arrivals (high Vp), and the Grafningur - fissure swarm - Hengill - Ölfus zone with relatively late arrivals (low Vp). The maximum difference in average arrival time between stations was about 0.2 sec. These delays are probably associated with structures shallower than 15 km. Three local and two regional explosions were detonated during the 1981 field project, sampling the crust beneath the Hengill area down to about 5 km depth. The deviations of the observed travel times to the stations of the radio telemetered network from the expected were assessed and showed results consistent with those of the teleseismic study.

A possible interpretation of the teleseismic and explosion data combined was presented. The observations may be accounted for by velocity deviations of $\pm$ 5% from the average for the depth range 0-2 km, and $\pm$ 10% for the depth range 2-10 km. A "chimney" of low velocity material underlies Hengill, widening at depth, and flanked to the W and E by bodies with higher velocities. The low velocity material may not continuously underlie the fissure swarm, but be connected at depth to low velocity volumes associated with Grafningur and Ölfus. The data might alternativly be explained by smaller bodies and larger velocity contrasts.

6.2 A structural model for the Hengill area

6.2.1 Broad structure as indicated by previous work

A discussion of previous geological and geophysical work in the Hengill area is given by Foulger (1984). The broad picture that emerges from the application of many research methods to the Hengill area involves an extinct volcanic centre (herein referred to as the Grensdalur volcanic centre) located in the area N of Hveragerði, and an active one beneath Hengill (the Hengill volcanic centre). Volcanic activity is thought to have been transferred from the Grensdalur centre to the Hengill centre early in the Bruhnes geomagnetic epoch, about 700,000 yrs ago. Geochemical, hydrological and borehole studies indicate that the high temperature geothermal area may be fed by two separate heat sources, one associated with the presently active Hengill centre and the other with the cooling remnant of the extinct Grensdalur centre. Geochemical data indicate the possibility that a third, minor heat source may be associated with the Klambragil area.

6.2.2 The transverse structure

A transverse structure that runs from Mosfellsheiði in the W, SE to Ingolfsfjall has long been recognised. It is orientated approximately normal to the fissure swarm, transects Hengill and passes through the Grensdalur area. From NW to SE it is delineated by hyaloclastite ridges, fissures, erosional features (Kýrgil and Klambragil), a topographical high (Ölkelduhals) and changes in surface fault trends.

It is proposed here that this transverse structure represents the trajectory of migration of the Grensdalur volcanic centre off the accretionary plate boundary to its present site N of Hveragerði.

The presence of a volcanic centre on an accretionary plate boundary affects the development of the area locally in two ways. Firstly the axial stress field of the spreading plate boundary will be modified by a radial field associated with the volcanic centre, and secondly volcanic production both intrusive and extrusive may be enhanced in the immediate vicinity of the centre, resulting in the formation of a topographic high.

The local modification of the stress field will cause local variations in the trend of features such as dykes, faults and fissures whose orientation is governed by the orientation of the principal axes of stress. The stress trajectories resulting from the superposition of a relatively weak radial tensional stress field (associated with the central volcano) onto a strong axial tensional stress field

(associated with the fissure swarm) is illustrated schematically in Fig. 6.1.

The relative strength of the tensional stress in the direction normal to the fissure swarm is not greatly influenced by the addition of the weak radial field. However, in the longitudinal direction the proportional increase in the strength of the tensional stress field is large. It might be expected that weak tensional features orientated in a direction normal to the fissure swarm might develop under such circumstances (faults, fissures and dykes).
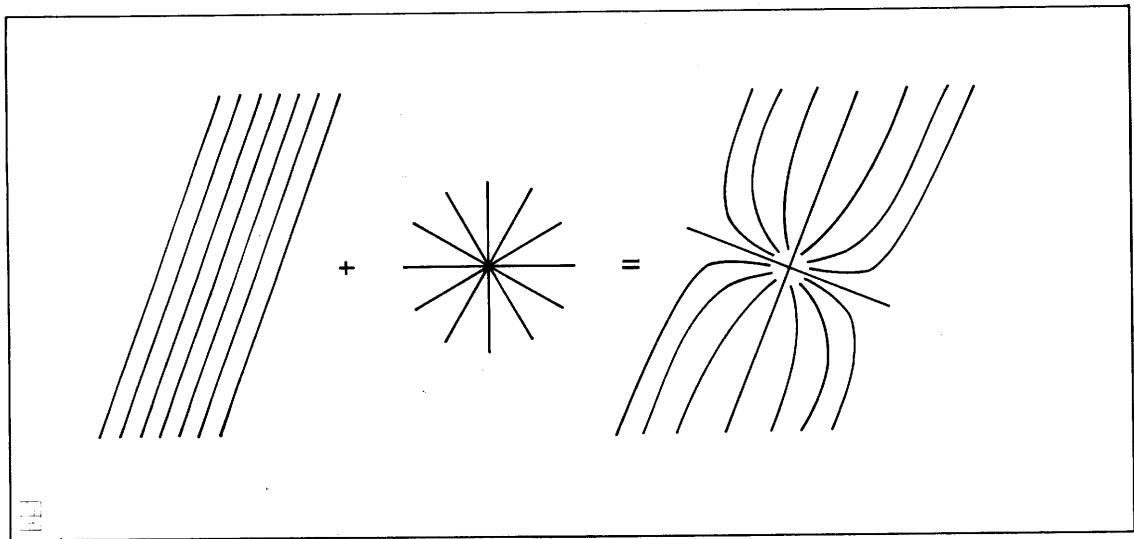
Fig. 6.1 Pattern of principal stress trajectories caused by the addition of a radial and a linear stress system (after Odé, 1957).

Whilst still active the site of the volcanic centre will be marked by a topographic high. After extinction its erosion will contrast with that of the surrounding areas because of its contrasting structure. Initially it will erode down faster than the surrounding areas because of its greater elevation. In later stages a fast erosion rate may be maintained by its elevated temperature, which speeds up chemical decomposition and enables the process of progressive fracturing by the action of groundwater (Section 6.2.3). This may result in the old volcanic centre being represented by a topographic depression in its final stages. Erosional features associated with faults, fissures and dykes will mirror their trends, and hence may exhibit a component

normal to the old spreading direction as well as parallel to it.

It is proposed here that in the Hengill area, NW-SE orientated tectonic features have formed in response to the modified stress regimes in the neighbourhood of the volcanic centres. In the NW these are recent tectonic features associated with the presently active Hengill volcanic centre, and in the SE they are erosional features associated with the extinct Grensdalur volcanic centre. A high volcanic production rate in the neighbourhood of the presently active Hengill centre has resulted in the build up of a topographic high whereas in the case of the extinct Grensdalur volcanic centre erosion has been speeded up by geothermal processes and the centre is marked by a topographic depression. Because the Grensdalur system is a remnant volcanic centre that drifted off axis with the E plate, and was replaced in the same location by the Hengill centre, its trajectory is parallel to the spreading direction and colinear with the transverse tectonic features of both volcanic centres described above. For this reason the transverse structures associated with the two volcanic centres are colinear and form a single, long, well developed structure.

In Fig. 6.2 a position for the axis of this structure is proposed based on the locations of surface tectonic features. Its strike is N 125°E. This is parallel to the direction of σ_3 inferred by the tensile crack type earthquakes observed in this area (Section 4.2.1).

As would be expected, volcanic activity associated with the Grensdalur centre continued longest on its NW margin, i.e. on Tjarnahnúkur, near Klambragil.

6.2.3 Cooling rock

It has been proposed that the penetration of water into hot rock boundaries is the mechanism by which heat is removed from hot rock intrusions at depth. Circulating groundwater causes rapid cooling, and small cracks form, continuously expanding the system of circulation channels and maintaining close contact between the groundwater and the retreating hot rock boundary (Björnsson et al. 1980).

This process can account for the very large heat losses observed over geothermal areas such as Yellowstone and Grimsvötn, which cannot be explained by thermal conduction alone. Also direct observations of the Heimey lava flow indicate that this process is probably occurring there. That background small magnitude seismicity is commonly observed in geothermal areas is in agreement with the hypothesis that the process may occur seismically. Where focal mechanism studies have been
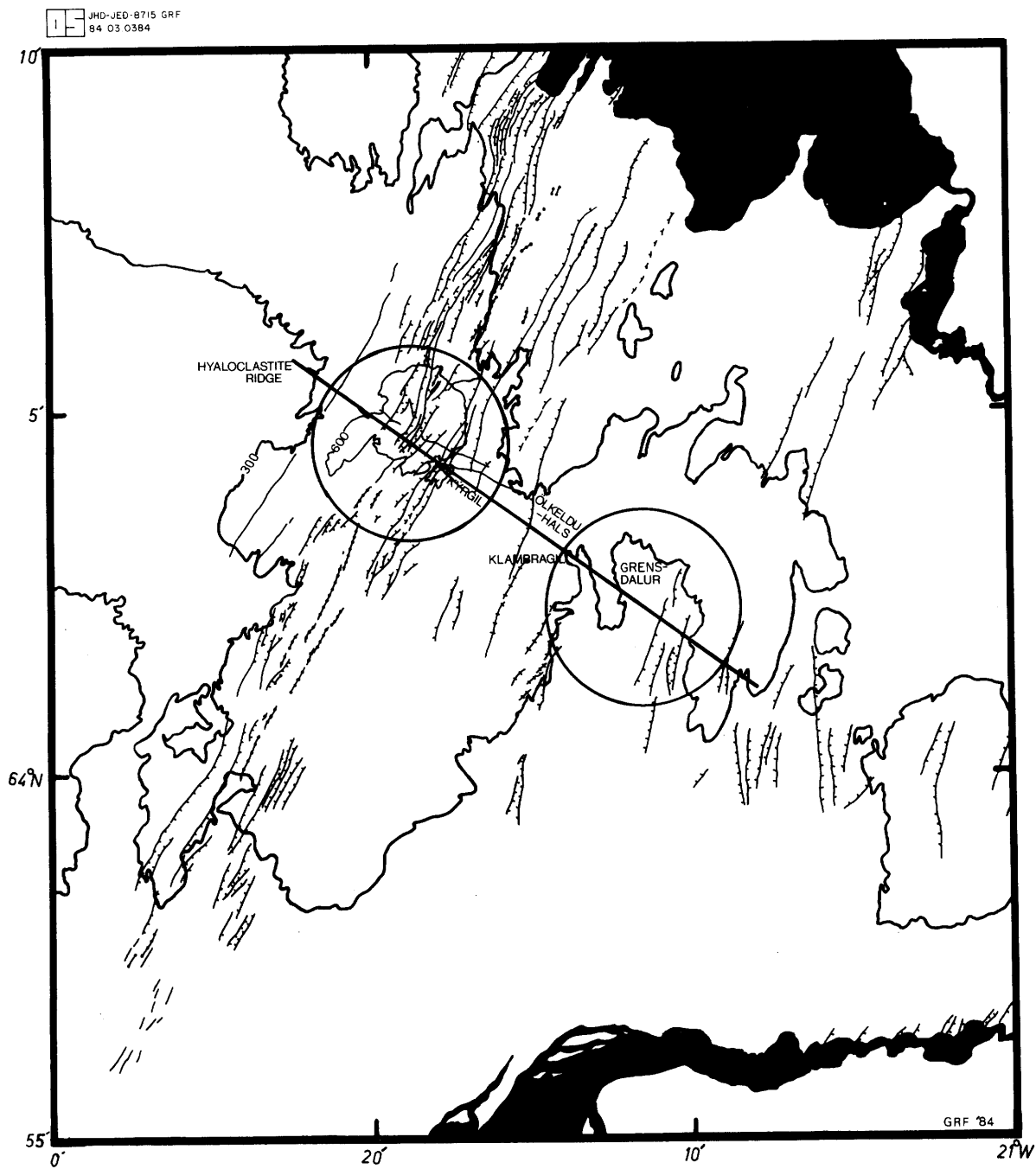
Fig. 6.2   Map of the Hengill area showing the proposed locations of the
double volcanic system and the transverse structure.

conducted, strain release is generally observed to conform with regional tectonics.

The seismicity of the Hengill area is consistent with this picture. The level of seismicity over the area correlates positively with surface heat loss. The area sits astride an accretionary plate boundary where strong extensional tectonics are displayed and over the high temperature geothermal area the mode of fracturing is predominantly tensile crack type. Observations conform with the theory that the tensile crack type events are confined to small magnitudes. In that case the larger magnitude events known to occur within the Hengill high temperature geothermal area may be shear type events associated with tectonic movements.

The spatial distribution of the tensile crack type events may thus be looked upon as a map of rapidly cooling volumes of rock that feed surface heat loss. In the case of the Hengill area they occur beneath the whole of the high temperature geothermal area. Heat is thus not only being removed from volumes of rock beneath Hengill and the fissure swarm, as may have been envisaged in the past, but also from beneath the area to the N of Hverageröi, supposedly the site of the extinct Grensdalur volcanic centre. This volume may not be the hottest heat source (Section 6.2.1) but the fact that it is the most active seismically indicates that it is probably delivering the most heat (or put another way, it is the fastest cooling down). In detail, small volumes were detected which exhibited especially high seismicity. These volumes may be connected to particularly good aquifers that allow efficient heat removal and hence encourage high seismicity. The most notable of these volumes lies at 3-4 km depth near Klambragil and exhibited a seismic rate of 1 magnitude -1.5 event per day during the 1981 monitoring project. It is possible that this seismicity demarcates a volume that is delivering a particularly large amount of heat and that feeds the intense geothermal displays of Klambragil and Ölkelduhals. This is consistent with geochemical and geological evidence suggesting the presence of a third, minor heat source in this area. The fact that only one out of five of the Mosfellsheiöi events was a tensile crack event implies that this area is peripheral to the high temperature field. This would indicate that the geothermal area is abruptly bounded on its W side.

6.2.4 The volume calculation

The total thermal contraction of the hot rock volume beneath the Hengill area can be estimated. The natural heat loss of the Hengill area is estimated to be 350 MW (Boövarsson, 1951). If attributed to a cooling intrusion, the rate of volume contraction can be calculated

using the equation:

$$\Delta V = \frac{H \, \gamma}{Cp \, \rho}$$

where ΔV is the contraction rate, H is the rate of heat loss, γ is the coefficient of thermal expansion($\simeq 16.2 \times 10^{-6} \, K^{-1}$), ρ is the density($\simeq 3 \times 10^3 \, kg \, m^{-3}$) and Cp is the specific heat of basalt at constant pressure($\simeq 1.3 \times 10^3 \, J \, kg^{-1} \, K^{-1}$). Application of this equation to the Hengill area gives a contraction rate of:

$$\Delta V = 4.5 \times 10^4 \, m^3 \, y^{-1}$$

The approximate volume of the tensile cracks formed seismically can be calculated from their local magnitudes using the relations:

$$\log Mo = 15.1 + 1.7 M_L \quad \text{(Wyss and Brune, 1968)}$$

$$Mo = 2 \mu V \qquad \text{(Appendix 2)}$$

where Mo is the seismic moment, M_L is local magnitude, μ is the rigidity modulus and V is the volume of the crack formed. Fig. 6.3 illustrates the relationship between magnitude and volume diagrammatically (line A). Also plotted in this Figure is the relationship corrected for the b-value of the Hengill area (line B). This shows the volume created per year against magnitude. The result is further corrected by assuming that only 5% of the seismic energy was released in tensile crack formation (line C) (Section 4.2.4). It should be pointed out that because the relationship is logarithmic, the total volume produced by events up to a given magnitude is approximately that of the largest event.

The contraction required to produce the natural heat loss is plotted as a horizontal line at $V = 4.5 \times 10^4 \, m^3 \, y^{-1}$ in Fig. 6.3 (line D). It can be seen that line D intersects line C at magnitude 6.3. This implies that events of up to this magnitude must occur within the geothermal area in order for the contraction predicted by the surface heat loss to be accommodated seismically.

It has been argued in Section 3.2.2.2 that earthquakes occurring in the geothermal area are probably confined to much lower magnitudes. Also the largest event observed with a tensile crack mechanism during the 3 month recording period had a magnitude of 1.2, and there is thus no evidence that tensile crack events occur with magnitudes greater than this. Thus the seismic rate of the geothermal area is insufficient to account for the required contraction rate and suggests
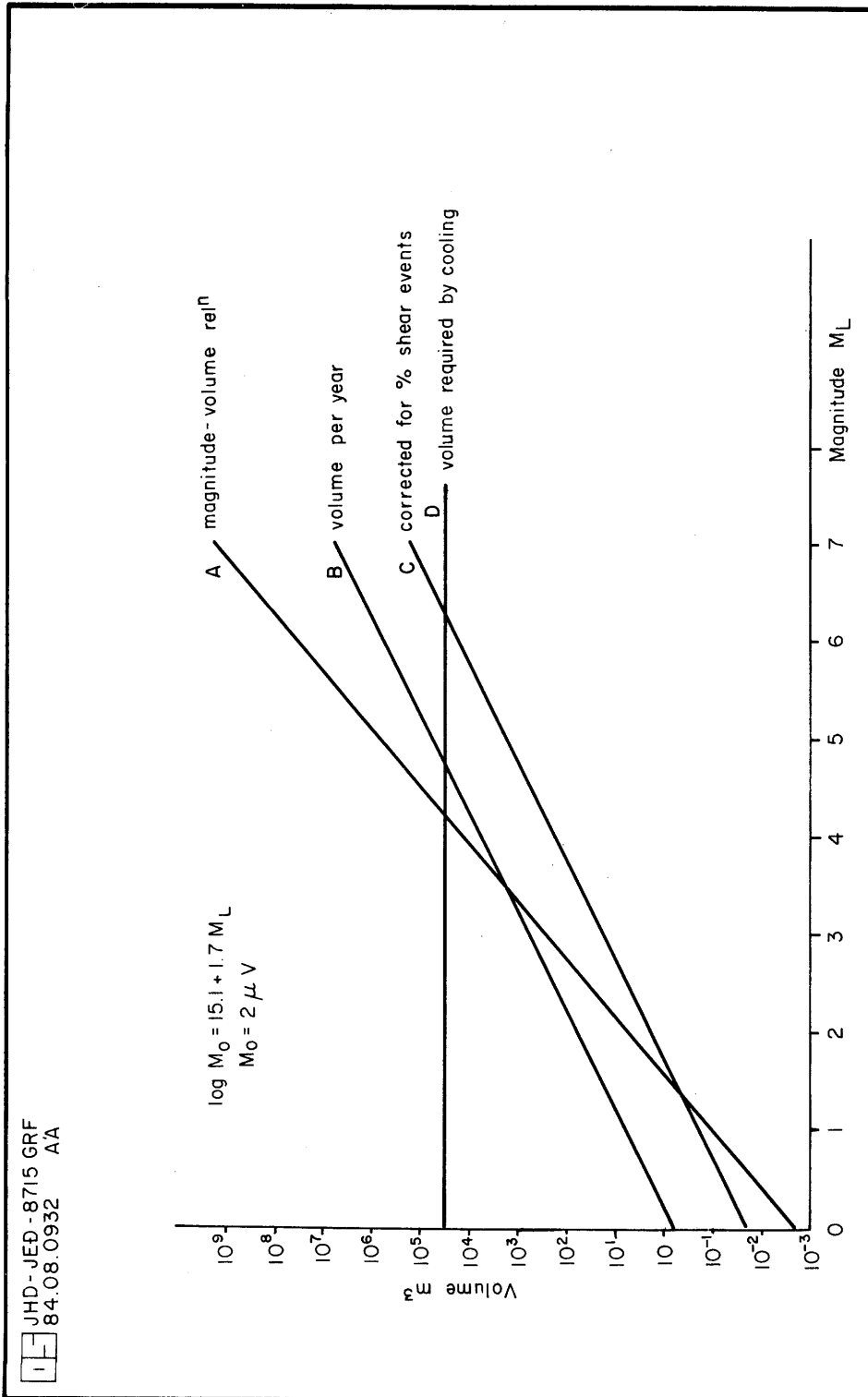
124

Fig. 6.3 Magnitude – volume relationships for tensile crack type
fracturing. See text for explanation.

that only a very minor part of the volume change resulting from the heat loss occurs seismically.

The implication of these facts is that if only a part of the contraction can be accounted for seismically then some, possibly most, must proceed aseismically. One explanation for this is as follows: as heat is removed by circulating fluids, the rock contracts and tensile stress builds up. When this reaches the breaking strength of the rock it fractures, forming a tensile crack which provides a new path for the fluids and enables cooling to proceed more quickly. Contraction due to this subsequent cooling will be accommodated by aseismic widening of the initial fracture and seismic fracture propagation. This process is illustrated schematically in Fig. 6.4.

6.2.5 The double volcanic system

In Fig. 6.2 a proposed structure for the Hengill area is illustrated. A position for the extinct Grensdalur volcanic centre is suggested, based on the geological and geophysical evidence available. This is represented by the SE circle in Fig. 6.2, and encloses the topographic low formed by the valleys Reykjadalur, Grensdalur and Sauðárdalur. The circle indicating the presently active volcanic centre encloses the topographic high of Hengill. The volcanic centres are given diameters of 5 km, based on the extent of their surface features. The axis of the transverse structure connecting their centres is also plotted. In Fig. 6.5, this proposed structure is plotted on a map of epicentres located during the 1981 monitoring project. Most of the earthquake epicentres identified in the area NW of Hveragerði lie within the extinct volcanic centre or on its proposed perimeter. This model implies that the Grensdalur volcanic centre has migrated 7.5 km in a N 125° E direction. If an approximate age of 700,000 yrs is assigned to it, an average migration rate of about 1 cm yr is indicated. This may be taken as a very rough estimate of the half spreading rate of the Western Volcanic zone at this point on the accretionary plate boundary in Iceland.

The spreading rate of the Reykjanes Ridge has been estimated to be about 1 cm per year (Talwani and Eldholm, 1977). Since the accretionary plate boundary in the south of Iceland is double a spreading rate of approximately 1/2 cm per year might thus be a more realistic estimate for the Western Volcanic Zone. The discrepancy between this and the geological estimate may be because the Grensdalur volcanic centre continued to be active until it had migrated several km away from the boundary. The geological estimate is, however, of the same order as the kinematic estimate. This indicates that the Grensdalur volcanic centre was probably transported off boundary by
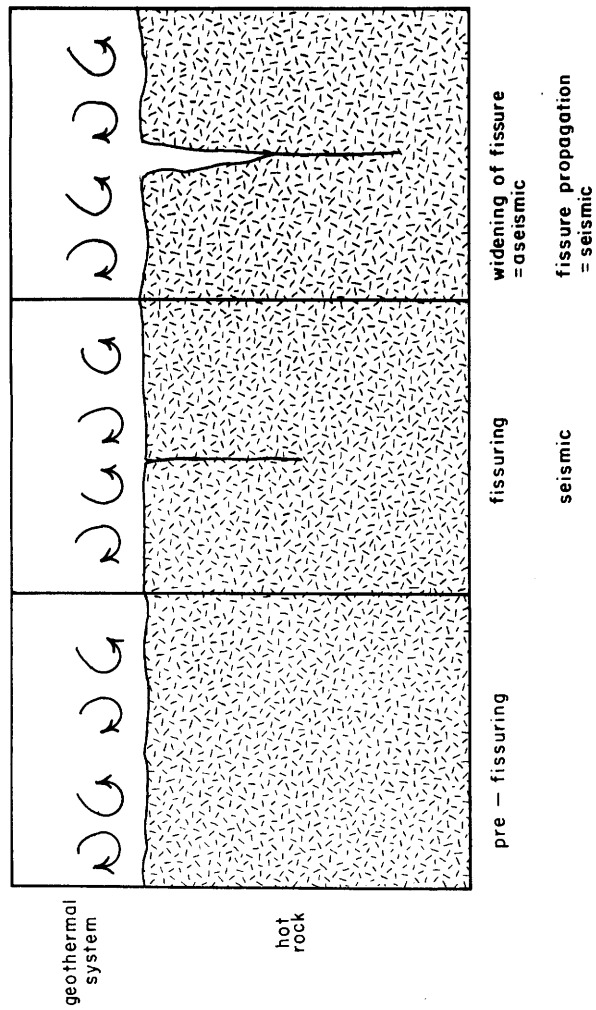
Fig. 6.4 Schematic illustration of the process of fracture formation, propagation and aseismic widening in a fluid cooled, hot rock environment.
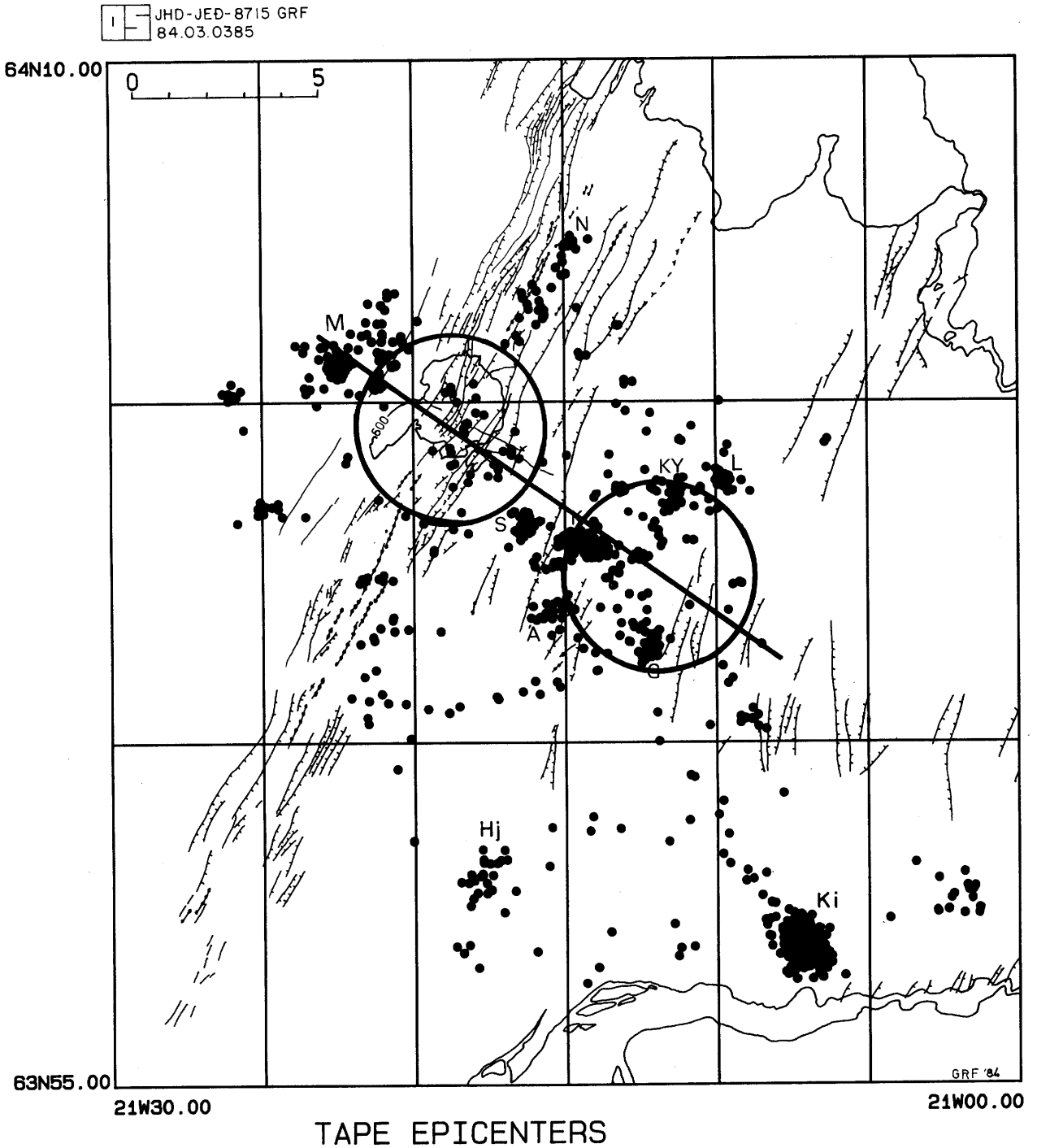
Fig. 6.5   The   double   volcanic system and connecting transverse structure
           plotted on a map of tape data epicentres (see Fig. 2.2).

plate movements and not that the accretionary plate boundary jumped west. It may be estimated that the Grensdalur volcanic centre lay on the accretionary plate boundary 1.4 Ma ago.

6.2.6 Implications for the geothermal reservoir

In Fig. 6.6 a proposed structure for the geothermal area is presented. The extent of the heat sources feeding the geothermal reservoir is outlined. It is suggested here that two major heat sources feed the geothermal area. One heat source is relatively cool and old and is associated with the extinct Grensdalur volcanic centre N of Hveragerði. The other is hotter and younger and is associated with the presently active Hengill volcanic centre. They are possibly connected to each other by a third, minor heat source associated with the Klambragil area. The few hot springs and fumaroles that do not lie directly above these heat sources may be explained by lateral subsurface flow along faults or fissures.

In Table 6.1 a suggested comparison of the two major systems is presented. The characteristics of the third, minor system may be intermediate. It may be noted in Figs. 6.5 and 6.6 that there is a paucity of earthquake hypocentres and hot springs in the E part of the Grensdalur centre. This may indicate that the centre is cooler there than on its W side where volcanic activity continued longer. The nature of the seismicity and the results of the refraction and teleseismic studies indicate that the structure associated with the Hengill centre may abruptly terminate on the W side of the fissure swarm. The heat sources are thus likely to be restricted to the inner part of the area outlined in Fig. 6.6.

The geothermal system of the Hengill area therefore consists of two major separate, merging systems fed by different heat sources and exhibiting different reservoir characteristics, possibly connected by a third, minor source.
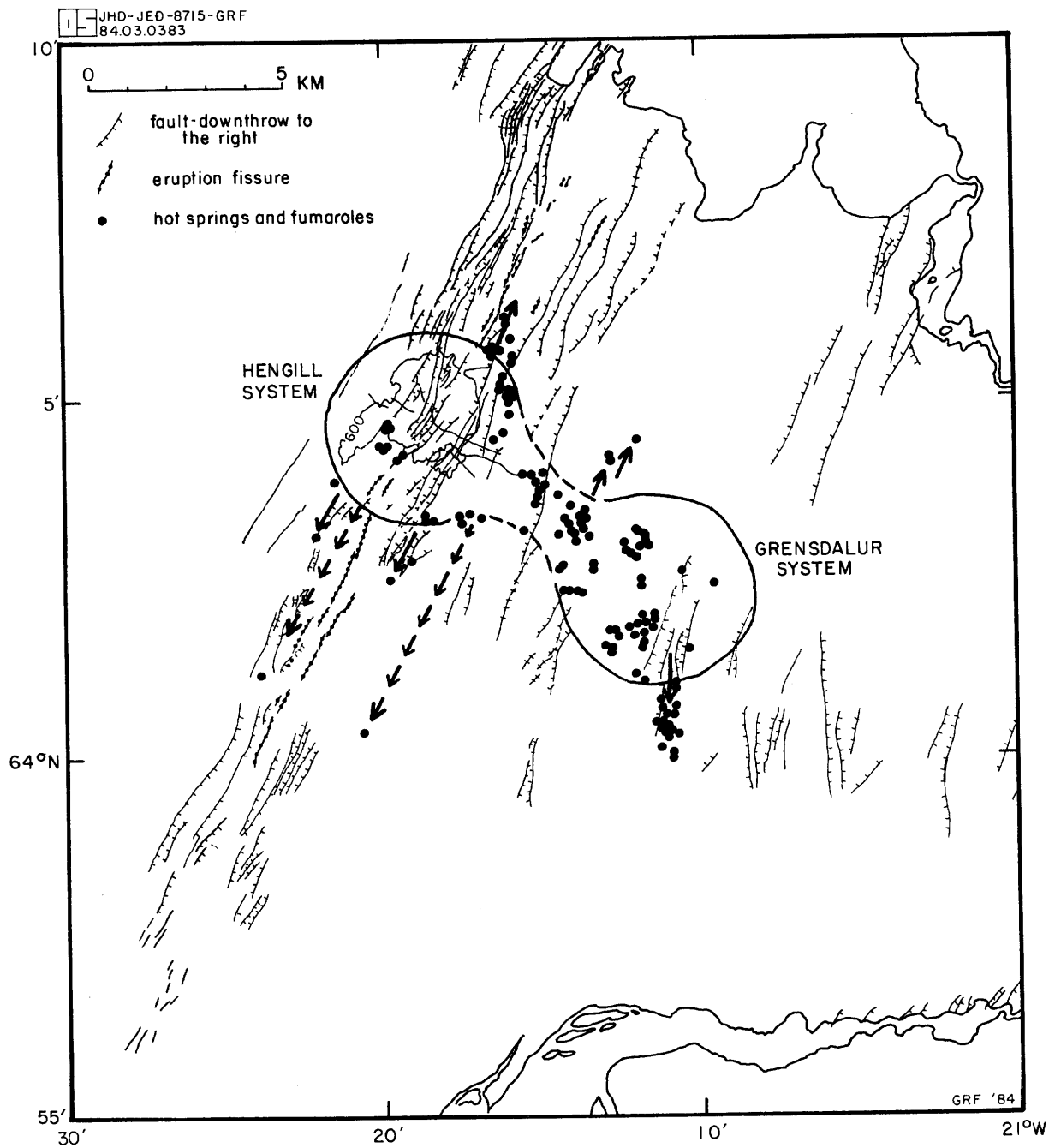
Fig. 6.6   Proposed structure of the high temperature area of the Hengill
area.   The   extents   of   the heat sources feeding the geothermal
fields are outlined and lateral subsurface flow is indicated   by
arrows.

Hengill system		Grensdalur system	
1.	Hot, partially molten source	1.	Hot, solidified source
2.	Periodic magma injections	2.	No periodic magma injections
3.	Reservoir hot	3.	Reservoir cool
4.	Good reservoir "cap"	4.	Poor, fissured reservior "cap"
5.	Thick pile of rock over reservoir	5.	Reservoir deeply eroded
6.	Small surface heat loss relative to heat content of source	6.	Large surface heat loss relative to heat content of source
7.	Periodic rifting episodes forming fissures	7.	No periodic rifting episodes
8.	Heat exchange maintained mainly from below by magmatic activity	8.	Heat exchange maintained mainly from above by groundwater activity
9.	Geothermal swarms and microearthquake activity continuous but infrequent	9.	Geothermal swarms and microearthquake activity continuous and frequent

Table 6.1 Comparison of the Hengill and Grensdalur geothermal systems

6.3 Wider implications

6.3.1 Icelandic geothermal areas

It has been suggested here (Section 6.2.3) that the continuous small magnitude background seismicity of the Hengill area is associated with rock volumes at depth that are cooling and contracting rapidly under the action of circulating ground water and steam. Because the area sits astride an accretionary plate boundary it is subject to a large tensional stress regime. Fracturing in this environment results in tensile crack formation.

The association of continuous background small magnitude earthquake activity and Icelandic geothermal systems has long been recognised (Ward and Björnsson, 1971). It has been argued here that the anomalously high level of seismicity in the Hengill area has much to do with the presence of a double (and therefore unusually large) high temperature geothermal area. The level of activity of the presently active Hengill central volcano-fissure swarm-geothermal system alone is not anomalous when compared with other Icelandic systems. The implication of this is that the background seismicity of Icelandic geothermal areas in general may mark the subsurface areas where heat is being removed from hot rock by circulating groundwater fluids. Perfect correlation with surface heat loss need not be observed since some lateral flow of the geothermal fluids may occur before they reach the surface. Such lateral flow probably does not occur over long distances, however, because of the very strong buoyancy forces associated with high temperature fluids. (The specific gravity of water above the critical temperature, for instance, is about 0.3). The absence of seismicity need not necessarily imply that the rocks in that volume are not hot, but simply that they are not rapidly cooling down (e.g. beneath Hengill).

The question is also raised as to whether tensile crack type seismicity does not occur in other central volcano-fissure swarm-geothermal systems. It is interesting to note that a large proportion of the solutions obtained for events within the Hengill fissure swarm were tensile crack type. To date, the only other earthquake study that has been done in sufficient detail in such an environment is the work done at Reykjanes by Klein et al. (1977). That study also revealed earthquake radiation patterns of a similar type to the Hengill tensile crack events. The fact that so many high temperature areas occur along the accretionary plate boundary in Iceland may well be due to the strong tensional stress regime associated with the boundary causing contraction fractures of the tensile crack type, which are optimum for aquifer formation.

Since Icelandic fissure swarm/geothermal systems also lie on or close to the plate boundary, it would be expected that periodic, tectonic episodes should occur, with accompanying seismicity that would probably exhibit shear mechanisms. This seismicity would be superimposed on the continuous, "geothermal" seismicity, but would display a contrasting temporal distribution. Sequences such as the Sept. 1972 swarm on Reykjanes, (Klein et al., 1977) and the Sept. 1981 Kirkjuferjuhjáleiga, Ölfus swarm were sequences of this type. It is appropriate to note that in the case of the background activity that could prove useful as a geothermal prospecting tool a continuous temporal distribution of activity would be anticipated that would ensure the successful aquisition of a data set by a relativly short monitoring project.

6.3.2 Dyke injection on accretionary plate boundaries

The observation of tensile crack formation at several kilometers depth in the earth's crust near to an accretionary plate boundary has wider implications for the crustal accretion process.

The accretion of the shallow crust by dyke injection is indicated by offshore research, and the mechanism by which this is achieved has been observed at Krafla. Such a process must necessarily involve large movements of crustal blocks in the direction normal to a fault plane that is itself orientated normal to the direction of least compressive stress. To date, however, neither the formation of such fractures nor movements normal to them have been observed seismically. Although some large teleseismic focal mechanisms with enhanced explosive components have been reported from the Mid Atlantic Ridge (see Foulger and Long, 1984, for summary) accretionary plate boundaries generally exhibit normal dip-slip shear faulting. Dyke injection events in the Krafla area are generally accompanied by relatively minor seismicity and much of the crustal widening is a result of the widening of pre-existing fissures. For example during the July 1978 event 30 km of the plate boundary was rifted and the crust widened by up to 1 m. The largest earthquake recorded during the swarm that accompanied this event was of magnitude $M_L = 4.1$ (Björnsson et al., 1979; Einarsson and Brandsdóttir, 1980).

It is proposed here that the formation of long fractures parallel to the accretionary plate boundary is achieved by cumulative small magnitude cooling-contraction fracture during inter-episodic periods of volcanic quiesence. This process may be short lived where narrow dykes are injected, which cool quickly. These form sheet complexes where the individual dykes are separated by fracture planes that are their cooled margins. This is consistant with the observation that

small magnitude background seismicity is absent in the fissure swarms away from central volcanoes. At central volcanoes, however, where there is a greater supply of magma, large heat losses may be maintained over long periods, and the cooling-contraction process be continuous.

During dyke injection events magma intrusion proceeds along the fracture planes that are the cooled edges separating the old dykes. These fracture planes are connected by shear movements on planes joining them and are widened aseismically to accomodate the dyke volume. The maintainance of a highly fractured and porous state by cooling contraction fracturing in the volume of a central volcano facilitates the upward migration and accumulation of magma and this process may thus be a contributary factor in the mechanism that perpetuates central volcanoes.

This concept may be summarised:

A feature of central volcanoes and their associated fissure swarm systems is fracture complexes that are zones of weakness in the brittle crust. Hot mantle material preferentially emplaces along those fracture complexes and engineers their perpetuation by thermal stresses.

6.4 Conclusions

Seismological studies were conducted in the Hengill area in the 7 year period 1978-1984. Local earthquake, teleseismic and explosion data were collected and processed. The results are consistent with a structure involving an extinct volcanic centre in the Grensdalur area and an active one now underlying Hengill. A transverse structure connects the two and represents the migration trajectory of the Grensdalur volcanic centre. The two volcanic centres are the sites of separate heat sources feeding merging geothermal fields with contrasting reservoir characteristics.

The action of cool circulating groundwater fluids on hot rock at depth results in the formation of cooling contraction cracks and accounts for the ongoing small magnitude seismicity observed over the geothermal area. In the tensile stress regime of the accretionary plate boundary the type of fracture formed is tensile crack. Volume calculations indicate that aseismic fracture opening occurs subsequent to formation.

The ongoing small magnitude seismicity that is a feature of Icelandic high temperature geothermal areas thus demarcates volumes of rock that are rapidly cooling down and feeding the geothermal system. It may therefore provide a geothermal prospecting tool. The formation of cooling contraction tensile cracks on accretionary plate boundaries offers an explanation for the mechanism of dyke injection.

7. RECOMMENDATIONS FOR FURTHER STUDY

7.1 Monitoring

It is recommended that the operation of seismographs be continued in the Hengill geothermal field if exploitation of the resource is under consideration, for the following reasons:

(1) Experience in other geothermal areas, e.g. The Geysers, Ca, has shown that production, and especially reinjection can affect the seismicity of the reservoir. In order to assess such effects it is important to monitor the seismicity for as long as possible prior to as well as during production. Whilst maintaining good network geometry, instruments should preferentially be deployed close to well sites.

(2) There is a real volcanic and seismic hazard in the Hengill area. Seismometers can provide direct, real-time monitoring over the long term, with detection capabilities through the whole of the volume of interest. The utility of this monitoring in reducing volcanic and earthquake hazard has been well proven elsewhere.

7.2 Data processing

As only 2 years were available to process the data collected during the 1981 monitoring project, and because the amount of data collected was far greater than anticipated, a number of possible lines of study were not pursued. For future reference these will be briefly listed below.

a) Modelling of the teleseismic data by the Aki inversion procedure.
b) Modelling of the local and regional explosions by ray tracing or Aki inversion.
c) Spectral analysis of the explosions, especially the fan shots.
d) Examination of the relative attenuation of P- and S- waves generated by regional earthquakes and recorded at various stations over the network.
e) Simultaneous inversion of local explosions and earthquakes to obtain a 3-dimensional velocity structure for the crust.
f) Inversion of P waveform data of the tensile crack type earthquakes of the geothermal field in order to calculate a best value for their seismic moment density tensors.

Other possible lines of investigation include further study of the apparent b-value variation during the Kirkjuferjuhjáleiga, Ölfus swarm, study of the periodicity of the $M_L = 4 - 6$ data recorded at REY, and investigation of possible variations in Poisson's ratio over the Hengill area.

REFERENCES

Angenheister, G., Bjornsson, Sv., Einarsson, P., Gebrande, H., Goldflam, P., Jacoby, W.R., Litvinenko, I.V., Loncarevic, B., Miller, H., Palmason, G., Pavlenkova, N.I., Richard, S., Solomon, S.C., Weigel, W. and Zverev, S.M. 1980. Reykjanes Ridge Seismic Experiment (RRISP 77). J. Geophys., 47, 228-238.

Bjornsson, A., Johnsen, G., Sigurdsson, S., Thorbergsson, G. and Tryggvason, E. 1979. Rifting of the plate boundary in North Iceland. J. Geophys. Res., 84, 3029-3038.

Bjornsson, H., Bjornsson, Sv. and Sigurgeirsson, Th. 1980. Penetration of water into hot rock boundaries of magma at Grimsvotn. Nature, 295, 580-581.

Bodvarsson, G. 1951. Skýrsla um rannsóknir á jarðhita í Hengli, Hveragerði og nágrenni, árin 1947 - 1949. Tím. V.F.I., 36, 1-48.

Bufe, C.G. 1970. Frequency-magnitude variations during the 1970 Danville earthquake swarm. Earthquake Notes, 41, 3-7.

Corbishley, D.J. 1969. Measurements of the derivative of the P-wave travel time curve by means of an array network. Ph.D. Thesis, University of Durham, pp. 99.

Einarsson, P. 1984. Seismicity along the eastern margin of the North American plate. Geol. Soc. Am., in prep.

Einarsson, P. and Eiriksson, J. 1982. Earthquake fractures in the districts Land and Rangarvellir in the South Iceland Seismic zone. Jokull, 32, 113-120.

Einarsson, P., Bjornsson, S., Foulger, G., Stefansson, R. and Skaftadottir, Th. 1981. Seismicity pattern in the South Iceland seismic zone. In: Earthquake Prediction - An International Review, Maurice Ewing Series 4, Am. Geophys. Union, 141-151.

Einarsson, P. and Brandsdottir, B. 1980. Seismological evidence for lateral magma intrusion during the July 1978 deflation of the Krafla volcano in NE Iceland. J. Geophys., 47, 160-165.

Einarsson, P., Klein, F. and Bjornsson, Sv. 1977. The Borgarfjordur earthquakes of 1974 in west Iceland. Bull. Seismol. Soc. Am., 67, 187-208.

Foulger, G.R. 1984. The seismological research programme of the Hengill area. Ph.D. Thesis, University of Durham, in prep.

Foulger, G. 1982. Geothermal exploration and reservoir monitoring using earthquakes and the passive seismic method. Geothermics, 11, 259-268.

Foulger, G. 1981. The seismological field project of June-October 1981 in the Hengill area. Science Institute, University of Iceland Report RH-81-18, pp. 50.

Foulger, G. and Long, R.E. 1984. Anomalous focal mechanisms: evidence for tensile crack formation on an accreting plate boundary. Nature, 310, 43-45.

Foulger, G. and Einarsson, P. 1980. Recent earthquakes in the Hengill-Hellisheidi area in SW Iceland. J. Geophys., 47, 171-175.

Francis, T.J.G. 1968a. The detailed seismicity of mid-ocean ridges. Earth Plan. Sci. Lett., 4, 39-46.

Francis. T.J.G. 1968b. Seismicity of mid-ocean ridges and its relation to properties of the upper mantle and crust. Nature, 220, 899-901.

Herrin, E. 1968. Introduction to 1968 seismological tables for P-phases. Bull. Seismol. Soc. Am., 58, 1193-1241.

Hill, D.P. 1977. A model for earthquake swarms. J. Geophys. Res., 82, 1347-1352.

Klein, F.W. 1978. Hypocenter location program HYPOINVERSE. U.S. Geol. Surv. Open-File Report, 78-694.

Klein, F.W., Einarsson, P. and Wyss, M. 1977. The Reykjanes Peninsula, Iceland, earthquake swarm of September 1972 and its tectonic significance. J. Geophys. Res., 82, 865-888.

Lahr, J.C. and Ward, P. 1975. Hypoellipse. A computer program for determining local earthquake hypocentral parameters, magnitude and first motion patterns. U.S. Geol. Surv. Open-File Report.

Lee, W.H.K. and Lahr, J.C. 1972. HYPO71: A computer program for determining hypocenter, magnitude and first motion pattern of local earthquakes. U.S. Geol. Surv. Open-File Report.

Long, R.E. and Mitchell, M.G. 1970. Teleseismic P-wave delay time in Iceland. Geophys. J.R. astron. Soc., 20, 41-48.

McKenzie, D.P. 1969. Earthquakes and the directions of principle stresses. Bull. Seismol. Soc. Am., 59, 591-601.

Ode, H. 1957. Mechanical analysis of the dyke pattern of the Spanish Peaks area, Colorado. Bull. Geol. Soc. Am., 68, 567-576.

Page, R. 1968. Aftershocks and microaftershocks of the great Alaska earthquake of 1964. Bull. Seismol. Soc. Amer., 58, 1131-1168.

Palmason, G. 1971. Crustal structure of Iceland from explosion seismology. Soc. Sci. Islandica Rit. 40, pp. 187.

Savage, J.E.G. 1979. A seismic investigation of the lithosphere of the Gregory Rift. Ph.D. Thesis, University of Durham, PP. 382.

Scholz, C. 1968. The frequency-magnitude relation of microfracturing in rock and its relation to earthquakes. Bull. Seismol. Soc. Am., 58, 399-415.

Suyehiro, S., Asada, T., and Ohtake, M. 1964. Foreshocks and aftershocks accompanying a perceptible earthquake in central Japan. Papers Meteorol. Geophys., 15, 71-88.

Sykes, L.R. 1970. Earthquake swarms and sea-floor spreading. J. Geophys. Res., 75, 6598-6611.

Talwani, M. and Eldholm, O. 1977. Evolution of the Norwegian-Greenland Sea. Bull. Geol. Soc. Am., 88, 969-999.

Tryggvason, E. 1979. Jarðskjálftar á Íslandi 1950-1959. Science Institute, University of Iceland Report, RH-79-06, pp. 90.

Tryggvason, E. 1978a. Jarðskjálftar á Íslandi 1930-1939. Science Institute, University of Iceland Report, RH-78-21, pp. 92.

Tryggvason, E. 1978b. Jarðskjálftar á Íslandi 1940-1949. Science Institute, University of Iceland Report, RH-78-22, pp. 51.

Tryggvason,E. 1973. Seismicity, earthquake swarms and plate boundaries in the Iceland region. Bull. Seismol. Soc. Am., 63, 1327-1348.

Ward, P.L. and Bjornsson, S., 1971. Microearthquakes, swarms and the geothermal areas of Iceland. J. Geophys. Res., 76, 3953-3982.

Wyss, M. 1973. Towards a physical understanding of the earthquake frequency distribution. Geophys. J. R. astron. Soc., 31, 341-359.

Wyss, M. and Lee, W.H.K. 1973. Time variations of the average earthquake magnitude in central California. In: R.L. Kovach and A. Nur ed., Proceedings of the Conference on Tectonic Problems on the San Andreas Fault system. Stanford Univ. Publ., Geol. Sci., 13, 24-42.

Wyss, M. and Brune, J.N. 1968. Seismic moment, stress and source dimensions for earthquakes in the California-Nevada region. J. Geophys. Res., 73, 4681-4694.

APPENDIX 1

SEISMOMETER STATION LOCATIONS AND THE HENGILL - SOUTH ICELAND CRUSTAL
MODEL

This Appendix contains:
(1) The list of station locations. Stations with two letter code
     names are (or were) of the drum recorder type, and part of the
     Icelandic regional network, with the exception of HK (Krókur),
     see Section 1.3. Stations with 3 letter code names were stations
     of the radio telemetered network deployed in 1981. They are as
     follows:

Telemetered to Blákollur (BBL)

        BSL –   Sleggjubeinsdalur
        BHU –   Húsmúli
        BVA –   Vallalda
        BLA –   Lakakrókur
        BEN –   Engidalur
        BMO –   Mosfellsheiði

Telemetered to Kambar (KKA)

        KST –   Stapholt
        KDN –   Djúpgrafningur
        KKL –   Klóarfjall
        KDL –   Djúpagil
        KDA –   Dalaskarð
        KMI –   Miðdalur
        KHE –   Hengladalsá
        KHA –   Háaleiti
        KSA –   Sauðá

Telemetered to Lambhagi (LLA)

        LBO –   Botnadalur
        LDY –   Dyrafjöll
        LGR –   Grafningsrétt
        LDJ –   Djáknapollur
        LKA –   Kattatjarnir

  (2) the crustal model parameters. The depth column gives the depth to
       the top of each layer, and the velocity column gives the velocity
       at the top of that layer. The velocity within each layer
       increases linearly to that given for the top of the layer

beneath. Layer 5 is a constant velocity halfspace.

This crustal model was derived by making a composite travel time plot of all first arrivals for explosion profiles 35 - 42 and L3, shot by Palmason (Palmason, 1971). These profiles cover the Hengill area and South Iceland. The program TTGEN (Klein, 1978) was then used to model this data to find a crustal structure that fitted the observational data. A halfspace velocity of 7.0 km sec^{-1} was used, based on the results of Angenheister et. al. (1980).

(3) a list of test parameters used by HYPOINVERSE for Iceland. Items (1), (2) and (3) are presented in Tables A1.1 and A1.2.

(4) a diagram of the velocity-depth profile for the Hengill-South Iceland crustal model (Fig. A1.1).

(5) HYPOINVERSE printout for each of the 5 explosions detonated, tabulating observed and calculated travel times from source to recievers (Tables A1.1 to A1.5).

Variations in the crustal structure within the area and their effect on the hypocentral locations

Examination of explosion data taken from Palmason (1971) indicated variations in the velocity structure within the Hengill area. Profile 42 was taken as indicative of the velocity structure N of 64°N. Profiles L3, L4 and L5 were taken as representitive of the area S of 64° N. Profiles L3, L4 and L5 consistantly indicated lower velocities than profile 42. The indication of these data is hence that the velocities S of 64° N may be lower than those of the Hengill-South Iceland crustal model, and those N of 64°N higher.

The explosion data described in this report (see Section 5.2) indicate an area of relatively high velocities to the N of Hveragerði, i.e. in the area of the central cluster of seismic activity. Velocities in the Grafningur-fissure swarm-Ölfus zone display velocities lower than those of the Hengill-South Iceland crustal model. These results are hence consistant with those of Palmason (1971).

Variations such as these, that may be up to 5% in magnitude are unlikely to affect the epicentral determinations significantly where station coverage is good. However the calculated hypocentral depth of an event is heavily dependant on the arrival times measured at close stations. Hence velocity variations in the immediate vicinity of the event may not be cancelled out and significantly distort the focal depth. Underestimation of the velocity in the hypocentral volume will result in the calculation of erroneously small hypocentral depths. Conversely, if the real velocities are lower than those defined in the

crustal model, hypocentral depths calculated will be too deep. In the
case of the Hengill area the local velocity variations described above
have the effect that hypocentres in the central cluster are
artificially shallowed and those in the Grafningur-fissure
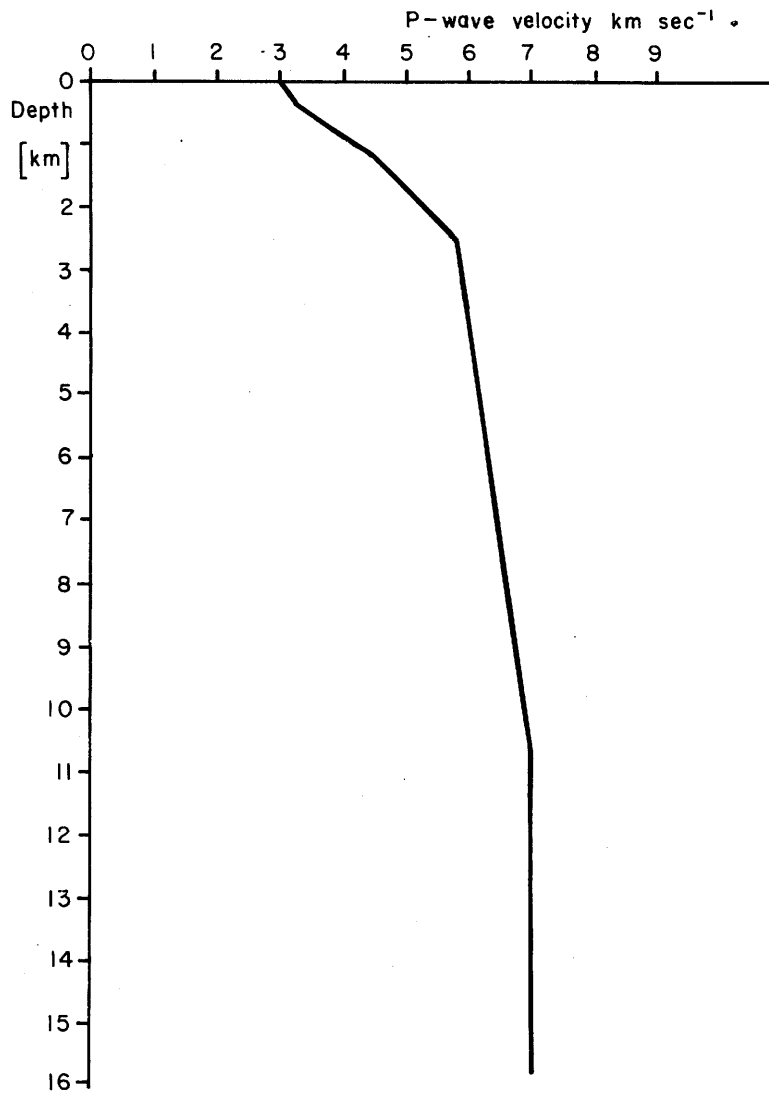swarm-Ölfus zone are artificially deepened by up to 5%.

Fig. Al.1 Velocity-depth profile for the Hengill-South Iceland crustal
model.

Table A1.1 Station locations of instruments in this study.

PROGRAM HYPINV (VERSION 1 - JUN 78) RUN ON 2/20/84 AT 13:10:05

STATIONS
CENTER 63. 0.00 25. 0.00   DLYAZ= 999.00   DLYWD= 0.00

I	NAME	---LAT---		---LON---		PDLY1	SDLY1	PDLY2	SDLY2	FMC	XMC	WT	MDL	CAL	PER	TYP	
1	KL	63.	55.52	22.	0.31	0.00	0.00	0.00	0.00	0.0	0.0	1	1	0.0	0.1	2	175
2	MV	64.	1.23	22.	17.78	0.00	0.00	0.00	0.00	0.0	0.0	1	1	0.0	0.1	2	
3	FJ	64.	2.77	20.	34.57	0.00	0.00	0.00	0.00	0.0	0.0	1	1	0.0	0.1	2	
4	BJ	64.	5.98	20.	47.69	0.00	0.00	0.00	0.00	0.0	0.0	1	1	0.0	0.1	2	
5	KI	64.	0.26	20.	46.89	0.00	0.00	0.00	0.00	0.0	0.0	1	1	0.0	0.1	2	
6	BJ	64.	3.95	20.	56.50	0.00	0.00	0.00	0.00	0.0	0.0	1	1	0.0	0.1	2	51
7	LS	64.	7.46	20.	0.80	0.00	0.00	0.00	0.00	0.0	0.0	1	1	0.0	0.1	2	300
8	RK	64.	8.30	21.	54.30	0.00	0.00	0.00	0.00	0.0	0.0	1	1	0.0	0.1	2	190
9	RN	63.	50.39	22.	39.17	0.00	0.00	0.00	0.00	0.0	0.0	1	1	0.0	0.1	2	10
10	MV	64.	1.23	22.	13.76	0.00	0.00	0.00	0.00	0.0	0.0	1	1	0.0	0.1	2	
11	RH	64.	8.40	21.	57.40	0.00	-0.20	0.00	0.00	0.0	0.0	1	1	0.0	0.1	2	20
12	GU	64.	3.24	20.	37.31	0.36	-0.25	0.00	0.00	0.0	0.0	1	1	0.0	0.1	2	24
13	HS	66.	6.70	20.	7.30	-0.44	-0.05	0.00	0.00	0.0	0.0	1	1	0.0	0.1	2	
14	AK	65.	41.20	18.	6.40	0.09	0.00	0.00	0.00	0.0	0.0	1	1	0.0	0.1	2	137
15	TN	63.	51.92	22.	26.62	0.00	0.00	0.00	0.00	0.0	0.0	1	1	0.0	0.1	2	300
16	VA	64.	1.09	21.	50.35	0.00	0.00	0.00	0.00	0.0	0.0	1	1	0.0	0.1	2	000
17	IR	64.	2.51	21.	22.54	0.00	0.00	0.00	0.00	0.0	0.0	1	1	0.0	0.1	2	100
18	SL	63.	56.63	21.	0.09	0.18	0.00	0.00	0.00	0.0	0.0	0	1	0.0	0.1	2	090
19	RE	64.	7.61	21.	54.70	0.00	0.60	0.00	0.00	0.0	0.0	1	1	0.0	0.1	2	180
20	LV	64.	12.93	20.	45.18	0.00	0.00	0.00	0.00	0.0	0.0	1	1	0.0	0.1	2	050
21	AR	63.	47.30	20.	0.90	0.00	-0.10	0.00	0.00	0.0	0.0	1	1	0.0	0.1	2	070
22	SE	63.	32.94	19.	36.56	0.00	0.00	0.00	0.00	0.0	0.0	0	1	0.0	0.1	2	640
23	SK	63.	27.21	19.	5.88	0.00	0.00	0.00	0.00	0.0	0.0	0	1	0.0	0.1	2	430
24	SM	64.	42.60	21.	2.80	1.07	0.00	0.00	0.00	0.0	0.0	0	1	0.0	0.1	2	120
25	HV	64.	52.10	19.	34.10	0.13	0.00	0.00	0.00	0.0	0.0	0	1	0.0	0.1	2	120
26	LA	64.	10.90	19.	13.40	0.00	0.00	0.00	0.00	0.0	0.0	1	1	0.0	0.1	2	560
27	SF	63.	30.00	18.	50.00	0.00	0.00	0.00	0.00	0.0	0.0	0	1	0.0	0.1	2	620
28	SH	63.	23.85	20.	17.60	0.00	0.00	0.00	0.00	0.0	0.0	0	1	0.0	0.1	2	200
29	BV	64.	5.87	19.	0.43	0.00	-0.46	0.00	0.00	0.0	0.0	1	1	0.0	0.1	2	026
30	VF	64.	12.07	13.	59.02	0.32	0.00	0.00	0.00	0.0	0.0	0	1	0.0	0.1	2	030
31	SB	63.	43.25	13.	37.30	0.00	0.00	0.00	0.00	0.0	0.0	1	1	0.0	0.1	2	
32	KK	63.	47.10	18.	3.50	0.00	0.00	0.00	0.00	0.0	0.0	0	1	0.0	0.1	2	580
33	KV	63.	58.60	16.	26.30	0.00	0.00	0.00	0.00	0.0	0.0	1	1	0.0	0.1	2	100
34	SA	64.	3.09	20.	25.04	0.00	0.00	0.00	0.00	0.0	0.0	0	1	0.0	0.1	2	210
35	SG	64.	10.76	19.	7.19	0.00	0.00	0.00	0.00	0.0	0.0	1	1	0.0	0.1	2	80
36	HL	64.	0.44	20.	0.60	0.00	-0.12	0.00	0.00	0.0	0.0	0	1	0.0	0.1	2	180
37	ST	64.	12.63	21.	29.12	0.21	0.00	0.00	0.00	0.0	0.0	1	1	0.0	0.1	2	100
38	HG	64.	1.03	21.	11.31	0.00	0.00	0.00	0.00	0.0	0.0	1	1	0.0	0.1	2	40
39	HN	64.	6.93	21.	15.44	0.00	0.00	0.00	0.00	0.0	0.0	1	1	0.0	0.1	2	120
40	HH	64.	2.00	21.	7.46	0.00	0.00	0.00	0.00	0.0	0.0	1	1	0.0	0.1	2	
41	HB	63.	56.59	21.	18.16	0.00	0.00	0.00	0.00	0.0	0.0	1	1	0.0	0.1	2	
42	HK	64.	5.94	21.	7.01	0.00	0.00	0.00	0.00	0.0	0.0	1	1	0.0	0.1	2	

Table Al.2 Station locations, crustal model parameters and test parameters used by HYPOINVERSE.

#	Sta	Lat (deg)	Lat (min)	Lon (deg)	Lon (min)									
43	HF	65.	30.05	16.	44.26	0.00	0.00	0.00	0.000	0.000	0.0	0.1	2	110
44	HE	64.	0.34	19.	40.90	0.00	0.00	0.00	0.000	0.000	0.0	0.1	2	940
45	MI	64.	23.90	15.	20.79	0.00	0.00	0.00	0.000	0.000	0.0	0.1	2	060
46	BSL	64.	3.03	21.	22.12	0.00	0.00	0.00	0.000	0.000	0.0	0.1	2	380
47	BHU	64.	5.69	21.	24.08	0.00	0.00	0.00	0.000	0.000	0.0	0.1	2	260
48	DBL	64.	2.26	21.	28.31	0.00	0.00	0.00	0.000	0.000	0.0	0.1	2	310
49	BVA	64.	4.62	21.	26.19	0.00	0.00	0.00	0.000	0.000	0.0	0.1	2	230
50	BLA	64.	0.36	21.	21.61	0.00	0.00	0.00	0.000	0.000	0.0	0.1	2	410
51	BEN	64.	4.80	21.	22.63	0.00	0.00	0.00	0.000	0.000	0.0	0.1	2	260
52	BMO	64.	6.78	21.	21.17	0.00	0.00	0.00	0.000	0.000	0.0	0.1	2	320
53	KST	63.	56.33	21.	9.19	0.00	0.00	0.00	0.000	0.000	0.0	0.1	2	5
54	KDN	64.	0.15	21.	6.34	0.00	0.00	0.00	0.000	0.000	0.0	0.1	2	185
55	KKL	64.	2.81	21.	10.17	0.00	0.00	0.00	0.000	0.000	0.0	0.1	2	280
56	KDL	64.	1.72	21.	13.30	0.00	0.00	0.00	0.000	0.000	0.0	0.1	2	200
57	KDA	64.	2.65	21.	12.54	0.00	0.00	0.00	0.000	0.000	0.0	0.1	2	350
58	KMI	64.	2.97	21.	19.19	0.00	0.00	0.00	0.000	0.000	0.0	0.1	2	460
59	KHE	64.	2.34	21.	16.59	0.00	0.00	0.00	0.000	0.000	0.0	0.1	2	370
60	KKA	63.	58.22	21.	15.66	0.00	0.00	0.00	0.000	0.000	0.0	0.1	2	150
61	KSA	63.	59.90	21.	15.17	0.00	0.00	0.00	0.000	0.000	0.0	0.1	2	310
62	KSA	64.	1.85	21.	9.68	0.00	0.00	0.00	0.000	0.000	0.0	0.1	2	390
63	LBO	64.	8.12	21.	15.32	0.00	0.00	0.00	0.000	0.000	0.0	0.1	2	250
64	LDY	64.	6.48	21.	16.89	0.00	0.00	0.00	0.000	0.000	0.0	0.1	2	380
65	LLA	64.	8.52	21.	6.34	0.00	0.00	0.00	0.000	0.000	0.0	0.1	2	130
66	LGR	64.	4.93	21.	5.36	0.00	0.00	0.00	0.000	0.000	0.0	0.1	2	240
67	LDJ	64.	5.28	21.	9.94	0.00	0.00	0.00	0.000	0.000	0.0	0.1	2	230
68	LKA	64.	4.48	21.	11.08	0.00	0.00	0.00	0.000	0.000	0.0	0.1	2	360

LINEAR GRADIENT CRUST MODEL 9 SRUCT. GP R

LAYER	VEL	DEPTH
1	3.000	0.000
2	3.300	0.400
3	4.500	1.200
4	5.800	2.500
5	7.000	10.800

TEST PARAMETERS

-ITERATION AND CONVERGENCE-

20=ITRLIM	0.9000=DAMP
0.0400=DQUIT	0.0010=DRQT
5.0000=DXFIX	0.0120=EIGTOL
7.0000=DZMAX	0.0200=RBACK
0.5000=DZAIR	0.6000=BACFAC

-WEIGHTING, ERRORS, TRIAL DEPTH-

130.0000=DISCUT	0.1600=RMSCUT
1.0000=DISW1	1.5000=RMSW1
3.0000=DISW2	3.0000=RMSW2
1.0000=SWT	0.1000=PDERR
5.0000=ZTR	1.0000=ERCOF

-DURATION MAG CONSTANTS-

-5.0000=FMA1	-0.7050=FMA2
3.8900=FMB1	2.0260=FMB2
0.0000=FMZ1	0.0000=FMZ2
0.0000=FMD1	0.0000=FMD2
210.0000=FMBRK	1.7800=POS

Table A1.3 Observed and calculated travel times for Ölfus explosion.

12 AUG 81, 16:21 EVENT NO. 1 RUN .. 2/23/84 AT 12:38:00

I ORIGIN	LAT N	LON W	Z	NWR	RMS	DT	ADJUSTMENTS (KM)				
							DLAT	DLON	DZ	RR	NF
1	16.27 63	56.27 21	9.50	0.01	23 0.C9	0.052	0.307	-0.134	0.000	0.335	3

EIGENVALUES
(4.347 0.600 0.160 0.000)

EIGENVECTORS OF ADJUSTMENT

				COVARIANCE				ERRORS	#ERROR ELLIPSE		
OT (	-0.990	-0.017	0.143	0.000)(	0.015	0.098	0.008	0.000)	0.123 #	SERR	AZ	DIP
LAT(	0.142	0.078	0.987	0.000)(	0.095	0.677	0.048	0.000)	0.823 #	31.61	0	90
LON(	0.028	-0.997	0.075	0.000)(	0.006	0.043	0.053	0.000)	0.230 #	0.82	175	0
Z (	0.000	0.000	0.000	0.000)(	0.000	0.000	0.000	0.000)999.000)	31.607 #	0.22	85	0

YR MO DA	ORIGIN	LAT N	LON W	DEPTH	RMS	ERH	ERZ	GAP	XMAG	FMAG	STAND
81- 8-12	1621 16.27	63 56.27	21 9.50	0.01	0.09	0.82	31.61	206			0.437

RMSWT	DMIN	ITR	NFM	NWR	NWS	REMK
0.09	0.3	1	0	23	0	

STA	DIST	AZM	AN	P/S W	SEC+CCOR	(TOBS	-TCAL	-DLY	=RES)	WT	XMG	FMG	R INFO
KST	0.3	69	97	P	16.33 0.00	0.06	0.08	0.00	-0.02	1.00			0.447
KST	0.3	69	97	P	16.33 0.00	0.06	0.08	0.00	-0.02	1.00			0.447
KHA	6.3	305	39	P	18.04 0.00	1.77	1.77	0.00	0.00	1.00			0.107
HB	7.1	275	37	P	18.20 0.00	1.93	1.93	0.00	0.00	1.00			0.616
KDN	7.6	19	35	P	18.17 0.00	1.90	2.03	0.00	-0.13	1.00			0.111
KKA	8.2	326	34	P	18.44 0.00	2.17	2.13	0.00	0.04	1.00			0.071
HG	8.9	351	32	P	18.50 0.00	2.23	2.28	0.00	-0.05	1.00			0.082
KSA	10.3	3	31	P	18.88 0.00	2.61	2.51	0.00	0.10	1.00			0.071
HH	11.9	24	30	P	19.00 0.00	2.73	2.78	0.00	-0.05	1.00			0.067
KDA	12.1	349	30	P	19.03 0.00	2.76	2.81	0.00	-0.05	1.00			0.071
KKL	12.1	358	30	P	19.17 0.00	2.90	2.82	0.00	0.08	1.00			0.110
BLA	12.4	308	30	P	19.37 0.00	3.10	2.87	0.00	0.23	1.00			0.056
KHE	12.7	333	30	P	19.21 0.00	2.94	2.91	0.00	0.03	1.00			0.068
IR	15.7	313	30	P	19.90 0.00	3.63	3.43	0.00	0.20	1.00			0.062
BSL	16.2	321	30	P	19.83 0.00	3.56	3.52	0.00	0.04	1.00			0.070
LGR	16.3	10	30	P	19.97 0.00	3.70	3.54	0.00	0.16	1.00			0.071
LDJ	16.6	359	30	P	19.83 0.00	3.56	3.60	0.00	-0.04	1.00			0.068
BHU	18.6	318	30	P	20.19 0.00	3.92	3.92	0.00	0.00	1.00			0.058
BEN	19.6	324	30	P	20.35 0.00	4.06	4.09	0.00	-0.03	1.00			0.063
LDY	19.9	343	30	P	20.39 0.00	4.12	4.15	0.00	-0.03	1.00			0.057
BMO	21.6	335	30	P	20.63 0.00	4.41	4.45	0.00	-0.04	1.00			0.073
BVA	21.7	316	30	P	20.67 0.00	4.40	4.46	0.00	-0.06	1.00			0.071
LLA	22.8	6	30	P	20.84 0.00	4.57	4.65	0.00	-0.08	1.00			0.000
SL	35.5	48	29	P	18.00 0.00	1.73	6.76	0.00	-5.03	0.00			0.000

Table Al.4 Observed and calculated travel times for Djáknapollur explosion.

I	ORIGIN	LAT N	LON W	Z	NWR	RMS	DT	DLAT	DLON	DZ	RR	NF
1	15.80	64 5.17	21 10.10	0.01	26	0.09	0.014	-0.309	-0.137	0.000	0.333	3

```
        EIGENVALUES
   ( 5.123 0.705 0.607 0.000)
   EIGENVECTORS OF ADJUSTMENT
                                        COVARIANCE              ERRORS    #ERROR ELLIPSE
                                                                          # SERR AZ DIP
OT ( -0.995  0.094 -0.026 -0.229)(  0.001 -0.002  0.003  0.000)   0.033  # 31.61   0 90
LAT( -0.070 -0.872 -0.485  0.115)( -0.002  0.006  0.000)          0.202  #  0.23 300  0
LON(  0.068  0.481 -0.374 -0.242)(  0.003  0.048  0.000)          0.219  #  0.19  29  0
Z  (  0.272  0.020 -0.223 -0.936)(  0.000  0.000999.000)         31.607  #
```

YR	MO	DA	ORIGIN	LAT N	LON W	DEPTH	RMS	ERH	ERZ	GAP	XMAG	FMAG	STAND
81-	8-	13	1645 15.80	64 5.17	21 10.10	0.01	0.09	0.23	31.61	63			0.500

```
RMSWT DMIN ITR NFM NWR NWS REMK
 0.09  0.2   1   0   26   0
```

STA	DIST	AZM	AN	P/S	W	SEC+CCOR	(TOBS	-TCAL	-DLY	=RES)	WT	XMG	FMG	R INFO
LDJ	0.2	37	96	P	0	15.92 0.00	0.12	0.06	0.00	0.06	1.00			0.403
LKA	1.5	213	79	P	0	16.41 0.00	0.61	0.49	0.00	0.12	1.00			0.146
LGR	3.5	97	57	P	0	16.86 0.00	1.06	1.10	0.00	-0.04	1.00			0.336
KKL	4.4	181	45	P	0	16.93 0.00	1.13	1.35	0.00	-0.22	1.00			0.117
KDA	5.1	203	42	P	0	17.26 0.00	1.46	1.51	0.00	-0.05	1.00			0.078
HN	5.4	307	41	P	0	17.40 0.00	1.60	1.57	0.00	0.03	1.00			0.169
KSA	6.2	176	39	P	0	17.51 0.00	1.71	1.74	0.00	-0.03	1.00			0.106
LLA	6.8	26	37	P	0	17.76 0.00	1.96	1.88	0.00	0.08	1.00			0.214
LBO	6.9	323	37	P	0	17.87 0.00	2.07	1.89	0.00	0.18	1.00			0.169
KDL	7.0	202	37	P	0	17.65 0.00	1.85	1.90	0.00	-0.05	1.00			0.068
KHE	7.5	226	36	P	0	17.77 0.00	1.97	2.00	0.00	-0.03	1.00			0.058
HG	7.8	188	35	P	0	17.80 0.00	2.00	2.06	0.00	-0.06	1.00			0.077
HH	7.8	136	35	P	0	17.90 0.00	2.10	2.08	0.00	0.02	1.00			0.158
KMI	8.4	241	33	P	0	18.03 0.00	2.23	2.19	0.00	0.04	1.00			0.059
BMO	9.4	289	31	P	0	18.35 0.00	2.55	2.37	0.00	0.18	1.00			0.102
KDN	9.8	161	31	P	0	18.20 0.00	2.40	2.42	0.00	-0.02	1.00			0.103
BSL	10.6	248	30	P	0	18.38 0.00	2.53	2.55	0.00	-0.03	1.00			0.059
KKA	10.7	203	30	P	0	18.32 0.00	2.52	2.57	0.00	-0.05	1.00			0.055
BEN	11.0	267	30	P	0	18.48 0.00	2.68	2.63	0.00	0.05	1.00			0.077
IR	11.3	244	30	P	0	18.50 0.00	2.70	2.67	0.00	0.03	1.00			0.057
BHU	12.3	257	30	P	0	18.57 0.00	2.77	2.34	0.00	-0.07	1.00			0.067
BLA	12.9	227	30	P	0	18.79 0.00	2.99	2.96	0.00	-0.03	1.00			0.050
KHA	13.8	200	30	P	0	18.84 0.00	3.04	3.10	0.00	-0.06	1.00			0.057
BVA	14.7	267	30	P	0	19.09 0.00	3.29	3.26	0.00	0.03	1.00			0.077
BBL	16.1	251	30	P	0	19.38 0.00	3.58	3.50	0.00	0.08	1.00			0.062
SL	28.0	75	29	P	0	19.50 0.00	3.70	5.52	0.00	-1.32	0.00			0.000
VA	33.5	257	29	P	0	22.00 0.00	6.20	6.43	0.00	-0.23	1.00			0.063

Table A1.5 Observed and calculated travel times for Þingvallavatn explosion.

13 AUG 81 / 21: 1   EVENT NO.   4   RUN ..   2/23/84   AT 12:38:00

I	ORIGIN LAT N	LON W	Z	NWR	RMS	DT	ADJUSTMENTS (KM) DLAT	DLON	DZ	RR	NF
1	15.49 64	9.07 21	11.40	0.01 26	0.07	0.000	-0.024	-0.015	0.000	0.028	3

EIGENVALUES
5.149   0.544   0.258   0.000

EIGENVECTORS OF ADJUSTMENT

					COVARIANCE				ERRORS	#ERROR ELLIPSE # SERR AZ DIP
OT (	-0.990	-0.052	-0.129	0.131)(	0.004	-0.023	0.000	0.000)	0.065	# 31.61 0 90
LAT(	-0.133	0.081	0.938	0.350)(	-0.028	0.211	0.015	0.000)	0.460	# 0.46 174 0
LON(	0.041	-0.995	0.088	-0.129)(	0.000	0.015	0.050	0.000)	0.223	# 0.22 84 0
Z (	0.229	0.332	0.101	0.910)(	0.000	0.000	0.000	799.000)	31.607	#

YR MO DA	ORIGIN	LAT N	LON W	DEPTH	RMS	ERH	ERZ	GAP	XMAG FMAG STAND
81- 8-13	21 1	15.49 64	9.07 21 11.40	0.01	0.07	0.46	31.61	186	0.484

RMSWT	DMIN	ITR	NFM	NWR	NWS	REMK
0.07	3.7	1	0	26	0	0

STA	DIST	AZM	AN	P/S	W	SEC+CCOR	(TOBS	-TCAL	-DLY	=RES)	WT	XMG	FMG	R INFO
LBO	3.7	241	54	P		16.70 0.00	1.21	1.16	0.00	0.05	1.00			0.172
LLA	4.2	104	48	P		16.83 0.00	1.34	1.30	0.00	0.04	1.00			0.349
HN	5.2	220	42	P		16.90 0.00	1.41	1.52	0.00	-0.11	1.00			0.088
LDJ	7.2	170	36	P		17.51 0.00	2.02	1.94	0.00	0.08	1.00			0.127
LGR	8.9	149	32	P		17.84 0.00	2.35	2.27	0.00	0.08	1.00			0.110
BMO	9.0	242	32	P		17.89 0.00	2.40	2.29	0.00	0.11	1.00			0.133
KKL	11.7	175	30	P		18.17 0.00	2.68	2.74	0.00	-0.06	1.00			0.073
KDA	11.9	185	30	P		18.30 0.00	2.81	2.79	0.00	-0.02	1.00			0.063
BEN	12.7	232	30	P		18.43 0.00	2.94	2.92	0.00	0.02	1.00			0.085
KMI	12.9	210	30	P		18.51 0.00	3.02	2.96	0.00	0.06	1.00			0.047
KHE	13.2	199	30	P		18.48 0.00	2.99	3.00	0.00	-0.01	1.00			0.050
KSA	13.4	174	30	P		18.57 0.00	3.08	3.05	0.00	0.03	1.00			0.075
KDL	13.8	187	30	P		18.57 0.00	3.08	3.10	0.00	-0.02	1.00			0.061
BSL	14.2	218	30	P		18.69 0.00	3.20	3.18	0.00	0.02	1.00			0.052
HH	14.4	153	30	P		18.70 0.00	3.21	3.22	0.00	-0.01	1.00			0.097
BHU	14.8	228	30	P		18.69 0.00	3.20	3.28	0.00	-0.08	1.00			0.072
HG	14.9	179	30	P		18.70 0.00	3.21	3.30	0.00	-0.09	1.00			0.069
IR	15.2	217	30	P		18.90 0.00	3.41	3.34	0.00	0.07	1.00			0.051
BVA	15.9	239	30	P		19.03 0.00	3.54	3.47	0.00	0.07	1.00			0.116
KDN	17.1	166	30	P		19.11 0.00	3.62	3.67	0.00	-0.05	1.00			0.083
KKA	17.3	191	30	P		19.14 0.00	3.65	3.71	0.00	-0.06	1.00			0.056
BLA	18.1	208	30	P		19.33 0.00	3.84	3.85	0.00	-0.01	1.00			0.046
BBL	18.9	229	30	P		19.51 0.00	4.02	3.98	0.00	0.04	1.00			0.075
KHA	20.5	191	30	P		19.65 0.00	4.16	4.25	0.00	-0.09	1.00			0.056
LV	22.3	71	30	P		20.00 0.00	4.51	4.56	0.00	-0.05	1.00			0.628
VA	34.9	245	29	P		22.00 0.00	6.51	6.65	0.00	-0.14	1.00			0.153

Table A1.6 Observed and calculated travel times for Grænavatn explosion.

```
12 AUG 81, 19:15  EVENT NO.  2              RUN ..  2/23/84  AT 12:33:00

                                                       ADJUSTMENTS (KM)
I ORIGIN  LAT N    LON W     Z   NWR  RMS  DT    DLAT   DLON    DZ     RR NF
1  16.52 63 53.05  22  3.40  0.01  20  0.26 -2.042 -6.639  9.845  0.00011.874 3

     EIGENVALUES
  ( 4.527  0.118  0.018  0.000)
     EIGENVECTORS OF ADJUSTMENT                COVARIANCE                ERRORS   #ERROR ELLIPSE
                                                                                 # SERR AZ DIP
OT ( -0.988  0.002  0.154  0.038)(  5.801 17.182-32.980  0.000)   2.409 # 31.61   0 90
LAT(  0.073  0.887  0.456 -0.645)( 17.182 55.373-95.352  0.000)   7.441 # 15.45  62  0
LON( -0.136  0.462 -0.876 -0.262)(-32.980-95.352188.923  0.000)  13.745 #  2.40 152  0
Z  (  0.233  0.660  0.044  0.713)(  0.000  0.000  0.000  0.000)  31.607 #

YR MO DA  ORIGIN     LAT N    LON W   DEPTH  RMS  ERH   ERZ   GAP  XMAG FMAG STAND
81- 8-12 1915 16.52 63 53.05  22 3.40  0.01 0.26 15.45 31.61 316           0.021

RMSWT DMIN ITR NFM NWR NWS REMK
0.26  18.3   1   0  20   0
```

STA	DIST	AZM	AN	P/S W	SEC+CCOR		(TOBS	-TCAL	-DLY	=RES)	WT	XMG FMG R	INFO
VA	18.3	35	30	P	20.50	0.00	3.98	3.88	0.00	0.10	1.00		0.528
BBL	32.9	58	29	P	22.91	0.00	6.39	6.33	0.00	0.06	1.00		0.237
BVA	35.8	53	29	P	23.01	0.00	6.49	6.80	0.00	-0.31	1.00		0.136
BLA	36.6	68	28	P	23.33	0.00	6.81	6.93	0.00	-0.12	1.00		0.133
BHU	37.0	57	28	P	23.21	0.00	6.69	7.00	0.00	-0.31	1.00		0.113
HB	37.5	79	28	P	23.40	0.00	6.88	7.07	0.00	-0.19	1.00		0.230
IR	37.5	62	28	P	23.60	0.00	7.03	7.09	0.00	-0.01	1.00		0.107
BSL	38.3	61	28	P	23.51	0.00	6.99	7.21	0.00	-0.22	1.00		0.091
BEN	39.0	56	28	P	23.53	0.00	7.01	7.31	0.00	-0.30	1.00		0.083
KHA	39.9	76	28	P	23.77	0.00	7.25	7.45	0.00	-0.20	1.00		0.171
KMI	40.4	62	28	P	23.96	0.00	7.44	7.53	0.00	-0.09	1.00		0.066
KKA	41.3	72	28	P	23.98	0.00	7.46	7.67	0.00	-0.21	1.00		0.108
KHE	41.8	65	28	P	24.04	0.00	7.52	7.76	0.00	-0.24	1.00		0.060
BMO	42.7	53	28	P	24.11	0.00	7.59	7.90	0.00	-0.31	1.00		0.097
HG	44.9	70	27	P	24.40	0.00	7.83	8.24	0.00	-0.36	1.00		0.102
KDA	45.0	66	27	P	24.34	0.00	7.82	8.27	0.00	-0.45	0.92		0.055
LDY	45.3	56	27	P	24.48	0.00	7.96	8.30	0.00	-0.34	1.00		0.081
KKL	46.9	67	27	P	24.77	0.00	3.25	8.55	0.00	-0.30	1.00		0.095
LDJ	49.0	62	26	P	25.01	0.00	8.49	8.37	0.00	-0.33	1.00		0.128
LLA	54.5	58	26	P	25.90	0.00	9.38	9.68	0.00	-0.30	1.00		0.369

Table A1.7 Observed and calculated travel times for Reykjavík explosion.

```
                                                      ADJUSTMENTS (KM)
I  ORIGIN  LAT N     LON W      Z    NWR  RMS   DT    DLAT   DLON   DZ    RR     NF
1          55.20  64 11.07  21 51.12  0.02  5  0.98 -0.059  5.746  1.785  0.000  6.017  3
```

```
           EIGENVALUES
        2.338   0.264   0.044   0.000
    EIGENVECTORS OF ADJUSTMENT                COVARIANCE                  ERRORS    #ERROR ELLIPSE
                                                                                   # SERR AZ DIP
OT ( -0.988 -0.043 -0.146  0.000)( 10.677 -62.864 -32.797   0.000)   3.268   # 31.61   0  90
LAT( -0.149  0.464  0.873  0.000)(-62.864 377.132 193.498   0.000)  19.420   # 21.91 151   0
LON( -0.030 -0.885  0.465  0.000)(-32.797 193.498 116.931   0.000)  10.813   #  3.72  61   0
Z  (  0.000  0.000  0.000  0.000)(  0.000   0.000   0.000 999.000)  31.607   #
```

```
YR MO DA   ORIGIN         LAT N      LON W    DEPTH  RMS   ERH   ERZ   GAP  XMAG FMAG STAND
81- 9-18   1713 55.20  64 11.07  21 51.12  C.02  0.98  21.91 31.61  277             0.009
```

```
RMSWT DMIN ITR NFM NWR NWS REMK
0.99  5.8   1   0   5   1
```

STA	DIST	AZM	AN	P/S	W	SEC	+CCOR	(TOBS	-TCAL	-DLY	=RES)	WT	XMG	FMG	R INFO
RK	5.8	207	40	P	2	57.80	0.00	2.60	1.65	0.00	0.95	1.13			0.931
VA	18.5	178	31	P	4	59.90	0.00	4.70	2.94	0.00	1.76	0.48			0.868
BVA	22.1	122	31	P	4	60.20	0.00	5.00	3.91	0.00	1.09	1.13			0.281
BBL	24.3	132	30	P	4	0.00	0.00	-55.20	4.52	0.00	-59.72	0.00			0.000
BEN	25.1	117	30	P	4	0.00	0.00	-55.20	4.90	0.00	-60.10	0.00			0.000
BHU	25.3	122	30	P	4	0.00	0.00	-55.20	5.03	0.00	-60.23	0.00			0.000
BMO	25.5	108	30	P	4	0.00	0.00	-55.20	5.06	0.00	-60.26	0.00			0.000
BSL	27.8	122	29	P	4	0.00	0.00	-55.20	5.10	0.00	-60.30	0.00			0.000
IR	28.1	124	30	P	4	61.60	0.00	6.40	5.48	0.00	0.88	1.13			0.511
LDY	29.0	107	30	P	4	0.00	0.00	-55.20	5.67	0.00	-60.87	0.00			0.000
LBO	29.5	100	30	P	4	0.00	0.00	-55.20	5.76	0.00	-60.96	0.00			0.000
KMI	29.9	120	30	P	4	0.00	0.00	-55.20	5.83	0.00	-61.03	0.00			0.000
BLA	31.1	129	29	P	4	0.00	0.00	-55.20	6.03	0.00	-61.23	0.00			0.000
KHE	32.3	120	29	P	4	0.00	0.00	-55.20	6.23	0.00	-61.43	0.00			0.000
LKA	34.6	110	29	P	4	0.00	0.00	-55.20	6.61	0.00	-61.81	0.00			0.000
KDA	34.9	116	29	P	4	0.00	0.00	-55.20	6.66	0.00	-61.86	0.00			0.000
LDJ	35.0	107	29	P	4	0.00	0.00	-55.20	6.67	0.00	-61.87	0.00			0.000
KDL	35.2	119	29	P	4	0.00	0.00	-55.20	6.70	0.00	-61.90	0.00			0.000
KKA	35.8	125	29	P	4	0.00	0.00	-55.20	6.79	0.00	-61.99	0.00			0.000
LLA	36.5	97	29	P	4	0.00	0.00	-55.20	6.91	0.00	-62.11	0.00			0.000
KKL	36.5	114	29	P	4	0.00	0.00	-55.20	6.91	0.00	-62.11	0.00			0.000
KHA	37.2	129	28	P	4	0.00	0.00	-55.20	7.03	0.00	-62.23	0.00			0.000
KSA	37.7	117	28	P	4	0.00	0.00	-55.20	7.10	0.00	-62.30	0.00			0.000
HB	37.9	135	28	P	4	63.10	0.00	7.90	7.13	0.00	0.77	1.13			0.406
LGR	38.4	107	28	P	4	0.00	0.00	-55.20	7.21	0.00	-62.41	0.00			0.000
KDN	41.5	119	28	P	4	0.00	0.00	-55.20	7.71	0.00	-62.91	0.00			0.000
KST	43.6	128	28	P	4	0.00	0.00	-55.20	8.04	0.00	-63.24	0.00			0.000

APPENDIX 2

A BRIEF INTRODUCTION TO THE TREATMENT OF ANOMALOUS
EARTHQUAKE RADIATION PATTERNS

with special reference to the anomalous
events recorded in the Hengill area, 1981

CONTENTS

This appendix is intended to provide a brief introduction to
a general notation for the seismic source, and a few
selected examples to illustrate its use. It is not in any
way intended to be a thorough treatment of this subject.

1. INTRODUCTION

Hitherto it has been customary amongst seismologists to assume that earthquakes are caused by sudden shear failure in rock, and to fit focal mechanism solutions of a type predicted by this theory, to data. The widespread acceptance of this theory is doubtlessly influenced by the facts that much data is consistant with it and seismic sources that are not shear present conceptual and theoretical difficulties.

In the last 10 years a more general theory for the earthquake source has been developed. A number of case histories of anomalous radiation patterns have been documented, and a computer methodology developed that enables data to be reduced without a priori assumptions as to source mechanism (e.g. Randall and Knopoff, 1970). By implementing this methodology:

a) The nature of the source may be described by a general representation that is not based on an assumption of source mechanism, but which is readily interpretable in terms of known source types. This representation is known as the moment tensor representation of the source.

b) Wave form and amplitude data contained in seismograms can be used in addition to polarity data, and thus a "best fit" solution can be calculated, instead of expressing the results as a range of possible solutions.

2 GENERAL TREATMENT OF THE SEISMIC SOURCE

Let us consider a general seismic source having a body force equivalent given by couples alone. For 3 components of force and 3 possible arm directions, there are 9 generalised couples:
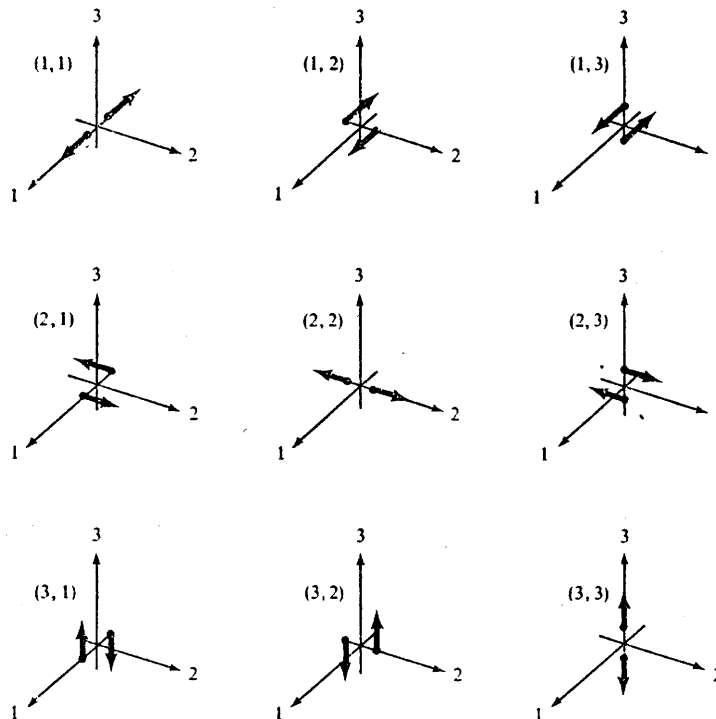
The nine possible couples that are required to obtain equivalent forces for a generally oriented displacement discontinuity in anisotropic media.

We will introduce the concept of the moment density tensor tensor m having 9 components equal to the strengths of the 9 generalised couples.

$$
m = \begin{vmatrix} m_{11} & m_{12} & m_{13} \\ m_{21} & m_{22} & m_{23} \\ m_{31} & m_{32} & m_{33} \end{vmatrix} \cdot
$$

The components of this tensor are obtainable from the far field radiation pattern (Aki and Richards, 1980):

$$
u_n(x,t) = \iint_\Sigma m_{pq} * G_{np,q} \, d\Sigma
$$

displacement   Green function

For a <u>shear source,</u> this tensor, the "seismic moment density tensor" is of the form:

$$m = const \times \begin{vmatrix} 0 & 0 & 1 \\ 0 & 0 & 0 \\ -1 & 0 & 0 \end{vmatrix}$$

The body force equivalent is:
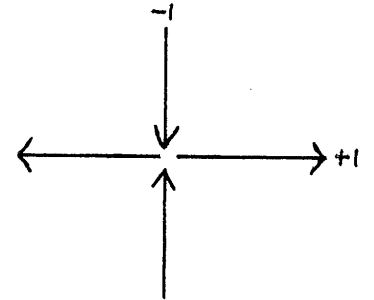
for an <u>explosion</u>:

$$m = const \times \begin{vmatrix} 1 & 0 & 0 \\ 0 & 1 & 0 \\ 0 & 0 & 1 \end{vmatrix}$$

the body force equivalent is
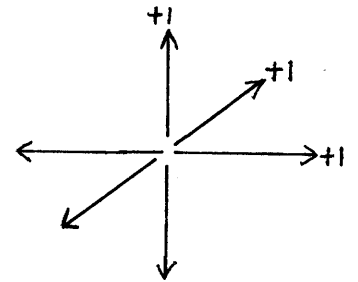
for a <u>tensile crack</u>

$$m = const \times \begin{vmatrix} \lambda & 0 & 0 \\ 0 & \lambda & 0 \\ 0 & 0 & (\lambda+2\mu) \end{vmatrix}$$

the body force equivalent is
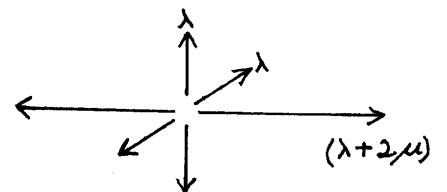
3. THE MODELLING OF COMPLEX SOURCES

The concept of the <u>seismic moment density tensor</u> is a useful one for considering seismic sources, since tensor representations of simple sources may be <u>combined linearly</u> to model complex sources. The <u>body force equivalent</u> representation is a useful device to help us visualise the result.

It is important to note that volume is conserved if the sum of the seismic moment density tensor components is equal to zero, i.e. volume is conserved for the shear mechanism, but not for the explosion or the tensile crack.

<u>Examples</u>

No.1 Shear source of amplitude 1 plus explosion of amplitude 1. The result is a source with an all-compressive far field radiation pattern with amplitudes ranging from 0 (in the 3 direction) to 2 (in the 1 direction).
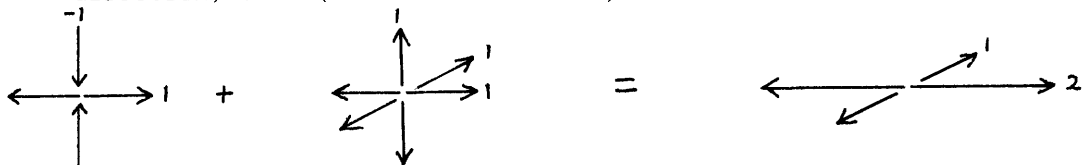
$$\begin{vmatrix} 1 & 0 & 0 \\ 0 & 0 & 0 \\ 0 & 0 & -1 \end{vmatrix} \quad + \quad \begin{vmatrix} 1 & 0 & 0 \\ 0 & 1 & 0 \\ 0 & 0 & 1 \end{vmatrix} \quad = \quad \begin{vmatrix} 2 & 0 & 0 \\ 0 & 1 & 0 \\ 0 & 0 & 0 \end{vmatrix}$$
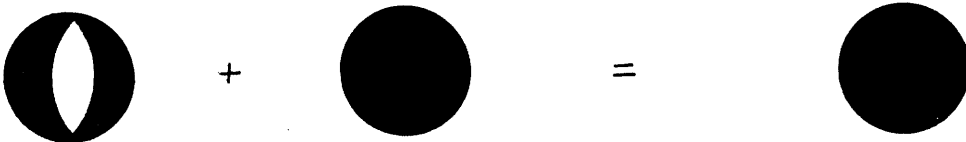
No.2 Shear source of amplitude 1 plus explosion of amplitude 1/2. The result is a source with shrunken dilatational quadrants. Amplitudes range from -1 (in the 3 direction) to 3 (in the 1 direction).

$$\begin{vmatrix} 1 & 0 & 0 \\ 0 & 0 & 0 \\ 0 & 0 & -1 \end{vmatrix} \quad + \quad \frac{1}{2} \begin{vmatrix} 1 & 0 & 0 \\ 0 & 1 & 0 \\ 0 & 0 & 1 \end{vmatrix} \quad = \quad \frac{1}{2} \begin{vmatrix} 3 & 0 & 0 \\ 0 & 1 & 0 \\ 0 & 0 & -1 \end{vmatrix}$$

No.3 Addition of two shear sources, one rotated through $90°$ with respect to the other. The result is a CLVD (compensated linear vector dipole) source, that conserves volume. These have been documented at Long Valley, California. The question is, though: is two simultaneous, orthogonal, superimposed double couple sources a reasonable model for an earthquake source?

$$\begin{vmatrix} 1 & 0 & 0 \\ 0 & 0 & 0 \\ 0 & 0 & -1 \end{vmatrix} + \begin{vmatrix} 1 & 0 & 0 \\ 0 & -1 & 0 \\ 0 & 0 & 0 \end{vmatrix} = \begin{vmatrix} 2 & 0 & 0 \\ 0 & -1 & 0 \\ 0 & 0 & -1 \end{vmatrix}$$

No.4 It should be pointed out that any complex source that conserves volume may theoretically be decomposed into two shear sources, sometimes referred to as the "major and minor double couples".

$$a = b + c$$

4. THE TENSILE CRACK: DERIVATION OF THE SEISMIC MOMENT DENSITY TENSOR AND THE VOLUME RELATIONSHIP

M , the _seismic moment,_ is a fundamental parameter used to measure the strength of an earthquake. For double couple sources it is:

$$M_o = \mu \times \text{average slip} \times \text{fault area}$$
$$\uparrow$$
rigidity
modulus

The following calculation derives this formula from the fundamental stress-strain relationships, and extends it to the tensile crack model.

Standard stress-strain relationships:
(Generalised form of Hooke's Law for isotropic solid – see for example Ewing et al., 1957).

$$\theta = \frac{\partial u}{\partial x} + \frac{\partial v}{\partial y} + \frac{\partial w}{\partial z}$$

components of stress

$$P_{xx} = \lambda\theta + 2\mu\frac{\partial u}{\partial x}$$

$$P_{xy} = \mu\left(\frac{\partial u}{\partial y} + \frac{\partial v}{\partial x}\right)$$

$$P_{yy} = \lambda\theta + 2\mu\frac{\partial v}{\partial y}$$

$$P_{yz} = \mu\left(\frac{\partial v}{\partial z} + \frac{\partial w}{\partial y}\right)$$

$$P_{zz} = \lambda\theta + 2\mu\frac{\partial w}{\partial z}$$

$$P_{zx} = \mu\left(\frac{\partial w}{\partial x} + \frac{\partial u}{\partial z}\right)$$

Consider a shear seismic source. Slip occurs on a vertical plane normal to the y axis and proceeds in the x direction. The couples involved are xy and yx.

$$P_{xy} = \mu\left(\frac{\partial u}{\partial y} + \frac{\partial v}{\partial x}\right)$$

$$P_{yx} = -\mu\left(\frac{\partial u}{\partial y} + \frac{\partial v}{\partial x}\right)$$
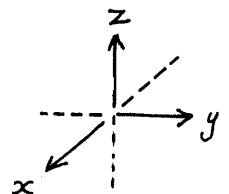
for displacement in the x dcn only:

$$P_{xy} = \mu\frac{\partial u}{\partial y} \qquad\qquad P_{yx} = -\mu\frac{\partial u}{\partial y}$$

for $\dot{u}$ we may substitute $\bar{u}$, where $\bar{u}$ is the average displacement.

$$A\, P_{xy}\, \partial y = A_{\mu}\bar{u} \qquad A\, P_{yx}\, \partial y = -A_{\mu}\bar{u}$$

area of fault plane.

mean displacement

M_{yx} component of the seismic moment tensor

the seismic moment tensor representation of a shear source is therefore:

$$M = A_{\mu}\bar{u} \begin{vmatrix} 0 & 1 & 0 \\ -1 & 0 & 0 \\ 0 & 0 & 0 \end{vmatrix}$$

(moment $= \mu \times$ average slip x fault area)

where M is the seismic moment tensor.

<u>Consider tensile crack.</u> For a crack in the plane normal to the x axis:

$$P_{xx} = (\lambda + 2\mu)\frac{\partial u}{\partial x} \qquad P_{yy} = \lambda\frac{\partial u}{\partial x} \qquad P_{zz} = \lambda\frac{\partial u}{\partial x}$$

$$A\, P_{xx}\, \partial x = A(\lambda + 2\mu)\,\bar{u} \qquad A\, P_{yy}\, \partial x = A\lambda\bar{u} \qquad A\, P_{zz}\, \partial x = A\lambda\bar{u}$$

the tensor representation of a tensile crack is therefore:

$$M = A\bar{u} \begin{vmatrix} (\lambda + 2\mu) & 0 & 0 \\ 0 & \lambda & 0 \\ 0 & 0 & \lambda \end{vmatrix}$$

volume of crack

5. APPLICATION OF THIS METHODOLOGY TO ANOMALOUS EARTHQUAKE RADIATION PATTERNS OF HENGILL EVENTS.

We have now let our imaginations run riot a little. We will now consider the anomalous Hengill events. These events are characterised by a large preponderance of compressional arrivals. Dilatational arrivals project in a narrow transverse zone on the focal sphere. The preponderance of compressional arrivals indicates a net explosive component at source, i.e. non-conservation of volume, and the dilatational belt indicates planarity of the source. The tensile crack displays both these features, so it was taken as the basis of a model.

As mentioned before, the seismic moment density tensor of a tensile crack is

$$
\begin{vmatrix}
(\lambda + 2\mu) & 0 & 0 \\
0 & \lambda & 0 \\
0 & 0 & \lambda
\end{vmatrix}
$$

which gives an all-compressive radiation pattern. It differs from a pure explosion only in as much as the amplitude of the radiation is not spherically symmetrical. In order to produce a dilatational portion in the total radiation pattern, we must superimpose some kind of implosion. A spherically symmetrical implosion, for example, will suffice:

$$
\begin{vmatrix}
\lambda & 0 & 0 \\
0 & \lambda & 0 \\
0 & 0 & (\lambda+2\mu)
\end{vmatrix}
+
\begin{vmatrix}
-(\lambda+\delta\lambda) & 0 & 0 \\
0 & -(\lambda+\delta\lambda) & 0 \\
0 & 0 & -(\lambda+\delta\lambda)
\end{vmatrix}
=
\begin{vmatrix}
-\delta\lambda & 0 & 0 \\
0 & -\delta\lambda & 0 \\
0 & 0 & (2\mu-\delta\lambda)
\end{vmatrix}
$$

The flow of magma, e.g. dyke injection, has been suggested as a possible cause of such an implosive component (Julian, 1983), but such a phenomenon would probably proceed slowly relative to the speed at which a fracture forms. What is required is some process that occurs instantaneously with the rock fracture. It is here suggested that at the instant of fracture formation there is a pore pressure drop in the volume occupied by the new void. This pore pressure drop generates an omnidirectional implosive pressure pulse. The pressure differential is subsequently equalised aseismically by diffusion of the pore fluid (Foulger and Long, 1984).

Calculation of the seismic moment density tensor for the Hengill
events: It will hereafter be assumed that the anomalous Hengill events
are caused by the formation of tensile cracks in the presence of
restricted pore fluid flow. This implies that the nodal surfaces
trace small circles on the focal sphere of radius 80° (for a shear
source the nodal lines are great circles). In the case of the Hengill
data, this is a large assumption since the dilatational data points
are too few to constrain the shape of the nodal lines. The
possibility of obtaining such constraint is further discussed in
section 6.

$$U_n (x,t) = \iint_\Sigma m_{pq} * G_{np,q} \, d\Sigma$$

In the frequency domain, this reduces to (Julian, in press):

$$\vec{u}(\omega) = \vec{g}^T \, \vec{m}(\omega)$$

$\vec{g}^T(\omega)$ is a column vector whose elements are spectra of Green's functions.

$$\vec{g}(\omega) = \left[g_{rr}(\omega) \; g_{r\theta}(\omega) \; g_{\theta\theta}(\omega) \; g_{r\phi}(\omega) \; g_{\theta\phi}(\omega) \; g_{\phi\phi}(\omega) \right]^T$$

For a homogenous, isotropic medium, as functions of departure
angle i (zero=nadir) and departure azimuth J, for p waves:

$$g_{rr} = \cos^2 i \qquad\qquad g_{r\theta} = -\sin 2i \, \sin J$$

$$g_{r\theta} = \sin 2i \, \cos J \qquad\quad g_{\theta\phi} = -\sin^2 i \, \sin 2J$$

$$g_{\theta\theta} = \sin^2 i \, \cos^2 J \qquad\quad g_{\phi\phi} = \sin^2 i \, \sin^2 J$$

$\vec{m}(\omega)^T$ is a column vector of the 6 independant components of the moment
tensor for a point source

$$\vec{m}(\omega) = \left[m_{rr}(\omega) \; m_{r\theta}(\omega) \; m_{\theta\theta}(\omega) \; m_{r\phi}(\omega) \; m_{\theta\phi}(\omega) \; m_{\phi\phi}(\omega) \right]^T$$

r

J=0

J increases

φ

θ

i increases

i=0
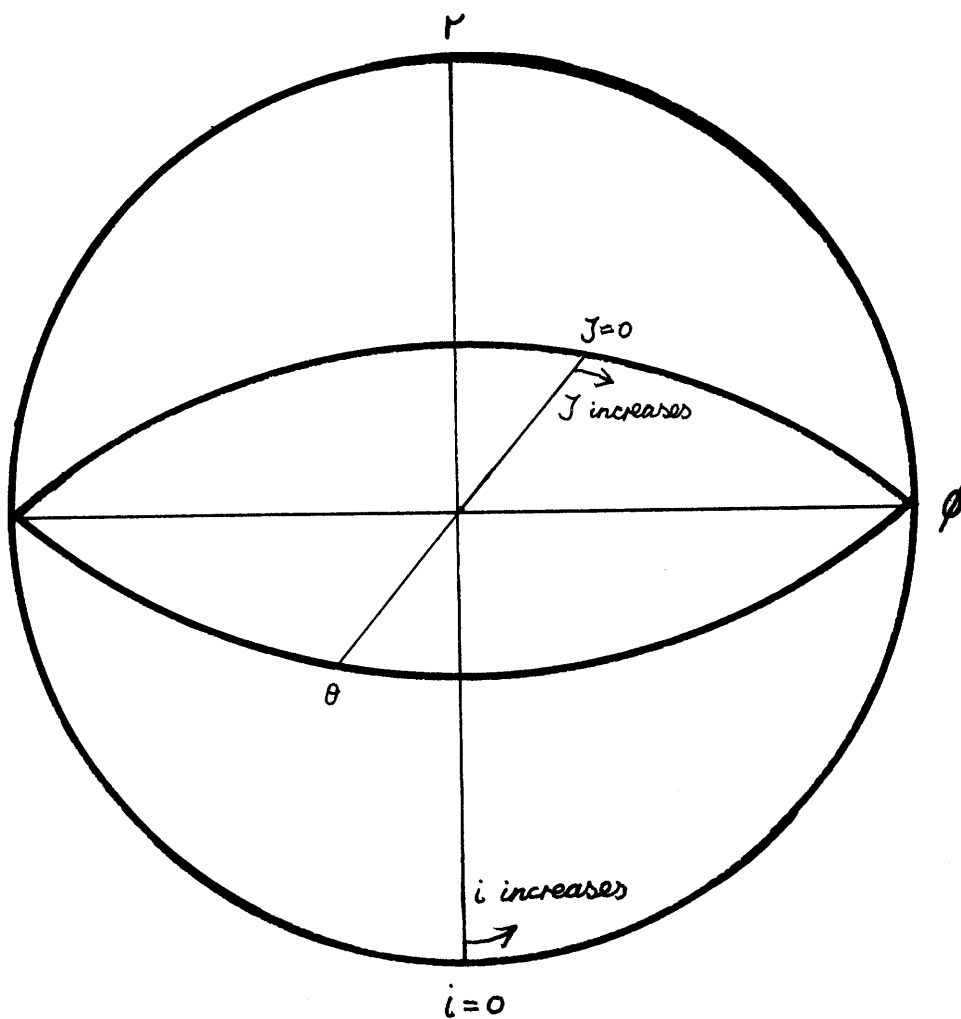
Double couple : $\vec{m}(\omega) = [0, 0, -1, 0, 0, +1]$

CLVD $\vec{m}(\omega) = [-1, 0, -1, 0, 0, 2]$

Consider the $\theta\phi$ plane.

$$i = \pi/2 \qquad \sin i = 1 \qquad \sin 2i = 0 \qquad \cos i = 0$$

$$\vec{g}(w) = [\, 0, 0, \cos^2 J, 0, -\sin 2J, \sin^2 J \,]$$

For a double couple:

$$\vec{u}(w) = [\, 0, 0, -1, 0, 0, +1 \,][\, 0, 0, \cos^2 J, 0, -\sin 2J, \sin^2 J \,]$$

$$= 0 + 0 - \cos^2 J + 0 + 0 + \sin^2 J$$

nodal point if amplitude = 0, i.e. if $\vec{u}(w) = 0$

$$i.e. \quad \cos^2 J = \sin^2 J$$

$$\underline{\underline{J = 45°}}$$

For a CLVD:

$$\vec{u}(w) = [\, -1, 0, -1, 0, 0, 2 \,][\, 0, 0, \cos^2 J, 0, -\sin 2J, \sin^2 J \,]$$

$$= 0 + 0 - \cos^2 J + 0 + 0 + 2\sin^2 J$$

nodal point if amplitude = 0, i.e. if $\vec{u}(w) = 0$

$$i.e. \quad \cos^2 J = 2\sin^2 J$$

$$\underline{\underline{J = 35°\,15'}}$$

For a Hengill event: let the dilatational components of the seismic moment density tensor be of magnitude x

$$\vec{u}(w) = [\, -x, 0, -x, 0, 0, 1 \,][\, 0, 0, \cos^2 J, 0, -\sin 2J, \sin^2 J \,]$$

$$= 0 + 0 - x\cos^2 J + 0 + 0 + \sin^2 J$$

for a nodal point, $\vec{u}(w) = 0$

$$i.e. \quad x\cos^2 J = \sin^2 J$$

$$\tan J = \sqrt{x}$$

for a typical Hengill event, $J = 10°$

$$\therefore \quad \underline{\underline{x = 0.03}}$$

moment tensor for this type of source is therefore:

$$m(w) \doteq [-1, 0, -1, 0, 0, 30]$$

Over what percentage of the focal sphere are dilatational first arrivals observed?

Surface area of sphere = $4\pi r^2$

Area of belt = $4\pi r^2 \sin\theta$

Area of 20° belt = $4\pi r^2 \sin 10°$

$= 0.1736 \cdot 4\pi r^2$

$\simeq$ $\underline{17\% \text{ of focal sphere}}$

What is the volume of a crack formed by this process?

It is shown above that for a tensile crack:

$$M = V \begin{vmatrix} \lambda+2\mu & 0 & 0 \\ 0 & \lambda & 0 \\ 0 & 0 & \lambda \end{vmatrix}$$

Approximating the Hengill events to a linear vector dipole, we must superimpose an implosion of amplitude proportional to λ:

i.e. of the form:

$$\begin{vmatrix} -\lambda & 0 & 0 \\ 0 & -\lambda & 0 \\ 0 & 0 & -\lambda \end{vmatrix}$$

then for a typical Hengill event:

$$M = V \begin{vmatrix} 2\mu & 0 & 0 \\ 0 & 0 & 0 \\ 0 & 0 & 0 \end{vmatrix}$$

$$\boxed{M_0 = 2\mu V}$$

6 RECOMMENDATIONS FOR FURTHER STUDIES

That the source mechanisms are anomalous is indisputable. The possibility that factors other than source mechanism are responsible for the anomalous radiation patterns (e.g. crustal inhomogeneity, equipment malfunction) are ruled out because:

a) explosions and teleseisms were recorded at intervals during the monitoring period and consistant polarities were recorded.

b) many double couple solutions were also obtained for local events. However as may readily be seen from the examples shown in Fig. 1, constraint on the shape of the nodal lines is very weak. Better constraint could be obtained by conducting a computer study to contour P-wave amplitudes on the focal sphere.

If such a study were conducted with the Hengill data, the benefits gained would be:

a) confirming or disproving whether we are indeed observing tensile crack formation at depth in the earth`s crust. At the moment this model remains a tentative proposal.

b) extracting more detail from the mechanisms e.g. the ratio of dilatational to shear movement. This would tell us if some of the mechanisms are mixtures of shear and tensile crack movement. 10% of the polarity plots would not permit either a shear or a tensile crack solution, possibly because they have composite mechanisms, and the nodal lines are hence neither small nor great circles.

The Hengill data are unique as far as is known, with the possible exception of a small amount of data collected on the Reykjanes peninsula. The implications of these results could profoundly affect our perception of:

- The tectonics and geothermal reservoir of the Hengill area.
- The behaviour in general of high temperature geothermal areas in tensional stress regimes - i.e. Icelandic high temperature geothermal areas
- The tectonics of the active rift system in Iceland, and hence the accretion of the Icelandic landmass.
- The tectonics of the mid ocean rift system and the mechanism of dyke emplacement.

REFERENCES

Aki, Keiiti and Richards, P.G., Quantitative Seismology, Freeman, San Francisco, 1980.

Ewing, W.M., Jardetzky, W.S. and Press, F., Elastic waves in layered media. McGraw - Hill, 1957.

Foulger, G. and Long, R.E., Anomalous focal mechanisms: Evidence for tensile crack formation on an accreting plate boundary. Nature, 310, 43-45, 1984.

Julian, B.R., Analyzing seismic-source mechanisms by linear programming. J.R. astr. Soc., in press.

Julian, B.R., Evidence for dyke intrusion earthquake mechanisms near Long Valley caldera, California. Nature, 303, 323-325, 1983.

Randall, M.J. and Knopoff, L., The mechanism at the focus of deep earthquakes. J. Geophys. Res., 75, 4965-4976, 1970.

POLARITY PLOTS

JHD JEÐ-8716 GRF
84.07 0881 SyJ

KLAMBRAGIL I OF 3

N

N

N

N

81.07.17 0555 d=3,56
M=-0,3

81.07.19 0743 d=5,24
M=-1,0

81.07.22 0626 d=3,83
M=-1,1

81.07.22 2138 d=5,90
M=-0,5

N

N

N

N

81.07.27 0548 d=3,99
M=0,0

81.07.28 0419 d=5,16
M=-0,5

81.07.28 0420 d=5,51
M=-1,3

81.07.28 1413 d=4,1
M=-1,4

N

N

N

N

81.07.28 1718 d=3,45
M=-1,1

81.08.01 2038 d=3,57
M=-1,4

81.08.02 1418 d=3,63
M=-0,7

81.08.03 1937 d=4,07
M=-0,8

N

N

N

N

81.08.13 0402 d=4,96
M=-0,5

81.08,14 0407 d=3,67
M=-0,9

81.08.14 0856 d=3,63
M=-1,5

81.08.14 2114 d=3,37
M=-1,8

Fig. A2.1 Polarity plots of events from Klambragil, 1 of 3.

167

KLAMBRAGIL 1 OF 3

810815 2025 d=5,15 M=0,9
81 0815 2030 d=4,97 M=0,1
810815 2041 d=4,95 M=-1,2
810815 2114 d=5,02 M=-1,1

810818 0722 d=3,87 M=-1,2
810819 1412 d=4,10 M=-0,1
810823 2050 d=3,67 M=-1,9
810828 1126 d=4,32 M=1,3

810828 1517 d=3,81 M=-0,9
810828 1545 d=4,24 M=-0,6
810829 0139 d=3,60 M=-0,8
810830 1400 d=3,75 M=-0,7

810830 1607 d=3,47 M=-0,1
810903 1419 d=3,35 M=-0,7
810903 1844 d=2,71 M=-1,5
810906 1151 d=3,61 M=-1,1

Fig. A2.2 Polarity plots of events from Klambragil, 1 of 3.

KLAMBRAGIL 1 OF 3

81.09.06 2018 d=4,28
M=0,8

81.09.07 0123 d=3,14
M=-0,1

81.09.12 2237 d=3,74
M=-0,3

81.09.18 0643 d=3,14
M=-0,4

81.09.23 0501 d=3,51
M=0,0

81.09.23 2111 d=3,62
M=-1,2

81.09.27. 0156 d=3,55
M=-0,8

SUMMARY – KLAMBRAGIL

81.09.28 1853 d=3,25
M=1,3

81.09.28 1923 d=2,97
M=0,1

81.09.28 2002 d=3,16
M=-0,5

81.09.28 2008 d=2,97
M=-0,6

81.09.29 2123 d=3,79
M=-0,7

81.10.03 0259 d=3,72
M=-0,8

Fig. A2.3 Polarity plots of events from Klambragil, 1 of 3.

Fig. A2.4 Polarity plots of events from the Fissure swarm, 1 of 2.

JHD-JEÐ-8716.GRF
84.07. 0886. SyJ.

FISSURE SWARM 1 OF 2

N

81 09 24 1103 d=6,71
M=-1,1

N

81 09 24 1956 d=6,24
M=-0,5

N

81 09 27 1049 d=4,56
M=-0,1

N

81 09 30 0211 d=4,61
M=0,6

MOSFELLSHEIÐI

N

81 07 25 1653 d=3,73
M=-0,7

N

81 08 21 1639 d=3,27
M=-1,7

N

81 09 02 1026 d=3,56
M=-1,5

N

81 10 05 0425 d=3,30
M=-0,3

N

81 10 05 0607 d=3,44
M=-0,6

N
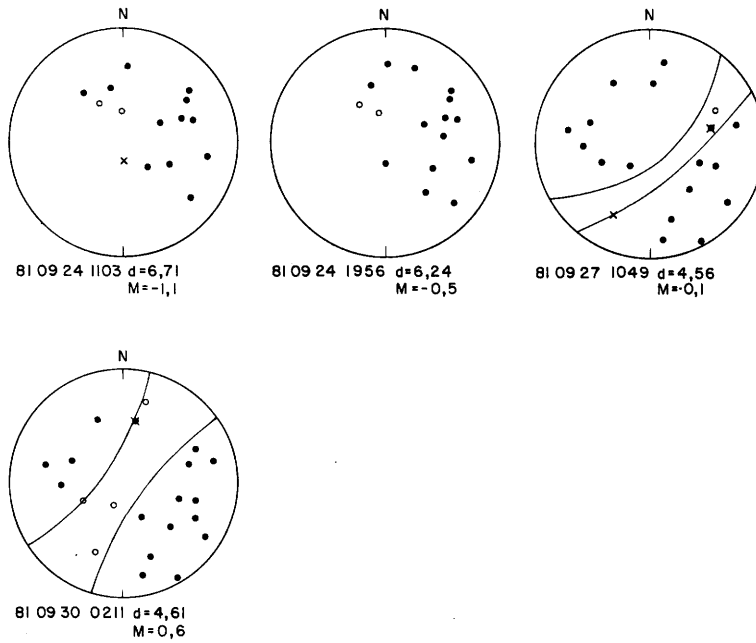
SUMMARY-MOSFELLSHEIÐI
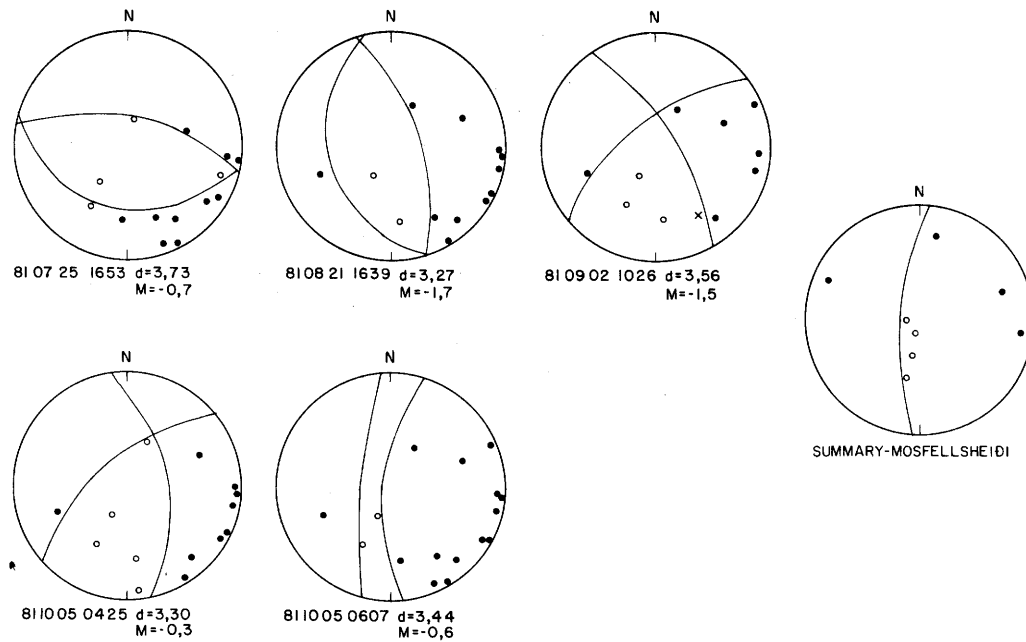
Fig. A2.5 Polarity plots of events from the Fissure swarm, 1 of 2,
and Mosfellsheiði.
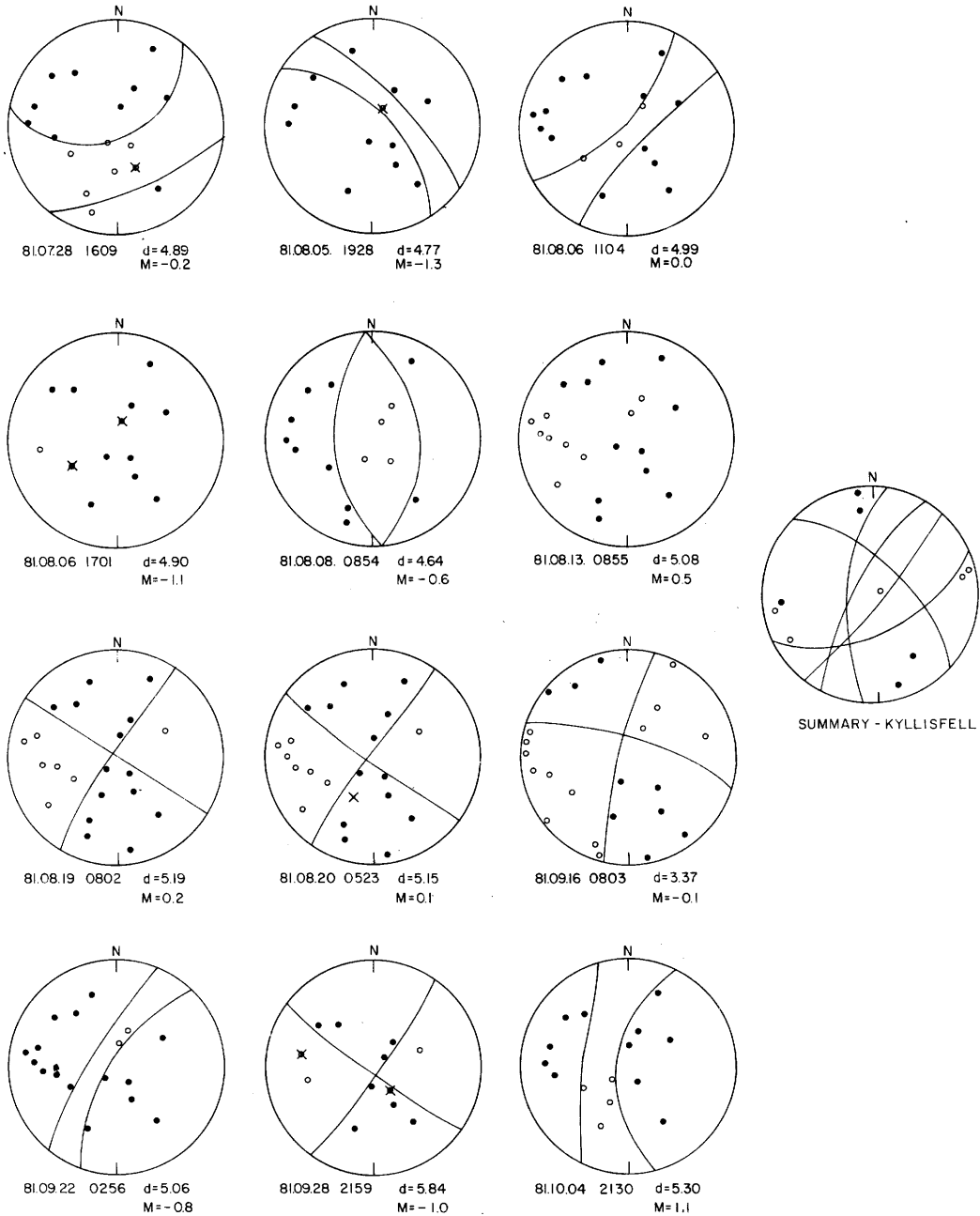
Fig. A2.6 Polarity plots of events from Kyllisfell.
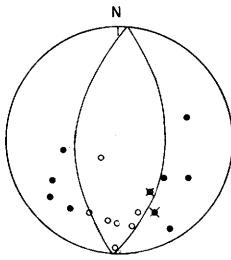
NESJAVELLIR

81 07 26 0124 d=5,10
M=-0,3
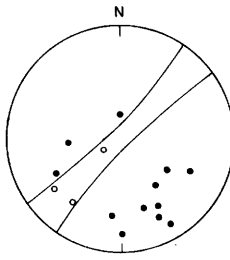
81 07 31 1634 d=5,32
M=-0,2
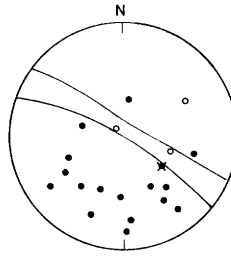
81 08 04 2112 d=6,08
M=0,50
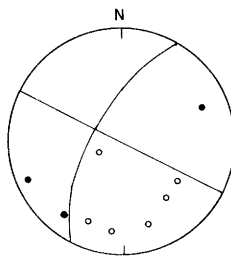
81 08 06 1414 d=3,97
M=-1,0
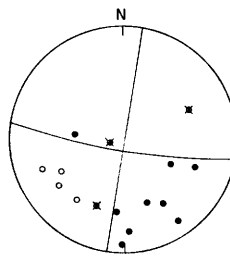
81 08 15 1119 d=5,46
M=-0,6
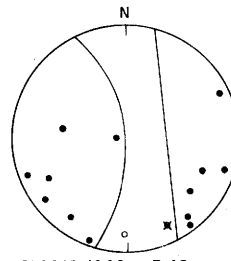
81 08 16 1020 d=3,42
M=-0,6
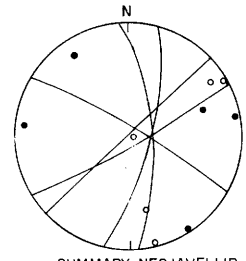
SUMMARY-NESJAVELLIR
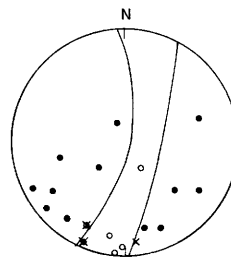
81 08 20 1004 d=4,48
M=0,1
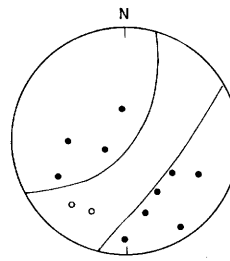
81 08 22 0205 d=4,80
M=-1,0
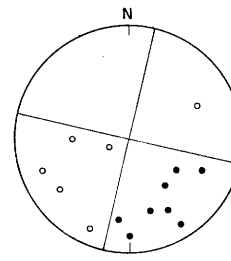
81 09 16 2206 d=4,94
M=-0,8
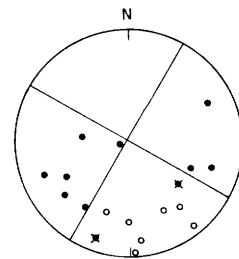
81 10 03 2153 d=4,71
M=-0,1

Fig. A2.7   Polarity plots of events from Nesjavellir.

JHD-JED-8716-GRF
84.07.0889. '0D

CLUSTER 1 OF 2

81.07.23. 1147   d=4.41
M=0.1

81.07.28.2351   d=5.12
M=-0.8

81.07.29 1952   d=4.06
M=-0.9

81.07.31. 2258   d=4.74
M=-0.2

81.08.01. 1910   d=4.94
M=-1.7

81.08.01. 1915   d=4.69
M=-0.9

81.08.03. 2355   d=3.20
M=0.0

81.08.10.1303   d=4.24
M=0.4

81.08.10.1308   d=4.28
M=-0.2

SUMMARY-CLUSTER

81.08.10.1558   d=5.0
M=-1.0

81.08.15.0302   d=4.44
M=0.0

81.08.17 2105   d=3.87
M=-0.8
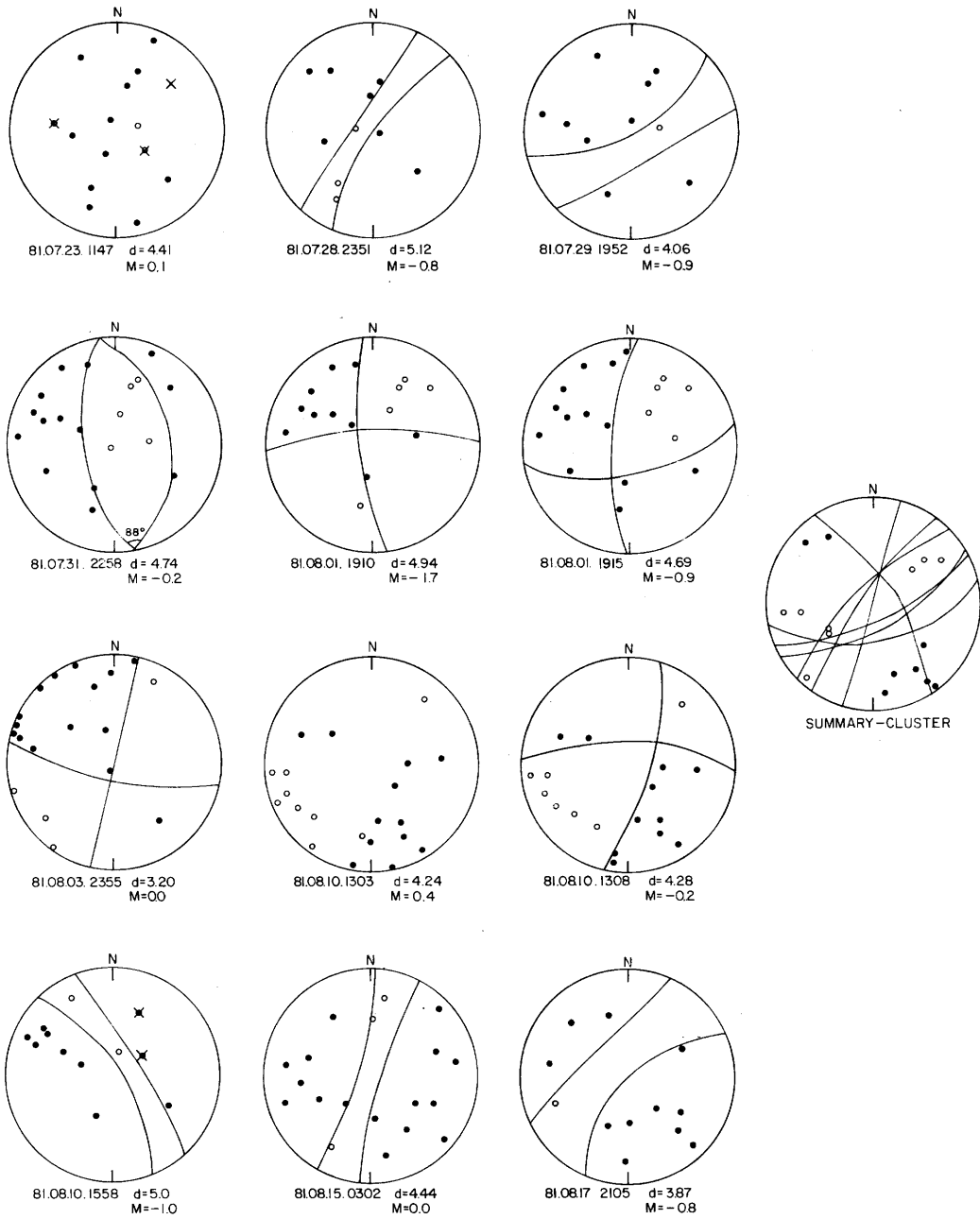
Fig. A2.8   Polarity plots of events from the central cluster, 1 of 2.

JHD-JED-8716.GRF
84.07.0877 SyJ

CLUSTER I OF 2

8108 21 2029 d=4,46
M=-1,1

8108 26 0355 d=3,97
M=-1,0

81 09 02 2002 d=3,65
M=-1,1

81 09 29 0624 d=5,23
M=0,3

81 09 13 1329 d=4,56
M=-1,0

81 09 21 1201 d=4,22
M=-0,7

81 09 28 0941 d=5,13
M=0,5

LAXÁRDALUR

810915 1459 d=3,38
M=-0,5

810915 1520 d=2,87
M=-0,4

81 09 15 1531 d=3,14
M=-0,3

SUMMARY-LAXÁRDALUR

810915 1535 d=3,01
M=-0,9

810915 1600 d=3,16
M=-0,2

81 09 15 1611 d=2,79
M=-0,5
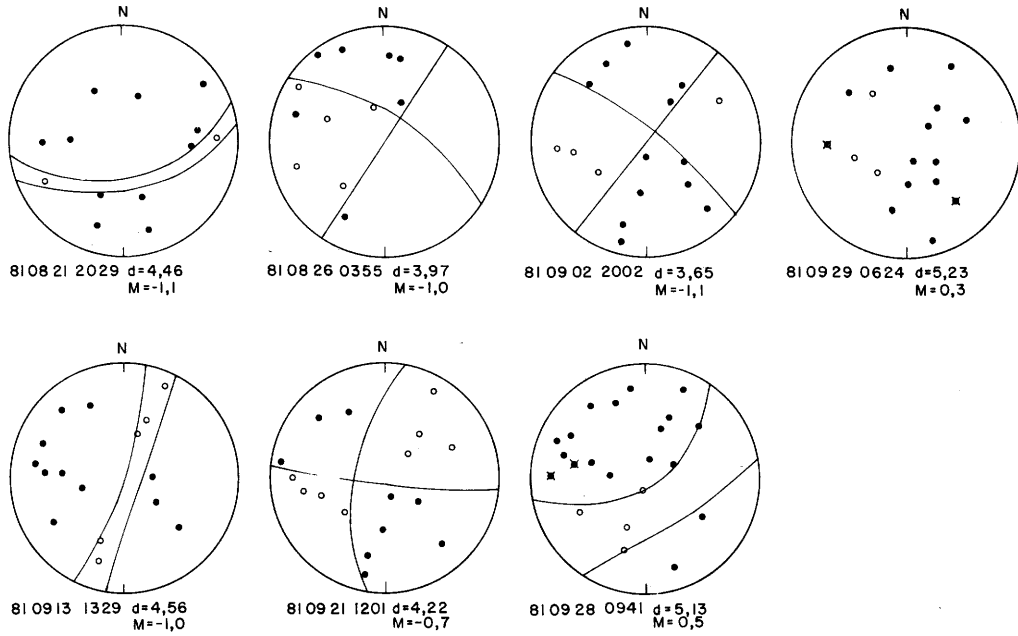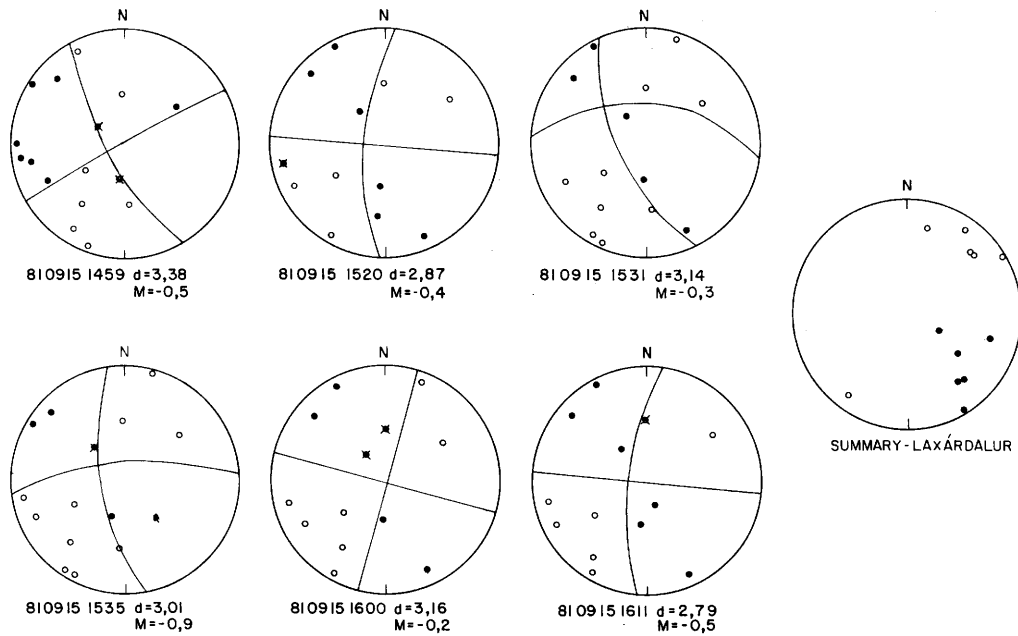
Fig. A2.9 Polarity plots of events from the central cluster, 1 of 2, and Laxárdalur.

JHD·JED·8716.GRF
84.04. 0882.SyJ

HVERAGERÐI

8I 07 20 0656 d=5,25
M=0,4

8I 07 20 2051 d=5,77
M=0,2

8I 07 30 0622 d=4,87
M=0,I

8I08 04 I233 d=I,94
M=-0,8

8I08 I2 08I4 d=2,79
M=-0,8

8I08 I2 08I8 d=3,42
M=0,5

8I08 I4 0346 d=4,40
M=-0,9

8I 09 02 0529 d=6,0
M=-0,I

8I0908 0240 d=6,I5
M=I,I

SUMMARY - HVERAGERÐI

8II0 03 0942 d=4,I5
M=-0,7
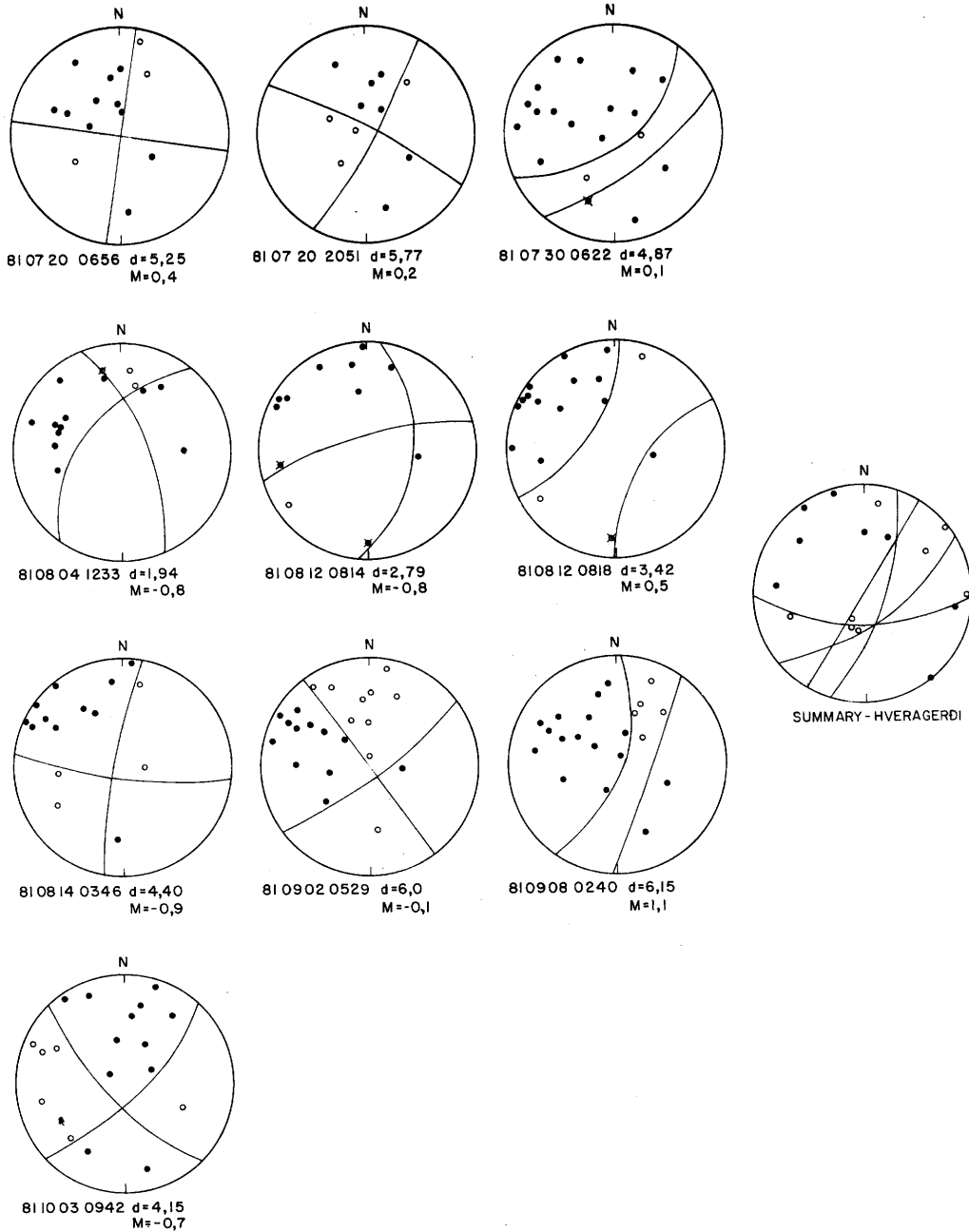
Fig. A2.I0 Polarity plots of events from Hveragerði.
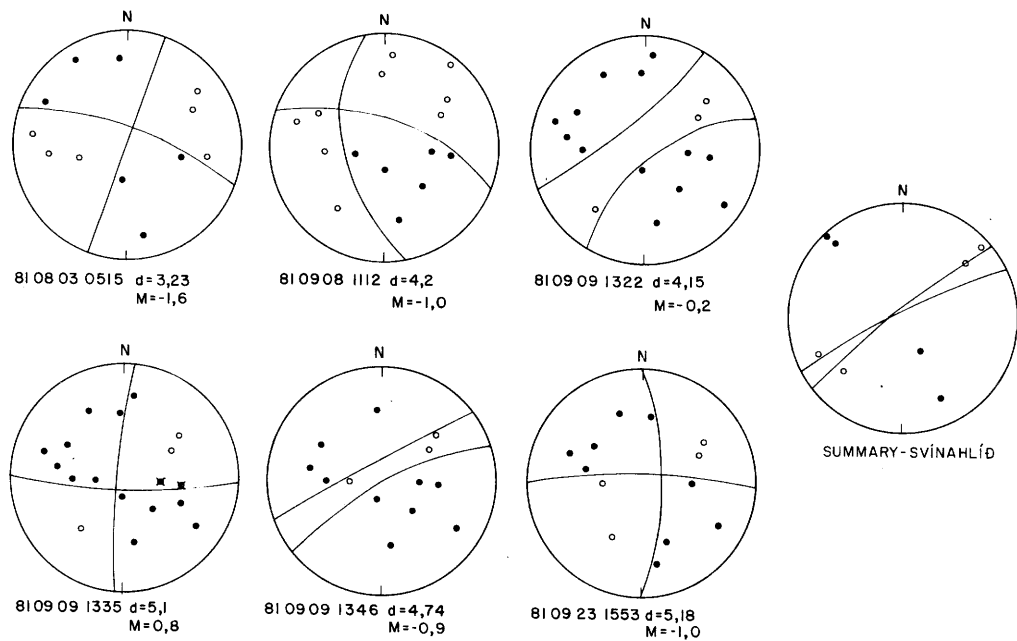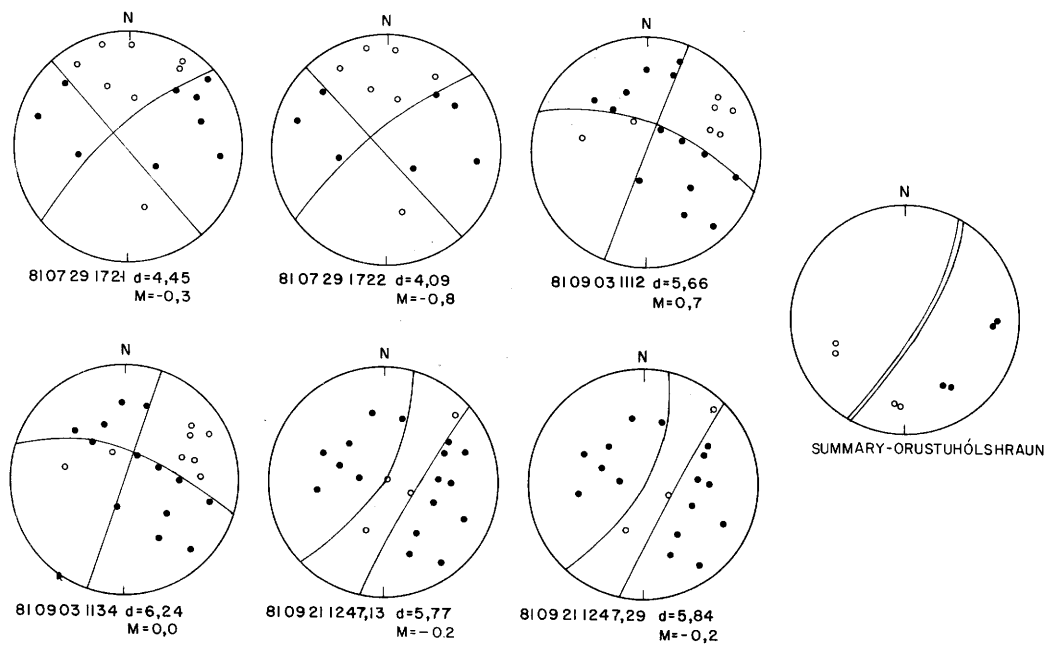
Fig. A2.11 Polarity plots of events from Svínahlð and Órustuhólshraun.

ÖLFUS I OF 2

81.07.24 0214 d=5,66
M=0,2

81.07.31 0246 d=6,74
M=-0,9

81.08.01 0810 d=6,70
M=-0,9

81.08.03 0236 d=6,85
M=-1,0

81.08.04 0928 d=4,29
M=-1,3

81.08.06 1012 d=6,45
M=-0,8

81.08.06 1018 d=6,48
M=-0,7

81.08.08 1728 d=7,05
M=-0,5

81.08.10 1236 d=6,87
M=-0,2

81.08.13 0010 d=7,04
M=-0,9

81.08.13 2144 d=7,33
M=-0,6

81.08.14 1749 d=6,02
M=-1,2

81.08.15 1819 d=5,44
M=-1,1

81.08.17 0946 d=7,11
M=0,20

81.08.17 0948 d=6,26
M=0,6

81.08.17 0955 d=6,62
M=1,0
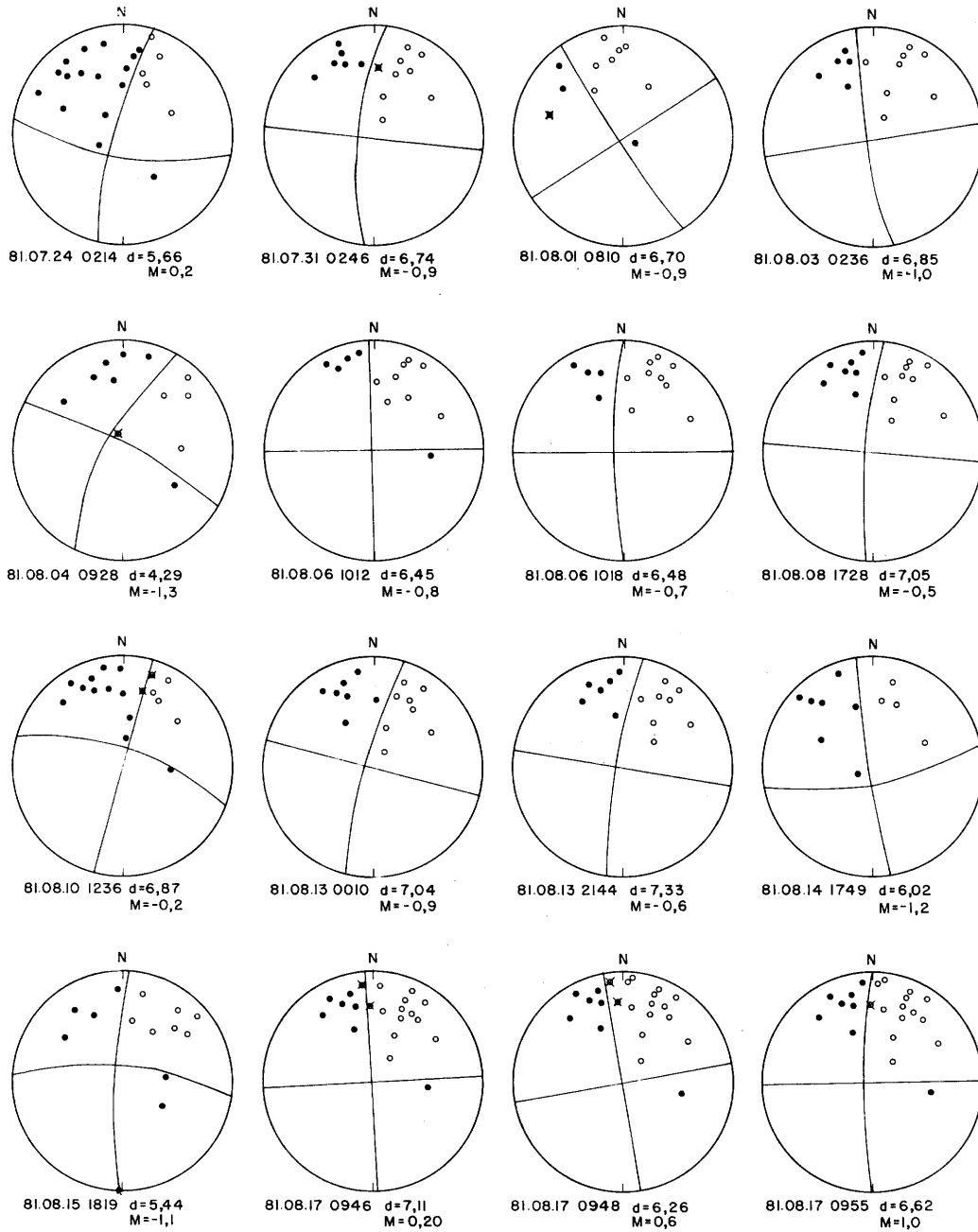
Fig. A2.12 Polarity plots of events from Ölfus, 1 of 2.

JHD-JE0-8716 GRF
84.07. 0884. SyJ

ÖLFUS I OF 2

810817 1006 d=6,69
M=-0,1

8108 22 0910 d=8,30
M=-0,3

81 09 02 0707 d=6,41
M=-0,1

810902 0711 d=6,55
M=-0,5

810904 2123 d=6,57
M=-0,6

810917 0718 d=6,42
M=-0,6

810918 0209 d=6,48
M=-0,6

81 09 20 0344 d=8,61
M=-0,1

810922 0134 d=3,77
M=-0,2

810922 0259 d=4,09
M=0,1

8109 22 1854 d=3,64
M=0,1

SUMMARY-ÖLFUS

810922 1941 d=4,07
M=-0,5

810922 2129 d=3,92
M=-0,8

8109 24 1219 d=4,66
M=0,9

A2.13 Polarity plots of events from Ölfus, 1 of 2.
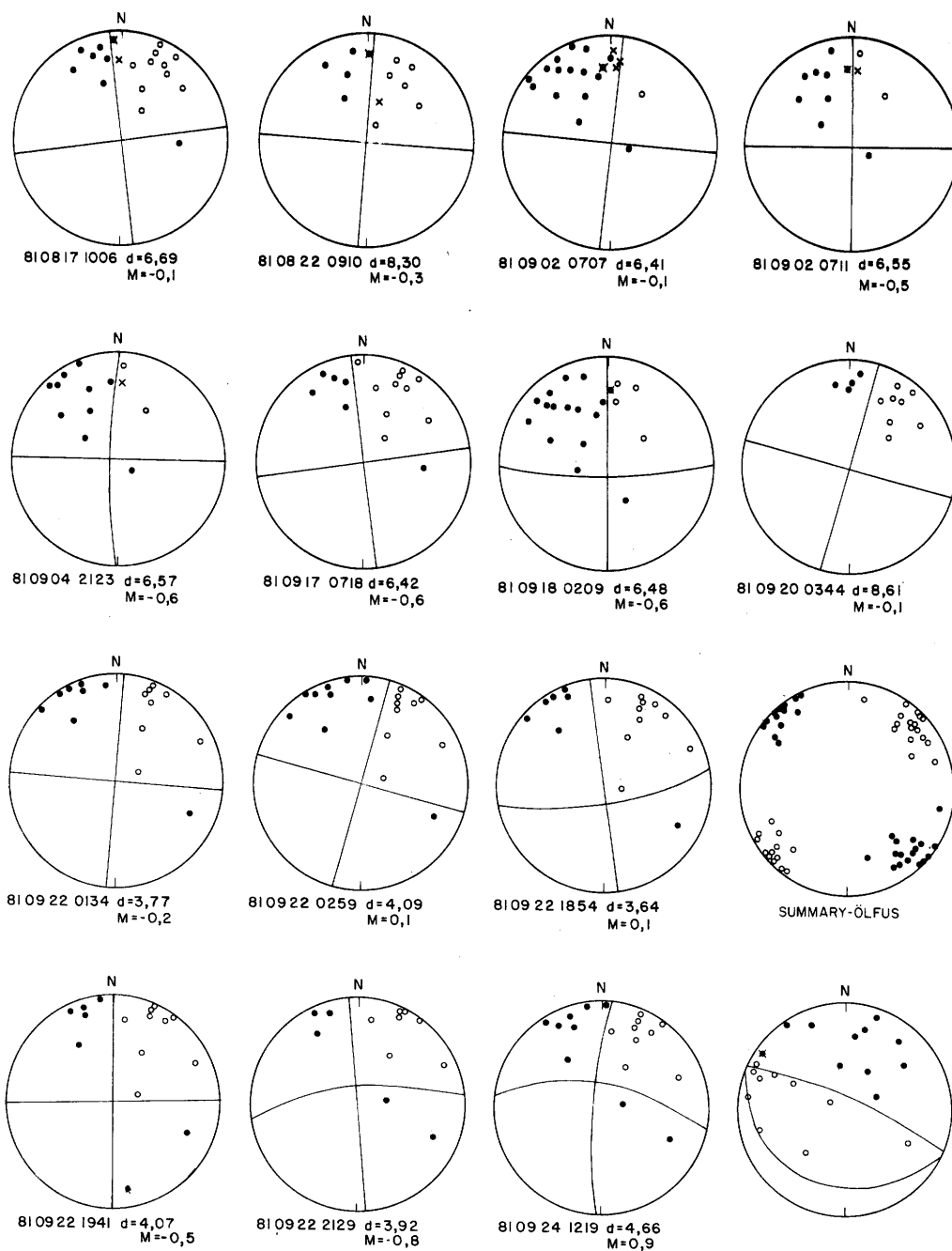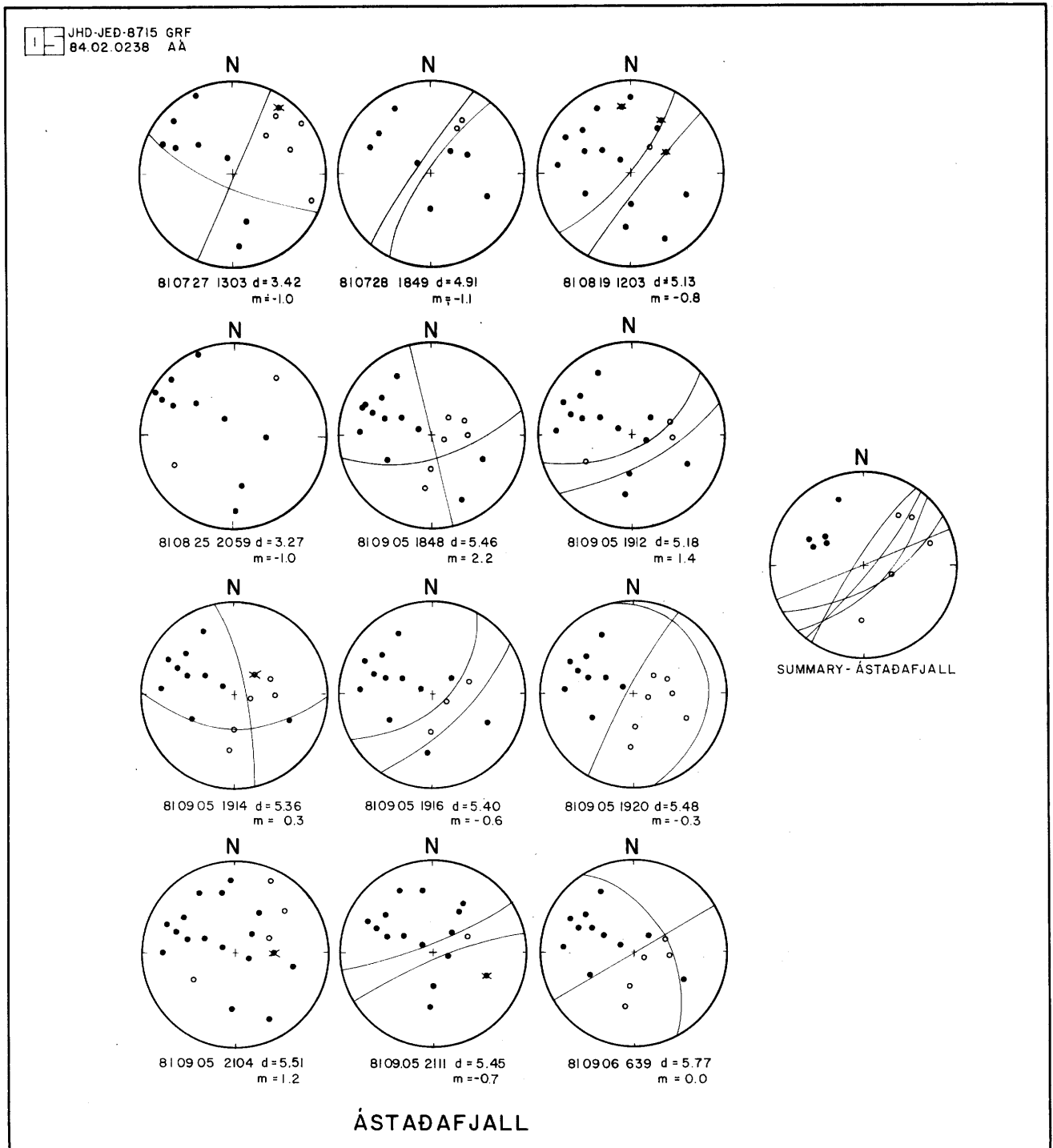
Fig. A2.14 Polarity plots of events from Ástaðafjall.

APPENDIX 3

DERIVATION OF THE EXPRESSION DESCRIBING THE FORM OF THE FREQUENCY - MAGNITUDE PLOT OF A COMBINATION OF TWO EARTHQUAKE SETS EXHIBITING DIFFERENT B-VALUES

for earthquake set (a): $\log_{10} N = a - bM$

for earthquake set (b): $\log_{10} N' = a' - b'M$

then $N = 10^{(a-bM)}$ $N' = 10^{(a'-b'M)}$

$$N + N' = 10^{(a-bM)} + 10^{(a'-b'M)}$$

if earthquake sets (a) and (b) were combined:

$$\log_{10}(N + N') = \log_{10}(10^{(a-bM)} + 10^{(a'-b'M)})$$

$$= \log_{10}\left[10^{(a-bM)} (1 + 10^{(a'-a)-(b'-b)M})\right]$$

$$\log_{10}(N + N') = a - bM + \log_{10}(1 + 10^{(a'-a)-(b'-b)M})$$

if $a = a'$, then

$$\log_{10}(N + N') = a - bM + \log_{10}(1 + 10^{(b-b')M})$$

This expression is non-linear and describes the expected form of the frequency-magnitude plot for the composite data set.

The slope of the plot decreases with increasing magnitude i.e. the plot is always upwards concave.

SEISMICITY CHARTS 1930 - 1983

Figs. A3.1 - A3.9 Seismicity charts based on the station REY. Events reported as felt but not recorded are indicated as magnitude 1 events
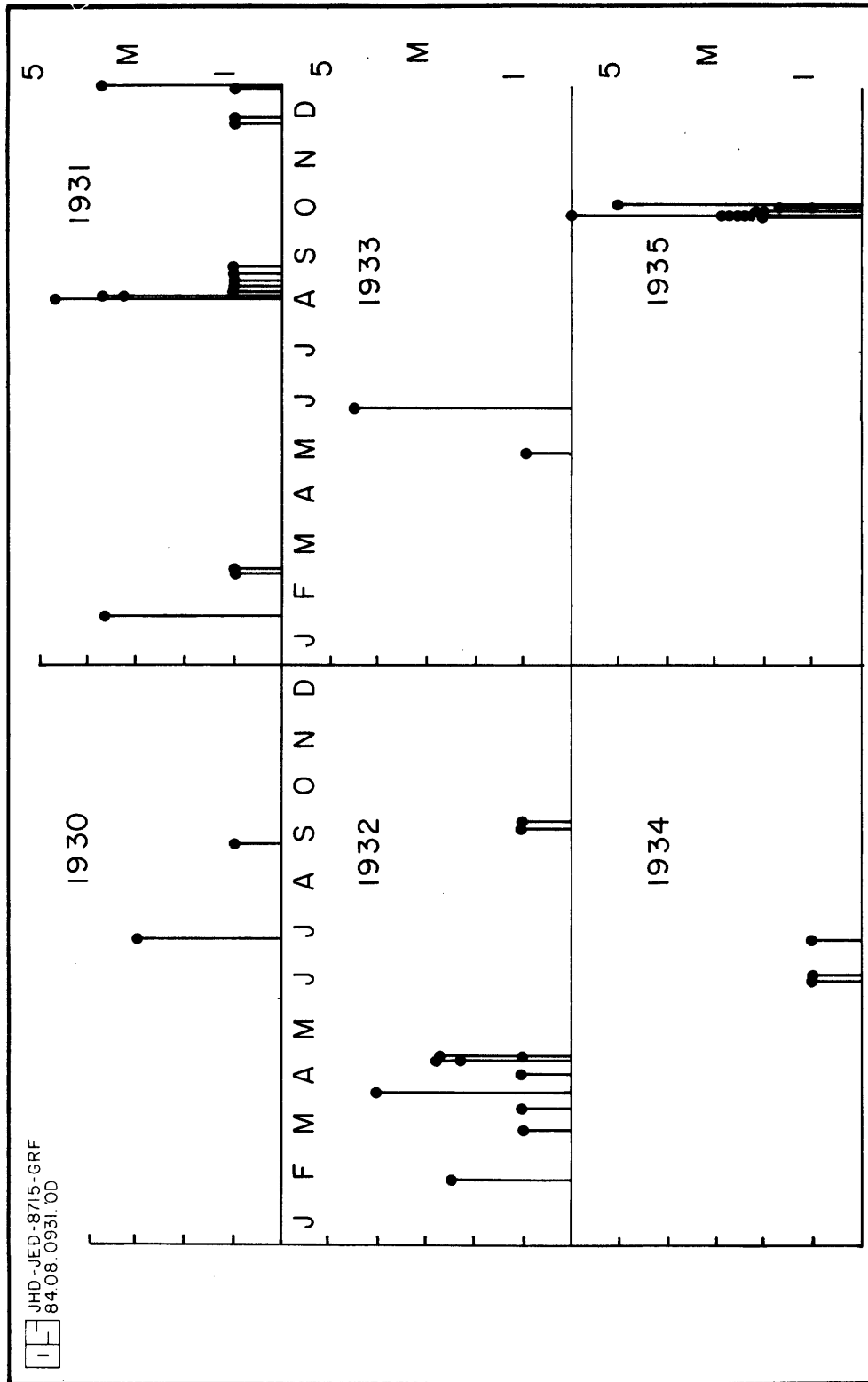
Fig. A3.1 1930 - 1935
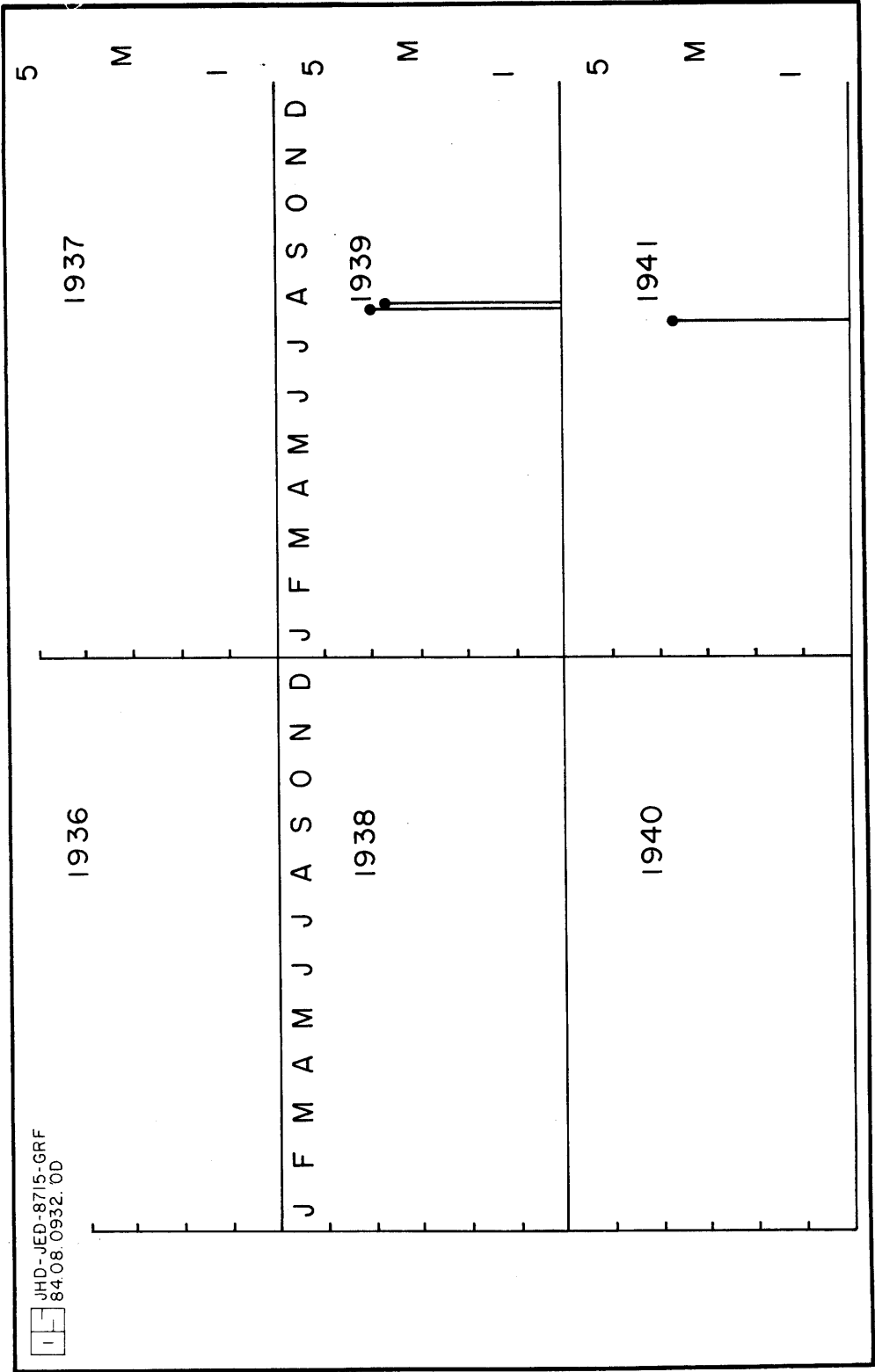
Fig. A3.2   1936 - 1941
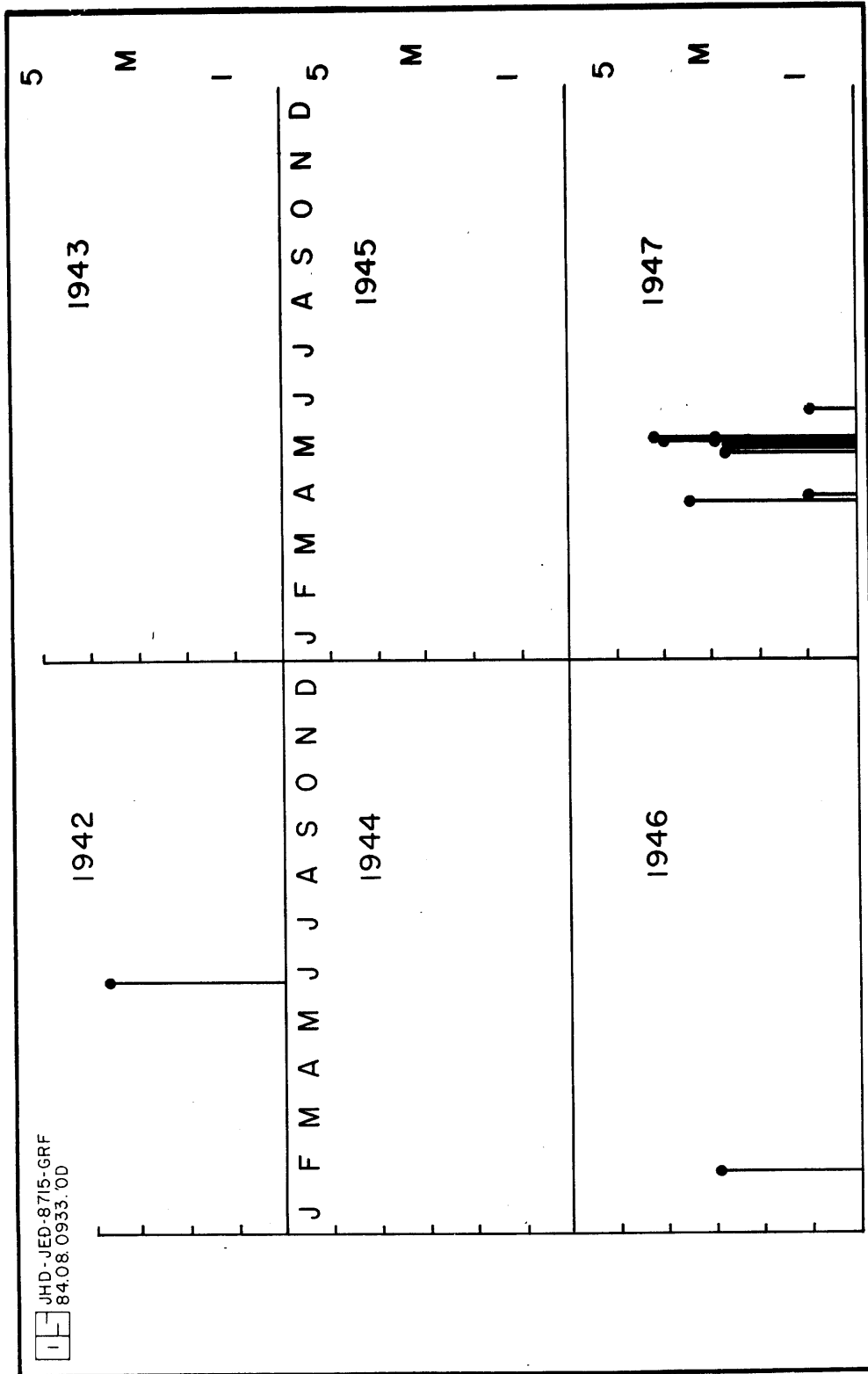
Fig. A3.3 1942 – 1947
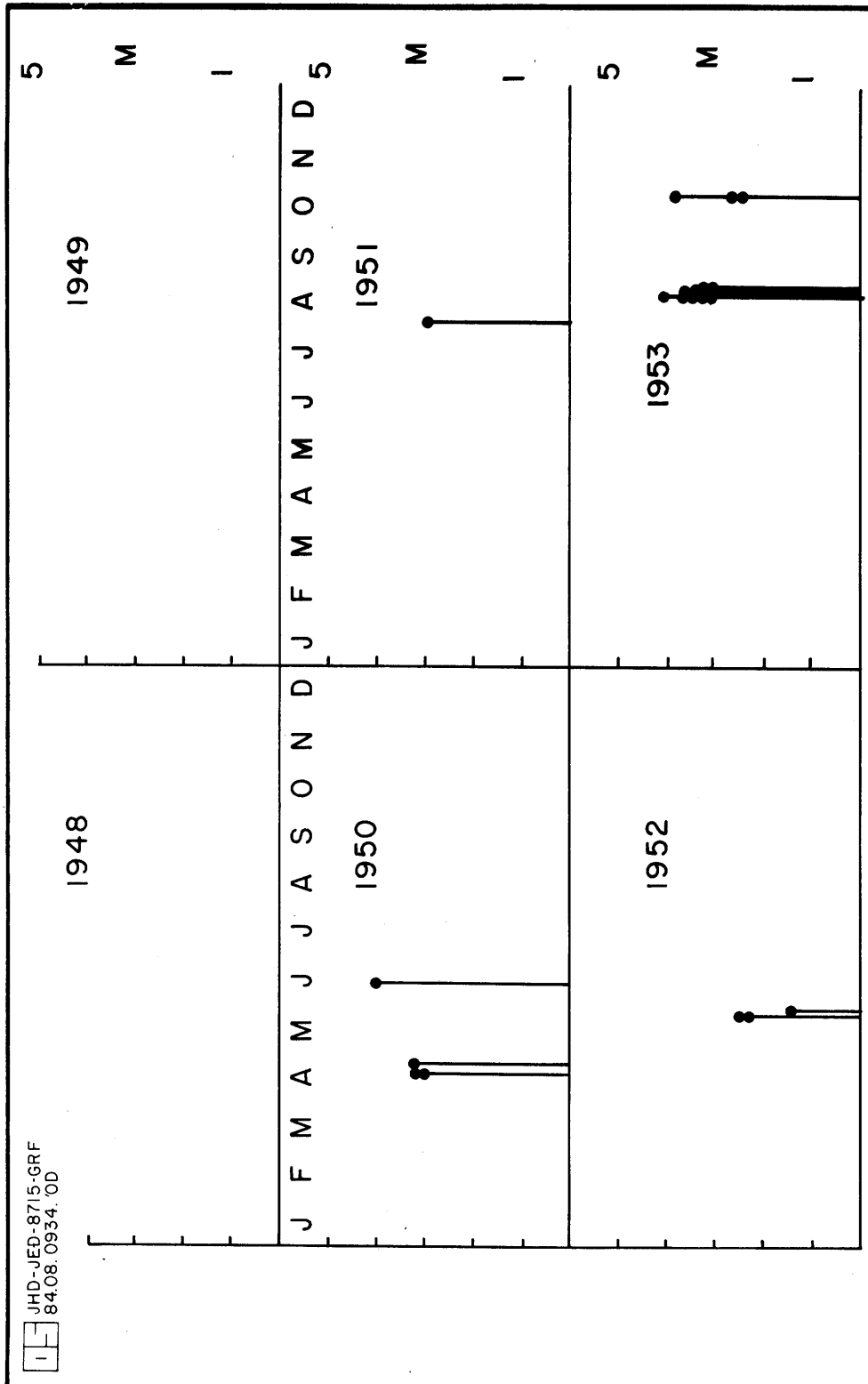
Fig. A3.4 1948 - 1953
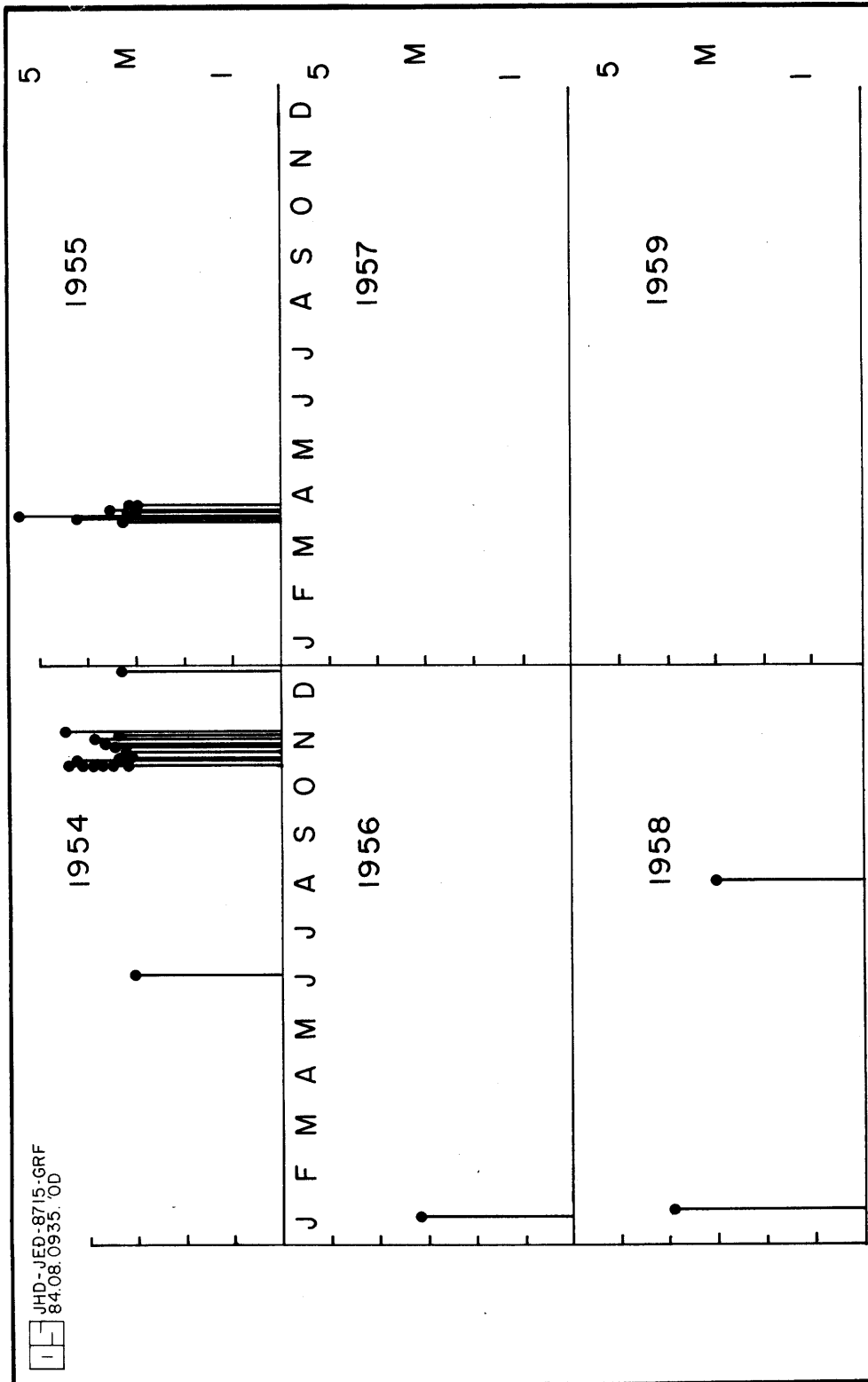
Fig. A3.5 1954 - 1959
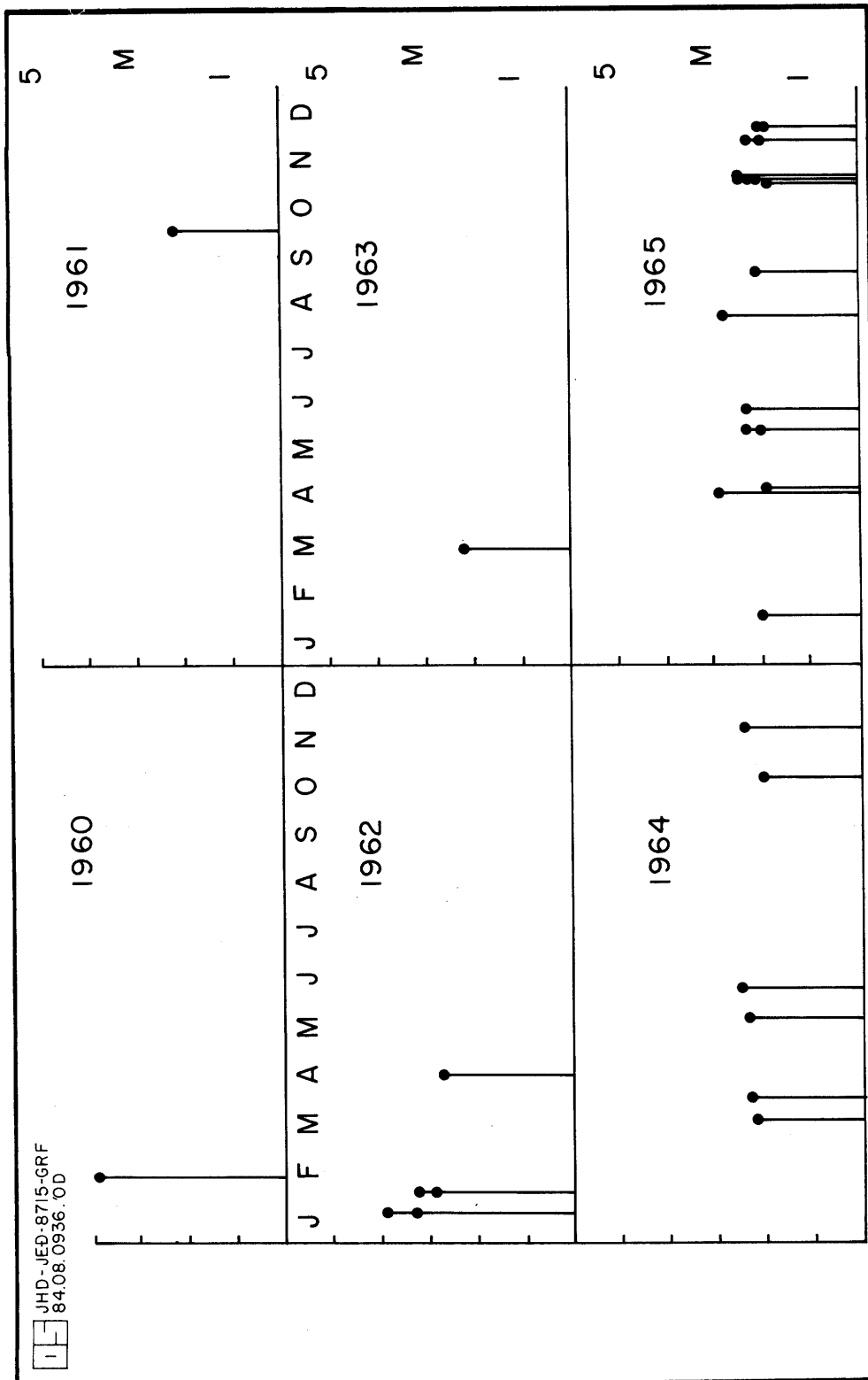
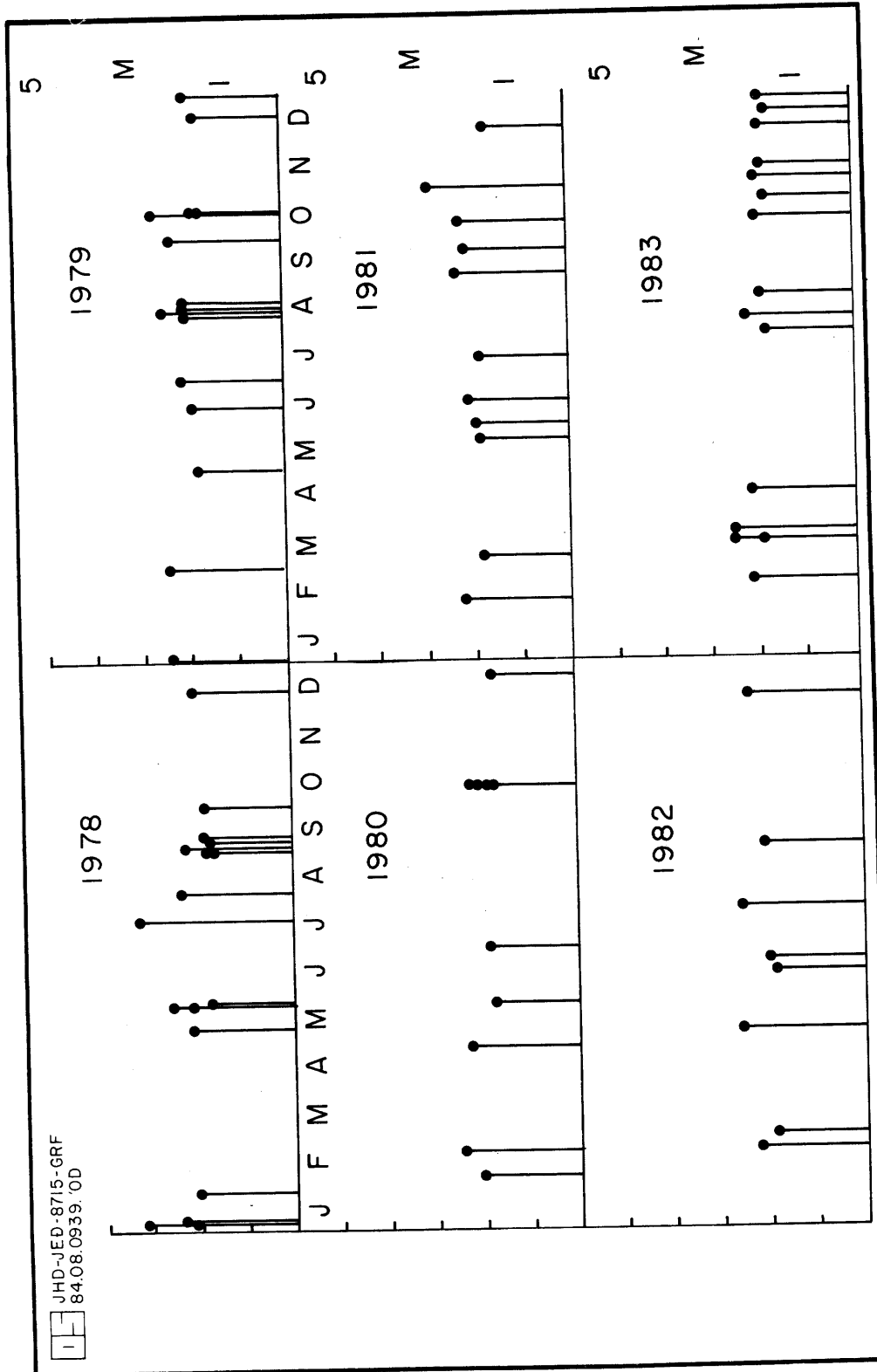Fig. A3.6 1960 - 1965
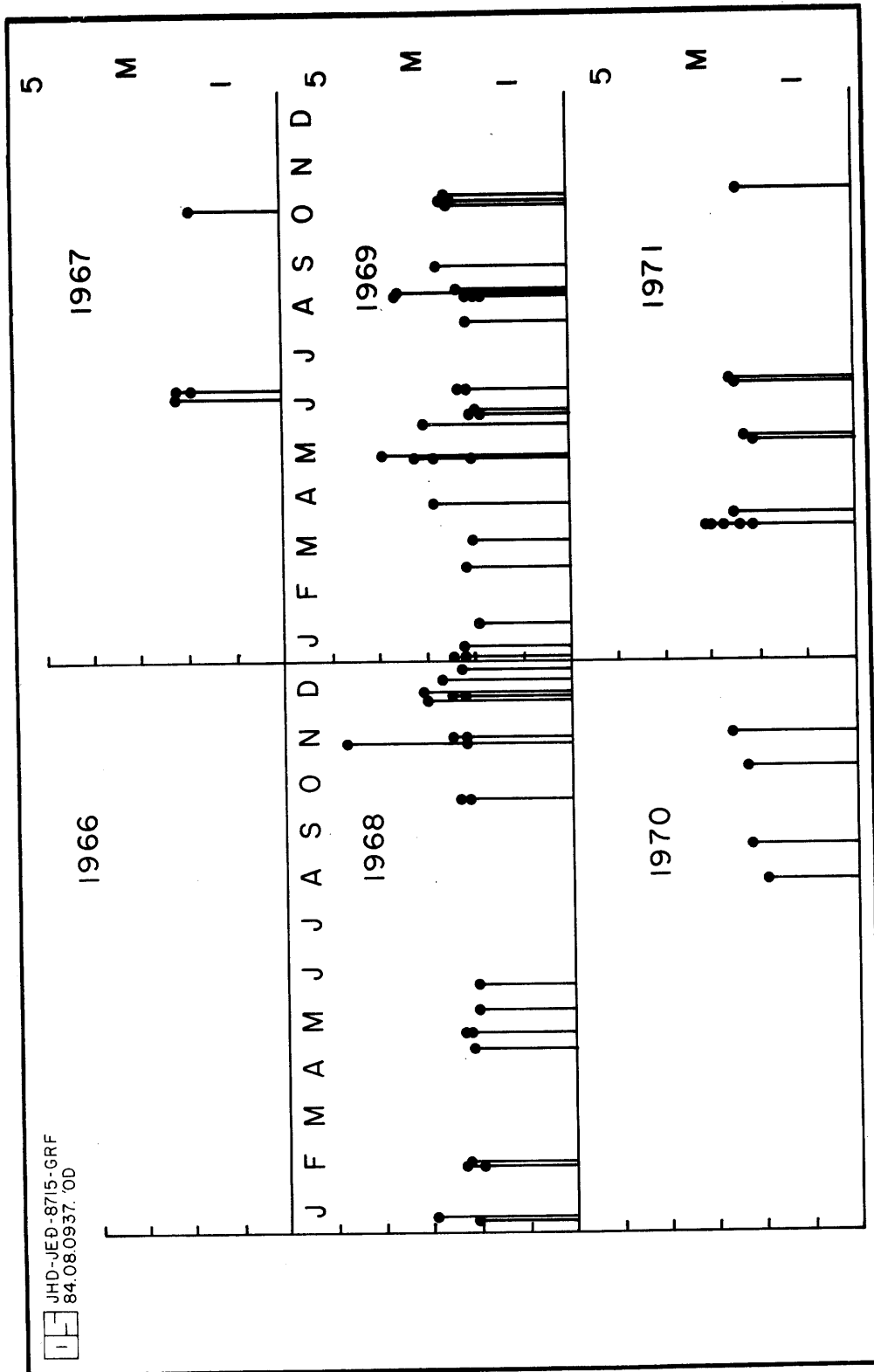
Fig. A3.7 1966 - 1971
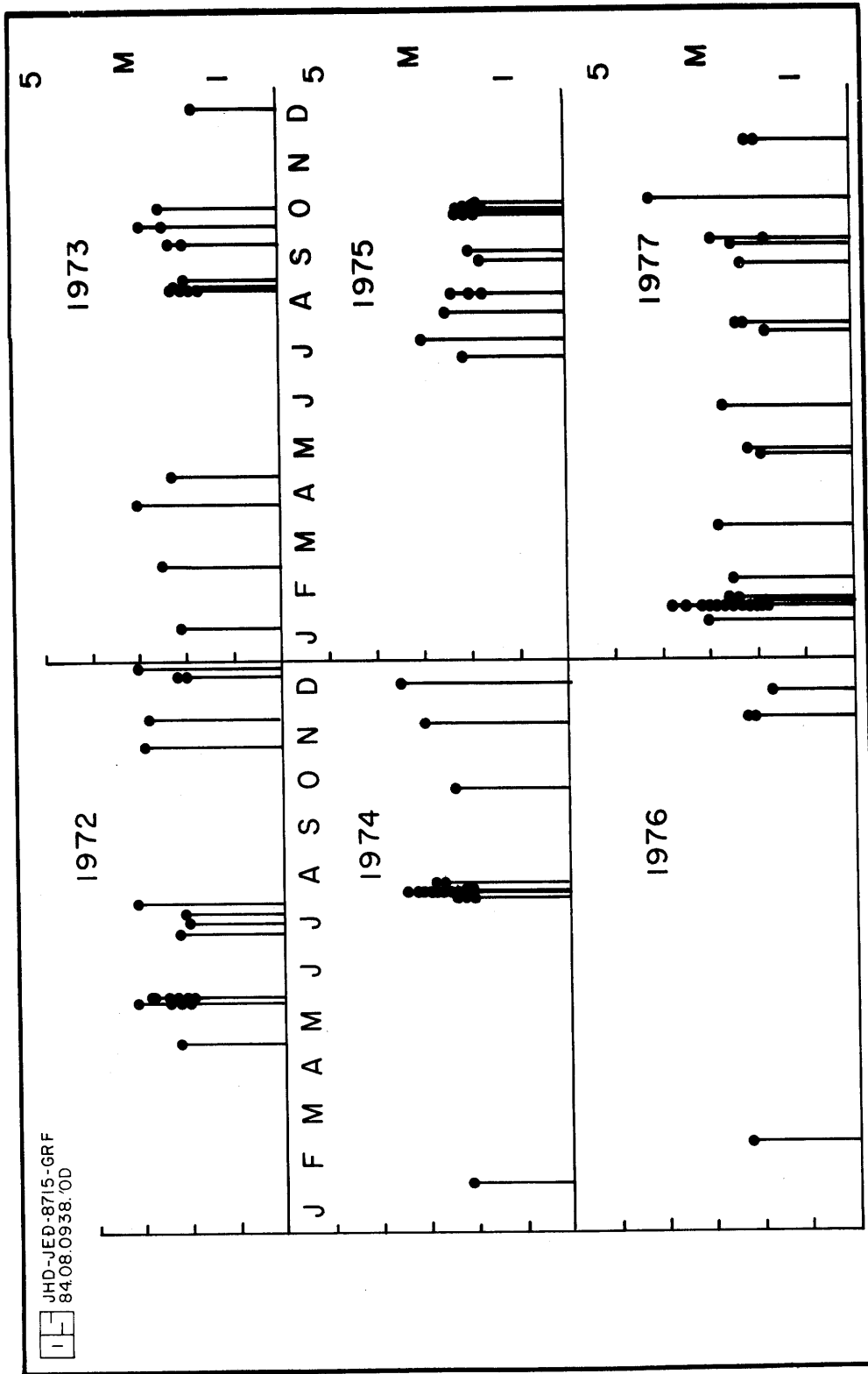
Fig. A3.8 1972 – 1977

Fig. A3.9 1978 – 1983

Figs. A3.10 - A3.16 Seismicity charts based on the station IR. $M_{IR}^{'}$ is coda length magnitude computed for IR, N is number of events.
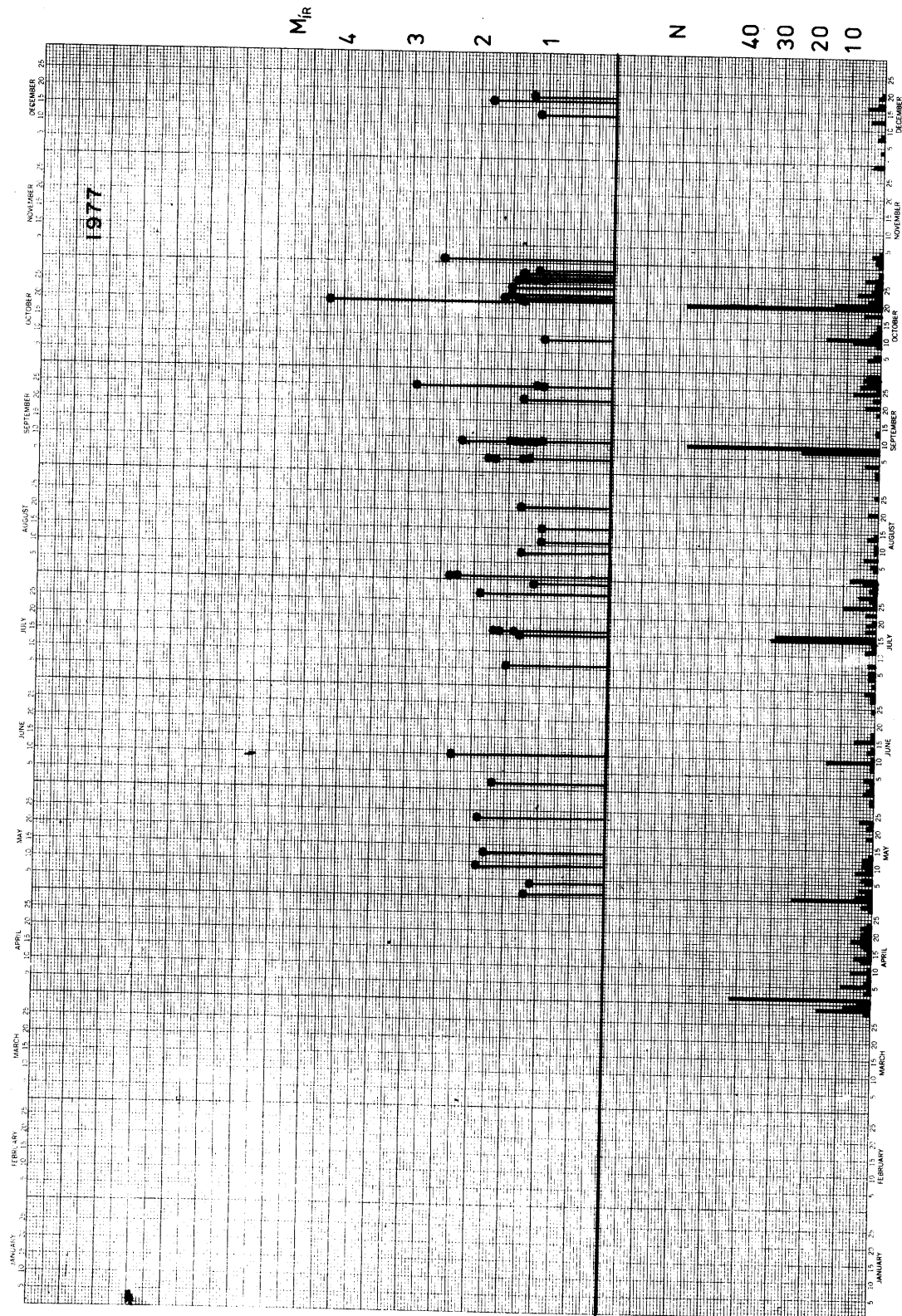
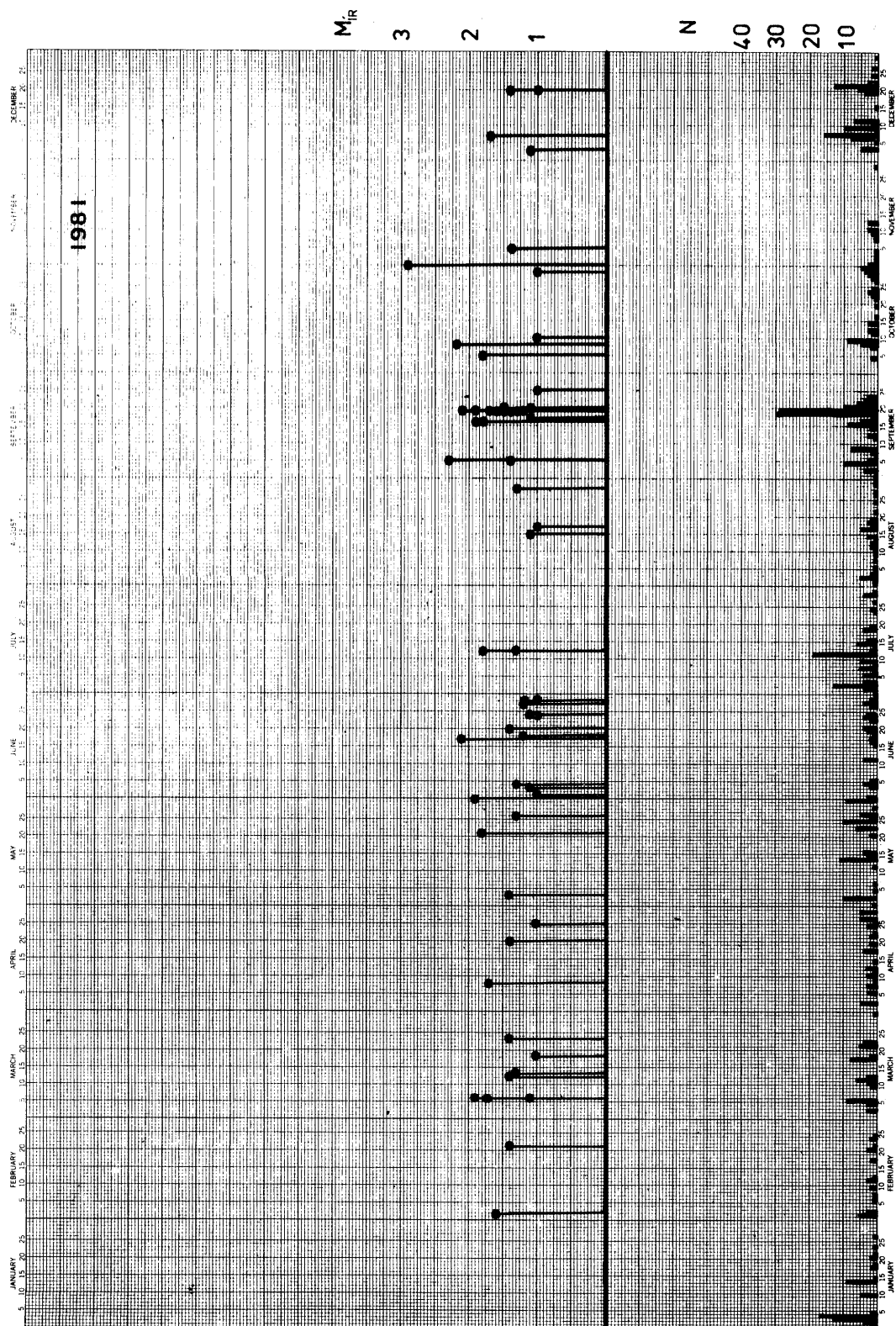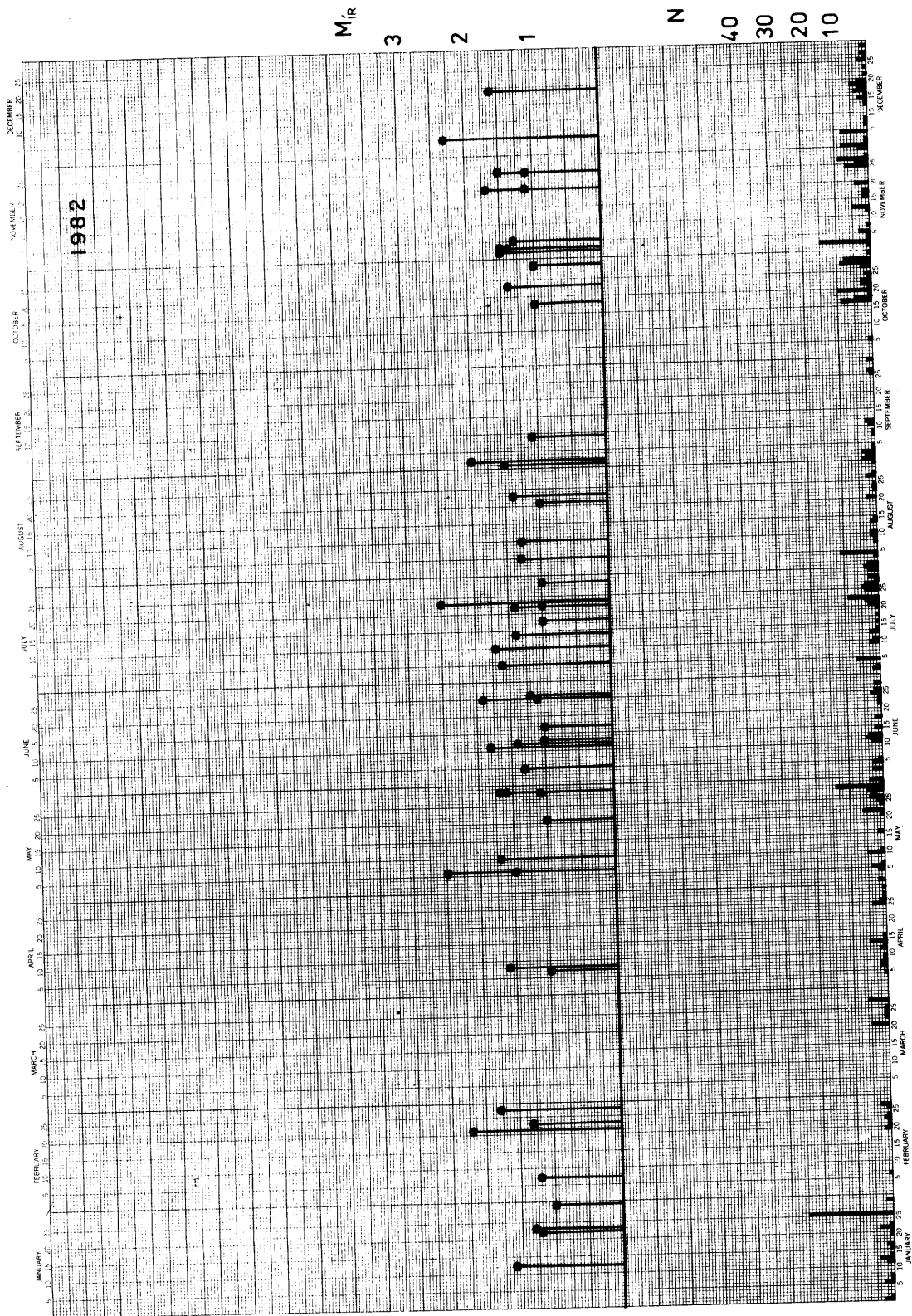Fig. A3.10 1977
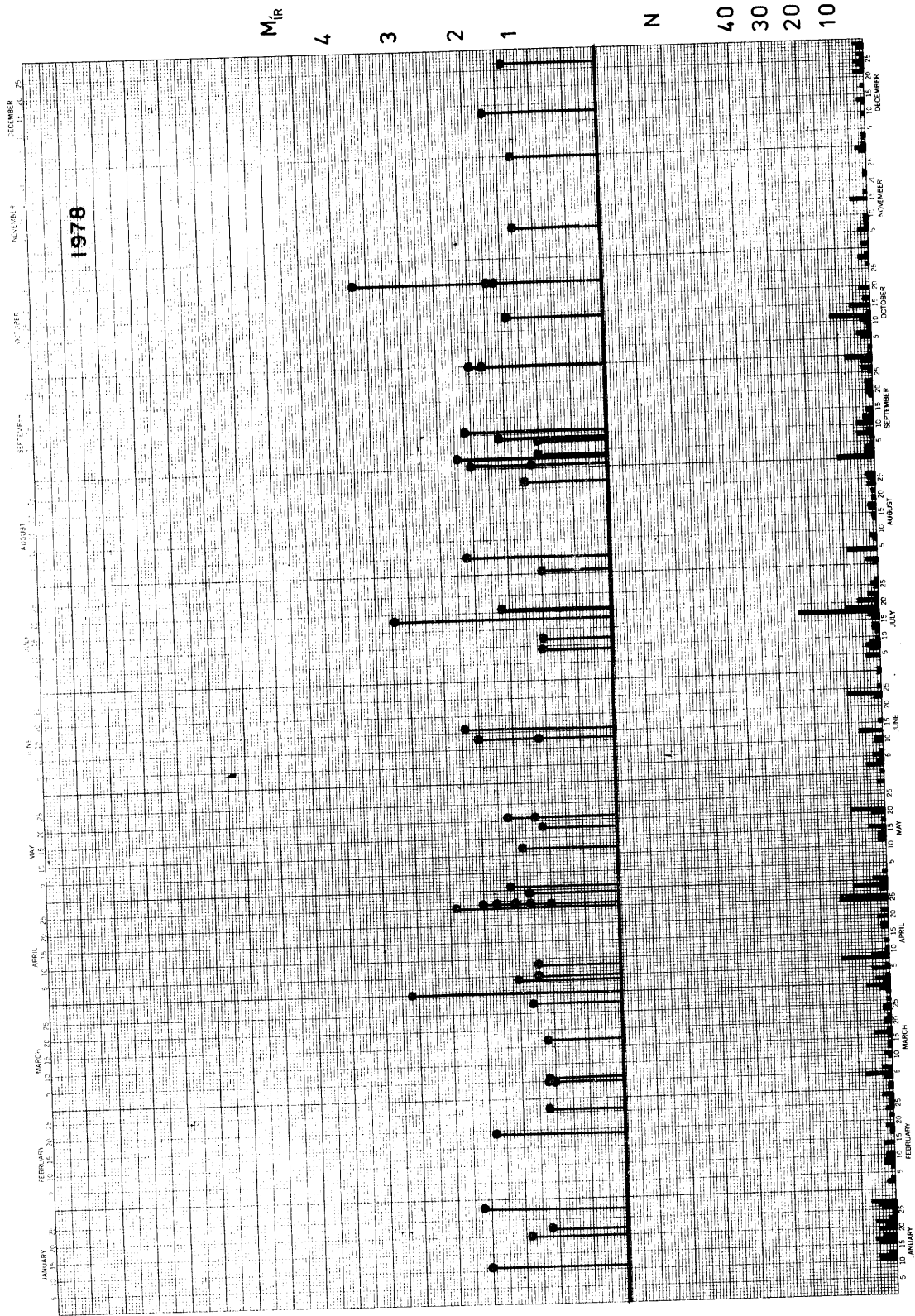
Fig. A3.11 1978
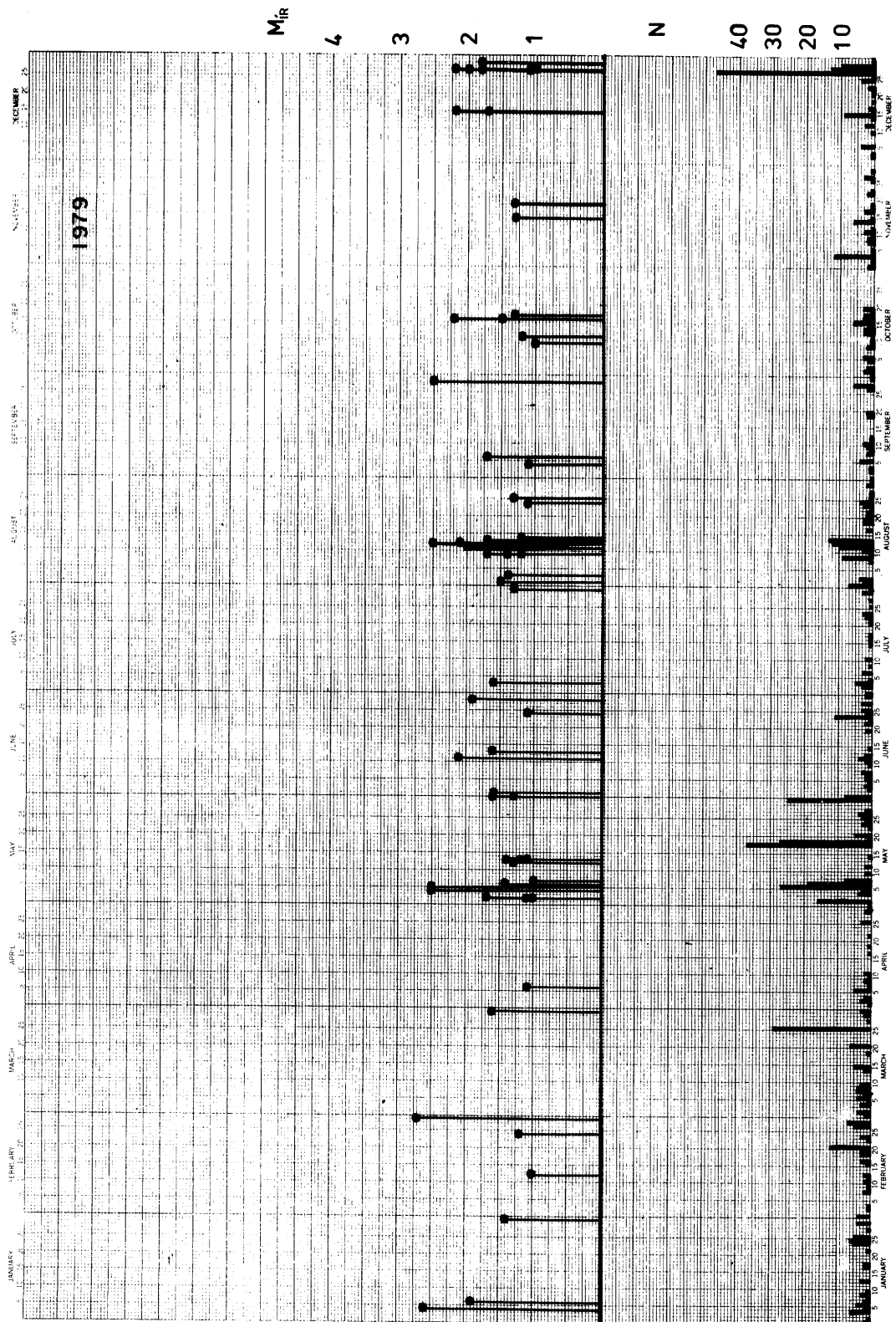
Fig. A3.12 1979

Fig. A3.13 1980

194
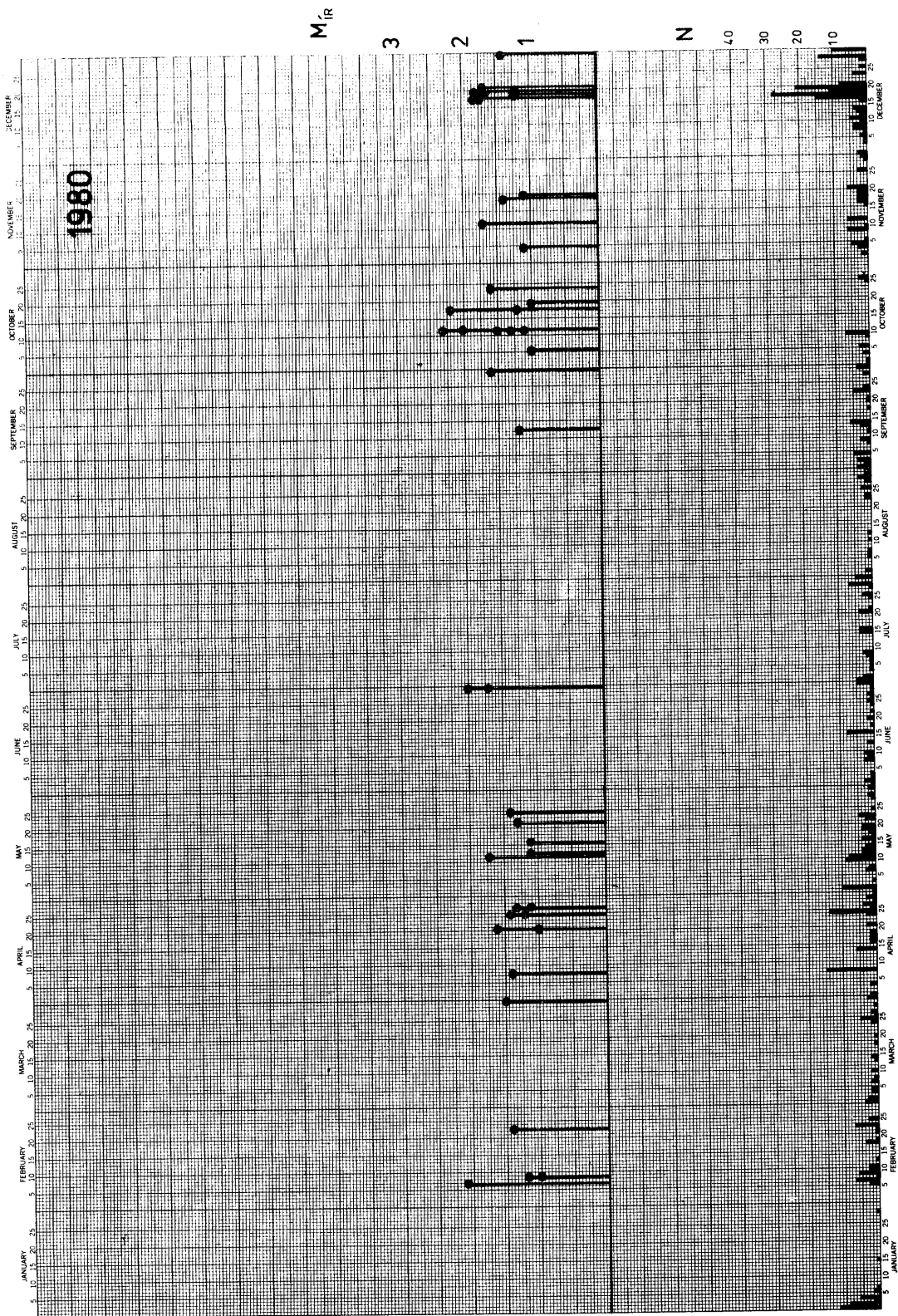
Fig. A3.14 1981

Fig. A3.15 1982

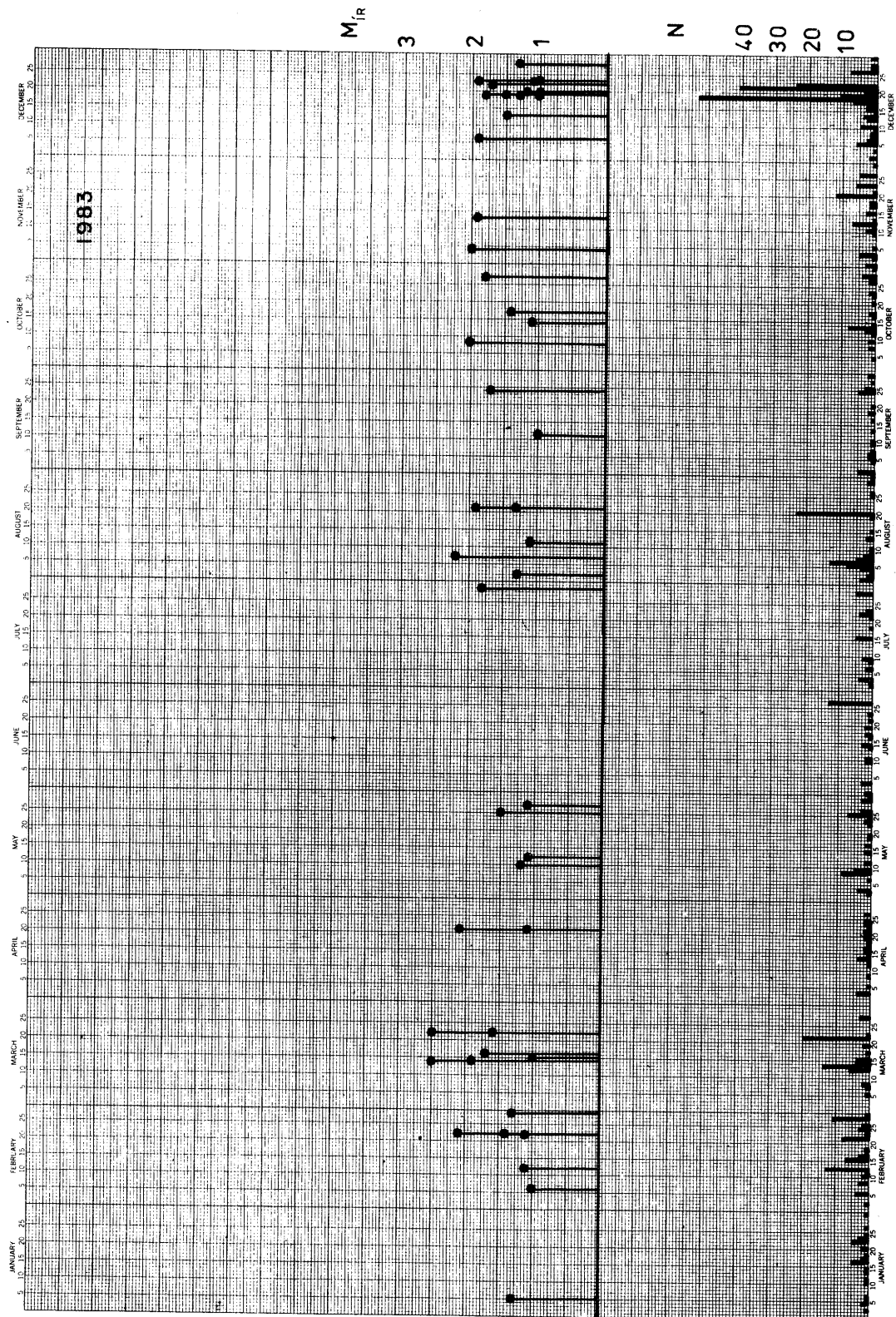Fig. A3.16 1983